Molecular characterisation of the recombinant Vesicular Stomatitis Virus- ZEBOV-GP virus, prototype vaccine against Ebola virus

Nicolas Danet

N° d'ordre NNT : 2019LYSE1009

THÈSE de DOCTORAT DE L'UNIVERSITÉ DE LYON
opérée au sein de
l'Université Claude Bernard Lyon 1

Ecole Doctorale N° 340
Biologie Moléculaire Intégrative et Cellulaire

Spécialité de doctorat : Virologie
Discipline : Biologie moléculaire

Soutenue publiquement le 01/02/2019, par :
Nicolas DANET

Molecular characterisation of the recombinant *Vesicular Stomatitis Virus*-ZEBOV-GP virus, prototype vaccine against Ebola virus

Devant le jury composé de :

Jamin Marc, Professeur, Institut de Biologie Structurale - CEA Grenoble, Rapporteur et Président du jury.

Blondel Danielle, Directeur de Recherche CNRS, Institut de Biologie Intégrative de la Cellule Université Paris-Saclay, Rapporteuse.

Gonzales-Dunia Daniel, Directeur de Recherche CNRS, Centre de Physiopathologie Toulouse-Purpan - Université de Toulouse, Examinateur.

Manet Evelyne, Directrice de Recherche CNRS, Centre International de Recherche en Infectiologie - Université Claude Bernard Lyon 1, Examinatrice.

Gilbert Christophe, Maître de Conférences UCBL, Centre International de Recherche en Infectiologie - Université Claude Bernard Lyon 1, Examinateur

Volchkov Viktor, Professeur UCBL, Centre International de Recherche en Infectiologie, Directeur de Thèse.

INDEX

LIST OF FIGURES AND TABLES

ABBREVIATIONS

- (-)ssRNA: Single-stranded negative-sense RNA
- ~: About
- ADAM: A disintegrin and metalloproteinase
- ADE: Antibody-dependant enhancement
- APC: Antigen presenting cells
- BHK T7: Baby hamster kidney cell T7
- BOMBV: Bombali virus
- Bp: Basepairs
- BSL2: Biosecurity level 2
- BUDV: Bundibugyo ebolavirus
- C1q: Complement component 1q
- cAd: Chimpanzee Adenovirus
- CatL/B: Cathepsin L/B
- CD: Cluster differentiation
- CFR: Case Fatality Rate
- CLEC-2: C-type lectin-like receptor 2
- COPII: Coat protein complex II
- CRD: Carbohydrate recognition domain
- CTLA-4: cytotoxic T-lymphocyte-associated protein 4
- CX3CL-1: Chemokine (C-X3-C motif) ligand 1
- DC: Dendritic cells
- DC-SIGN: Dendritic cell-specific intercellular adhesion molecule 3-grabbing non integrin
- DIC: Disseminated intravascular coagulation
- DMEM: Dulbuecco's modified Eagle's medium
- DNA: Deoxyribonucleic acid
- DRM: Detergent-resistant membranes
- DSM: Detergent-sensitive membranes
- dsRNA: double stranded RNA
- EBOV: Zaire ebolavirus
- EGF: Epidermal growth factor
- Endo H: Endoglycosidase H
- ER: Endoplasmic reticulum
- ESCRT: Endosomal sorting complex required for transport
- E-value: Expect-value
- EVD: Ebola Virus Disease
- F: Phenylalanine
- FB: Fibrinogen
- FBS: Fetal bovin sera
- Fc: Fragment crystallizable
- Fig: Figure
- FVII: Coagulation factor VII
- GE: Gene End
- GE: Gene end
- GFP: Green fluorescent protein
- GlcNAc: N-acteyl-glucosamine
- GP: Glycoprotein
- $GP_{2\text{-RES}}$: $GP_{2\text{-RESISTANT}}$

- GPcl: Cleaved GP
- GS: Gene Start
- GS: Gene start
- HBSS: Hanks' balanced salt solution
- HeV: Hendra virus
- His: Histidine tag
- HIV: Human immunodeficiency virus
- HK: High molecular weight kininogen
- HLA-DR: Human leukocyte antigen-DR isotype
- HPIV3: Human parainfluenza virus type 3
- HR1/2: Heptade region ½
- Hrs: Hours
- HSPA8: Heat shock 70 kDa protein 8
- IB: Inclusion bodies
- ICAM-1: Intercellular adhesion molecule 1
- IFA: Indirect fluorescence assay
- IFL: Internal fusion loop
- IFN: Interferon
- IFNAR: Interferon alpha receptor
- IFNGR: Interferon gamma receptor
- IgG/M: Immunoglobulin G/M
- IID: Interferon inhibitory domain
- IL: Interleukines
- IL-1RA: Interleukine-1 receptor antagonist
- IO: Iodixanol
- IR: Intergenic Regions
- IRES: Internal ribosome entry site
- IRF-3: Interferon-regulated factor 3
- ISG: Interferon stimulated genes
- JAK-STAT: Janus kinase-Signal transducer and activator of transcription
- Kb: Kilobase
- kDa: Kilodalton
- KPNA: Karyopherin Alpha
- LDL: Low density lipoportein
- LLOV: Lloviu cuevavirus
- LN: Lymph nodes
- LPS: Lipoplysaccharide
- LR: Lipid rafts
- LSECtin
- L-SECTIN
- L-SIGN/CLEC4M: C-type lectin domain family 4 member M
- MAp19/44: MBL-associated protein of 19/44 kDa
- MARV: Marburg virus
- MASP: Mannose-associated serine protease
- MBL: Mannose binding lectin
- MCP1: Monocyte chemoattractant protein 1
- M-CSF: Macrophage colony-stimulating factor
- MDA-5: Melanoma differentiation-associated protein 5
- MFI: Median Fluorescence Intensity

- MIP-1α/1β: Macrophage inflammatory protein 1α/1β
- MkDa: Million kiloDalton
- MLD: Mucin-like domain
- mM: Millimolar
- MOI: Multiplicity of infection
- MPER: Membrane proximal external region
- mRNA: Messenger RNA
- MVA: Modified vaccinia Ankara
- N/CTD: N/C-terminal domain
- NC: Nucleocapsid
- Nedd4: Neural precursor cell expressed developmentally down-regulated protein 4
- NHP: Non-Human Primates
- NK: Natural Killer
- nm: Nanometer
- NNS: Nonsegmented negative-sense
- NP: Nucleoprotein
- NPC1: Niemann-Pick C1
- Nt: Nucleotide
- OPS: O-phospho-L-serine
- ORF: Open reading frame
- PAR: Protease-activated receptor
- PBS: Phosphate buffer saline
- PCR: Polymerase chain reaction
- PD-1: Programmed cell death protein 1
- PE: Promoter element
- PFA: Paraformaldehyde
- PLT: Platelets
- PFU: Particle Forming Unit
- PhD: Philosophiæ doctor
- PK: Prekallikrein
- PNG F: Peptide N-glycosidase F
- PPP: Platelet-poor plasma
- Pre-GP: Precursor Glycoprotein
- Pre-GP_{ER}: Precursor glycoprotein endoplasmic reticulum
- Pre-sGP: Precursor soluble Glycoprotein
- PRP: Platelet-rich plasma
- PRR: Pathogen recognition receptor
- PS: Phosphatidylserine
- qRT-PCR: quantitative Retrotranscription Polymerase Chain Reaction
- RA: Roussetus aegyptiacus
- rAd: Recombinant Adenovirus
- RANKL: Receptor activator of nuclear factor kappa-b ligand
- RAVV: Ravn virus
- RBC: Red blood cells
- RBD: Receptor binding domain
- rEBOV: Recombinant EBOV
- RESTV: Reston ebolavirus
- RIG-I: Retinoic acid-inducible gene I
- RLR: Rig-I like receptor

- rMBL: recombinant MBL
- RNA: Ribonucleotide Acid
- rNAPc2: Recombinant nematode anticoagulant protein c2
- RNP: Ribonucleocapsid
- rRNA: Ribosomal RNA
- RT: Retrotranscription
- rVSV/LASVGPC: rVSV/Lassa virus glycoprotein
- rVSV-GP-HS: rVSV-GP High shed mutant
- rVSV-GP-LS: rVSV-GP Low shed mutant
- rVSV-ZEBOV: recombinant VSV-ZEBOV
- Sec34c: SEC24 homolog C
- sGP: Soluble GP
- sIL-6R: Soluble interleukine 6 receptor
- siRNA: small interfering RNA
- SNP: Single Nucleotide Polymorphism
- SPNT: Supernatant
- ssGP: Super small GP
- sTNF-R: Soluble Tumor necrosis factor receptor
- SUDV: Sudan ebolavirus
- TACE: TNFα-converting enzyme
- TAFV: Taï Forest ebolavirus
- TCID50: 50% Tissue culture infective dose
- TF: Tissue Factor
- Tgs101: Tumor susceptibility gene 101
- TIMP3: Tissue inhibitor of metalloproteinase 3
- TLR: Toll-like receptor
- TM: Transmembrane domain
- TNFα: Tumor necrosis factor α
- TRAIL: TNF-related apoptosis-inducing ligand
- TRAP: Thrombin receptor activator peptide 6
- UC: Ultracentrifuged supernatant
- µg: Micrograms
- UTR: Untranslated regions
- VCAM-1: Vascular cella dhesion protein 1
- VEEV: Venezuelan equine encephalitis virus
- VeroE6: Verda reno E6
- VLP: Virus-like particle
- VP: Viral protein
- VP35 NPBP: VP35 NP Binding Peptide
- vPAMP: Viral pathogen associated molecular pattern
- VRP: Venezuelan equine encephalitis virus replicon
- VSV: Vesicular stomatitis virus
- Washed PLT: Washed platelets
- WT: Wild-type
- WWP1: WW doain containing E3 ubiquitin protein ligase 1
- Y: Tyrosine
- α: Alpha
- β: Beta
- Δ: Delta

RESUME

Ebolavirus (EBOV) est un filovirus responsable de fièvres hémorragiques virales sévères chez l'humain, qui peuvent être létales dans 90% des cas. L'actuelle épidémie en République Démocratique du Congo et l'ampleur démesurée de l'épidémie de 2014-2016 en Afrique de l'Ouest, qui a causé la mort de plus de 11 000 personnes, ont poussé les agences sanitaires internationales à tester plusieurs approches thérapeutiques afin d'essayer d'endiguer rapidement la propagation virale et de limiter la mortalité liée au virus lors de futures épidémies. Parmi toutes les stratégies testées, le virus recombinant réplicatif rVSV-ZEBOV qui exprime la glycoprotéine de surface d'EBOV, semble offrir la meilleure protection, aussi bien en modèle animaliers que sur le terrain. Avant d'être testé chez l'humain, de nombreuses études ont permis de mettre en évidence l'efficacité et l'innocuité de ce vaccin prototype. Pourtant et malgré le fait que de nombreuses études ont démontré l'importance et le rôle de la glycoprotéine GP dans l'efficacité des vaccins contre ce virus, aucune étude n'a encore été réalisé sur la nature des glycoprotéines virales synthétisées par le gène GP d'EBOV inséré dans le génome du virus VSV. Ainsi, les caractérisations moléculaires des protéines virales produites lors de l'infection par le virus rVSV-GP décrites dans ces travaux de thèse offrent de nouvelles perspectives pour comprendre le succès de ce vaccin mais aussi l'origine virales dans les effets secondaires sévères observés lors de la vaccination, et pourront aider à développer un vaccin plus sûr, qui n'est actuellement pas utilisable chez les personnes immunodéprimées.

Mots clefs : *Ebolavirus*, rVSV-ZEBOV, vaccin, glycosylations, *R. aegyptiacus*, *Marburgvirus*.

ABSTRACT

The filovirus Ebolavirus (EBOV) is the causative agent of severe viral haemorrhagic fevers in humans that can be lethal in 90% of cases. The current outbreak in the Democratic Republic of Congo and the extraordinary scale of the 2014-2016 outbreak in West Africa, that caused the death of more than 11 000 disease victims, lead the international public health agencies to test several therapeutic approaches to limit viral spreading and mortality. Amongst those, the recombinant replication-competent rVSV-ZEBOV virus, that expressed EBOV GP glycoprotein, appears to offer the best protection in animal models and outbreak settings. While its effectiveness and safety have been widely investigated before human trials and despite numerous studies that showed the importance the nature of the glycoproteins which are produced during the infection from the EBOV GP gene that has been inserted in VSV genome are unknown. In this respect, the molecular characterisation of the viral glycoproteins synthesised during rVSV-GP presented in this thesis, offer new insights with which to understand the success of the rVSV-GP vaccine but also the potential viral origins of the severe adverse side effects observed during vaccination and could help in developing a safer vaccine, which currently cannot be used in an immunocompromised population.

Keywords: *Ebolavirus*, rVSV-ZEBOV, vaccine, glycosylations, *R. aegyptiacus*, *Marburgvirus*

INTRODUCTION

EBOLA VIRUS: IDENTIFICATION, TRANSMISSION AND NATURAL RESERVOIR

FILOVIRUS OUTBREAKS

Ebola virus is an enveloped, non-segmented single-stranded negative-RNA virus that was first isolated in 1976 following outbreaks in South Sudan and Zaire (now the Democratic Republic of Congo) [1]. It is a zoonotic virus and the causative agent of Ebola virus disease (EVD), a severe disease in humans and non-human primates (NHP) with a fatality rate that can reach 90% in some outbreaks. As there are currently no vaccine or therapeutic approaches approved, Ebola virus is a major public health concern.

Ebola virus is part of the *Ebolavirus* genera, which alongside *Marburgvirus* and *Cuevavirus* compose the Filoviridae family (Fig. 1). They are currently five recognised genetically distinct species of Ebolavirus: *Zaire ebolavirus* (EBOV), *Sudan ebolavirus* (SUDV), *Taï Forest ebolavirus* (TAFV), *Bundibugyo ebolavirus* (BUDV) and *Reston ebolavirus* (RESTV). Marburgvirus is composed of a single species *Marburg marburgvirus* with two members Marburg virus (MARV) and Ravn virus (RAVV). Finally, discovered in 2011, Cuevavirus is formed of a unique species, *Lloviu cuevavirus* (LLOV) [2,3] .

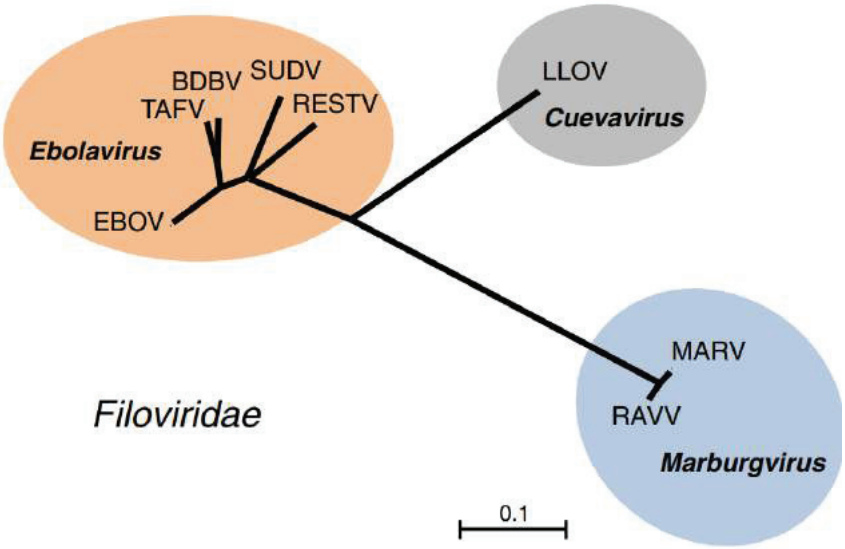

FIGURE 1. PHYLOGENIC TREE OF THE *FILOVIRIDAE* FAMILY.

Obtained from [9]. Phylogenetic tree representing the three major Filovirus genera: Ebolavirus, Marburgvirus and Cuevavirus. Ebolavirus is composed of five species: Zaire ebolavirus (EBOV), Sudan ebolavirus (SUDV), Tai Forest ebolavirus (TAFV), Bundibungyo ebolavirus (BEBOV) and Reston ebolavirus (RESTV). Marburg marburgvirus (MARV) and Ravn virus (RAVV) are forming the Marburgvirus genus and Lloviu virus, the Cuevavirus genus. The scale bar represents evolutionary distance between each node.

Since the first filovirus outbreak in 1967, caused by MARV, forty different outbreaks have been recorded, with their majority being caused by one of the five species of Ebolavirus. So far, LLOV has not caused any outbreak in humans but was detected only in dead insectivorous bats (Table 1). The majority of the outbreaks occurred in Central and South Africa, which suggests that filoviruses are endemic of these regions. However, the 2014 outbreak that occurred in West Africa, the isolation of RESTV from infected monkeys imported from the Philippines, the identification of LLOV in the north of Spain and its re-emergence in 2013 in Hungary, as well as the detection of partial RNA sequences of filoviruses in central China, are incrementing elements pointing out that Filoviruses are not restricted to Central and South Africa as initially thought (Fig. 2) [3–7]. The increasing number of Ebolavirus outbreaks since 2000 has been suggested to be caused by an augmentation of accidental contacts between humans and the natural or amplifying hosts of the virus, occurrences often associated with certain social and economic activities, such as deforestation, hunting and bushmeat consummation [8–11].

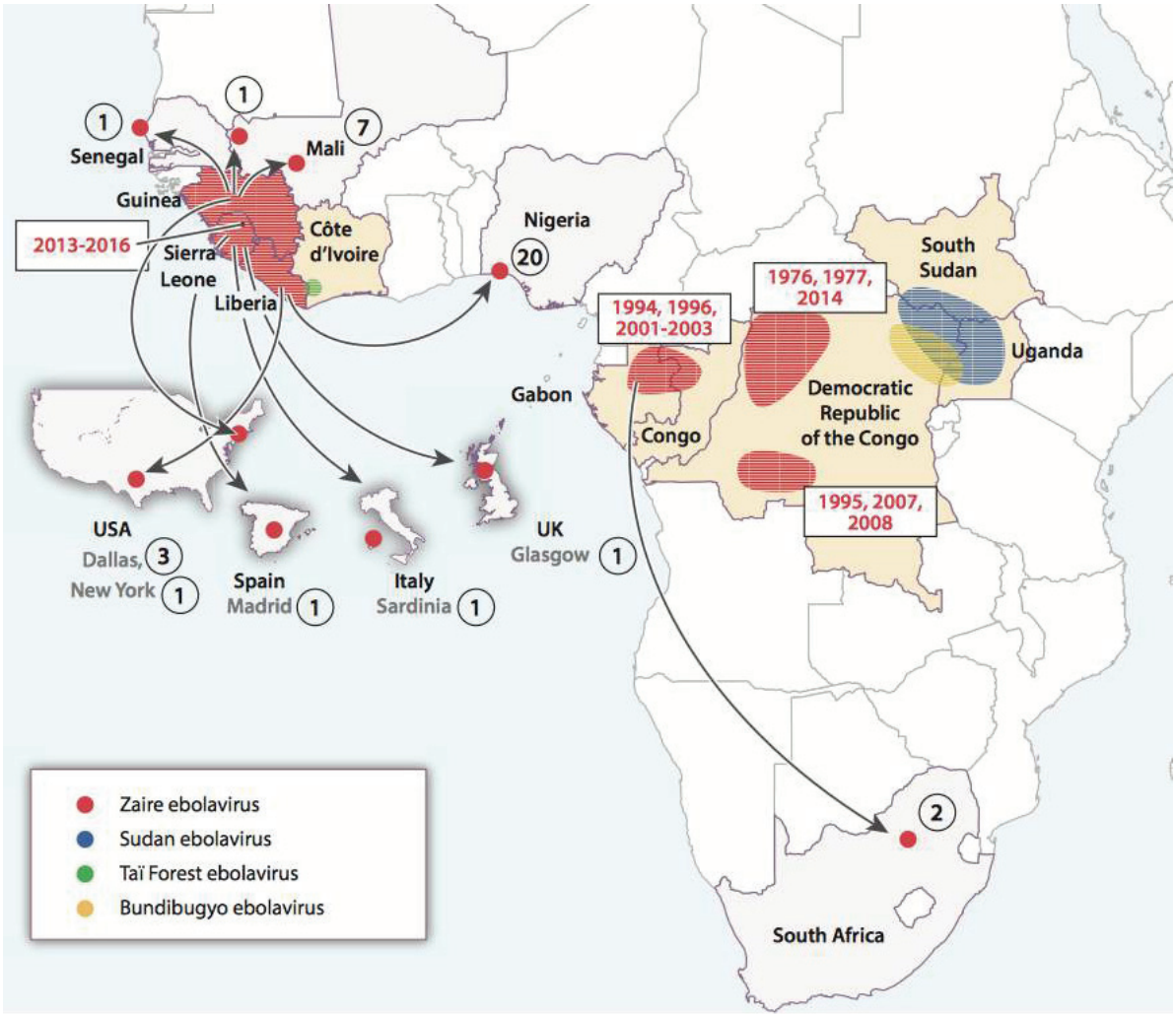

FIGURE 2. EBOLAVIRUS OUTBREAKS MAP.

Obtained from [15]. Modified map of Africa showing the date and the localisation of the different Ebolavirus outbreaks. The arrows are representing the human movements that lead to the exportation of EBOV to different countries, during the 2014 outbreak, and the encircled number the number of associated cases.

Filovirus	Year(s)	Country	Reported number of human cases	Reported number of fatalities
Marburg marburgvirus	1967	Germany and Yugoslavia	31	7
Marburg marburgvirus	1975	Johannesburg, South Africa	3	1
Sudan ebolavirus	1976	South Sudan	284	151
Zaire ebolavirus	1976	Democratic Republic of Congo	318	280
Zaire ebolavirus	1977	Democratic Republic of Congo	1	1
Sudan ebolavirus	1979	South Sudan	34	22
Marburg marburgvirus	1980	Kenya	2	1
Marburg marburgvirus	1987	Kenya	1	1
Marburg marburgvirus	1990	Russia	1	1
Taï Forest ebolavirus	1994	Côte d'Ivoire (Ivory Coast)	1	0
Zaire ebolavirus	1994	Gabon	52	31
Zaire ebolavirus	1995	Democratic Republic of Congo	315	250
Zaire ebolavirus	1996	South Africa	2	1
Zaire ebolavirus	1996	Gabon	60	45
Zaire ebolavirus	1996	Gabon	37	21
Marburg marburgvirus	1998-2000	Democratic Republic of Congo	154	128
Sudan ebolavirus	2000	Uganda	425	224
Zaire ebolavirus	2001	Republic of Congo	57	43
Zaire ebolavirus	2001	Gabon	65	53
Zaire ebolavirus	2002	Republic of Congo	143	128
Zaire ebolavirus	2003	Republic of Congo	35	29
Sudan ebolavirus	2004	South Sudan	17	7
Marburg marburgvirus	2004-2005	Angola	252	227
Bundibugyo ebolavirus	2007	Uganda	149	37
Zaire ebolavirus	2007	Democratic Republic of Congo	264	187
Marburg marburgvirus	2007	Uganda	4	1
Zaire ebolavirus	2008	Democratic Republic of Congo	32	15
Marburg marburgvirus	2008	USA"	1	0
Marburg marburgvirus	2008	Netherlands"	1	1
Sudan ebolavirus	2011	Uganda	1	1
Sudan ebolavirus	2012	Uganda	6*	3*
Bundibugyo ebolavirus	2012	Dem. Rep. of Congo	36*	13*
Sudan ebolavirus	2012	Uganda	11*	4*
Marburg marburgvirus	2012	Uganda	15	4
Zaire ebolavirus	2014-2016	Multiple Countries**	28652	11325
Zaire ebolavirus	2014	Democratic Republic of Congo	66	49
Marburg marburgvirus	2014	Uganda	1*	1
Marburg marburgvirus	2014	Uganda	2	5
Zaire ebolavirus	2017	Democratic Republic of Congo	8	4
Zaire ebolavirus	2018	Democratic Republic of Congo	Ongoing	Ongoing

" Exported cases from Uganda

* Laboratory cases confirmed only

** Guinea, Serria Leone, Liberia, USA, Nigeria, Mali, USA, Senegal, Spain, United Kingdom, Italy

TABLE 1. LIST OF EBOLAVIRUS OUTBREAKS.

Modified from [9].

NHP are highly susceptible to EBOV infection and are commonly used as a model of human transmission. It has been shown that NHP could be infected through oral, conjunctival, submucosal and respiratory routes [12,13]. NHP infection studies also showed that EBOV is highly infectious and those cynomolgus macaques were able to succumb to the infection when exposed to very low dose of infectious virus (from 0.01 PFU to 1 PFU; Plaque Forming Unit) [14]. In humans, the overall case fatality rate[1] (CFR) of Ebolavirus ranges from 34% to 88% depending on the species; EBOV being the most lethal and, with the exception of RESTV, which is considered to be asymptomatic in humans, BEBOV appears to be the less pathogenic of the five known Ebolavirus species. For Marburg virus, the CFR is around 80% [15].

Based on the NHP studies and retrospective analysis of epidemiological data of chain of transmissions, It is now clear that EBOV is mostly transmitted between humans through direct exposure with an infected person or disease victim through broken skin or mucous membranes [9,12]. During the acute phase of the illness, the virus is present at high titters in different bodily fluids such as the blood, saliva, sweat, tears, vomit, semen and stools. Improper handlings of the patients or burial practises are considered to be the main cause of virus transmission. Initially, it was thought that EBOV could not be transmitted outside of the symptomatic phase. However, the virus was found to be able to persist for a longer time in some immune-privileged sites following clearance from the bloodstream [16]. Viral RNA has been detected in breast milk, vaginal secretions, ocular aqueous humors and semen several weeks to several months after remission. In this regard, infectious EBOV was also isolated from semen more than three months after viral clearance from blood, and sexual transmission of EBOV has been reported and linked to the start of new transmission chains several days after Ebola-free declaration in the countries [17–19].

The presence of the virus in multiple bodily fluids would suggest that transmission through fomites[2] is also a key in EBOV transmission and would place the handling of the patients or the cadavers at the centre of the transmission event and propagation of the outbreak. In this regard, a study where EBOV was spiked directly into human blood, has shown that the virus was stable in both dry and liquid blood and that live virus could be retrieved up to 14 days after spiking [20]. Similarly, *in vivo* studies showed that EBOV could be detected and retrieved from the corpses of dead monkeys several days after their death [21].
The possibility of airborne[3] or aerosol transmission during filovirus outbreaks is unclear. Filovirus outbreaks are usually restricted in term of size and the viruses do not spread rapidly into the human population, as it can be observed with similar viruses such as Influenza or Measles viruses, suggesting that filoviruses are not airborne viruses. Experimentally infected pigs with a RESTV pig isolate were shown to shed the virus asymptomatically from the nasopharynx and EBOV has been found in human alveoli. Those data, therefore, raise the

[1] CFR: Proportion of cases within a designated population who die as a result of an infection [15].
[2] Fomites: Inanimate object or substance capable to carry infectious organism and to transfer it from one individual to another.
[3] Airborne transmission: As defined by [22]: 'Transmission resulting from the inhalation of small respirable infectious particles (<5µm in size) dispersed over long distances by air currents.

possibility that droplet transmission[4] is possible, and has been suspected to explain some chain of transmissions when no direct contact with an infected person was reported [24,25]. Finally, while NHP were successfully infected following EBOV aerosolization in a controlled environment, it is not known whether the virus could be transmitted this way in a natural setting. Indeed, the virus was shown to be extremely unstable following aerosolization and as such, even though it is not possible to completely rule out aerosols as a transmission route, it would be a very unlikely event, especially in the different tropical or arid environments of the African continent [9,12,26,27].

Several risk factors for filovirus transmission have been identified, based on the previous outbreaks and are associated to an increased risk [15,28]. As expected, the chances of being infected are much more important when being in direct contact with an infected individual at home, or at the hospital, or with infected fluids. As such, the use of inappropriate personal protective equipment or poor medical practises such as exposure to unsterilized/contaminated needles have also played an important role in spreading the disease in some of the EBOV and MARV outbreaks. Taking part in funeral rituals (preparing and touching the cadaver), also significantly increases the chance of getting infected. Interestingly, children (5 to 19 years old of age) seem to be relatively spared from contracting the disease and recent data suggest that they are actually less susceptible to filovirus infections [15,29]. Therefore, genetic factors could play a role in filovirus susceptibility as it has been shown for some Single Nucleotide Polymorphisms (SNP) in the Niemann-Pick C1 (NPC1) gene (encoding a cellular endosomal protein which is the necessary receptor for EBOV entry [30,31]; see below 'Full-length $GP_{1,2}$) or using a genetically diverse panel of recombinant inbred mice [32].

NATURAL AND ACCIDENTAL HOSTS OF FILOVIRUSES

There is no consensus definition for what classifies a species as a natural reservoir for a specific pathogen but it can be defined as 'one or more epidemiologically connected populations or environments in which a pathogen can be permanently maintained and from which infection is transmitted to the defined target population' [33]. Another commonly accepted definition is that natural reservoirs are able to replicate the virus but show little or no sign of disease compared to an accidental/amplifying host. Additionally, natural hosts have a higher seroprevalence than active infection prevalence [34].

Despite intensive efforts to identify reservoir species for filoviruses over the past 40 years, it is still uncertain what the natural reservoirs for ebolaviruses actually are. Numerous studies have tried to identify viral hosts either by sampling animals for antibodies and/or RNA detection or for viral isolation or through experimentally infection in laboratory settings [34,35]. At first, it was hypothesized that, similarly to Lassa virus, small rodents could transmit filovirus and evidence of EBOV RNA was even found in one early study but similar results were never

[4] Droplet transmission: As defined by [23]: 'Form of direct contact transmission in which respiratory droplets (>5µm in size) carrying an infectious pathogen transmit infection when traveling short distances directly from the respiratory tract of the infectious individual to susceptible mucosal surfaces of the recipient.'

obtained again [1,36]. Experimental infection of different rodents, flying mammals and even plants performed by Swanepoel R *et al.* (1996) showed that only bats (both frugivorous and insectivorous) were able to replicate the virus with no sign of disease, pointing to bats as a potential candidate host [35].

Bats are the second most diverse mammalian order with over 1100 species and are present worldwide. They have been identified as the natural reservoir for numerous other re-emerging viruses such as coronaviruses, paramyxoviruses or Influenza A viruses. Their long lifespans, the use of torpor and flight, their diet, as well as the fact that there are living in large communities, with some roosts that can house more than a thousand individuals of the same or different species, are thought to facilitate virus maintenance and transmission [8,37,38].
The isolation in 2009 of MARV from *R. aegyptiacus* and the discovery of LLOV in *M. schreibersii* bats in different locations several years apart, is suggestive for bats being a natural reservoir for filoviruses [3,6,39]. Another piece of evidence is the identification of new RNA sequences from unidentified, potential filovirus species in China in *R. leschenaultia*, *E. spelaea* and *R.* spp bats [4,5]. The results from this study suggest that at least 3 potential new species or genera are present in Mainland China. Interestingly, while high numbers of genomic copies could be detected in some of the infected tissues, and that one bat was even infected with four different filoviruses, bats were according to the authors, seemingly healthy. Experimentally inoculations of arthropod-free *R. aegyptiacus* with MARV show that bats are permissive to virus replication with no apparent sign of diseases and are able to develop a long-lasting protective immunity against the virus following the resolution of the infection that protects animals from reinfection, at least, up to two months following the initial challenge. Oral and rectal shedding of infectious virus, as well as the presence of the virus in the urine have also been confirmed, suggesting that direct or indirect contact with infectious bodily fluids is likely responsible for the horizontal transmission of the virus between bats and probably between other species, including humans [40–44]. Thus, at least in the case of MARV, *R. aegyptiacus* fulfil all criteria to be called a natural reservoir.

So far, Ebolavirus has never been isolated directly from animal tissues and therefore the natural reservoir for Ebolavirus is still unknown. Several bat species are suspected to be potential hosts for Ebolavirus, including *H. helvum*, *R. aegyptiacus*, *E. gambianus* or *E. buettikoferi*, *E. franqueti* and *H. monstrosus*, but those assumptions are based only on antibodies or partial RNA sequence detection (Table 2) [45]. *In vivo* and *in vitro* studies have helped to shed light into potential reservoir hosts for EBOV. Indeed, it has been shown that *H. helvum* kidney fibroblast cell lines were drastically less susceptible to EBOV infection compared to fibroblasts derived from *R. aegyptiacus* and *E. buettikoferi* cell lines, due to a weak interaction between EBOV glycoprotein $GP_{1,2}$ that drives entry into cells and *H helvum* NPC1 (see below: Paragraph 'Full-length $GP_{1,2}$'). Interestingly, this limited binding has been mapped to a single amino acid in NPC1 and could be potentially used to predict whether a bat species is a candidate host for EBOV [46]. While, *in vitro* results support the hypothesis that *R. aegyptiacus* is a possible host for EBOV, as *R. aegyptiacus*-derived cell lines replicate the virus as efficiently as MARV, an *in vivo* experiment showed that following EBOV inoculation, *R. aegyptiacus* bats do not become viremic in the tested conditions (a single route of injection and a single dose of virus with a limited number of animals tested) [44]. Consequently, *in vitro* experiments using bat cell lines-derived from tissues that are not the primary targets of filoviruses (mononuclear phagocytic lineage cells, hepatocytes, splenocytes,) need to be

interpreted cautiously. Furthermore, the *in vitro* and *in vivo* experiments were performed using viruses that were isolated from humans and NHP and one cannot exclude that these viruses were more adapted to human/NHP than bats. Results from Jones ME *et al.* (2015) also encourage the idea that bat species are adapted to support the replication of one or closely related filoviruses and that the tropism of filovirus in bats is limited by different factors. Careful analysis of the phylogenetic analysis results obtained by Yang XL *et al.* (2017) also favours this hypothesis as the filoviruses discovered in Rousettus species are all clustered with MARV [5,44]. In July 2018, a sixth Ebolavirus species, Bombali virus was discovered in two different bat species (*C. pumilus* and *M. condylurus*) reinforcing again the idea of bats being the natural reservoir of filoviruses [298].

Bat species	EBOV	RESTV	LLOV	MARV	SEBOV	BEBOV	TAFV
Epomops franqueti	RNA / Antibodies	Antibodies	-	Antibodies	-	-	-
Hypsignathus monstrosus	RNA / Antibodies	Antibodies	-	Antibodies	-	-	-
Myoncyteris torquata	RNA / Antibodies	-	-	-	-	-	-
Miniopterus inflatus	-	-	-	RNA	-	-	-
Rhinolophus eloquens	-	-	-	RNA / Antibodies	-	-	-
Rousettus aegyptiacus	Antibodies	-	-	RNA / Antibodies / Viral isolation	-	-	-
Micropteropus pusillus	Antibodies	-	-	Antibodies	-	-	-
Microchiroptera	Antibodies	-	-	-	-	-	-
Rousettus amplexicaudatus	-	Antibodies	-	-	-	-	-
Miniopterus schreiberssi	-	RNA	RNA	-	-	-	-
Epomophorus gambianus	Antibodies	Antibodies	-	-	-	-	-
Eidolon helvum	Antibodies	Antibodies	Antibodies	Antibodies	Antibodies	Antibodies	Antibodies
Acerodon jubatus	-	Antibodies	-	-	-	-	-
Chaerephon plicatus	-	RNA	-	-	-	-	-
Cynopterus brachyotis	-	RNA	-	-	-	-	-
Miniopetrus australis	-	RNA	-	-	-	-	-
Pteropus vampyrus	-	Antibodies	-	-	-	-	-
Cynopterus sphinx	-	Antibodies	-	-	-	-	-
Hipposideros pomona	-	Antibodies	-	-	-	-	-
Hipposideros sp.	-	Antibodies	-	-	-	-	-
Myotis ricketti	-	Antibodies	-	-	-	-	-
Myotis sp.	-	Antibodies	-	-	-	-	-
Pistrellus pistrellus	-	Antibodies	-	-	-	-	-
Rhinolophus affinis	-	Antibodies	-	-	-	-	-
Rousettus leschenaultii	Antibodies	Antibodies	-	-	-	-	-
Scotophilus kuhlii	-	Antibodies	-	-	-	-	-

TABLE 2. LIST OF BAT SPECIES IDENTIFIED AS POTENTIAL FILOVIRUS RESERVOIR

In addition to bats as natural reservoirs for filoviruses, several other species were identified as amplifying hosts, such as NHP, duikers and swine (Fig. 3). Carcases of gorillas and chimpanzees, as well as antelopes, positive for the virus has been found at several occasions. Indeed, outbreaks in wild animals have commonly preceded outbreaks in the human population and would often appear to be the cause of the spillover into human society [47,48]. It has been estimated that the EBOV outbreaks between 2001 and 2003 in great apes has led to an alarming decline of more than 80% of the population [49]. In some areas, it is believed that EBOV is responsible for the disappearance of at least 50% of the duikers and 89% of the chimpanzees [50]. Group-to-group transmission of the virus between gorillas appears to be facilitated by their social habitude, especially their habits of inspecting carcases of other dead gorillas from outside of one's group or feeding on fruit from the same tree, which could be contaminated with infected bodily fluids from bats [51]. Similarly, RESTV was isolated initially

from cynomolgus monkeys imported from The Philippines [52]. For RESTV, while no Ebolavirus-like disease was observed in the adult humans that were infected (the virus is thus considered non-pathogenic in humans), it is highly lethal in monkeys, reinforcing the idea that NHP are highly susceptible to filovirus infection. Additionally, RESTV has been isolated from pigs in The Philippines and a direct contact between pigs and insectivorous bats (*M. schreibersii*) that were found positive by qPCR assays has been suggested to be the cause of the pigs' initial infection [53,54].

Based on these different studies, filoviruses appear thus to have a wide tropism and can infect multiple hosts, with some that can show no sign of disease. Considering the important economic value of the identified animals (pig farming, bushmeat for bats and NHP,), a routine animal sampling of those hosts for antibodies or RNA detection could help to prevent spreading of the virus into the human population.

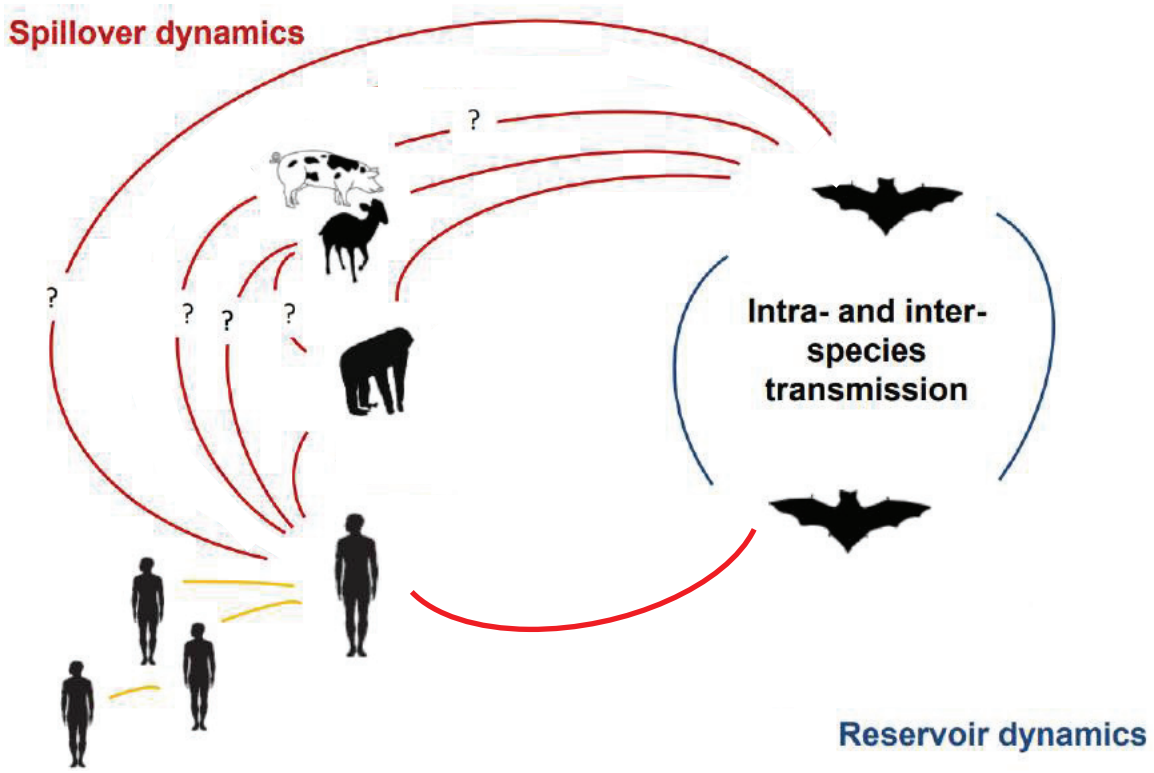

FIGURE 3. FILOVIRUS TRANSMISSION DYNAMICS

Modified from [296] representing the hypothesised existing relationship to allow either maintenance of filovirus in one or several bat species (Reservoir dynamics in blue), and their spillovers in accidental animal hosts (swine, duikers and great apes, and humans; Spillover dynamics, in red). Inter-human transmission is also represented (in yellow).

VIRION AND GENOMIC ORGANISATION

Filoviruses virions are filamentous, which make them the only currently known animal viruses with a filamentous structure. While filovirus' diameters are of about 80-90nm, and are consistent between the different filovirus genera, MARV virions length appears to be smaller than EBOV virions, with a size of about 800nm and 1200nm respectively. Electron microscopy analysis showed that the virions are flexible and it can form U or 9-shape (Fig. 4). This flexibility is suggested to be important to protect the single-stranded negative-sense RNA ((-)ssRNA) genome from breaking to limit the production of non-infectious viral particles [55–57].

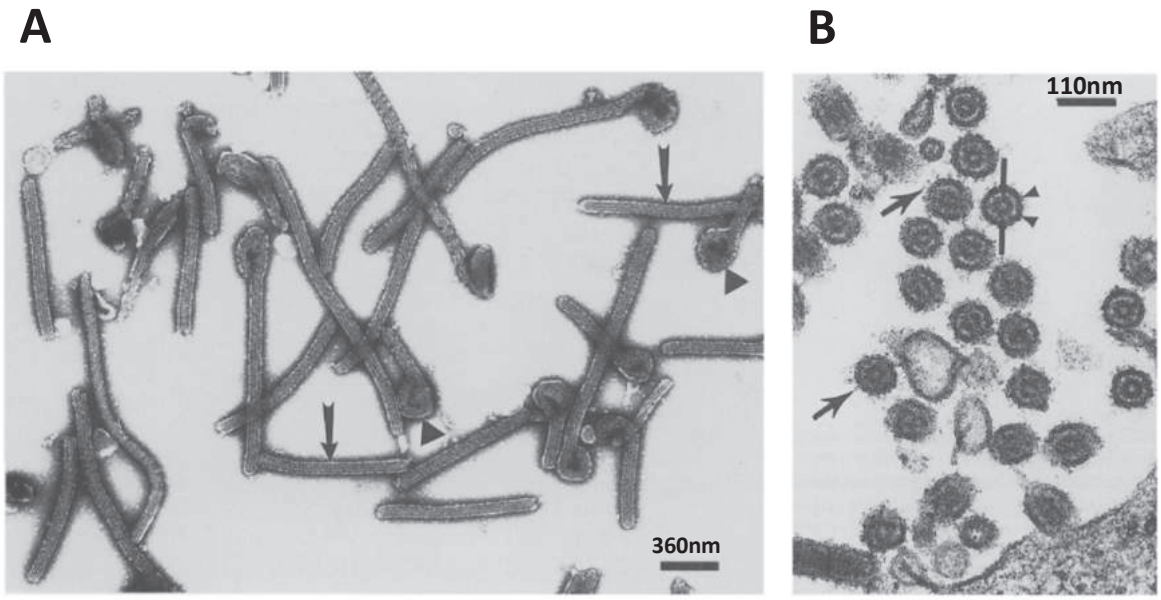

FIGURE 4. ELECTRON MICROSCOPY PICTURES OF FILOVIRUS VIRIONS

Obtained from [53]. Negatively contrasted EBOV virions (A), illustrating the filmanetous (full arrows) and 6-shaped forms (arrowheads) of the viral particles. EBOV virion cross-section (B) showing the 45-50nm nucleocapsid (arrowheads) and the viral host-derived membrane decorated by EBOV glycoprotein spikes (spearheads).

Ebola virus has a 19kb genome that starts by a 3' leader non-coding region, followed by seven genes arranged in tandem encoding seven structural proteins: The nucleoprotein NP, VP35, VP40, VP24, the glycoprotein $GP_{1,2}$ and the RNA-dependant RNA-polymerase polymerase L and two secreted non-structural proteins, the soluble GP (sGP), and the super small GP (ssGP). The genome is terminated by a 5' trailer non-coding region (Fig. 5). At the exception of the GP gene which gives rise to three different proteins through transcriptional editing, all other EBOV genes produce a single viral protein [58].

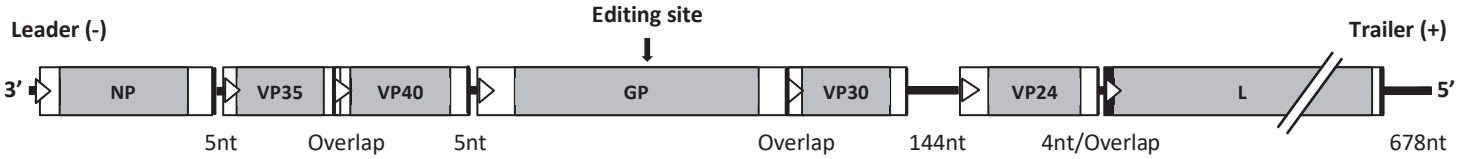

FIGURE 5. EBOV GENOME STRUCTURE

Modified from [60]. Schematical representation of EBOV genome organization. At the exception of the L gene, the genes are drawn to scale. Open reading frame are painted in grey and the untranslated regions in white. White triangles are showing gene start and black bars, gene ends. The length and the nature and size of the intergenic regions (not to scale) are indicated, as well as the position of GP editing site.

TRANSCRIPTION AND REPLICATION REGULATION

The 3' leader is a 55 nucleotides region formed of a cis-acting promoter, which drives the formation of a complementary antigenome that is used as a template for the replication of the genome (Fig. 6). The 676-nucleotide complementary 5' trailer end serves as a significantly stronger promoter than the 3' leader promoter and allows for intense replication of the viral genome. Predictions of secondary structure suggest that both the leader and trailer regions can interact together to form a panhandle structure, yet, it is not clear if they indeed form such structure during the infection. However, it has been shown that the introduction of mutations that modify the secondary structures of either EBOV leader or trailer impair genome replication [59–62]. Analysis of the EBOV leader region revealed that it is formed of a bipartite promoter, separated by a spacer, and that a loop is formed inside of the first promoter element, which is essential for replication (Fig. 6, lower part). Similarly, the cellular HSPA8 protein is able to bind a small stem-loop structure present in the EBOV trailer. Introduction of mutations to impair the formation of this structure and the binding of HSPA8 make it impossible to rescue the virus, again highlighting the key role of secondary structures in this region for regulation [59–62].

During transcription, EBOV polymerase scans the genome from the 3' end to the 5' end for the highly conserved gene start signals (GS) and gene end signals (GE) [63,64]. While the GS marks the initiation of the mRNA transcription, the GE marks the termination of the transcript (Fig. 6, upper part). It is believed that filovirus polymerase function through a stop-and-start mechanism similarly to other non-segmented negative-sense (NNS) viruses. When the polymerase encounters a GS signal, it will start to transcribe a mRNA, that is co-transcriptionally capped and methylated, and will be terminated at its associated GE signal. The GE signal consists of a stretch of uridine residues, which will lead to the formation of a poly(A) tail, by a mechanism called stuttering. Finally, the newly synthesised mRNA is detached from the polymerase [65]. At this point, the polymerase is either released from the template or continues to scan the genome to detect a new GS and initiate the transcription of a new mRNA from an upstream gene. In some rare instance, when the GS is not well recognised, read-through mRNA are produced [66,67]. When the polymerase is detached from the genome, and as it can only enter it from the 3' end, it will have to restart the transcription from the beginning. This leads to a transcription gradient, which can be observed during infection, with the more proximal genes (with respect to the 3' leader) being more transcribed than the most distal ones. This gradient represents a first layer of transcription regulation to

control viral protein levels during the infection and is necessary for a proper viral fitness. Accordingly, an excess of L proteins was shown to reduce viral replication [68–71].

Gene expression is also controlled by *cis*-acting element present between the GS and the GE signals, notably the intergenic regions (IR) and the untranslated regions (UTR) appears to be play a significant role [72]. The GS of the following gene is either separated from the GE of the downstream gene by a short, 4 to 5 nucleotide-long IR (NP/VP35; VP40/GP; VP24/L), a 144 nucleotide-long IR (VP30/VP24) or are partially overlapped (VP35/VP40; VP24/L) (Fig. 6, upper part). It was shown that the IR and their length were involved in the regulation of the reinitiation rates of the polymerase: Shortening, increasing or removing the IR lead to a specific decrease of the downstream gene. However, this effect seems to be gene-dependent, suggesting that other elements control gene transcription, including the length of the GE sequence and the UTR (Fig. 6, white boxes in genes). Indeed, compared to other NSS viruses, EBOV has relatively long 3’ and 5’ UTR that can potentially form secondary structures involved in mRNA stability [72]. It was shown that the 3’UTR and 5’UTR have antagonist roles: The 3’UTR downregulates the expression of the upstream gene, whereas the 5’UTR is necessary for the proper expression of the downstream gene [63]. Finally, it was shown that all of these regulatory mechanisms could also have an action on each other, creating an interplay that can further impact EBOV genomic regulation [67].

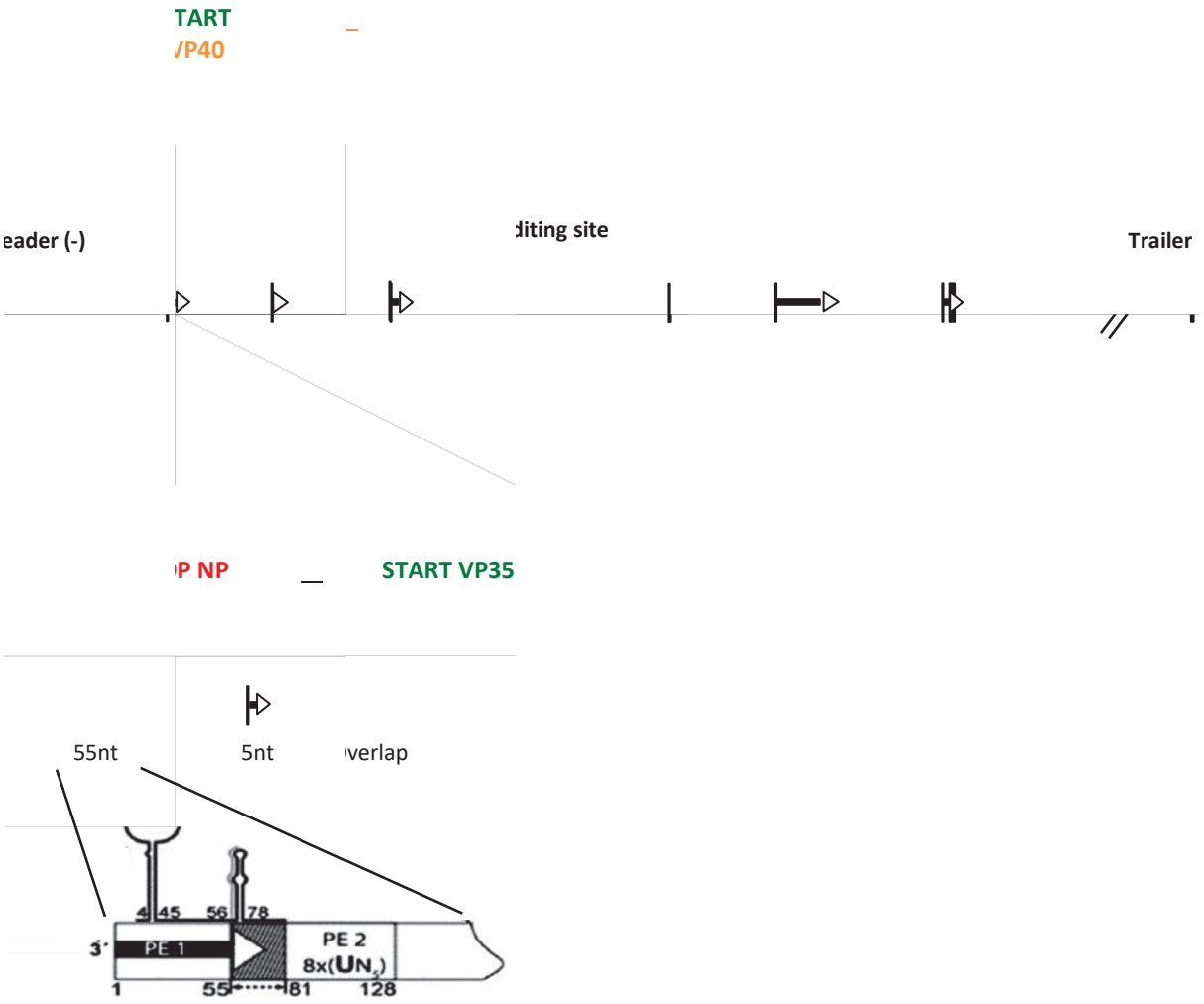

FIGURE 6. EBOV GENE BORDERS ORGANISATION AND LEADER STRUCTURE

Modified from [60]. Representation of the sequences and the structure of EBOV NP:VP35 and VP35:VP40 gene borde (upper part) and the organisation of the leader region (lower part). The leader is formed of a bipartite promot composed of the promotor elements PE1 and PE2 that are separated by a 26 nucleotides spacer. The predicted RI

VIRAL LIFE CYCLE AND NUCLEOCAPSID ASSEMBLY

Following infection, the viral genome is released inside of the cytoplasm of infected cells. Both antigenomes and viral mRNA are then produced in the cytoplasm, resulting in the translation of newly synthesised viral proteins. A hallmark of filovirus infection is the observation of inclusion bodies (IB) in infected cells. Such bodies can be defined as 'sites of viral transcription and genome replication that are readily apparent in cells by light microscopy' [73,74]. It has been shown that with the exception of the glycoprotein $GP_{1,2}$, all viral proteins colocalize within these cellular compartments, which are filled with nucleocapsid (NC)-like structures, indicating that IB are an important site for viral replication. Throughout infection IB grow larger and closer to the nucleus. Whilst transcription starts initially in the cytoplasm, viral transcription moves to the IB at late stages of the infection where the viral RNA is intensively replicated and encapsidated to form NC, close to the edge of the IB. NC are then transported to the cell

plasma membrane where the viral particles will bud, preferentially from filopodia-like structures (Fig. 7) [75,76].

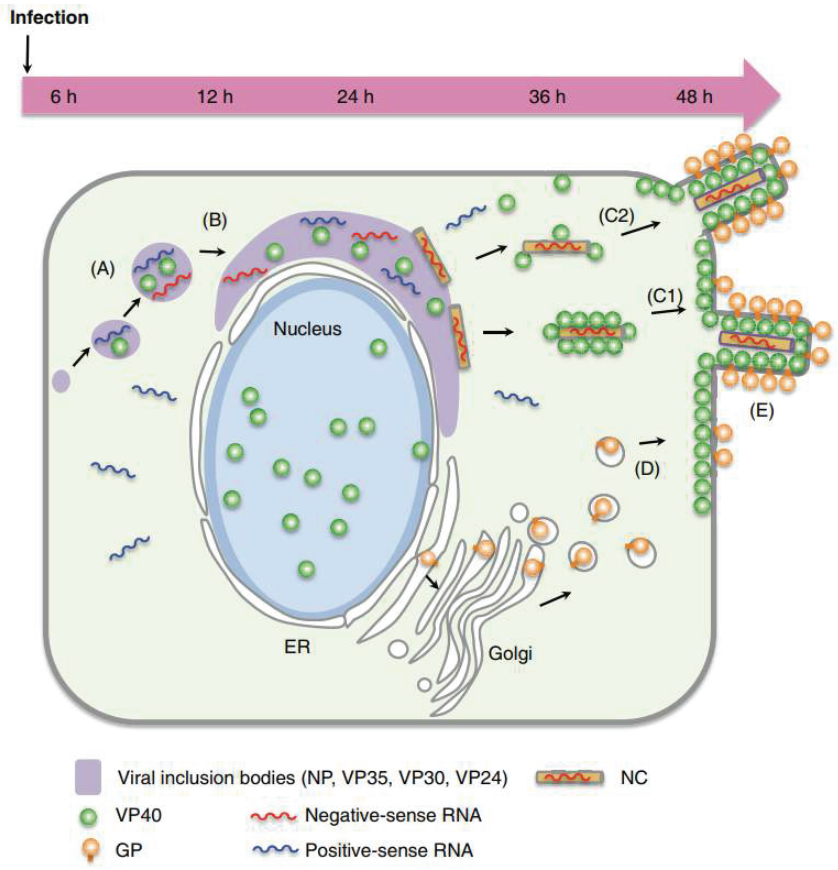

FIGURE 7. EBOV ASSEMBLY AND VIRAL RELEASE

Adapted from [72]. Viral transcription and antigenome formation (blue RNA) start in the cytoplasm. It is then rapidly transported to the inclusion bodies (A) where newly synthesised proteins will participate in the intense viral replication (red RNA) and transcription (blue RNA) (B). Over the course of the infection, the inclusion bodies are growing and nucleocapsid-like structure (NC) can be detected and are associating with VP40 to be transported to the plasma membrane (C1 and C2). EBOV glycoprotein is synthesised as a precursor in the endoplasmic reticulum (ER), which is then transported to the Golgi apparitus where it will be cleaved and proccesed into a mature form that will be inserted into the plasma membrane (D). The viral particles are budding preferentially from filopodia lipid rafts (E).

During the assembly process, the viral genome forms a 30 nm NC complex together with the nucleoprotein NP and viral proteins VP30, VP35, VP24 and L. NP, VP24 and VP35 are required for the assembly of the NC-like structure in IB, a process which is, however, not dependant on the presence of RNA [76,77]. VP24:VP35 bridges help to stabilize the NC formed of VP30:NP:RNA complexes [78]. The matrix protein VP40 forms a regular lattice which is associated with the inner layer of the plasma membrane (Fig. 8). VP40 drives the transport of the nucleocapsid to the membrane through a direct interaction with NP, as well as the budding of the virion. When released from cells, either horizontally or vertically, the surface of the viral host cell-derived membrane is decorated by the viral glycoprotein $GP_{1,2}$. Of note, $GP_{1,2}$ is not necessary for viral release, as virus-like particles (VLP) are efficiently released in the sole presence of VP40 [77].

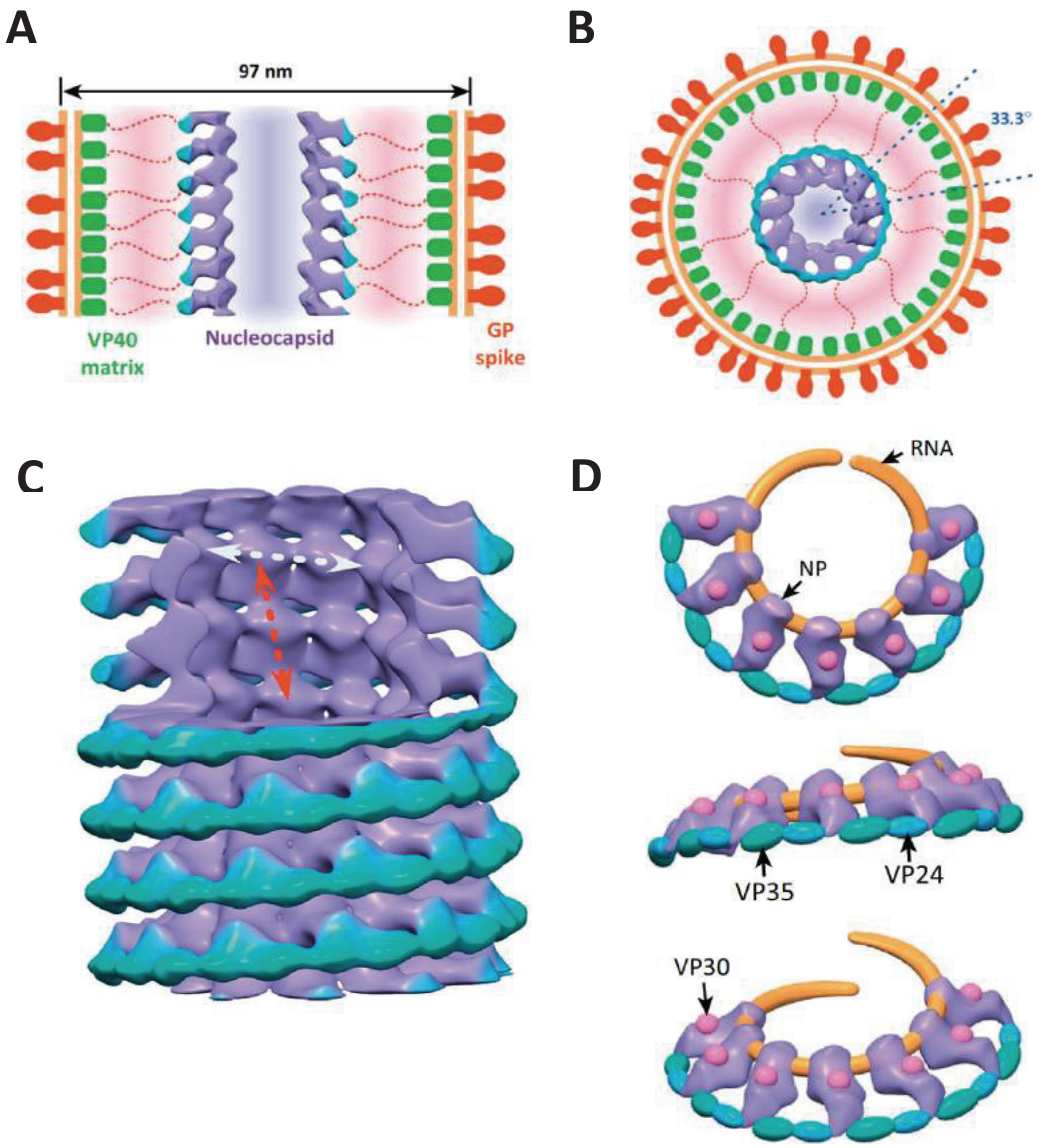

FIGURE 8. EBOV NUCLEOCAPSID STRUCTURE

Adapted from [55]. Schematic representation of a straight filovirus particle (A) and its cross-section (B). Interaction between the matrix protein VP40 and the nucleocapsid is showed by dashed lines. The host-derived membrane is colored in orange. 3D visualisation of EBOV nucleocapsid in a partial cutway view (C). The interactions between the viral RNA:NP, VP30:NP, VP35:VP24 and the potential positions for VP35:NP and VP24:NP contacts are shown (D). The white arrow shows NP:RNA interactions and the red arrow, protein:protein interactions.

NUCLEOPROTEIN

EBOV nucleoprotein is a 739-amino acid protein encoded by the first gene of the viral genome. It is a glycosylated and sialylated protein that possesses in its N-terminal domain (NTD) a self-oligomerization domain. While it is not clear what type of glycosylations are present in NP, it was identified that they are important for NP:VP35 interactions. Ectopic expression of NP induces the formation of IB-like bodies in which helicoidal tube structures can be detected. Co-expression of NP with VP35 and VP24, induces the formation of NC-like structures, a phenomenon dependant on NP NTD. It is suggested that the protein acts as a scaffold for the construction of NC-like structures that are essential for EBOV replication [79,80]. Recently, the NP crystal structure was resolved and a model for NP NC-like self-assembly was proposed [81,82]. These studies, highlight the importance of several regions, including the helices α21–α22 (amino acids 341 to 365 and 371 to 403 respectively) and a region called the VP35 NP Binding Peptide (VP35 NPBP), that controls NP:VP35 interaction. Helices α21-α22 were shown to regulate NP self-assembly, and while dispensable, they also favour NP binding to ssRNA, suggesting that NP binding to EBOV genome is dependent on oligomerization and NP molecule orientation. Furthermore, VP35 NTD and its binding to VP35 NPBP modulates NP oligomeric states and its association with viral RNA [83,84]. The recent models propose that NP has two distinct conformations: Opened and closed. When in contact with VP35, NP is forced into a closed conformation and cannot interact with the viral RNA. An unknown stimuli will displace the NP:VP35 interaction and NP will be able to oligomerize and to interact with the viral RNA and subsequently start RNA encapsidation. The NP:RNA structure is further condensed by possible direct interactions between the C-terminal domain (CTD) of NP with VP24, and by VP24:VP35 contacts (Fig. 9) [81,82].

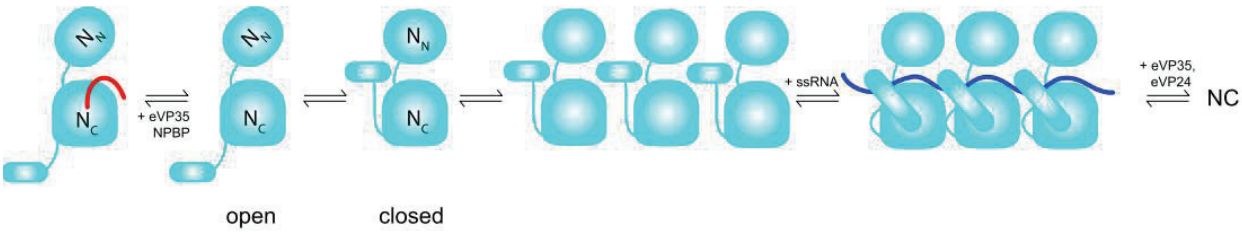

FIGURE 9. EBOV NP ASSEMBLY AND REGULATION DURING RNA SYNTHESIS

Obtained from [77]. Cartoon representation of the proposed model for NP:NP interactions and the role of VP35 in controlling NP oligomerisation state. When VP35 is bound to VP35 NP Binding Pocket (VP35 NPBP) it forces NP into an opened conformation. A displacement of NP:VP35 interactions leads to a shift of NP into a closed conformation that can then oligomerize and interact with the viral RNA.

The first line of defence against virus infections is the induction of the innate immune response, which is activated after recognition of a viral Pathogen Associated Molecular Pattern (vPAMP) by Pathogen Recognition Receptors (PRR). Each PRR are specialised in the recognition of specific vPAMP: ssRNA and dsRNA viruses can be either detected by endosomal-associated PRR (from the Toll-like Receptors, TLR family) or by a cytosolic receptor (from the RIG-I like Receptors, RLR family). Ultimately, PRR activation leads to the induction of an antiviral state, through the cooperation of two essential transcription factors, IRF-3 and NF-κB to stimulate the Type I Interferon system (IFN-α and IFN-ß) and the production of pro- and anti-inflammatory cytokines [85,86]. Early stages of fatal EVD are characterised by an important immunosuppressive state followed by an excessive and uncontrolled sustained activation of the inflammatory and the coagulation response, resembling what is observed with sepsis [87]. On the other side, survivors are able to rapidly activate an immune response directed against the virus and to control its replication [88]. Consequently, EBOV pathogenicity is partially dictated by its ability to block the host immune system during the first steps of the infection, notably in mononuclear phagocytic cells, which are the primary targets of the virus *in vivo* [89].

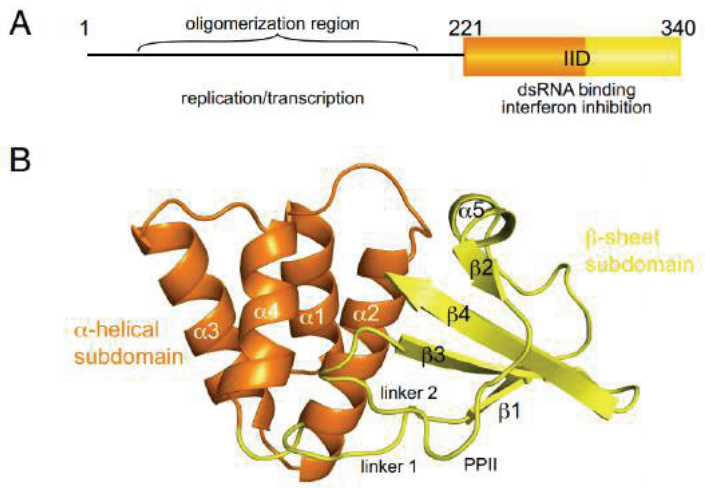

FIGURE 10. CRYSTAL STRUCTURE OF VP35 IFN-INHIBITORY DOMAIN

From [79]. VP35 organisation (A) and ribbon representation (B) of VP35 IFN-inhibitory domain (IID).

Besides its role in nucleocapsid formation and viral RNA synthesis, VP35 is a key virulence factor that is able to limit the activation of the innate immune system by interfering with the induction of the type I IFN system [80,90,91]. VP35 possesses in its CTD an IFN inhibitory domain (VP35 IID), with a dsRNA-binding activity that is necessary for blocking RIG-I activation and the nuclear translocation of IRF-3 (Fig. 10) [92]. VP35's ability to suppress RIG-I recognition of immunostimulatory viral RNA secondary or intermediate structures is essential for EBOV pathogenicity, as its activation was shown to render cells resistant to EBOV infection [93,94]. A reverse genetics approach and the generation of recombinant mice-adapted EBOV further demonstrated this with a single amino acid change in VP35 IID that renders the recombinant EBOV completely attenuated in mice. Studies performed on human Dendritic Cells (DC) demonstrated that VP35 inhibitory function participates in limiting DC maturation and cyto- and chemokine productions. Infected DC are then incapable to properly present EBOV antigens to CD8+ and CD4+ T cells and are thus cannot initiate the activation of an adaptive immune response specific to EBOV [95,96]. Crystallography studies revealed that the VP35 IID is formed of a set of three clusters of basic residues. The central basic patch was mapped to regulate dsRNA binding. Furthermore, VP35 IID RNA binding activity has been shown to be independent of VP35 viral polymerase cofactor function [97]. Indeed, to participate in viral RNA synthesis, VP35 is required to directly interact with NP and the viral polymerase. Single point mutations in the first patch of basic residues are sufficient to destabilise VP35:NP interactions but not VP35:L interactions, leading VP35 to lose its cofactor activity [98].

VP40 is the major matrix protein and a 326-amino acid protein with a molecular weight of 40kDa involved in the regulation of viral transcription and viral budding [99]. VP40 possesses two domains, a NTD and a CTD connected by a flexible linker, that control its functions as well as its different oligomerization states. In infected cells, VP40 is majoritarly present as a dimer. It was shown that VP40 dimers through their CTD were able to interact with phosphatidylserine (PS) allowing its association with the plasma membrane inner-leaflet [100,101]. Following binding to PS, the dimers reorganise to form hexamers [102–104]. Furthermore, VP40 was shown to be associated with PS in lipid rafts localised in filopodia-like projections. The fact that VP40 is alone able to form and release virus-like particles (VLP), highlights his central role for viral budding [105]. A hydrophobic loop region is present in the CTD that drives VP40 insertion into the plasma membrane, controlling its localisation to the plasma membrane as well as for its hexamerization, plasma membrane remodelling and consequently virus egress [106,107]. While, the CTD controls binding to the plasma membrane, VP40 NTD is necessary for VP40 dimerization. VP40 dimers have a butterfly-shaped like structure, with a 'body' formed of the interface of the NTD of two VP40 molecules, and the CTD that will form the wings and expose its membrane binding and penetrating domains. Bornholdt ZA *et al.* (2013) propose the following model to explain VP40 interaction with the plasma membrane and how it controls viral budding: The CTD domains of a VP40 dimer interact first with the plasma membrane and its lipids. This will lead to a conformational change of VP40 homodimers into antiparallel zigzagging hexamers. According to their data, only VP40 dimers can bind the plasma membrane as monomers have too weak an affinity for such a purpose. They suggest that VP40 possess 'sticky' ends that allow the formation of the EBOV matrix into long filaments of VP40 hexamers and eventually forcing the curvature of the plasma membrane and the release of virions (Fig. 11) [101,107].

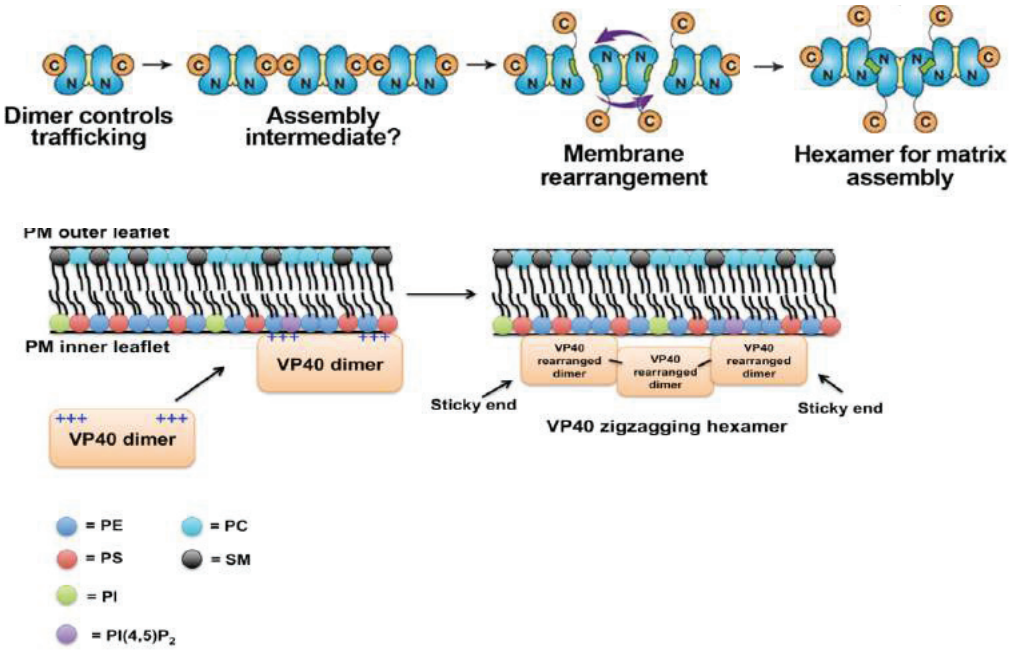

FIGURE 11. VP40 OLIGOMERISATION AND INTERACTION WITH THE CELLULAR PLSAMA MEMBRANE

Adapted from [96] and [102]. Cartoon representing VP40 monomers interacting through their N-terminal domain interfaces (N) to form VP40 dimers (upper part). VP40 dimers interaction with phosphatidylserine (PS) lead to a conformational change and their rearrangement into zigazagging hexamers that assemble into a filamentous structure to form the virion matrix (lower part).

Several studies revealed the mechanism involved in VP40 transport to the cell membrane. It was shown that two N-terminal domains called 'Late domain' motifs, formed of tetra-peptide motifs (PTAP and PPEY), were involved and necessary for hijacking the Endosomal Sorting Complex Required for Transport (ESCRT) pathway, which is required for EBOV budding by facilitating the virion scission from the plasma membrane. Indeed, through its Late domains VP40 interacts with Nedd4 and WWP1, two ubiquitin ligases that will ubiquitinate VP40 allowing it to interact with Tgs101, a necessary host factor that is recruited by VP40 into lipid rafts and that greatly participates in VP40 mediated viral budding [105,108–110]. Another key cellular factor for EBOV release is the Sec24c protein, which is part of the Coat Protein Complex II (COPII) transport system. The COPII transport system is involved in the initial steps of the ER-Golgi transport and uses microtubules for transporting vesicles. Accordingly, upon infection VP40 initially interacts with the COPII transport system through Sec34c to initiate its transport in a microtubule-dependant manner to the plasma membrane. It will then dissociate from the COPII transport system to interact with proteins from the ESCRT pathway to induce budding [111]. Although VP40 is not necessary for EBOV nucleocapsid transport, it is required to address it to filopodia, the preferred site of EBOV budding [112].

In addition to control viral egress, VP40 was shown to be able to form large aggregates, which have an octameric ring structure, formed by four antiparallel homodimers of VP40 NTD (Fig. 12). This octameric form is arranged following a conformational change of the VP40 dimer interface, resulting in the exposure of an RNA binding pocket located in VP40 NTD. Importantly, it was shown that RNA binding is essential for the formation and stabilization of the octameric rings [107,113]. The roles of this form are not fully elucidated and the nature of the bound RNA has yet to be found. It appears to have no role in viral budding but instead seems to be important for viral transcription [114]. Indeed, it was demonstrated that the Arginine in position 134 is essential for VP40 RNA binding and as such for octamer formation. No virus could be rescued by reverse genetics when introducing a mutation at this position, proving the importance of this form in the EBOV life cycle. Additional studies showed that the VP40 ring structure is able to negatively regulate viral transcription. Similarly to other NNS viruses, it was suggested that the octameric rings are involved in viral RNP compaction and thus overexpression of this form blocks the access of the polymerase to the genome, rendering it inactive for replication or transcription [107,115].

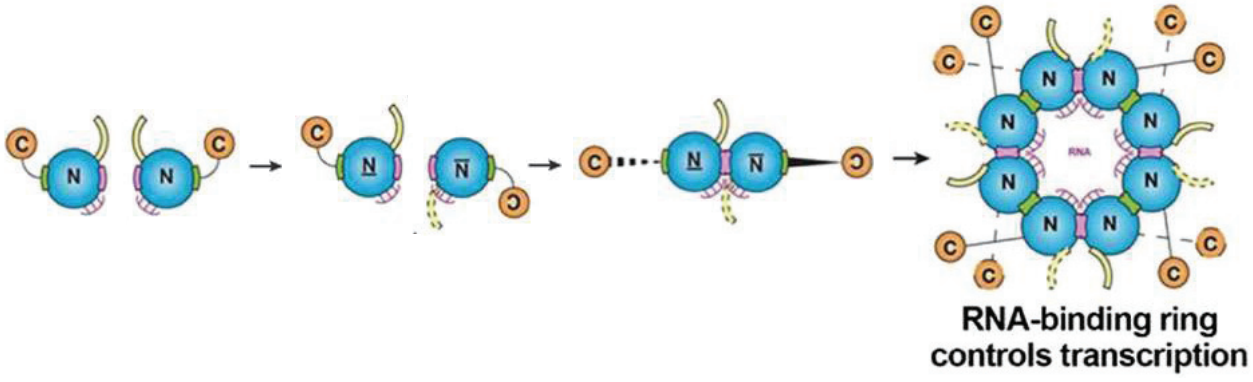

FIGURE 12. VP40 OCTAMERIC RING FORMATION

Adapted from [102]. Following binding to an unknown RNA to VP40, VP40 monomers assemble into dimers through their N-terminal domains to form in the cell cytoplasm an octameric ring. This structure was shown to be able to regulate viral transcription.

TRANSCRIPTIONAL EDITING

EBOV glycoprotein $GP_{1,2}$ has been actively studied for its different roles in EBOV pathogenicity. EBOV GP gene is the only viral gene that encodes several products following transcriptional editing [58]. The pre-soluble GP (Pre-sGP) mRNA, that ultimately leads to production of the soluble, released form of the viral glycoprotein and known as sGP, is the main product of the unedited GP mRNA and is produced similarly to the other viral gene following the recognition by the polymerase of the conserved GS and GE sequences and its subsequent polyadenylation. While it is cell type dependant, it is admitted that this transcript represents about 75% of the GP associated mRNA transcribed in infected cells in cell culture. EBOV full-length $GP_{1,2}$ is only produced following a frameshift mutation in the GP ORF due to co-transcriptional editing, which occurs when the polymerase adds an additional single adenine at the editing site; the mRNA produced is commonly called 8A and represents about 20% of the GP mRNA produced in infected cells [70]. In around 5% of the cases, a 9A mRNA is transcribed and encodes for an additional non-structural secreted GP called super small GP (ssGP) of currently unknown functions (and will therefore not be discussed here) [116]. Due to their transcription strategy, all EBOV glycoproteins have a conserved NTD and differ only by their CTD (Fig. 13).

The editing site is composed of a stretch of seven uridine residues in the viral genome and is resembling EBOV GE sequences (Fig. 13A). Consequently, it is believed that the mechanism allowing transcriptional editing is similar to the stuttering process that leads to viral mRNA polyadenylation (Fig 13B). A similar sequence is present also in EBOV L gene, however, no editing is observed, suggesting that the editing to be GP-specific. Furthermore, whilst viral polymerases from other viruses were shown to be able to successfully edit the GP gene and to produce an 8A mRNA in *in vitro* systems, it appears that during EBOV infection, VP30 is necessary to resolve a stem-loop structure present before the editing sequence and helps to edit GP mRNA (Fig 13B) [117–119].

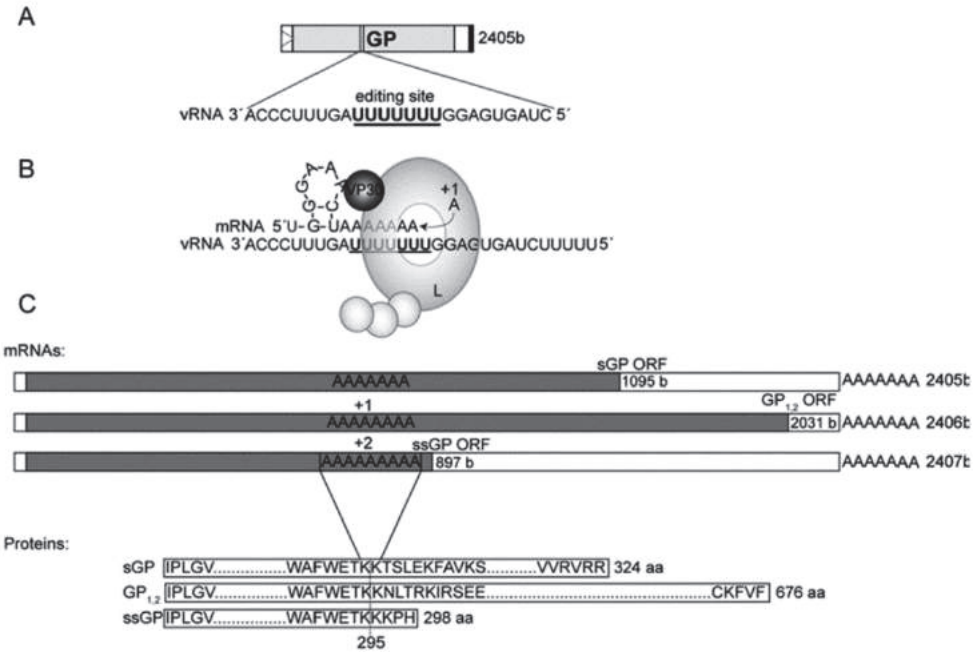

FIGURE 13. GP TRANSCRIPTIONAL EDITING

Obtained from [60]. Representation of the GP gene as shown in Fig. 6 and of its editing site (A). The model proposed to explain GP editing is represented in (B). In this model, the polymerase is scanning and transcribing the viral RNA (vRNA) into a mRNA. VP30 helps to resolve a secondary structure created during transcription. Editing leads to the production of different mRNA and proteins (C).

SOLUBLE GP

The viral protein sGP is first synthesized as a precursor, Pre-sGP, in the endoplasmic reticulum (ER) and is then transported to the Golgi apparatus where it will acquire glycosylations and its mature form following cleavage by the cellular proprotein convertase Furin (Fig. 14) [120]. Of note, and as shown in Fig. 14, Furin cleavage of Pre-sGP also liberates the Pre-sGP CTD part of the protein, producing a short peptide known as the viral Δ-peptide (see below). sGP lacks a transmembrane domain and is secreted as a disulfide bond-linked dimer during EBOV infection through the classical secretory pathway. sGP is believed to play a key role in antibody subversions by attracting antibodies directed against the full-length $GP_{1,2}$ protein to prevent viral neutralisation [121]. It appears to also have an anti-inflammatory action by limiting the activation of macrophages and endothelial cells. Importantly, being the main product of the GP gene, sGP expression has been shown to play a role in controlling the cytotoxicity of the unique EBOV surface virion glycoprotein (discussed further below) [122–124]. In cell culture, sGP is not necessary and indeed it has been shown that in this system, the EBOV wild-type 7U genome is rapidly edited through genomic insertion of an uridine residue at the editing site (8U genome) to encode almost exclusively for the full-length $GP_{1,2}$ (although some sGP is still produced either by deletion or skipping of an adenine residue) [125]. On the other side, infection of guinea-pigs with a guinea-pig adapted virus with an altered editing site (8U genome), rapidly converts to its original 7U genotype. Similarly, infection of guinea pigs with an EBOV virus with no editing site, but that is still able to encode for EBOV glycoprotein shows a significant reduction in virus pathogenicity [126]. The importance for sGP in EBOV pathogenicity was also highlighted during the recent EBOV outbreak, as a systemic analysis of EBOV mRNA produced in infected humans showed that the 8A mRNA transcript only represented around 1% of the GP mRNA produced [127].

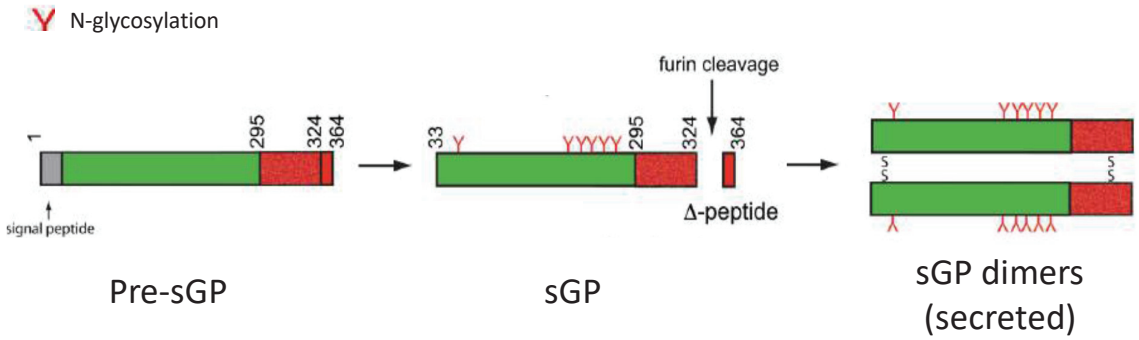

FIGURE 14. SOLUBLE GP STRUCTURE AND SYNTHESIS

Obtained and adapted from [367]. The soluble GP (sGP) is first synthesised in the endoplasmic reticulum as a 364 amino acids precursor, Pre-sGP. Pre-sGP is glycosylated and transported to the Golgi where it will acquire complex glycans and be processed by the proprotease Furin into the mature sGP and Δ-peptide. Following cleavage, sGP monomers form parallel dimers and due to a lack of transmembrane domain, they are released into the cell extracellular domain.

Δ-PEPTIDE

Little is known about the role of the Δ-peptide, it represents the 40 last amino acids of the CTD of sGP and as mentioned above is liberated following Pre-sGP intracellular processing. It was shown to be a O-glycosylated and silylated peptide which is secreted and that is able to bind non-infected cells and to block EBOV entry (Fig. 15) [128,129]. Recently, the Δ-peptide was shown to be able to bind to cells and induce their permeabilization at micromolar concentrations, establishing the Δ-peptide as a viroporin [130]. Considering the large amount of sGP (in micromolar amounts) released into the patient sera [131], the authors suggest that EBOV Δ-peptide is also actively secreted during EBOV infection and that through its local binding to cells and its viroporin activity could act similarly to an enterotoxin and participate in the severe gastrointestinal disorders observed during the EVD.

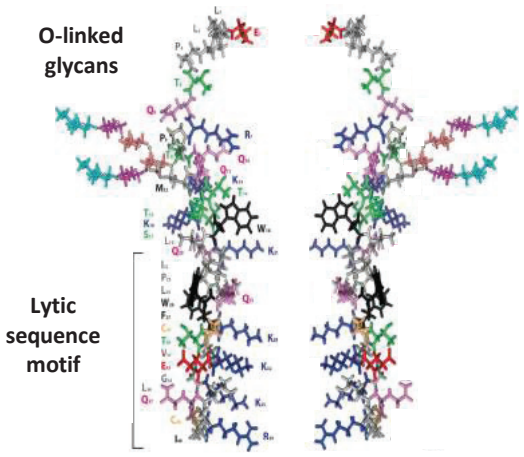

FIGURE 15. Δ-PEPTIDE STRUCTURE

Adapted from [125]. During Pre-sGP processing by Furin, the Δ-peptide, that represents the 40 last amino acids of Pre-sGP C-terminal domain is liberated. In the golgi, it will acquire O-glycosylations and will be silylated before being released into the sera as a dimer. The lytic sequence motif responsible for its viroporine activity is shown.

FULL-LENGTH $GP_{1,2}$

The full-length $GP_{1,2}$ is a highly glycosylated type I protein produced in the ER as a precursor called Pre-GP_{ER}, where it acquires immature oligomannosidic N-glycans. The 110 kDa glycoprotein Pre-GP_{ER} is then transported to the Golgi apparatus to obtain mature N-glycosylations and O-glycosylations and represents the second precursor, the 160 kDa pre-GP. Pre-GP is cleaved into a 140 kDa GP_1 and a 26 kDa GP_2 subunit by the cellular enzyme Furin. The two subunits are linked by a disulfide bond between the cysteine 56 of GP_1 and the cysteine 609 of GP_2 and form a trimer, dictated by the presence of a N-heptade repeat domain in GP_2. The $GP_{1,2}$ trimer is inserted into the virion host-derived membrane through the GP_2 transmembrane domain [58,120,124,132,133]. The currently available resolved structures of $GP_{1,2}$ reveal that the protein resembles a chalice with GP_1 forming the cup and GP_2 its base (Fig. 16).

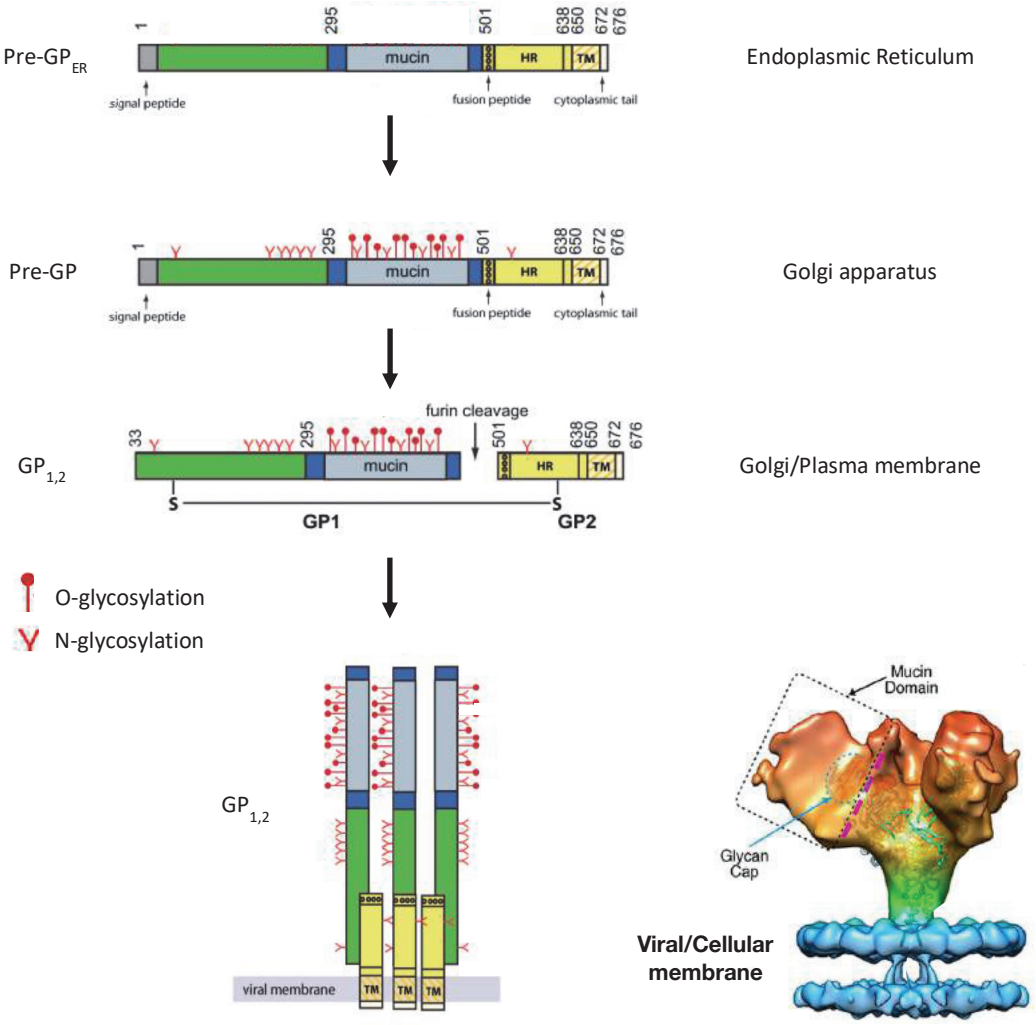

FIGURE 16. EBOV GLYCOPROTEIN $GP_{1,2}$

Adapted from [367,368]. EBOV glycoprotein $GP_{1,2}$ is synthesised first in the endoplasmic reticulum as a precursor protein called Pre-GP_{ER}, where it will acquire immature glycosylations. Pre-GP_{ER} is then transported to the Golgi apparatus to be further processed. In the Golgi, the golgi-specific precursor Pre-GP is cleaved by the proprotein Furin into two subunits GP_1 and GP_2, linked by a disulfide bond. Of note, Pre-GP, acquires before cleavage mature N- and O-glycosylations, which are mostly present in the glycan cap and the mucin-like domain. The 3D structure of the trimer inserted into the host-derived viral membrane with the position of the Glycan cap (blue arrow) and the Mucin-like domain (dashed box) and the supposed position of the receptor binding domain (purple dashed line) is shown (lower left),

GP_1 possesses four distinct domains: base, receptor binding domain (RBD), Glycan cap, and the mucin-like domain (MLD). The glycan cap and the MLD contain the majority of N- and O-linked glycans. Structural analysis revealed that the RBD is hidden by the glycan cap, which has solely N-glycosylations, protecting the RBD from different immune pressures. The MLD is a serine-threonine-rich region and the most variable domain between ebolavirus species. It is also the most glycosylated domain of GP_1 with N- and O-glycosylations that contributes to half of the protein molecular weight. Whilst the MLD is not necessary for EBOV infectivity, several groups reported that the MLD is involved in EBOV $GP_{1,2}$ high cytotoxicity and immune cell activation [131,134–137]. Furthermore, it was suggested that the MLD creates a glycan shield that protects EBOV $GP_{1,2}$, and notably its RBD from neutralising antibodies. Antibodies directed against the MLD are rarely neutralising against this domain. Indeed, as both the MLD and the glycan cap are removed during EBOV entry by intracellular cathepsin in endosomes (to allow the interaction between the RBD and its intracellular receptor, the cholesterol transporter NPC1), these domains are not thought to be actively involved in viral entry and as such unlikely targets for antibodies able to block the viral entry process [31,138,139]. In addition, EBOV $GP_{1,2}$ shielding was shown to hide cell surface proteins, such as T-cell receptors or the Major Histocompatibility Complex-I, rendering infected cells less susceptible to recognition by T and NK cells [140]. Besides their protective roles, EBOV GP_1 glycosylations are important for their interaction with C-type lectins such as DC-SiGN, L-SIGN or LSECtin that acts as attachment receptors and mediate EBOV attachment and entry into cells [141,142]. While GP_1 drives viral attachment and cellular tropism, GP_2 governs viral entry by mediating viral membrane fusion in endosomes [143]. GP_2 contains two N-glycosylations, which are important for EBOV $GP_{1,2}$ immunogenicity as well as for its proper conformation and expression [141]. GP_2 possesses several identified domains: its transmembrane domain (TM) that retains the glycoprotein in the cells and the virion, a membrane proximal external region (MPER), a C and N-heptad repeat region (CHR and NHR) and the internal fusion-loop (IFL) domain [132,144]. Interestingly, all five GP_2 domains appear to participate in EBOV $GP_{1,2}$ fusion.

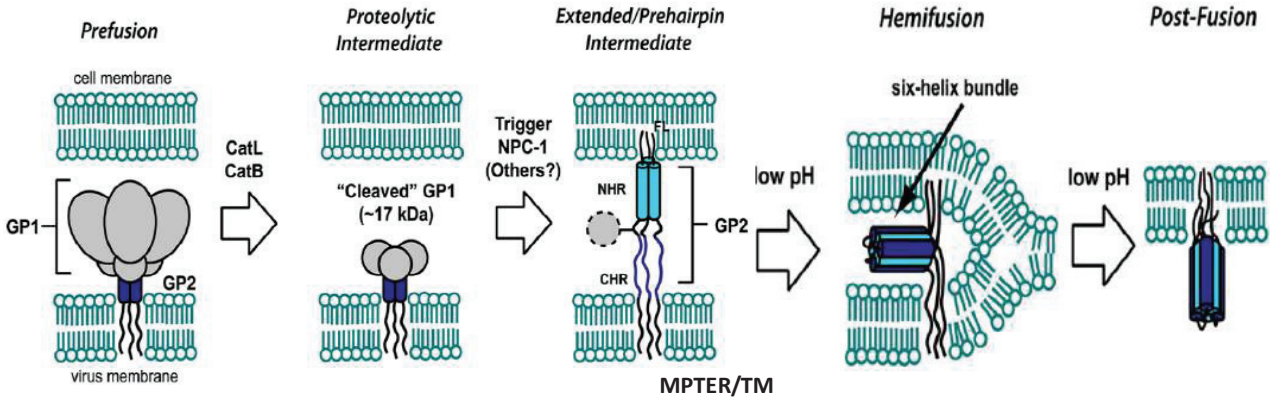

FIGURE 17. GP MEDIATED FUSION MODEL

Modified from [145]. In its prefusion conformation, the viral glycoprotein is inserted in the virion membrane through its transmembrane domain (TM). Following cellular uptake and internalisation in the late endosomes/lysosomes, the glycan cap and the mucin-like domain of EBOV GP_1 are cleaved off by the cellular proteases, Cathepsin L and B, resulting in a 17 kDa protein called Cleaved GP_1 (GPcl). Its subsequent interaction with the endosomal receptor NPC1 and the exposure of the protein to the endosomes/lysosomes acidic pH, lead the viral glycoprotein to change into a hemifusion conformation, which will be able to initiate membrane fusion through the exposure of GP_2 Internal Fusion Loop (FL) that will be inserted into the endosome membrane. Fusion occurs when the N- and C-heptad repeat regions (NHR and CHR) fold back to form a six-helix bundle structure that participates to bring the viral and cellular membrane in close proximity to allow fusion.

Following EBOV uptakes by macropinocytosis, the virion ends up inside of late endosomes/lysosomes where the glycoprotein will be cleaved by cellular proteases, notably Cathepsin L and B [145,146]. This result in the removal of the glycan cap and the MLD and the formation of a primed 19 kDa GP_1:GP_2 protein called GP cleaved (GPcl) that is ready for fusion and necessary for EBOV infection [147]. The exposure of $GP_{1,2}$ to the acid pH of the late endosomes, its processing into GPcl that is subsequently capable to bind to NPC1-C domain lead to conformational changes in GPcl and the exposure of the GP_2 IFL that triggers membrane fusion [148]. In GP_2 IFL contains hydrophobic residues located at the tip of the FL that are inserted into the host membrane. At this point the CHR folds back onto the NHR to form a six-helix bundle that brings the viral and the cellular membrane close enough to allow fusion, which is possible following the interaction between the IFL and the MPER/TM domain (Fig. 17) [132].

SHED GP

In addition to the transcriptional editing of GP, another strategy is used by the virus to increase its panel of glycoproteins and to control $GP_{1,2}$ cytotoxicity. During EBOV infection, EBOV $GP_{1,2}$ is shed from the cellular membrane and released as a soluble form in the blood of infected patients and experimentally infected animals, as a truncated polymer, termed $GP_{1,2\Delta}$ or shed GP. The cellular metalloprotease TACE (TNFα-converting enzyme) a member of the ADAM family (a disintegrin and metalloproteinase), also known as ADAM17, has been identified as being responsible for $GP_{1,2}$ shedding (Fig. 18) [149]. It was shown that shed GP is able to block virus-neutralizing antibodies against surface GP and to participate in the immune response dysregulations observed during EBOV infection by binding macrophages, DC and endothelial cells that, in response, will release inflammatory cytokines, as well as by disrupting the endothelial barrier either by a direct action of $GP_{1,2\Delta}$ or indirectly through the effects of pro-inflammatory cytokines [131].

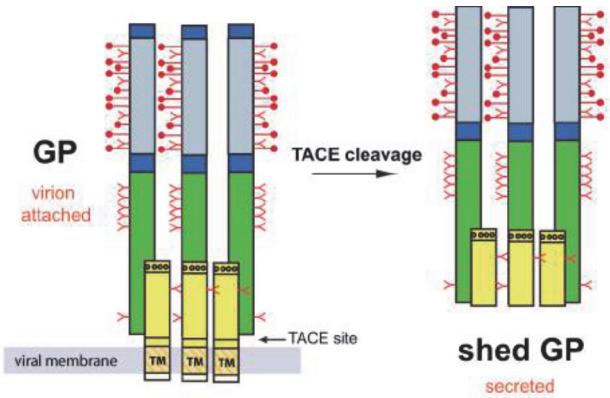

FIGURE 18. EBOV $GP_{1,2\Delta}$ STRUCTURE

Obtained from [367]. When present at the plasma membrane, the viral glycoprotein $GP_{1,2}$ can be shed from the membrane by the cellular enzyme TACE/ADAM17 (TNF-α Converting Enzyme/A Disintegrin And Metalloproteinase 17) and released into the extracellular domain as a truncated trimeric protein.

INSIGHTS INTO ADAM17 SHEDDING MECHANISM

The enzyme or “sheddase” ADAM17 regulates numerous key physiological processes by releasing membrane-anchored cellular factors through a proteolytic cleavage of its substrate membrane proximal domains. ADAM17 was shown to control TNF-α release and is therefore involved in the early steps of innate immune activation. Since its discovery in 1997, several other cyto- and chemokines (MCP-1, CX3CL-1, RANKL…), as well as multiple growth factors (M-CSF, EGF) and adhesion molecules (L-selectin, ICAM-1, VCAM-1), were shown to be shed by ADAM17 [150,151]. Cleaved molecules can then either interact with receptors on the same or neighbourhood cells, or from the same tissue and can even enter the bloodstream. This sheddase can also downregulate cellular pathways by cleavage of its substrate receptors, as was shown for TNF-α or M-CSF, to avoid their sustained activation [152]. Of note, ADAM17 over-expression and unregulated activation have been linked to several pathologies, including chronic inflammatory diseases and cancer. To avoid such a scenario, ADAM17 activity is tightly regulated by several posttranslational mechanisms (Fig. 19). First, it is synthesised as a 110 kDa proprotein in the ER, where it associates with iRhom proteins that promote its transport to the Golgi apparatus. Furin cleaves off its inhibitor pro-domain inside of the Golgi. ADAM17 is then addressed to the secretory pathway in an ERK-dependant manner in order to reach the plasma membrane. During this process, ADAM17 is packaged into lipid rafts to sequestrate it away from its substrate that are majoritarily present outside of this membrane microdomain. At the plasma membrane, mature ADAM17 associates with TIMP3 to force its dimerisation and prevent its activity. Its phosphorylation by kinases from the MAPK or p38 ERK pathways release ADAM17 dimers from TIMP3 that will then dissociate into active monomers that can recognise and cleave its ectodomain targets [153]. It has been shown that ADAM17 is active only in lipid rafts as its interaction with phosphatidylserines helps ADAM17 to be brought closer to the membrane proximal domain of its targets leading to their ectodomain cleavage [154,155].

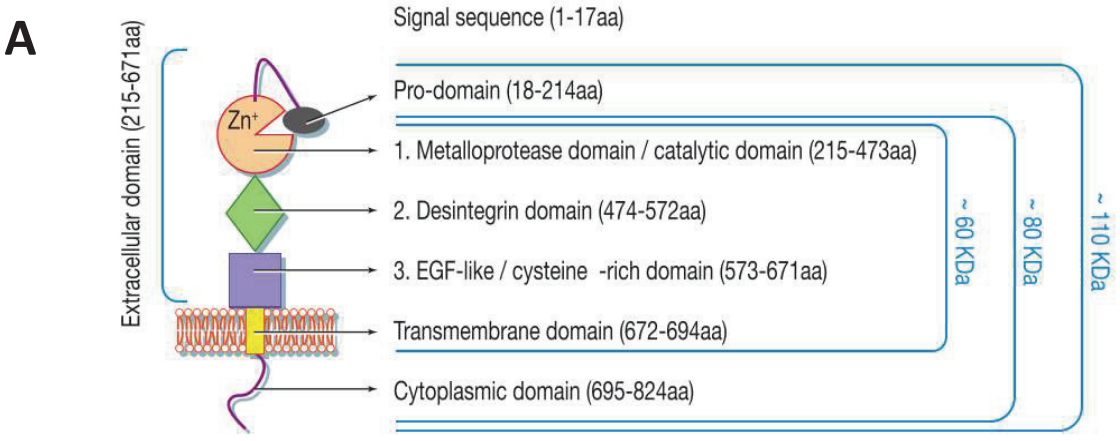

B

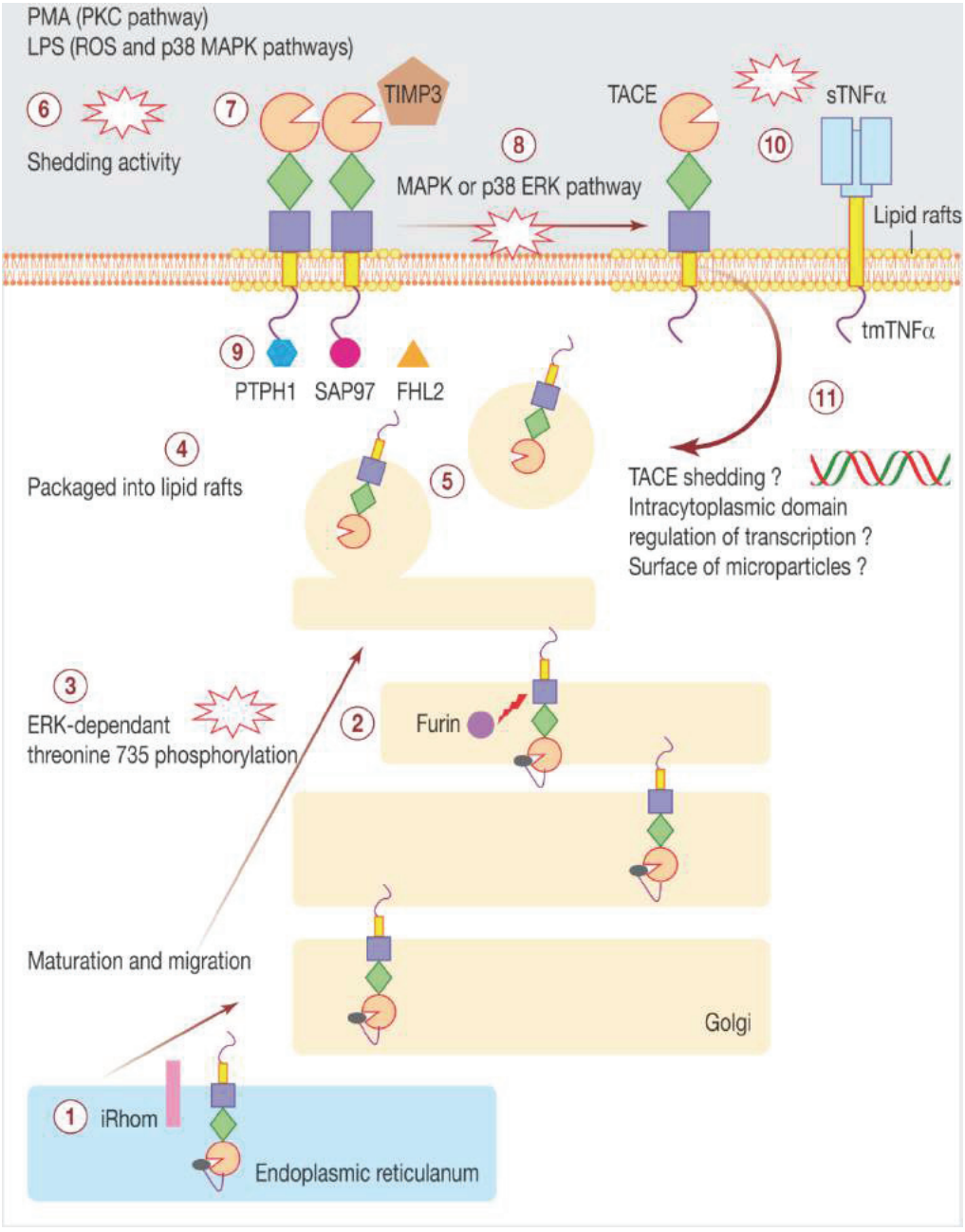

FIGURE 19. ADAM17 POST-TRANSLATION REGULATION

Structure and domains of ADAM17 (A). After synthesis, ADAM17 is stocked in the Endoplasmic reticulum (ER). Following binding to iRhom proteins, it leaves the ER for the Golgi apparatus where it will be maturated (1). ADAM17 regulator pro-domain is cleaved by the proprotease Furin in the Golgi (2). It will then be addressed to the secretory pathway in an ERK-dependant manner (3). During its transport to the plasma membrane, it is packaged into lipid rafts (4) and transported to the plasma membrane. At the plasma membrane, ADAM17 is present as a dimer that binds its inhibitor TIMP3 (7).

VP30

The EBOV VP30 gene encodes for a multifunctional phosphoprotein that acts as a transcription factor and that is part of the nucleocapsid [91]. It was shown that the 288-amino acid protein is phosphorylated on two different clusters of three serines located in its NTD (Position 29 to 31 and 42 to 46). Phosphorylations of VP30 control its interaction with NP as well as its ability to transcribe the EBOV genome. Indeed, when VP30 is phosphorylated, it associates in NP-induced IB and is not able to sustain viral transcription, while a fully phosphorylated VP30 loses its ability to locate inside IB but can activate the production of viral mRNA [156]. A follow-up study revealed that the serine at position 29 is majoritarily responsible for sustaining EBOV transcription. In the current proposed model, VP30 needs to be phosphorylated by an unknown kinase to ensure its transport to the site of EBOV transcription by interacting with NP through its CTD, where it will be dephosphorylated by the phosphatases PP1 and PP2A. Its dephosphorylation in the IB will release VP30 from NP that will then interact with VP35 to form an active transcription complex. At some point, VP30 is phosphorylated again to insure its incorporation into the virion and ensure initiation of viral transcription at the beginning of the infection (Fig. 20) [157,158]. VP30 is able to form homodimers that bind a secondary stem-loop structure present in EBOV leader in a zinc-dependant manner. Moreover, binding to the RNA is essential for the dephosphorylated VP30 to interact with VP35 and initiate transcription. It was suggested that VP30 stabilizes the viral polymerase and VP35 interactions and increases the affinity of the complex to the viral genome to ensure its transcription [159]. In accordance, dephosphorylated VP30 allows the transcription reinitiation of the EBOV genome, suggesting that VP30 helps to resolve secondary structures present in the 5'UTR of EBOV genes [160]. While it was thought that VP30 is not necessary for viral replication, several recent studies proposed that VP30 could participate in genome, antigenome and mRNA synthesis. Indeed, blocking the binding of VP30 to NP NTD greatly reduced the amount of all viral RNA species. As such, it was postulated that VP30, when it is bound with high affinity to NP, could stabilize the NC and restrain the accessibility of the genome for the viral polymerase. However, those recent results were obtained using minireplicon systems and were not yet validated by reverse genetics and as such, certain differences may be observed compared to what was previously shown for these interactions [160–162].

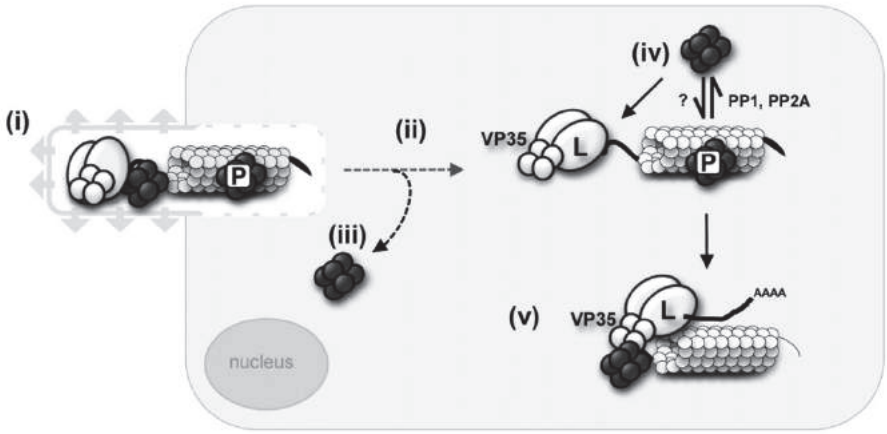

FIGURE 20. ROLE OF VP30 IN VIRAL TRANSCRIPTION

Adapted from [149]. In the virion, VP30 is present in phosphorylated and dephosphorylated forms that interact with NP and VP35, respectively (i). In the cytoplasm of infected cells, the phosphorylated VP30 is transported with the nucleocapsid into the inclusion bodies (ii), while the dephosphorylated form will stay in the cytoplasm (iii). In inclusion bodies VP30 will be dephosphorylated by the phosphatase PP1 and PP2A to be released from its interaction with NP resulting in its interaction with VP35 and the formation of an active transcription complex, alongside the polymerase L (iv), to allow viral transcription (v).

VP24

Initial biochemical studies of EBOV VP24 showed that, similarly to VP40, the protein is able to associate to the plasma membrane and is localised in the perinuclear region and to form homo-oligomers. It was consequently initially suggested that VP24 is a second but minor matrix protein [163]. Since then, several roles were described for VP24. Although it is not necessary for VLP budding, it was shown that alongside NP and VP35, VP24 NTD and CTD domains are necessary for proper NC formation and transport. Silencing of VP24 in EBOV infected cells further confirmed those results [80,112,164–166]. Moreover, as VP24 is able to negatively regulate both EBOV viral replication and transcription it was proposed that VP24 participates in the NC condensation and can seal it to ensure its transport. Indeed, VP24 mutants that no longer have the ability to bind NP showed NC formation and packaging defects that were linked to VP24 NP-dependant NC condensation activity [167]. During adaptation to a new host, EBOV acquires mutations in VP24 that have been shown to be necessary for adaptation. Indeed, in addition to its role in viral production, VP24 is an important viral pathogenicity factor and cooperates with EBOV VP35 to inhibit interferon signalling to prevent immune cell activation [96,169]. Following recognition of a pathogen, cells will release IFN-α/ß and IFN-γ molecules that will bind IFNAR and IFNGR receptors, respectively, of neighbouring cells. This will lead to the activation of the JAK-STAT pathway and the nuclear translocation of the phosphorylated transcription factors STAT1 and STAT2 leading to the induction of a cellular antiviral state (Fig. 21). VP24 binding to the nuclear transporters Karyopherin-α (KPNA1, 5 and 6) involved in STAT1 and STAT2 nuclear shuttling abolishes the induction of the IFN signalling. Differences in the ability of VP24 to block the IFN signalling and differences in affinity for the different KPNA family members was demonstrated to exist between different species of EBOV and was suggested to participate in the differences between the different EBOV species pathogenicity [170].

In addition, wild-type VP24 has been shown to produce large aggregates in guinea pig macrophages compared VP24 from a guinea pig-adapted strain, a phenomenon which could be potentially attributed to impaired functions of VP24 and an inability of the viral protein to properly interact with NP and therefore to correctly condense the viral NC [168,171].

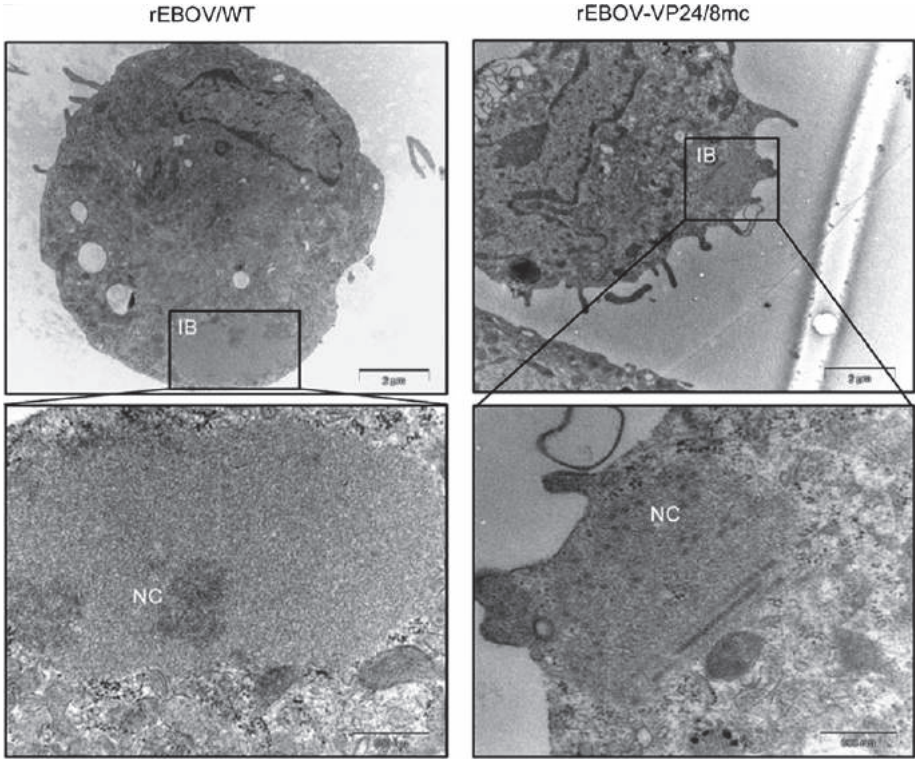

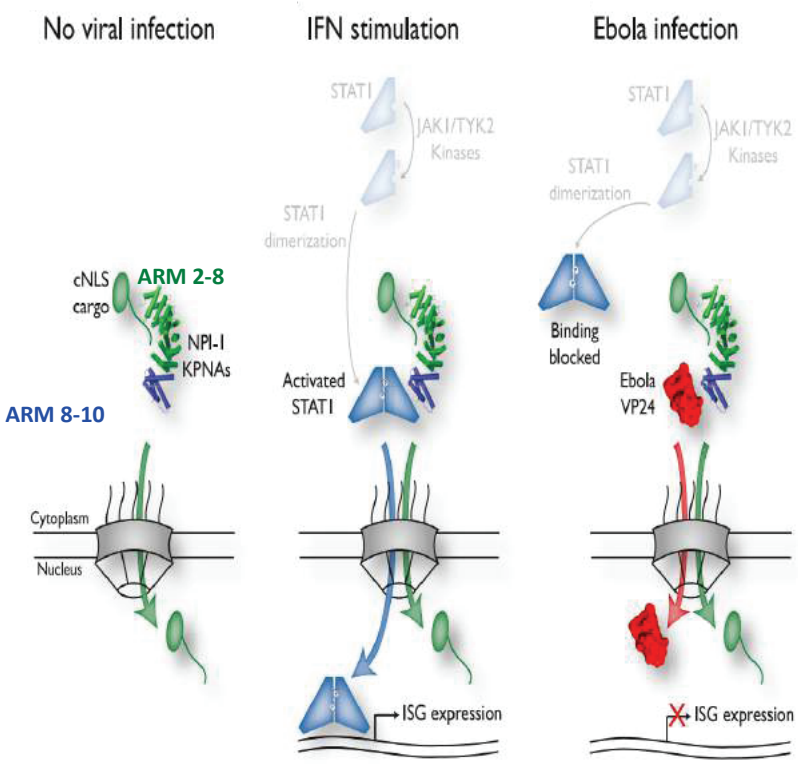

FIGURE 21. VP24-DEPENDANT NUCLEOCAPSID FORMATION AND INTERFERON ANTAGONISM

Obtained from [171, 369]. Upper panel: Guinea-pig macrophages infected with non-adapted rEBOV virus (rEBOV/WT) fails to produce typical NCs as observed with the adapted guinea-pig virus (rEBOV/VP24-8mc). Lower part: In the absence of viral infection (A), proteins adressed to the nucleus possess a classical nuclear localisation signal (cNLS) that afording their binding to armadillo repeats 2-8 (ARM 2-8, green) localised in nuclear transporter proteins of the KPNA family, such as NPI-I. During an infection (B), the production of interferon molecules (IFN) lead to STAT1 phosphorylation by JAK1/TYK2 kinases and its subsequent dimerisation. STAT1 dimers have a non-classical NLS that is able to bind to ARM 8-10 repeats to be able to shuttle to the nucleus to initiate the transcription of Inteferon-Stimulated Genes (ISG). During EBOV infection (C), VP24 blocks STAT1 binding to KPNA proteins by competing for its binding with the ARM 8-10 repeats.

RNA DEPENDANT-RNA POLYMERASE L

Compared to the other viral proteins, little is known about the 250 kDa RNA-dependant RNA polymerase L and most of its functions were attributed by comparison with other NNS viral polymerases. The enzyme is encoded by the most distal gene on the genome and is the least expressed viral protein [59,71]. It is involved in viral replication and transcription and, similarly to other NNS viral polymerases, is able to cap and to polyadenylate mRNA following the recognition of the GE sequence. In addition, it would appear to be able to make homo-dimers [172]. As it was shown for the *Vesicular Stomatitis Virus* (VSV) viral polymerase, EBOV scans the viral genome from the 3' to the 5' end and also appears, in some occasions, to be capable to scan the viral template from 5' to 3' [67]. Importantly, EBOV L requires interacting with VP35 to form a functional polymerase complex [172]. Considering its necessary role in viral replication and transcription, mutations in the polymerase are suspected to represent adaptation to a new host or a fitness gain and were thus tightly monitored during the 2014 EBOV outbreak to try to assess whether EBOV multiple passaging in humans could lead to its adaptation and maintenance [9]. Indeed, mutations in a viral protein can severely affect its functions and modify viral fitness, consequently, viral adaptations are commonly associated with co-mutations that compensate specific mutations to restore viral fitness [173]. To fully assess the effect of a mutation on viral fitness, it is thus important to analyse it by itself and in association with other co-mutations to fully understand the 'mutation cross-talk' that exists and unveils the molecular determinants of pathogenicity [174]. In this context, *in vitro* studies showed that a mutation identified during the West Africa outbreak in L, and which was suggested to modify the structure of the catalytic site, increased viral replication and transcription and could provide a growth advantage in humans by increasing viral fitness. Concomitantly, co-mutations also identified in 2014 between GP and L further increased this fitness [175]. Similarly, analysis of RESTV variants isolated either from monkeys or from humans that diverged mainly by non-synonymous mutations identified in the viral polymerase showed a growth adaptive gain in a species-dependant manner [176].

EBOLA VIRUS DISEASE: PATHOLOGY AND IMMUNE RESPONSE DYSREGULATIONS

Lethal cases of EBOV are caused by a sepsis-like shock syndrome, characterised by a widespread massive viral replication, a sustained and uncontrolled release of pro- and anti-inflammatory cytokines and at later stages, disseminated intravascular coagulation (DIC), leading to multiple organ failure [177]. As discussed above, several viral factors are admitted to participate in EBOV pathogenesis by either inducing an immunosuppressive state in infected cells or by activating immune cells. In this part, the current knowledge about EVD pathology will be discussed with a particular focus on EBOV-induced inflammation and coagulation disorders.

EBOLA VIRUS DISEASE PATHOGENESIS

How exactly EBOV initiates the infection and which cells are immediately infected is not precisely known, however, it is admitted that the primary targets of the virus are from the mononuclear phagocytic lineage, especially monocytes and dendritic cells [178]. They serve as an initial viral reservoir and help the virus to be transported to the lymph nodes where it will replicate extensively prior to dissemination to other organs (Fig. 22) [177]. EBOV possesses a wide tropism that allows it to infect multiple cell types to sustain its replication. Rapidly after the beginning of the infection, the liver, the spleen and the lungs are infected and become the primary sources of virus replication. At the late stages of the disease, the infection becomes systemic and the virus can be detected into the kidneys, intestines, pancreas, the bladder, endothelium, as well as immune-privileged sites such as the testis, the ovaries or the eyes, where the virus can persist for several months after recovery [17,25,179].

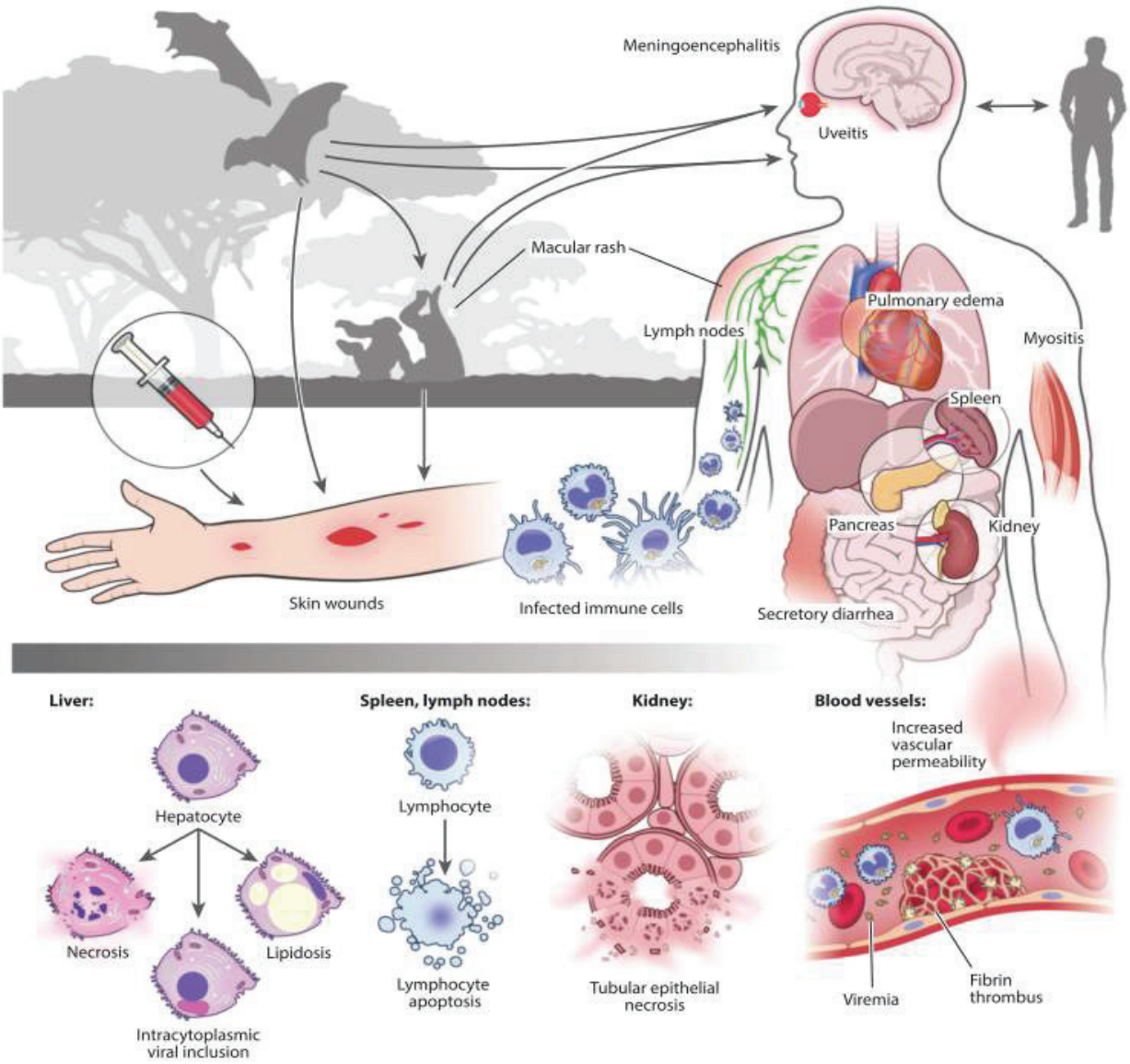

FIGURE 22. EBOV PATHOGENESIS OVERVIEW

From [179]. Direct contacts with an infected animal or another individual led to the infection of cells from the mononuclear phagocyte lineages (monocytes, dendritic cells, macrophages), that will replicate and transport the virus to auxiliary lymph nodes. Is followed a widespread dissemination and intense replication of the virus, especially in the liver, spleen, kidneys and lungs. The viral replication, the release of soluble glycoproteins of viral origin as well as the intense inflammatory response will lead to tissue and vascular damages.

Ebola virus disease is an acute disease and the clinical illness lasts for about four weeks and can be described as four distinct periods: The incubation period, the early illness, the peak illness and the recovery phase (Fig. 23) [179]. Until recently, most of the data about EBOV pathogenesis were obtained from animal models, however, the West Africa outbreak, helped to gain great insights in the development of EVD in humans.

The incubation period varies and is Ebolavirus species- and even strain-dependant. Epidemiological studies showed that the incubation period could be as short as two days after the first contact with an infected person/surface and could last up to 21 days. As such, if in a country affected by EBOV, no cases were reported for 42 days, two times the maximum incubation time, the outbreak is declared over. For EBOV, the mean incubation time ranges

from 5.3 days to 12.7 days. During that period, no symptoms are observed and the persons are not considered infectious. If shedding during the incubation period has been at least documented, it is not clear whether the viral load would have been sufficient to transmit the virus [180].

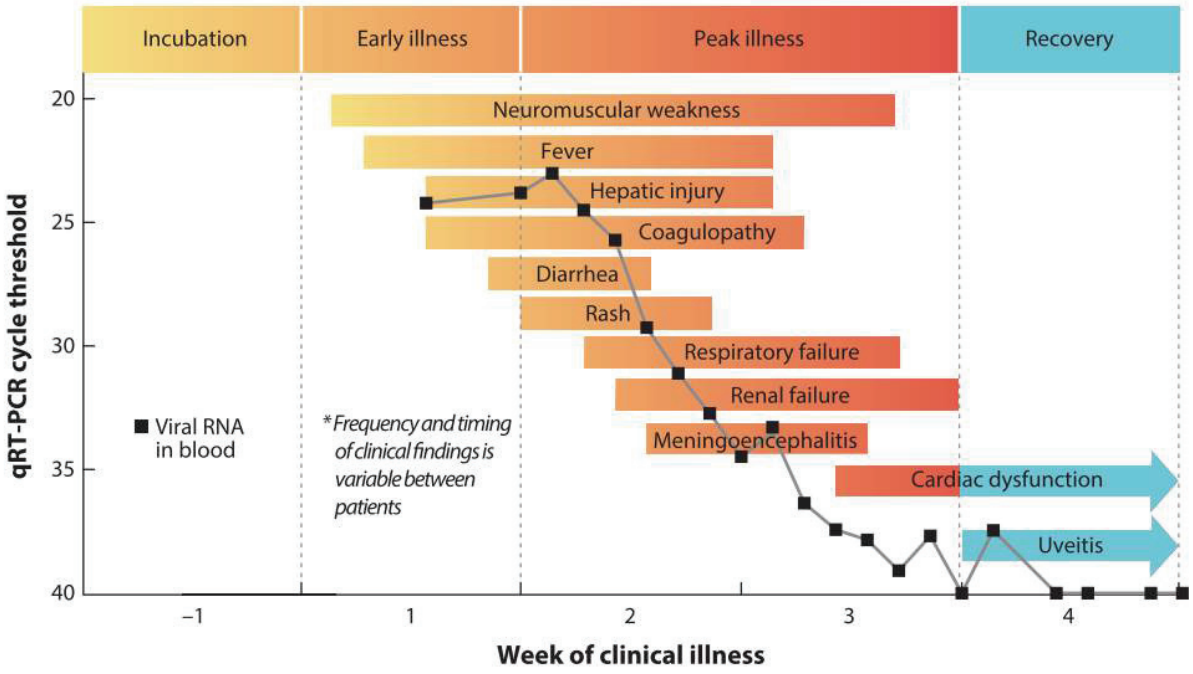

FIGURE 23. CLINICAL COURSE OF EBOV INFECTION

Obtained from [179]. The evolution of the viral RNA quantity in the blood (black lines, detected by qRT-PCR and represented as cycle threshold) during the different phases of the disease is represented. During recovery, no viral RNA is detected in the blood but infectious viruses have been shown to be able to persist into immune-privilege sites. The different symptoms and how long they usually persist is pictured.

Next comes the early illness with the onset of symptoms that are nonspecific and resemble a flu-like disease, with a persistent high fever (~40°C), headache, muscle weaknesses and pains (myalgia), fatigue and malaise. This phase lasts for about 3 days. As EBOV is usually not detected directly in the blood after the first symptoms occur, its resemblance with most other viral diseases makes it difficult to detect the beginning of EBOV outbreaks and to rapidly contain them [179,181]. With the disease progressing, the patients commonly start to display multiple severe gastrointestinal symptoms such as nausea, abdominal pain, vomiting, watery diarrhea, that last for about 7 days. This leads to an extreme loss of fluids (up to 5 to 10L of water lost due to the watery diarrhea) that is believed to contribute to multiple organ failure and death due to severe dehydration and hypovolemia shock during the peak illness. Coagulation disorders can already be detected in this phase. In addition to gastrointestinal symptoms, patients may show associated neurologic symptoms, being often in hypoactive and/or hyperactive delirious state, and confused. The neurologic disorders can continue during the peak of the disease and lead to meningoencephalitis. Viral-induced hepatic injuries are also detected and will persist during the peak illness phase.

The peak illness starts usually a week after symptom onset and this period is critical for the disease outcome. In an Ebola management centre in Liberia, it was shown that 60% of the patients will develop a sepsis-like shock that usually lead to death in the next five days [87,180]. The shock phase is associated with loss of consciousness, coma and multiple organ failure. Renal failure is a common feature of EVD and is attributed to viral replication in renal tubular cells and glomerular endothelium. Respiratory failure is also observed in 30% of the cases that could also be caused by EBOV infection of alveolar macrophages and probably other lung cells. In a similar manner, cardiac dysfunctions are suggested to be either due to EBOV replication or secondary effects of the disease. Moreover, the coagulation abnormalities observed during the early illness will persist during the peak illness and lead to disseminated intravascular coagulation (DIC). The DIC syndrome amplifies EBOV-induced damage to organs by blocking the blood circulation through the formation of fibrin clots and therefore participates in the observed ischemia and multiple organ failure [182].

The other 40% of the infected persons will start recovering from the disease. Recovery is associated with viral clearance and tissue repair as well as the development of a specific humoral response to the virus, with specific IgG antibodies against EBOV that can be detected in the blood for after recovery [183]. The ability of the host to control viral replication is also critical for survival, as survivors have significant lower viral load in the blood [184,185]. As stated above, during the convalescence phase, live EBOV is able to persist in immune-privileged sites several months after recovery and contribute to some of the after effects of the infection. Ocular complications are often observed in addition to long lasting fatigue, muscle pains and weakness, hearing loss or tinnitus and cognitive issues [186,187]. To this list should be added an important stigmatisation of the survivors from the local communities that can result in an important social burden [188].

INNATE AND ADAPTIVE IMMUNE RESPONSE DYSREGULATIONS DURING EBOLA VIRUS INFECTION

The immune response to an infection can be divided into two distinct responses: The innate immune response, which is rapidly induced following pathogen recognition but is largely nonspecific and the adaptive response that is activated by antigen presenting cells (APC) and is specific to a pathogen. The adaptive response is further divided into the humoral immunity and cellular immunity. A proper activation of the innate immune response and the adaptive response were shown to be essential for surviving EBOV infection.

As already discussed above (see VP35 paragraph), the innate immune response is initiated following the detection of the infectious agent by pathogen receptors called PRR by sensor cells, especially resident macrophages, DC and monocytes. These PRRs recognise specific motifs or PAMPS of an infectious agent. The engagement of the PRR with a viral PAMP leads to the induction of a panel of anti-viral genetic programs, notably the NF-κB-dependant cytokines and IRF-regulated IFN-α/-β responses, that initiate inflammation through the upregulation of pro-inflammatory genes, but also genes involved in the first steps of the adaptive response [86]. The recognition of a pathogen represents the first phase of the inflammation. The next phases will be (ii) the recruitment of specialised immune cells, namely monocytes, neutrophils and NK and T cells, to the site of infection through the secretion of pro-inflammatory cytokines and chemokines, (iii) the resolution of the infection and (iv) the return to homeostasis by inducing tissue repair programs and anti-inflammatory cytokines [86,189]. In this part, we will discuss EBOV-induced dysregulation of each of these phases.

PATHOGEN DETECTION

EBOV can be recognised by the surface pathogen receptor TLR-4 and the intracellular receptors RIG-I and MDA-5. $GP_{1,2}$ was shown to interact with TLR-4 *in vitro* and EBOV dsRNA intermediates are suggested to activate the RIG-I and MDA-5 pathways but can be blocked by EBOV VP35, as already discussed above [92,190]. The link between EBOV $GP_{1,2}$ and release of pro-inflammatory cytokines has been established by several groups (see below). Recently, it was proved that while infected at similar levels, monocytes-derived macrophages, when infected with RESTV do not release pro-inflammatory cytokines, contrary to EBOV. This difference was linked to the absence of engagement between RESTV $GP_{1,2}$ and TLR-4 and the absence of a sustained induction of innate immune programs was proposed to explain the absence of pathogenicity in humans for RESTV [191].

IMMUNE CELLS RECRUITMENT

The intense viral replication and the host response to the virus has been linked to the extensive organ damage that can be observed in infected animal models or humans. In response to EBOV $GP_{1,2}$, human macrophages release IL-1β, TNF-α, IL-6; a continuous macrophage activation is associated with fatal outcome in humans [131,192,193]. Early reports showed that similar cytokines can be readily detected in infected patient plasma and infected NHP. However, the profile of these released cytokines is different between survivors and non-survivors. In survivors, in the first days of the disease, the release of pro-inflammatory

cytokines, notably IL-1β, TNF-α, IL-6 and the T cell recruiter chemokines MIP-1α and MIP-1β is more rapid and pronounced than in non-survivors. Fatal cases are associated with a more intense induction of the pro-inflammatory cytokines IL-6, IL-8 and TNF-α but also the anti-inflammatory cytokine IL-10 at late stages of the infection [88,182,194]. TNF-α and other pro-inflammatory cytokines control several key aspects of the immune system. Of interest, they regulate immune cell migration by increasing vasodilation, permeability and presentation of surface adhesion molecules by endothelial cells, as well as coagulation pathway activation [195]. The early and controlled induction of pro-inflammatory cytokines as well as the adequate release of their antagonists (IL-1RA, sTNF-R, sIL-6R, or moderate levels of IL-10) to limit immune cell activation and to ensure the return to homeostasis is associated with survival. It is important to note that while reports and results are contradicting concerning the protective role of an intense but controlled inflammatory response during the early stage of the infection — likely due to different sampling times — it is well admitted that the 'cytokine storm' observed during EBOV infection (meaning the massive release of pro-inflammatory cyto- and chemokines to recruit additional, and *in fine* more immune cells that can be further targeted for viral replication, to the site of infection), is detrimental and associated with a fatal outcome, while a transient and controlled inflammation is necessary and beneficial to control viral replication and activate an adaptive response [88,196–198]. In addition, EBOV $GP_{1,2}$'s role in cell cytotoxicity, cell rounding and detachment has been proved to be in part responsible for the necrosis observed in infected organs, notably in hepatocytes and kidneys and to participate in vascular leakage [131,134].

RESOLUTION OF THE INFECTION

During an infection, DC play a central role in coordinating the innate and the adaptive immune response. Following the detection of a pathogen, DC will produce large amounts of IL-12 and type I IFN molecules that will regulate the cytotoxic activity of NK and CD8+ T cell and will induce an antiviral state to prevent the pathogen from further propagating. The role of the Type I IFN IFN-α and IFN-β and the T cell specific Type II IFN IFN-γ during EBOV infection is still debated. Some studies were able to detect the release of the three IFN species into the blood of infected persons and associate it to fatal infection, while others were not able to detect IFN-α, IFN-β and IFN-γ or found that they were more released in survivors [88,196,199,200]. The recruitment of specialised immune cells, notably NK and CD8+ T cells, which are involved in the clearance of infected cells, is believed to participate in EBOV pathogenesis [88,137].

The role of NK cells during EBOV infection is not clear. *In vitro* studies showed that monocytes, macrophages and DC were all able to release IL-12 in response to the virus but this seems to not be secreted during human infection [88,131,201]. Whilst suggested to participate in organ damage by destroying infected cells, recent data suggests that NK cells are not able to efficiently detect EBOV infected cells and that their proper activation is associated with recovery [140,202].

DC are antigen-presenting cells (APC) and as such are able to mount non-self-peptides onto a class II MHC (HLA-DR) and present it to the surface of its plasma membrane before migrating in the draining lymph node sites. With the help of the class II MHC and costimulatory molecules (notably CD80, CD86, CD40, CD11c, CD83), the newly maturated DC, is able to activate naive

CD4+ and CD8+ T cells that in response will proliferate and migrate to the site of the infection to resolve it. During EBOV infection, DC are readily infectable, however, the cooperation of VP35 and VP24 blocks DC maturation. In this respect, infected DC present an aberrant maturation profile with an upregulation of CD40 and CD80, a slight increase of CD86 and HLA-DR but no CD11c and CD83 and also fail to induce T cell proliferation [89,96,203].

In addition to the lack of proliferation signals by DC, lymphopenia is a hallmark of EBOV infection. Classically, during an infection, CD4+ T cells will, after encountering a mature DC, be activated and different CD4+ T cells subsets will actively participate in fighting the infection by helping DC-priming of CD8+ T cells and by playing a central role in their recruitment to the site of the infection. CD4+ T cells are also necessary for B cells to produce neutralizing antibodies, as was shown for the production of specific EBOV $GP_{1,2}$ antibodies during vaccination trials. Finally, they can also directly kill infected cells through a cytolytic activity [204–206]. CD8+ T cells are cytosolic cells that expand and migrate to the site of the infection to destroy or promote the death of infected cells through the release of TNF-α, IFN-γ or perforin and granzymes [207]. Alongside EBOV $GP_{1,2}$ that directly promotes lymphocyte death through direct binding, the upregulation of Fas/FasL and TRAIL molecules, the intense release of TNF-α and the improper maturation of DC that lead to a deregulated DC/T synapse are believed to participate in the lymphopenia observed in the spleen and lymph nodes during EVD [195,208,209]. Furthermore, the high production of reactive oxygen species and nitric oxide species released by infected macrophages has been identified in lethal infections of NHPs and humans and could participate as much as in tissue damage as in T cell death [88]. The role of T cell activation during EBOV has been long postulated to be essential for protection [182,210]. While in fatal infections CD4+ and CD8+ T cells are still activated, further analysis showed that their activation was abnormal and correlated with an increased expression of both CTLA-4 and PD-1, which are markers of loss of function, probably in response to the strong inflammatory microenvironment and viral replication [196,211]. On the other side, in survivors CD8+ T cells were able to set a strong EBOV-specific T cell response, especially against NP and VP24 peptides [212].

The role of the humoral response and the production of specific anti-EBOV IgG is evident. Analysis of sera from humans that survived infection all show a rapid production of specific-IgM about 10 to 29 days after symptom onset, which are then progressively replaced starting from around 19 days post-onset by high amounts of IgG, that can persist for several decades. Recent data showed for the first time that plasmablast proliferation was observed 2 to 3 weeks after symptom onset in human [183,213,214]. However, in lethal cases, the presence of IgM and IgG are not observed, suggesting that these disease victims were not able to mount a proper humoral response. In line with this result, animals pre-challenged with candidate vaccines were able to induce a robust B and CD4+ T cells response, which was associated and necessary for high titers of IgG anti-EBOV, and survived lethal infection [206,215].

RETURN TO HOMEOSTASIS

The inflammatory effectors released to eliminate the pathogen and to remodel the infection environment to ensure the rapid arrival of specialised immune cells is deleterious for the host if it is not controlled back to its normal levels. During EVD, several lines of evidence have shown that non-survivors are not able to regulate the activation of inflammation, while for

survivors, the secretion of anti-inflammatory cytokines, as well as tissue repair proteins such as the platelet derived sCD40L is observed during the infection [216]. Interestingly, anti-inflammatory cytokines are released at lower levels in survivors than in non-survivors, especially at the late stage of the disease. This suggests that the timing of and the proper release of anti-inflammatory cytokines is necessary to return to homeostasis, otherwise it can only further destabilize the immune response and participate in EBOV pathogenicity [88,196].

In summary, it appears that survival to EBOV is associated with a rapid but controlled induction of the inflammatory response to be able to rapidly mount a specific humoral and cytotoxic response against the virus and to control viral replication. In lethal cases, viral infection cannot be restrained, which leads to a sustain and important dysregulated activation of the inflammatory response with the release of both pro and anti-inflammatory cytokines. This will lead to an improper activation of the different immune cells, especially DC cells and T cells, and important tissue damage participating in the observed pathogenesis.

COAGULATION DISORDERS

Coagulation is part of hemostasis, a highly ordered and complex process that controls vascular integrity. Over the last few years, it became more and more evident that coagulation pathways are involved in innate immunity by helping to prevent pathogen dissemination in the bloodstream. Importantly, coagulation and inflammation are tightly interwoven with multiple cross-talk: activation of inflammation modulates coagulation activity and coagulation is able to impact inflammation by either inhibiting or amplifying it. Any changes in the balance can result in a complete dysregulation of both systems and lead to life threatening pathologies [217–219]. Coagulation is activated by several interconnected pathways: The extrinsic pathway, the intrinsic pathway or the lectin pathway, either simultaneously or separately and ultimately lead to fibrin deposition and the formation of a fibrin clot. Complement is also known to be able to amplify coagulation. EBOV coagulation disorders are well known and are described for NHP and human infection with fatal cases being associated with the development of a DIC syndrome during the late stage of the disease. Indeed, numerous markers of coagulation activation can be observed during EVD, with a decrease of levels of fibrin and the coagulation inhibitor protein C in plasma, an increase in prothrombin time and fibrin degradation products (D-dimers) and thrombocytopenia are commonly described [182,194,216,220,221]. How exactly EBOV impacts the coagulation system is not well characterised but growing evidence shows that it can directly impact some of the coagulation activator pathways that will further be described here.

EXTRINSIC PATHWAY

The extrinsic pathway activated by type I integral glycoprotein Tissue Factor (TF). Exposure of TF to plasma protein Factor VII forms the TF/FVIIa complex that initiates the activation of the coagulation pathway. The formation of the TF/VIIa complex results in the activation of serine proteases that can interact with plasma membrane receptors that control inflammation such as PAR receptors and TLR-4 (Fig. 24) [222]. In a normal physiological state, TF is both constitutively expressed in cells that are hidden from blood cells in the subendothelium or is expressed at low levels in an inactive form in monocytes and endothelial cells. In those cells, inflammatory cytokines and infection are known to be able to up-regulate TF expression at their surface, which can also be secreted into the bloodstream in the form of microparticles. Alternatively, endothelium injuries expose the TF normally concealed from the bloodstream. During EBOV infection, upregulation of TF is observed at the surface of monocytes and is believed to strongly participate in the early activation of coagulation [220]. Furthermore, treatment of EBOV-infected monkeys with rNAPc2, a specific recombinant inhibitor of the TF/FVIIa complex showed a significant decreased in active TF that correlated with an increased survival and lower inflammation, highlighting the role of coagulation disorders in EBOV pathogenicity as well as the bidirectional control existing between the coagulation and the inflammation [223].

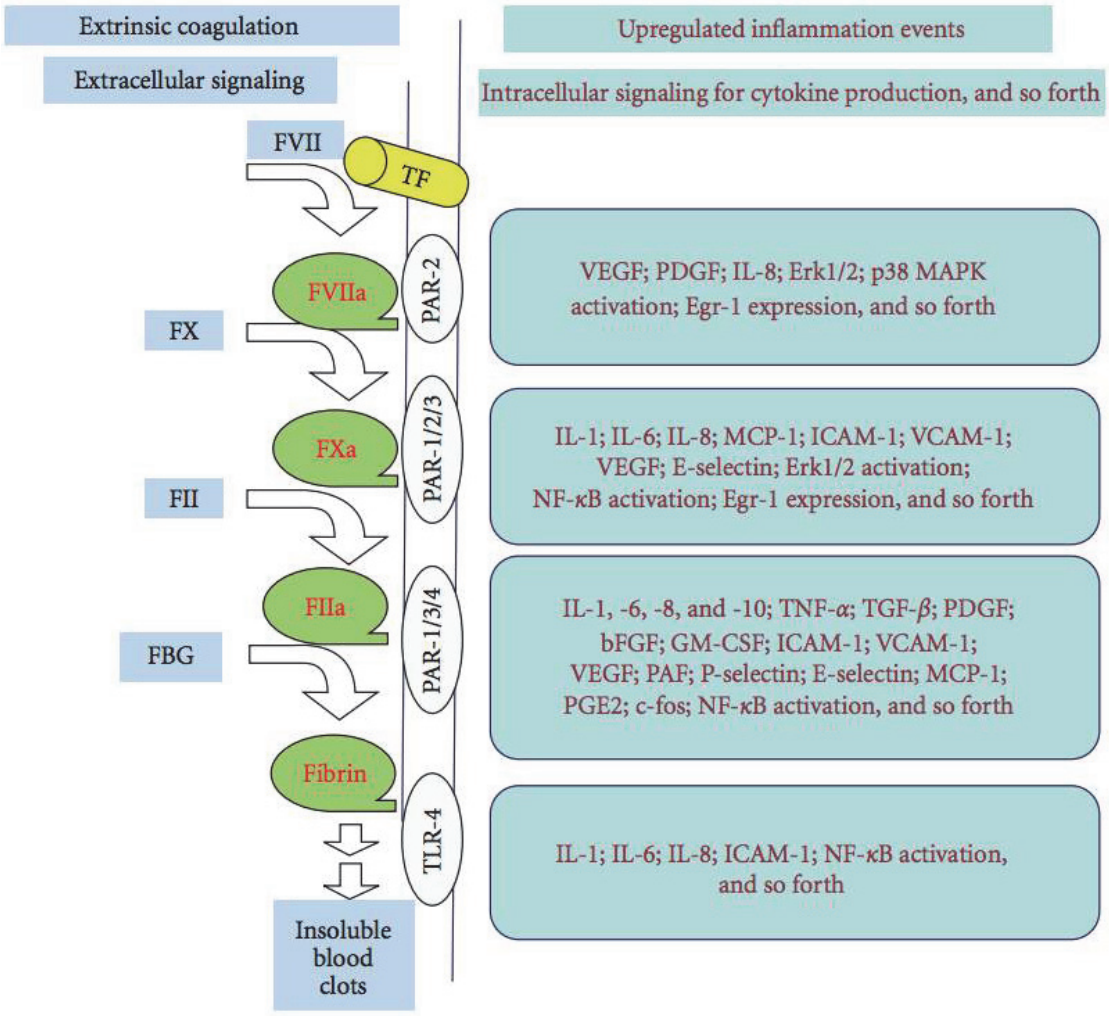

FIGURE 24. TISSUE FACTOR-DEPENDANT EXTRINSIC COAGULATION ACTIVATION AND INTERPLAY WITH INFLAMMATION

Obtained from [211]. The interaction between Tissue Factor (TF) and the coagulant mediator FVII initiates the extrinsic coagulation pathway (left). It leads to the generation of active serine proteases (in red) from their inactive zymogens (in black) that will ultimately result in the cleavage of Fibrinogen (FB) into Fibrin that polymerizes and cross-link to form fibrin clot to stop bleeding or pathogen spreading. The interactions existing between the different coagulant mediators and cellular receptors that can activate the pro-inflammatory response are shown (right).

INTRINSIC PATHWAY

The intrinsic pathway involves the formation of a complex of three serine proteinases, the coagulation factor XII (FXII), FXI and plasma prekallikrein (PK) and a single non-enzymatic cofactor, high molecular weight kininogen (HK). As this process requires direct binding to negatively charged surface, it is also known as the contact pathway [224]. Direct evidence of intrinsic pathway activation by EBOV in humans or NHP are not known, however, a study performed in guinea pigs infected with MARV displayed an increase in circulating PK and bradykinin, factors produced during activation of the intrinsic pathway. The ability of HK to bind to phosphatidylserine molecules (PS), which are highly represented on EBOV virion surfaces, and the results obtained for MARV infection could suggest that the intrinsic pathway is potentially also upregulated during EBOV infection [224–226].

The lectin pathway is the perfect example of a cellular pathway that communicates with other pathways to control both the innate immune response and the coagulation cascade. The C-type lectins, mannan-binding lectin (MBL) and the H-, L- and M-ficolins are specialised complement-activating PRR that predominantly recognise mannose and N-acetylglucosamine (GlcNAc) that are mostly present on bacterial and viral glycoproteins [227,228]. MBL and ficolins are homo-oligomeric proteins formed of a collagen-like domain that allows homo-oligomerization of three subunits that form the structural subunits, and 3 to 6 of these trimeric subunits will associate to form the functional protein. MBL proteins recognise and bind their target proteins through its carbohydrate-recognition domain (CRD). Ficolins on the other hand possess a fibrinogen-like domain that has a similar function to the CRD from MBL. The MBL and Ficolins are active when associated with the serine proteases Mannose-Associated Serine Protease 1 (MASP-1), MASP-2, MASP-3 and two non-enzymatic proteins, MAp19 and Map44, which are truncated forms of MASP-2 and MASP-1 respectively (Fig. 25). These truncated forms conserve their MBL binding domain and are thought to be regulators of MASP protein activities. Upon MBL binding to a carbohydrate group, MASP-1 auto-activates and cleaves MASP-2 to render it active. It was shown that both MASP-1 and MASP-2 can activate either the complement pathway or the coagulation system. The MBL:MASP-1:MASP-2 complex participates in the cleavage of the complement proteins C2 and C4 into their cleaved products C2a and C4a that together form the C3 convertase protein, which is the main effector of the complement cascade. How exactly MBL and Ficolins are able to initiate the coagulation cascade is not entirely understood, however, it was shown that MASP-1 and MASP-2 were able to cleave different coagulations factors, notably to cleave prothrombin into thrombin that then cleaves fibrinogen into fibrin to create fibrin clot [229]. Furthermore, MBL-Knockout mice have a delayed activation of the coagulation cascade and when infected with *Staphylococcus aureus* develop DIC [230]. In a similar fashion, it was shown that Ficolin:MASP-1:MASP-2 complexes are activated following binding to activated platelets and fibrin clots and circulating D-dimers, again highlighting the cross-talk existing between inflammation and coagulation [231,232].

VSV viruses pseudotyped with EBOV glycoprotein were shown to interact with recombinant human MBL (rhMBL) and able to prevent its interaction with its attachment receptor DC-SIGN [233]. This study also shows that MBL actively participates in the complement-dependent neutralisation of pseudotyped EBOV viruses and thus potentially of EBOV. In another report, MBL was shown to be able to block EBOV $GP_{1,2\Delta}$-induced immune cell activation [131]. Surprisingly, M-Ficolin binding to EBOV $GP_{1,2}$ leads to an increased infectivity instead of neutralizing EBOV particles [142]. The protective role of of rhMBL during EBOV infection was further demonstrated by treating infected mice with large amount of rhMBL that resulted in an important increased survival [234]. MBL concentrations in humans are extremely variable (ranging from 0.002µg/mL to 10µg/mL) [228] and could thus represent a genetic factor that can determine EBOV infection outcome [131]. Interestingly, the results of Michelow IC *et al.* (2011) further highlight the role of the complement pathway, that appears to be necessary for MBL-dependant EBOV protection [234]

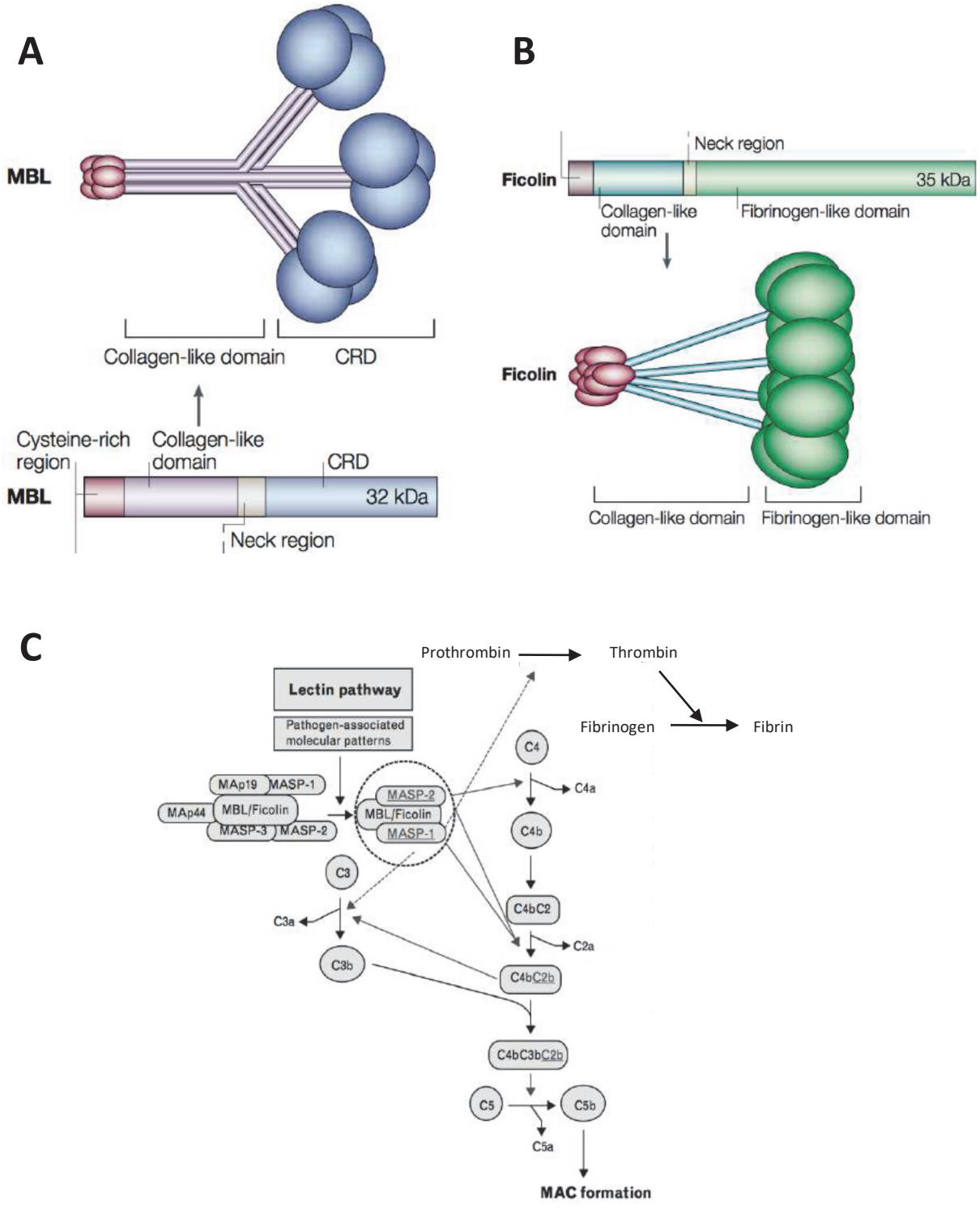

FIGURE 25. MBL AND FICOLIN STRUCTURE.

Modified from [227] and [228]. Schematic representation of MBL (A) and Ficolin (B) structures and how they can interact with the complement pathway (C). Both proteins are homo-oligomers formed of a collagen-like domain that allows self-oligomerisation. Through their interaction with MASP proteins, it was shown that MBL and Ficolins are able to cleave the complement protein C4 into C4a resulting in the activation of the complement pathway cascade. Alternatively, when bound to MBL, MASP-1 cleaves prothrombrin into thrombrin that is able to cleave fibrinogen products into fibrin.

The classical complement pathway is initiated by the C1q complex, formed of the C1q protein, a homo-oligomeric protein that resembles MBL and Ficolins, and two molecules of C1r and C1s. C1q possesses two distinct structures: A Six globular head and a collagenous region. The collagenous region is involved in anchoring the C1q complex to the cell plasma membrane through the recognition of a specific cellular ligand and the globular head is able to bind the Fc portion of an antibody that is fixed to its targets. Of importance, during EBOV infection, it was shown *in vitro* that antibodies bound to the virus were able to be recognised by the C1q complex and enhanced EBOV binding to its receptor and to promote EBOV infection [235]. The possibility of antibody-dependent enhancement (ADE) raises questions for vaccines development that could be potentially deleterious for the host. Recently, ADE was also shown to occur using antibodies from human survivors, however, the actual role of such antibodies for EBOV pathogenesis is not known [236].

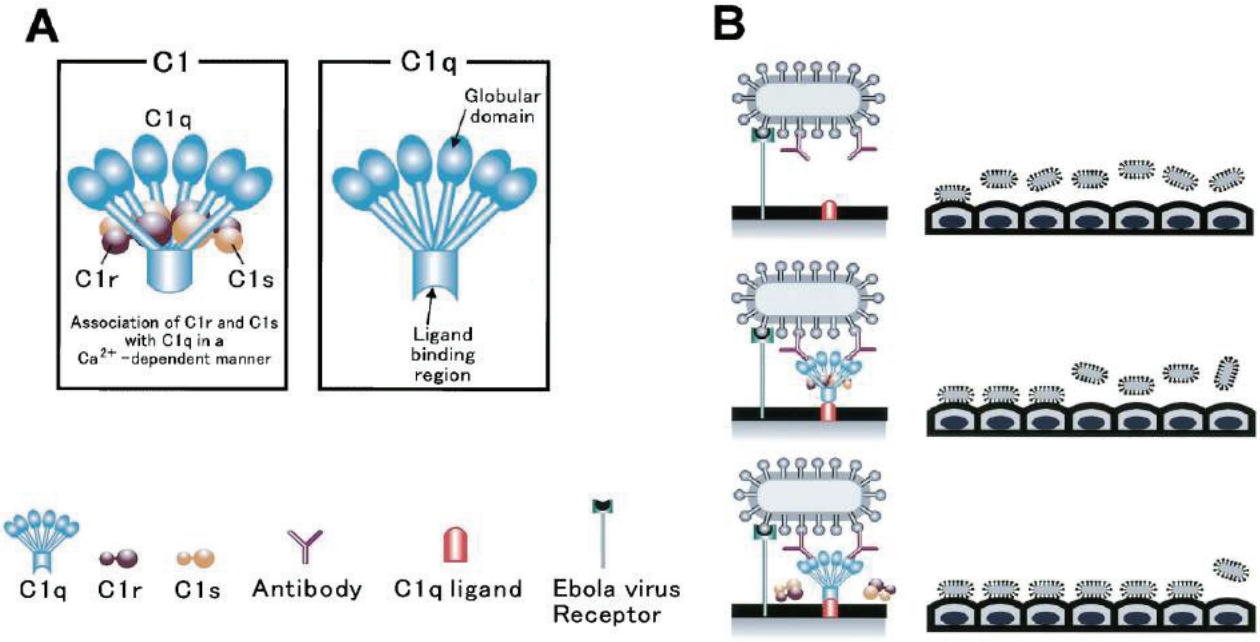

FIGURE 26. C1Q STRUCTURE AND ANTIBODY-DEPENDANT ENHANCEMENT

From [235]. Structure of C1q protein (A) showing its globular domain and the localisation of its cellular ligand binding region. In (B) is represented the proposed model for Antibody-dependant Enhancement (ADE) during EBOV infection. The FC portions of antibodies bound to EBOV are recognised and bound by C1q complex that is fixed to the plasma membrane through its cellular ligand binding region. In this context, EBOV interactions with its cellular attachment receptors are enhanced, facility its entry.

THERAPEUTIC STRATEGIES AGAINST EBOLA VIRUS

With the recurrent and recent EBOV outbreaks, intensive efforts were made to release approved therapeutic approaches based on the different strategies that have been developed over the years using different animal models to treat EVD. In the different attempts to find a way to protect from EBOV infection, two different approaches can be distinguished: Passive immunisation and active immunisation [237,238]. In this part, an overview of the different strategies will be given with a particular focus on the rVSV-ΔG-ZEBOV-GP vaccine and the results of the different studies are summarised in Table 3.

PASSIVE IMMUNISATION

Passive immunisation is based on the transfer of EBOV-specific neutralizing antibodies obtained either from survivors, through the use of convalescent plasma, or by directly injecting cocktails of monoclonal antibodies (e.g. ZMapp) directed against EBOV $GP_{1,2}$. During the last outbreak in West Africa, both strategies were tried. However, while they confer protection in NHP primates, their true efficiency in human remains uncertain and additional tests are required [237,238].

DIRECT IMMUNISATION

INACTIVATED EBOV

The first attempts of direct immunisation were performed in the 1980s with the use of EBOV inactivated viruses (heat, formalin or γ-irradiation). In addition to contradictory results about their ability to protect against EBOV, the use of such vaccination methods always raise important safety concerns [239–242].

DNA VACCINES

DNA vaccines tested for EBOV are based on the injection followed by electroporation of plasmid encoding either EBOV GP gene alone or with NP. The advantage of such a system is that it is possible to create plasmids encoding several filovirus GPs to create broad protection. This method showed promising results in NHP, offering 100% protection, but in humans, the seroconversion was below 50%. DNA vaccination using at the same time a plasmid encoding for IL-12 appears to significantly increase the seroconversion rates up to 90% in humans. The advantage of DNA vaccination compared to other strategies is that it is inexpensive to produce and extremely safe and stable. However, due to its poor immunogenicity, several injections are required to be able to mount a robust immune response to the virus [237,242,243].

VIRUS-LIKE PARTICLES

Virus-like particles (VLP) are commonly used in laboratory settings to study the activation of immune cells. It is then not surprising that several attempts have been made to try to use them as vaccines. The advantage of this system is that it is relatively easy to produce as it primarily only requires transfection of cells with plasmids encoding for EBOV GP, VP40 and NP genes for the production of non-infectious viral particles that can then be easily purified. NHP immunised by VLP with different adjuvants were protected against EBOV lethal challenge four weeks after vaccination with the detection of antibodies against EBOV. So far, VLP have never been tested during outbreaks and while they offer advantages (cross-protection between different species, native antigens, non-replicative and no pre-existing immunity), they are produced through transient transfection in mammalian cell lines, which is expensive and laborious [244,245].

REPLICATION-DEFECTIVE AND –COMPETENT VACCINES

Multiple different vector-based vaccines have been developed and offered positive results. Again, two types exist: Replication-defective and replication-competent viral vectors. The advantage of replication-defective vaccine is that they can be administered to immunocompromised individuals. Unfortunately, they usually induce a humoral and cellular response that is less potent compared to that seen with replication-competent vectors.

REPLICATION-DEFECTIVE VACCINES

MODIFIED VACCINA ANKARA VIRUS BASED VACCINES

The first attempts were made by generating a vaccinia Ankara virus expressing GP alone (MVA-BN), but they did not confer any protection in NHP. Recently, a MVA expressing both GP and VP40 genes (MVA-EBOV) was created and showed 100% protection in different animal models, including NHP, following a single dose injection [246]. MVA-EBOV infects cells which results in the production and the release of VLP. The MVA-BN vaccine is currently used in combination with the Ad26 vaccine and promising results were observed. It is now ongoing phase III trials in this form.

RECOMBINANT VENEZUELAN EQUINE ENCEPHALITIS VIRUS (VEEV) REPLICON

In this system, VEEV structural proteins were replaced with EBOV NP and EBOV GP genes leading to the formation of replicon-deficient viral particles (VRP-NP and VRP-GP). So far, only the VRP-GP showed protection in NHP [247].

KUNJIN VIRUS BASED-VACCINE

Kunjin-based vaccines expressing either a modified anchorless GP or a GP that has a mutation that increased its shedding (GP D637L) were generated and used to immunise guinea pigs. In the context of the transmembrane deleted mutant but also the shedding mutant, Kunjin VLP

are formed but when they are produced, no GP proteins are incorporated into the VLP. The results showed that animals immunised with the Kunjin GP D637L replicon were fully protected compared to animals immunised with the anchorless version. So far, no results are available for NHP immunisation [248].

RECOMBINANT EBOVΔVP30

A recombinant EBOV virus deleted for its VP30 gene was shown to induce complete protection in NHP. The advantage of this vaccine platform is that the vaccination is made, with the exception of VP30, with the full spectrum of EBOV antigens, including viral RNA. VP30 is absolutely necessary for viral replication and its deletion makes it a promising recombinant replication-deficient EBOV vaccine [249,250].

REPLICATION-COMPETANT VACCINES

During the 2014 EBOV outbreaks, several antiviral compounds were tested, such as favipiravir, brincidofovir, as well as a monoclonal based therapy with the ZMapp cocktail, the use of convalescent plasma from survivors, siRNA against GP, VP24 and L mRNA (TKM-Ebola). Of all the strategies used, replication-competent vaccines seem to provide the best protection so far [251–255].

HUMAN PARAINFLUENZA VIRUS TYPE 3 (HPIV3)

HPIV3 expressing EBOV GP protein (HPIV3/EboGP) demonstrated protection following intranasal immunisation in NHP [256]. The inconvenience of this vector vaccine is the existence of a very high pre-existing immunity (more than 94%) against HPIV3 in the human population. While it is possible to still bypass this pre-existing immunity through several vaccine doses, it appears to not be the best alternative for vaccination [237].

RECOMBINANT ADENOVIRUS 5 (RAD5)

Initially, a rAd5 expressing GP (rAd5-GP) was developed and a single dose injection was proved to be sufficient to provide full protection against EBOV lethal challenge in NHP [256]. Similarly to HPIV3, pre-existing immunity against Ad5 exists and to try to solve this issue, the human Ad26 and chimpanzee Ad3 (ChAd3), which are known to have a lower seropositivity in humans, vaccines were generated [258]. Of note, ChAd3 was chosen based on the seropositivity data from European population, and as such might not represent the actual seropositivity that could exist for the populations that are present in regions where the virus is endemic. As of today, both the Ad26 and the ChAd3 boosted with MVA-BN are undergoing human clinical trials. In NHP it was shown that this system provided complete protection with no clinical signs of EVD after viral challenge. Remarkably, in humans, the seroconversion rate is of 100% [259,260].

RECOMBINANT VESICULAR STOMATITIS VIRUS (RVSV)

The Vesicular Stomatitis virus (VSV), is an arthropod-borne virus and the prototype rhabdovirus. The bullet-shaped virus possesses a 11kb ss(-)RNA genome that encodes five genes organised in tandem: N, P, M, G and L (Fig. 28). N encodes the nucleoprotein that, alongside the phosphoprotein P, the polymerase L and the RNA, will compose the nucleocapsid [261]. The VSV M gene encodes three polypeptides, M1, M2 and M3, through alternative codon initiation. The matrix protein M1 controls several key aspects of the VSV life cycle, including viral budding, apoptosis, and interferon antagonism through the inhibition of host transcription and mRNA nucleo-cytoplasmic transport machineries. The M gene encodes two additional polypeptides denoted M2 and M3 that have a conserved CTD with the full-length M1 protein, as they are synthesised by alternative initiation at internal downstream codons. The M proteins form the matrix lattice of the virion. Finally, the glycoprotein G mediates viral binding and fusion. Its binding to phosphatidylserine, expressed on almost all cell types, and its interaction with the ubiquitous intracellular LDL receptor for fusion, allows VSV to infect a remarkable range of cell types and tissues [262,263].

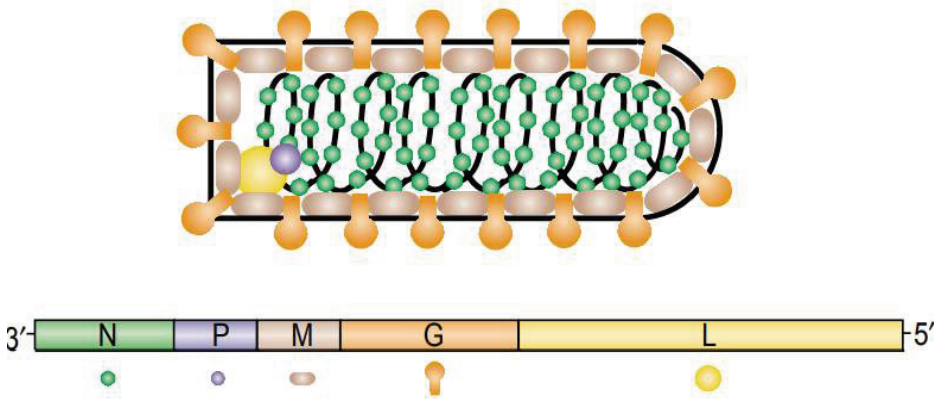

FIGURE 27. *VESICULAR STOMATITIS VIRUS* GENOMIC ORGANISATION AND STRUCTURE.

Obtained from [261]. The single-stranded negative RNA Vesicular Stomatitis Virus (VSV) genome is encoding for five different genes: The nucleoprotein N, the phosphoprotein P, the Matrix M, the glycoprotein G and the polymerase L. The nucleocapsid is formed of the VSV N, P and L proteins. The viral matrix is formed by the VSV M protein and the viral glycoprotein G is inserted into the host-derived membrane

The availability of the reverse genetic system for VSV makes it possible to generate biocontained recombinant Vesicular Stomatitis viruses (rVSV) in which the VSV G gene is replaced by a foreign viral glycoprotein gene [253,264]. These rVSV are able to successfully incorporate the new glycoprotein into infectious virions, while continuing to grow rapidly to high titers, similarly to those observed with the wild-type virus (Fig. 28) [253]. As such, rVSV are commonly used as tools to elucidate the role of the glycoproteins in viral entry and cell tropism, including for highly pathogenic viruses.

As a vaccine platform, rVSV-based vaccines are widely considered attenuated with respect to wild-type virus and usually display a restricted tropism. rVSV-based vaccines for EBOV have

demonstrated encouraging results. Indeed, the rVSV-ΔG-GP vaccine expressing the EBOV GP gene (rVSV-ZEBOV, or hereafter, rVSV-GP) has shown remarkable protective effects against EBOV infection in animal models and is currently undergoing clinical phase III trials to be used as a vaccine against Ebola virus disease [251,265]. Of interest for the development as a human candidate-vaccine, when used as a prophylactic vaccine it has been shown that the rVSV-based vaccine was able to protect NHP when vaccinated as a single shot a month before being challenged with high dose of EBOV (1000 PFU) and to completely prevent EBOV replication. This protection was associated with the development of an appropriate cellular and humoral response with the generation of neutralizing antibodies against EBOV glycoprotein. Vaccinated animals display a transient viremia that lasts for only two days and similar observations were made during human trials [251,252,266]. Shedding of the replicative vaccine from vaccinated animals has been detected by RT-PCR in rare cases, but it has never been isolated, highlighting its inability for vector transmission [264]. However, vaccinated animals with one Filovirus species are less protected against another, and attempts have been made to develop a rVSV expressing two different filovirus antigen that improved cross-protective efficacy [265,267]. Importantly, while lower, this vector still able to offer a significant protection in immunocompromised primates and is perfectly tolerated. This is of special importance when we take in account that Filovirus outbreaks occur in an African area where Human Immunodeficiency virus (HIV-1) prevalence is around 4% but can be as high as 14% in adults [266,268]. Furthermore, post-exposure vaccination was demonstrated to provide around 50% protection and is believed to have saved the life of a laboratory worker that was accidentally exposed to EBOV [269–271]. Vaccination appears to provide long-lasting protection as evidenced in small rodent models that were still protected against EBOV challenge up to 18 months after vaccination [271]. In addition to offering protection against EBOV and MARV infection, rVSV-based vaccines appear to offer a significant protection following lethal challenges with multiple viruses in NHP, including Lassa virus, Nipah virus or HIV and a rVSV virus expressing two different antigens (EBOV and the hantavirus Andes virus) offers protection against both viruses [273–276]. A non-negligible advantage of VSV for vaccine development is the very low pre-existing seroprevalence against the virus, which limits the risk of an existing immunity against the vector that could impair vaccine efficiency. Furthermore, NHP were successfully protected against EBOV lethal infection following rVSV-EBOV vaccination whilst they were already challenged before by a rVSV/LASVGPC (rVSV against the Lassa virus glycoprotein) and Lassa virus three months before [277]. Consequently, the ability of this vaccine vector to grow to high titer, the very low seropositivity in the human population and its apparent ability to offer protection against multiple viral infections following a single injection, make the rVSV-based vaccines very attractive.

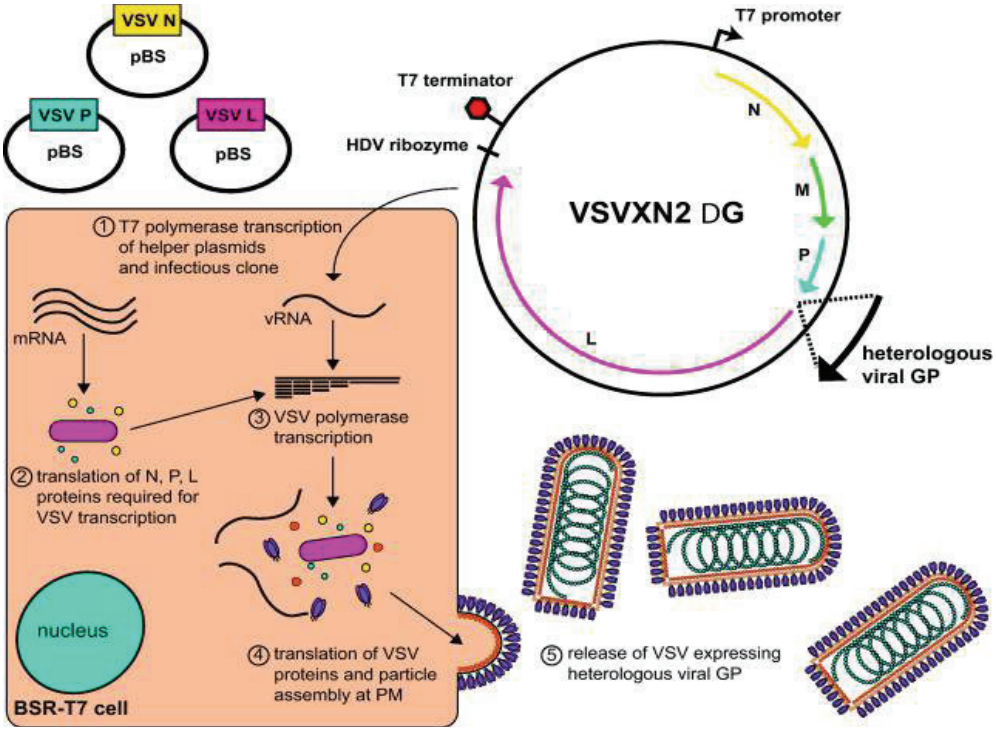

FIGURE 28. REVERSE GENETIC SYSTEM FOR THE GENERATION OF RECOMBINANT *VESICULAR STOMATITIS VIRUSES* (rVSV)

BHK stably expressing the T7 polymerase are transfected with helper plasmids encoding for VSV N, M and L genes as well as a full-length plasmid encoding for the VSV genome (under the T7 promotor) deleted of its G gene that has been replaced by a foreign glycoprotein gene (1). The viral (-)RNA is synthesised from the full-length plasmid by the T7 polymerase. In parallel, helper plasmids are transcribed and translated (2). The newly synthesised viral N, P and L proteins forms the nucleocaspid which is capable to replicate and transcribe the (-)RNA VSV genome (3) leading to the production of all VSV proteins, including VSV M and the foreign viral glycoprotein (4). Viral particles are assembled and released at the plasma membrane (5).

Vaccine type/Vector	Replication-competent	Immunogen	Animal studies / Clinical trials	Efficiency
Inactivated EBOV	No	NP, VP35, VP40, GP, VP30, VP24, L, vRNA	Guinea pigs	Uncertain
DNA	N/A	NP, GP	Phase I	Poor immunogenicity
VLP	N/A	NP, VP40, GP	NHP	100% protection (NHP)
MVA	No	VP40, GP	NHP	100% protection (NHP)
VEEV	No	VP40, GP	NHP	100% protection (NHP)
Kunjin	No	GP	Guinea pigs	100% protection (guinea pigs)
rEBOVΔVP30	No	NP, VP35, VP40, GP, VP24, L, vRNA	NHP	100% protection (NHP)
HPIV3	Yes	GP	NHP	100% protection (NHP)
ChAd/MVA	Yes	GP	Phase III	100% protection (NHP)
rVSV	Yes	GP	Phase III	100% protection (NHP and human in ring vaccination)

TABLE 3. CANDIDATE VACCINES AGAINST EBOLA VIRUS

MOLECULAR CHARACTERISATION OF THE rVSV-ΔG-ZEBOV-GP VIRUS, PROTOTYPE VACCINE AGAINST EBOLA VIRUS

OBJECTIVES

The recent EBOV outbreaks in West Africa and in the Democratic Republic of Congo lead to the death of about 11,000 disease victims for more than 30,000 confirmed cases [9]. To try to contain viral spreading and mortality, especially among health care workers, the World Health Organization pushed forward to test in humans several therapeutic strategies and candidate vaccines. Amongst all of the strategies developed in the last decade, the one that is offering the best protection in several animal models, including immunocompromised monkeys, is currently the rVSV-ΔG-EBOV-GP (rVSV-ZEBOV; rVSV-GP hereafter) candidate vaccine. In outbreak settings, rVSV-GP ring vaccination[5] trials are promising and are seemingly offering full protection from EBOV infection and transmission and are now entering Phase III clinical studies [251,252,278,279].
While rVSV-GP effectiveness and safety has been widely investigated before human trials, and since its initial development in our laboratory [253,265], the molecular characterisation of this replication-competent virus is still extremely limited to the point where the only data currently published are those confirming the correct expression of $GP_{1,2}$ in cells infected with the vector and its growth kinetic compared to the wild-type VSV virus [253,279]. Therefore, the molecular basis of how this vaccine provides disease protection is currently unclear. Further characterisation would provide insights into what make this vaccine so successful in protecting humans and animals against EVD and could help in the development of other rVSV-based vaccines with which to fight other viral diseases.

EBOV glycoprotein synthesis is a complex mechanism that requires transcriptional editing of the GP gene resulting in the production of several distinct viral glycoproteins that, in tandem, are likely central to the immunopathogenicity of the virus, as discussed above. EBOV full-length $GP_{1,2}$ protein is a highly glycosylated trimeric protein that is inserted into the viral host-derived membrane. Importantly, both the immunogenicity and the toxicity of the viral glycoprotein were linked to its glycosylations, which are also necessary from the point of view of the infected host to mount a successful immune response directed against EBOV [134,141,280–282]. In addition, the full-length $GP_{1,2}$ and its truncated soluble form, $GP_{1,2\Delta}$ which is shed by the cellular sheddase ADAM17 were shown to participate in immune cell activations and dysregulations as well as cellular damage [120,124,131]. Furthermore, it was shown that the soluble glycoprotein sGP is produced during the infection from an EBOV virus with an 8U genotype, and that it has the ability to interfere with the host antibody response directed against EBOV surface glycoprotein and to mediate inflammatory processes [58,121–123]. However, due to a lack of characterisation of the rVSV-GP virus, it is firstly, unknown if such viral glycoproteins are produced in the context of this vaccine vector and, secondly, if they resemble the ones produced during EBOV infection. It is of particular interest to understand this, as several candidates' vaccines that tried to express modified GPs proved unable to protect the host against EBOV infection. Indeed, as discussed above, a vaccine candidate expressing a transmembrane deleted mutant was unable to protect guinea pigs in a

[5] Ring vaccination: As defined in [278]: 'Vaccination of a cluster of individuals at high risk of infection, owing to their social or geographical connection to a confirmed index case.'

Kunjin-replicon based system and similar results were observed with a recombinant Adenovirus approach [248,257]. Furthermore, several studies pointed out the importance of the humoral immunity and the development of GP specific antibodies for survival during EBOV infection. In the context of vaccination, while it would also be vector-dependant, the activation of the humoral response but also apparition of protective, neutralizing antibodies are likely to be governed by the proper structure and nature of the viral glycoproteins that are presented [206,283,284]. Such elements emphasize the need to precisely characterise the nature of the glycoproteins, which are synthesised and released from the edited GP gene inserted into the rVSV genome (8U phenotype) during rVSV-GP infection. Therefore, in this work, we aimed to provide a better comprehension of the production and the processing of the EBOV glycoprotein from rVSV-GP infected cells.

To this end, we investigated and characterised the release of $GP_{1,2}$ into the cell culture supernatant of infected cells either as a virion-bound or as a shed form, using wild-type rVSV-GP or rVSV-GP modified viruses that have different shedding abilities. Furthermore, we addressed the ability of the VSV polymerase to edit 8U GP gene to identify the potential release of sGP or ssGP during infection [70,116,117]. Moreover, we studied the upregulation of several pathways known to participate in the cleavage of ADAM17 substrates to understand which molecular pathways could be involved in EBOV $GP_{1,2}$ shedding in the context of an infection and to identify new potential therapeutic targets.

During vaccination trails, multiple side effects have been reported, with most of the participants showing signs of fatigue, fever (up to 40°C), sweating, headache, chills, myalgia and in some limited cases, infectious colitis, that was associated with abdominal pain and mild diarrhea with blood, as well as arthralgia and nausea. Mild-to-moderate lymphopenia, neutropenia and thrombocytopenia were also observed in the first days following vaccination [251]. The molecular characterisations of the viral glycoproteins synthesised during rVSV-GP provided in our work and presented in this thesis offer new insights with which to understand the success of the rVSV-GP vaccine but also the potential viral origins of such side effects and could help in developing a safer vaccine, which currently cannot be used in an immunocompromised population.

EBOV $GP_{1,2\Delta}$ RELEASE FROM rVSV-GP INFECTED CELLS

Recombinant VSV expressing EBOV $GP_{1,2}$ (rVSV-GP) has been widely used to investigate specific steps of the EBOV life cycle, and is now used as a prototype vaccine, however, so far and as detailed above, the potential release of soluble glycoproteins during rVSV-GP and their characterisation has never been studied even though these soluble forms have clearly been implicated in multiple steps of virus development and pathogenicity mechanisms and may also be crucial in influencing the potential success of a vaccine candidate.
During EBOV infection, $GP_{1,2}$ is shed from the plasma membrane by the cellular sheddase ADAM17 as a form known as Shed GP or $GP_{1,2\Delta}$, a phenomenon which has been shown to control $GP_{1,2}$ cytotoxicity and to participate in EBOV pathogenicity mechanisms (Fig. 29A) [131,149,285]. Similarly, cells transfected with a plasmid expressing EBOV $GP_{1,2}$ are able to shed the glycoprotein, indicating that EBOV $GP_{1,2}$ is by itself self-sufficient to be recognised by ADAM17 and to be released as its soluble form into the cell culture supernatant [131]. Considering that shedding only requires that ADAM17 is active and that $GP_{1,2}$ is transported to the plasma membrane, it was hypothesised that during rVSV-GP infection, the viral glycoprotein could likewise be released as the soluble, truncated soluble $GP_{1,2\Delta}$ form.

To study this, both VeroE6 cells (Fig. 29B, lower panel) and 293T (Fig. 29C) were infected with rVSV-GP at the indicated MOI and cell culture supernatants were collected 36 hours post-infection. The supernatants were clarified from cellular debris and dead cells by low speed centrifugation ('SPNT') and then ultracentrifuged over a 20% sucrose cushion to separate the pelleted virion-bound $GP_{1,2}$ ('Virion') from unpelleted soluble proteins present in the upper 'supernatant' fraction ('UC'). All samples were analysed by western-blotting using rabbit sera that recognizes both the GP_1 subunit and the two forms of GP_2 (as detailed in Fig. 16 and Fig. 18). The different amounts of viral glycoproteins in the cell culture supernatant fractions were then estimated using ImageJ software [286].
In VeroE6 infected with rVSV-GP either at a MOI of 0.1 or 0.01, the GP_1 subunit was always detected as a single band in all analysed fractions, including in the ultracentrifuged supernatant fraction that should contain soluble glycoproteins, suggesting the presence of the viral glycoprotein as a soluble form (Fig. 29B, Lanes 'SPNT', 'UC' and 'Virion'). As demonstrated previously by Dolnik O *et al.* (2004), the virion-bound GP_2 has a lower electrophoretic mobility than the soluble $GP_{2\Delta}$ and migrates at around 25 kDa, whereas the soluble truncated form $GP_{2\Delta}$ migrates faster with a molecular weight of about 21 kDa. Both forms can be readily detected in the supernatant of EBOV-infected cell cultures [149]. For both MOI, in the low-speed clarified supernatant (lane 'SPNT'), two bands of different molecular weights were detected, corresponding to the GP_2 and $GP_{2\Delta}$ forms (Fig. 29A, left panel). Following ultracentrifugation, supernatants (lane 'UC') contained the single $GP_{2\Delta}$ band that migrated around 21 kDa and that was not pelleted alongside the virion (lane 'Virion'). Similarly, a single band of about 25 kDa is found in the virion/pelleted fraction but was excluded from the soluble ultracentrifuged supernatant fraction (Fig. 29B, left panel). The quantification of the signals of GP_2 and $GP_{2\Delta}$ in the clarified supernatant showed that $GP_{2\Delta}$ represents about 25% of the total viral glycoproteins released from cells infected at a MOI of 0.01 and about 20% from cells infected at a MOI of 0.1 (Fig. 29B, right panel).

In the human cell line 293T, the GP_1 subunit was also detected in all the analysed fractions (Fig. 29C, Lanes 'SPNT', 'UC' and 'Virions'). Similarly, to VeroE6 cells, in the clarified supernatant, two proteins of distinct molecular weight were observed. However, compared to VeroE6 (Fig. 1A, lane 'SPNT') their separation was less evident, suggesting potentially differences in their glycosylation profile. After ultracentrifugation, the band of higher molecular weight that corresponds to GP_2 was absent from the soluble fraction (Fig. 29C, Lane 'UC') and was detected as a single band in the pelleted virion fraction (Fig. 29C, Lane 'Virion'). As expected, on the other side, the protein of lower molecular weight was excluded from the membrane/virion-bound fraction and was only detected in the soluble 'UC' fraction. Densitometry quantification showed that around 15% of the viral glycoprotein present in the clarified supernatant was in a truncated soluble form (Fig. 29C, right panel).

Therefore, during rVSV-GP infection and in a similar fashion as during EBOV infection, the viral glycoprotein $GP_{1,2}$ is released in the cell culture supernatant as a virion-bound form (GP_2) and is shed from the infected cells as a soluble truncated form ($GP_{2\Delta}$).

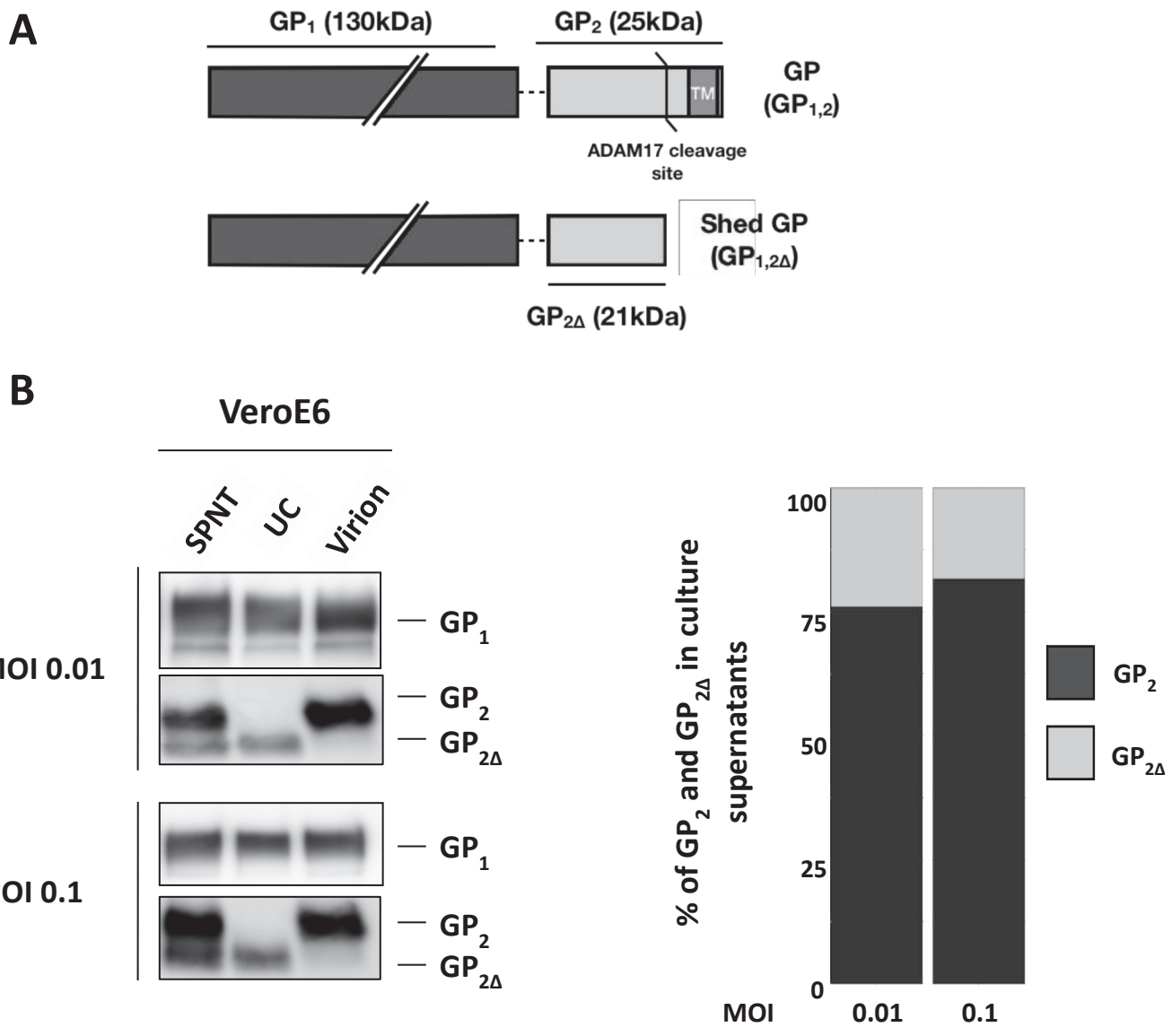

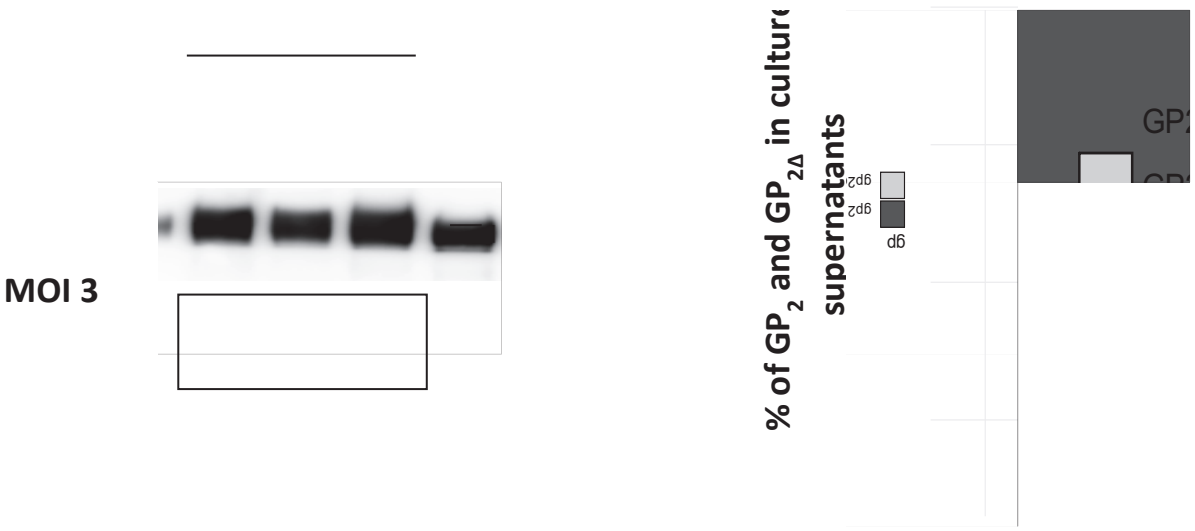

FIGURE 29. ANALYSIS OF $GP_{1,2\Delta}$ RELEASE FROM rVSV-GP INFECTED CELLS.

The structure of $GP_{1,2}$ and $GP_{1,2\Delta}$ is shown (A). VeroE6 (B) and 293T (C) cells were infected with rVSV-GP at the indicate MOI. Thirty-six hours post infection, supernatants were collected and clarified by low-speed centrifugation (SPNT) an the soluble proteins present in the supernatants (UC) were separated from the membrane-associated proteins (Virion by ultracentrifugation. Before analysis, the ultracentrifuged pellet was concentrated 5 times in DMEM 3%FBS. Sample were analysed by western-blotting in a 12% gel. The viral proteins were detected using sera recognising both EBO $GP_{1,2}$ subunits. Densitometry analysis was performed using the ImageJ software.

rVSV-GP-HS VIRUS RESCUE

To further study the release of $GP_{1,2\Delta}$ from infected cells in the context of the recombinant VSV vector system, an additional rVSV-GP virus engineered by reverse genetics and bearing the substitutions D637A and Q638V was rescued. Those mutations in the EBOV GP shedding site were identified as drastically modifying its shedding ability by modulating $GP_{1,2}$ recognition by ADAM17 to increase glycoprotein shedding during both EBOV infection and GP transfection. This “High Shedding” phenotype mutant will be referred to as GP-HS hereafter [131,285].

For virus rescue experiments, BHK cells stably expressing the T7 polymerase (BHK-T7) were transfected with plasmids encoding all VSV accessory proteins involved in nucleocapsid formation (VSV-L, VSV-P and VSV-N) and a rVSV-GP full-length plasmid encoding the VSV viral genome under the control of a T7 promoter. In this full-length plasmid, the VSV G gene has been replaced by EBOV GP gene with the D637A and Q638V mutations (Fig. 30A and see Fig. 28 for a detailed explanation of the rescue system to generate rVSV viruses). Up to seven days post-transfection, BHK-T7 cells were monitored for cytopathic effects and rescue was confirmed and amplified following passaging of BHK-T7 supernatants onto VeroE6 cells. Following transfection and subsequent amplification, the rVSV-GP-HS was successfully rescued and amplified and the presence of the mutations was confirmed by sequencing of the viral stock produced in VeroE6 cells (Fig. 30B).

Similarly to before, VeroE6 cells were infected with either rVSV-GP or rVSV-GP-HS and the differences in $GP_{1,2\Delta}$ release efficiency into the supernatants were then analysed by western-blotting and protein levels were quantified by ImageJ (Fig. 30C). As before, for both viruses, the GP_1 subunit was detected as a single band for all fractions (Fig. 30C, left panel, Lanes ‘SPNT’, ‘UC’ and ‘Virion’). However, compared to the rVSV-GP virus, the GP_1 band present in the soluble ultracentrifuged fraction (‘UC’) was more intense, whereas the GP_1 band in the virion was less pronounced, implicating an increased shedding that would result in less virion-associated $GP_{1,2}$ for this virus (Fig. 30C, left panel, see Lanes ‘Virion’ for rVSV-GP and -GP-HS). In the clarified supernatants of rVSV-GP and GP-HS viruses infected cells, GP_2 and $GP_{2\Delta}$ are both detected with a clear increase of $GP_{2\Delta}$ release observed from cells infected with the GP-HS variant (Fig. 30C, left panel, Lane ‘SPNT’). This was confirmed by densitometry quantification that showed that there was almost three times more $GP_{2\Delta}$ that accumulated in the supernatant of rVSV-GP-HS infected cells (Fig. 30C, right panel, 20% for rVSV-GP and 55% for rVSV-GP-HS). Accordingly, and as observed for GP_1, a higher shedding phenotype decreased the level of GP_2 in the virion fraction (Fig. 30C, left panel, Lane ‘Virion’ of rVSV-GP compared to rVSV-GP-HS).

Those results show that similarly to EBOV, a rVSV-GP high shed variant is viable and modifications of GP shedding site resulted in a significant increase in $GP_{1,2}$ shedding.

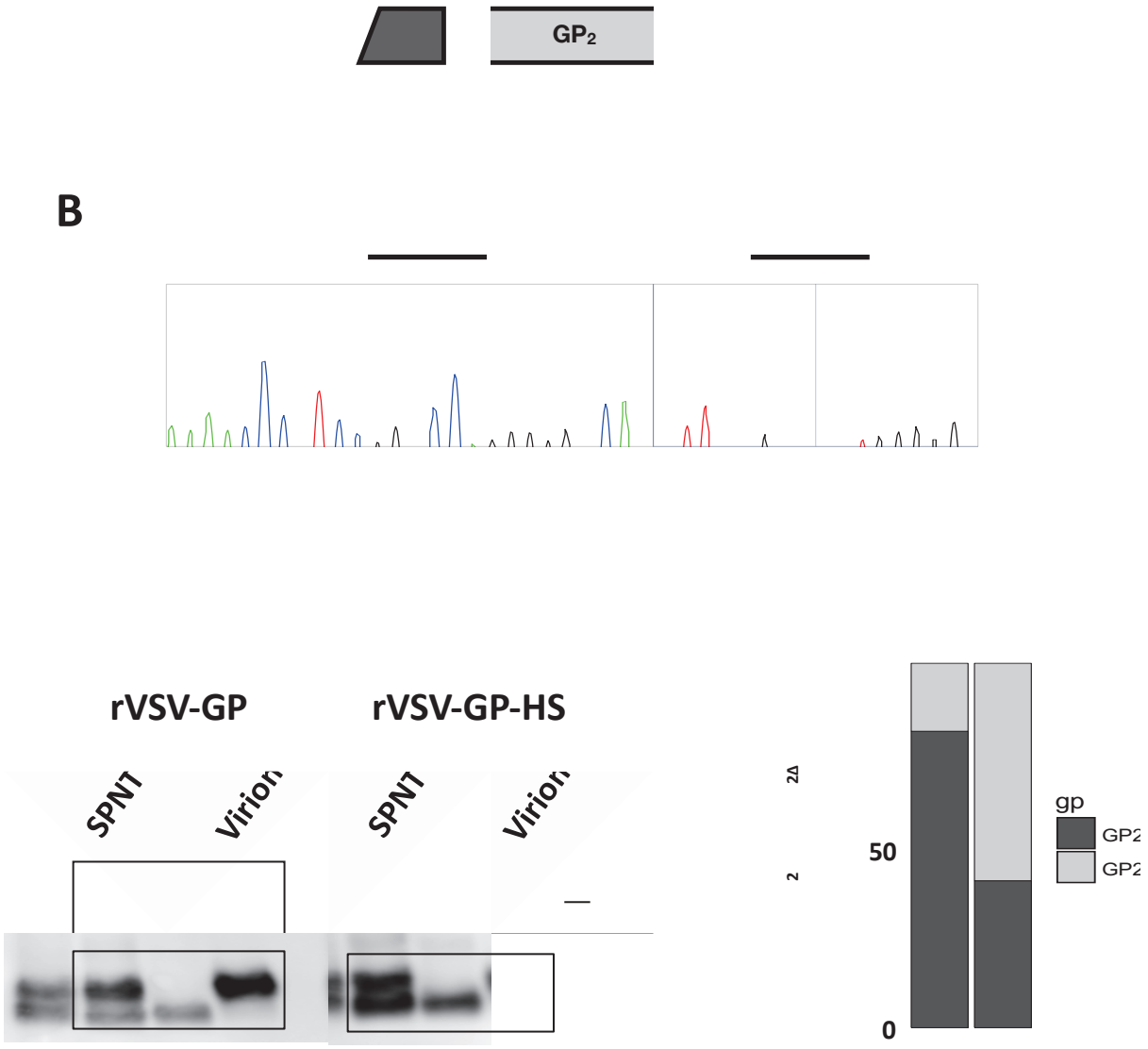

FIGURE 30. COMPARAISON OF $GP_{1,2\Delta}$ RELEASE EFFICIENCY BETWEEN rVSV-GP AND rVSV-GP-HS VIRUSES

Schematical representation of EBOV GP_2 subunit (A). Its wild-type shedding cleveage site and the high-shed muta (HS variant; in red) are shown. rVSV-GP-HS was rescued in BHK-T7 cells and the virus was amplified in VeroE6 cells presence of the mutation after one passage on VeroE6 cells was verified by RT-PCR and Sanger sequencing (B). Simil to before, VeroE6 cells were infected for thirty-six hours and the supernatant ('SPNT'), the ultracentrifuged supern ('UC') and the pelleted virion ('Virion') were analysed by Western-Blotting. The amount of $GP_{2\Delta}$ was quantified ImageJ.

KINETIC RELEASE OF $GP_{1,2\Delta}$ FROM INFECTED CELLS

It was shown for EBOV that $GP_{1,2}$ is continuously shed from the plasma membrane during infection [285]. The kinetics of $GP_{1,2\Delta}$ release for rVSV-GP infection was therefore investigated to understand if the viral protein was continuously shed into the supernatant of infected cells.

VeroE6 cells were infected with rVSV-GP at a MOI of 3 and the appearance of GP_1, GP_2 and $GP_{2\Delta}$ in cells and supernatant were monitored by western-blotting (Fig. 31, left panel). The amount of the virion-bound GP_2 and of the soluble $GP_{2\Delta}$ released in the cell culture media were then quantified and plotted over time (Fig. 31, right panel). In the first 12 hours of the infection few virion-bound GP_2 were detected in the cell culture supernatant. After 12 hours post-infection, an important and seemingly exponential GP_2 release was observed and continued until the end of the kinetic. In contrast, $GP_{2\Delta}$ was only detected in the culture media 18 hours post-infection and then gradually accumulates over time. As in the supernatant, in cells, GP_1 is rapidly detected and accumulates over time. Unexpectedly, the presence of a GP_2-specific band that migrated in a similar fashion to $GP_{2\Delta}$ was detected in cells 12 hours post-infection. While, virion-bound GP_2 levels were decreasing after reaching their maximum at around 24 hours post-infection, it would appear that this lower molecular weight protein that would appear to correspond to $GP_{2\Delta}$ continued to accumulate in infected cells. This protein was never previously observed either during EBOV infection or GP transfection and is indicated by 'Δ?' in the figure.

This experiment demonstrates that $GP_{1,2\Delta}$ is continuously released in the cell culture supernatant after infection with rVSV-GP. Furthermore, and contrary to EBOV, in during rVSV-GP infection, an intracellular $GP_{2\Delta}$-like protein was detected and accumulated over the time-course of the experiment.

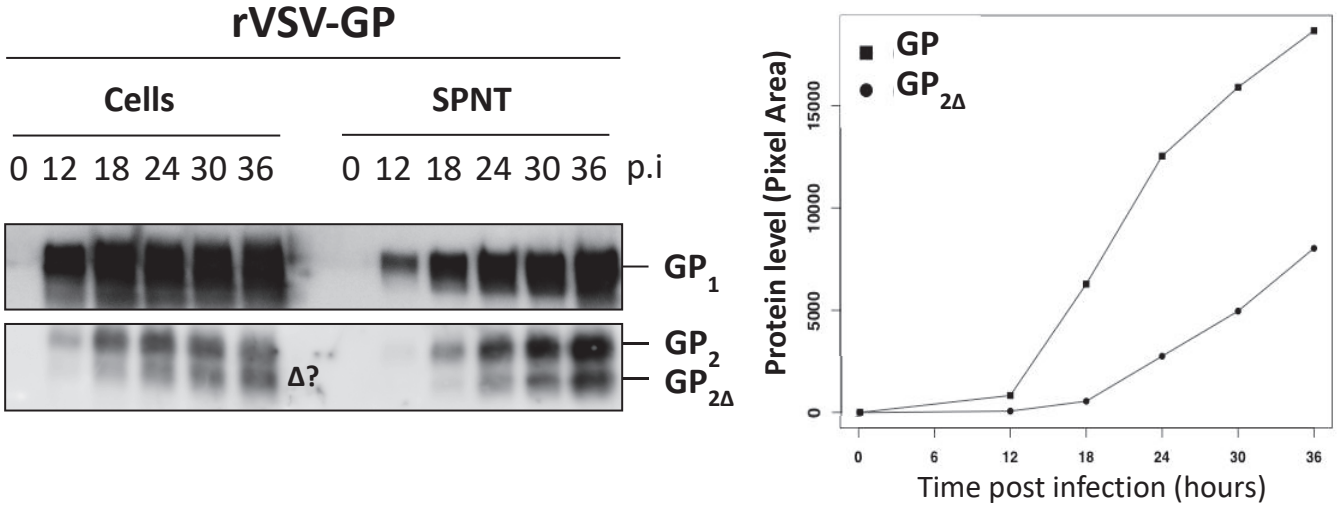

FIGURE 31. KINETIC OF $GP_{1,2\Delta}$ RELEASE FROM rVSV-GP INFECTED CELLS

VeroE6 cells were infected with rVSV-GP at a MOI of 3 in a 6-well plate. Cells and supernatants were collected at the indicated time-points. To collect cells, the media was removed and the same amount of fresh DMEM 3%FBS was added. Cells were then scraped from the well and collected. The cell culture media was prepared as before. Samples were run by Western-blotting in a 12% gel and the released of $GP_{2\Delta}$ was quantified by ImageJ. Δ? Indicates the position of the GP_2 protein that migrates in a similar fashion than $GP_{2\Delta}$ in cells.

IDENTIFICATION OF A FULLY MATURE GLYCOSYLATED GP_2 DURING rVSV-GP INFECTION

During its processing and trafficking to the plasma membrane, EBOV glycoprotein acquires multiple O- and N-glycosylations. In the Endoplasmic Reticulum (ER), the precursor Pre-GP_{ER} has N-glycosylations that are sensitive to the glycosidase Endo H (blue circles), whereas, in the Golgi apparatus and at the plasma membrane, both Pre-GP and $GP_{1,2}$ possess Endo H-resistant mature N-glycosylations (red circles) [120]. Of importance, GP_2 possesses only two N-glycosylation sites and only one acquires N-glycosylation complex glycans that resist Endo H cleavage. As a consequence, both GP_2 and $GP_{2\Delta}$ are partially resistant to Endo H [149]. All GP forms are, however, sensitive to the amidase PNG F that is able to cleave all glycans (Fig. 32). Therefore, by comparing Endo H and PNG F treatments, it is possible to reveal the actual size of the protein and to understand if differences in migration profiles between different glycoproteins are due to differences in glycosylations or are due to different amino acid sequences. Deglycosylation treatments help then to follow the intracellular transport of viral glycoproteins and to determine if electrophoretic mobility changes correspond to differences in glycosylations or in protein size.

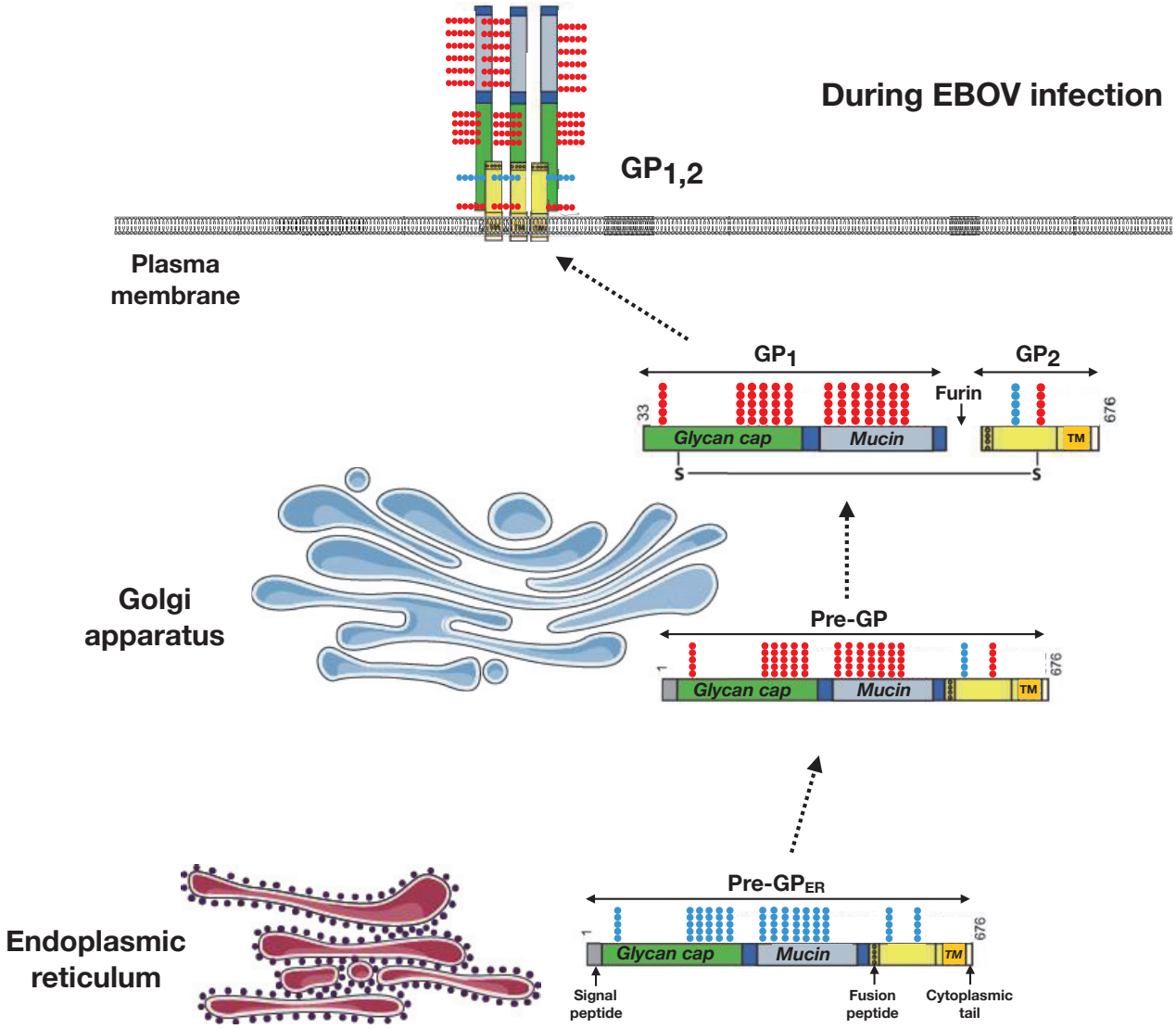

FIGURE 32. EBOV GP SYNTHESIS AND GLYCOSYLATIONS

The glycoprotein is first synthesised as a precursor in the Endoplasmic reticulum (Pre-GP_{ER}) which has immature N-glycosylations (shown by blue circles) that are mostly attached to the mucin-like domain (MLD) present in the future GP_1 subunit. In the Golgi, the glycoprotein High mannose N-glycosylations are matured into complex type N-glycans (Pre-GP) and is cleaved by the cellular enzyme Furin into GP_1 and GP_2, which associates into a dimer that are linked by a disfulde bound. At this point, it has complex N-glycans (red circles). In GP_2 two N-glycosylations sites exist but only one has complex N-glycans attached to it. The mature $GP_{1,2}$ is a trimeric protein inserted through its transmembrane domain (TM) into the host-cell derived membrane.

While intracellular cleavage of ADAM17 substrates had been suggested in early publications, it is now admitted that ADAM17 cleaves its target ectodomains only at the plasma membrane (Fig. 19) [287,288]. The observation of a protein that migrated similarly to $GP_{2\Delta}$ in western-blotting in the previous experiments presented above was thus surprising (Fig. 31). As such, to understand the nature of this '$GP_{2\Delta}$-like' protein product seen in infected cells and to confirm if this cellular-associated protein indeed originated from intracellular cleavage, the electrophoretic mobility of this newly detected form was compared to the GP_2 and $GP_{2\Delta}$ released from infected cells following glycosidase treatments. In this respect, rVSV-GP infected cells and supernatants were collected 36 hours post-infection and the soluble and virion-bound proteins were separated as before and all fractions were subjected to Endo H and PNG F treatments before western-blotting analysis.

In cells, in the mock-treated condition, a single GP_1 band was visible whereas after Endo H treatment, two bands of different size were observed (Fig. 33A, Lane 1 compared to Lane 2). Of the two bands detected after exposure to Endo H, only one stayed at the same position as the unique band detected in the mock condition. This demonstrates that one form is able to resist to Endo H, while the other one is sensitive to it. After PNG F treatment, both proteins underwent a mobility shift and were closely co-migrating. This shows that the proteins not only differ in their glycosylations but have also variations in their amino acid sequences (Fig 33A, Lane 3 compared to Lane 2). As expected, this analysis demonstrates that in rVSV-GP infected cells, GP_1 is present in two different forms: The Pre-GP_{ER} that is immaturely glycosylated and is therefore Endo H and PNG F sensitive (marked by a '# and a '##' respectively, Fig. 33A, Lanes 2 and 3), and the Endo H resistant Pre-GP/GP_1 that possess complex glycans. This form is also PNG F sensitive as mentioned above ('**' in the Fig. 33A). Similar results were obtained with rVSV-GP-HS infected cells (Fig. 33A, right panel).
GP_2 analysis showed that in cells, two forms were again also visible: The virion-bound GP_2 and the newly identified $GP_{2\Delta}$-like product, indicated as '$GP_{2?}$' in the Figure (Fig. 33A, Lane 1). For both viruses, after Endo H deglycosylation, the GP_2 band was no longer detected and a single band migrating at the same size as the $GP_{2?}$ protein was observed. The intensity of the signal of this band was stronger in the Endo H condition than in the mock condition (Fig. 33A, Lane 2 compared to Lane 1), indicating that the GP_2 and $GP_{2?}$ proteins co-migrated. This result shows that $GP_{2?}$ is Endo H resistant. In the PNG F condition, a unique band was seen, showing that they were again co-migrating (Lane 3, the PNG F sensitive forms are noted by a '**'). In addition, following Endo H treatment, the GP_2 subunit was migrating as a size between the mock-treated protein and the fully deglycosylated protein confirming that the GP_2 produced during rVSV-GP was resistant to Endo H (Fig. 33A, Lane 2 compared to Lanes 1 and 3). Therefore, the difference of size observed between the two proteins is not due to differences in amino acid sequences but in their glycosylation pattern. This $GP_{2\Delta}$-like protein would then appear to be not the result of an intracellular cleavage but of an abnormally glycosylated $GP_{1,2}$

resulting in a protein that migrates at the same size than $GP_{2\Delta}$. It will consequently be referred to as $GP_{2\text{-}RES}$ ($GP_{2\text{-}RESISTANT}$; Fig. 33C).

Examination of the GP_1 signals obtained in the low-speed centrifuged supernatant (Lanes 1 to 3, 'SPNT', Fig. 33B), showed that the subunit is always detected as a single, fully matured form, as it can be seen by the absence of Endo H sensitive forms. However, it is, as expected, PNG F sensitive (marked by a '**, Fig 33B, 'SPNT', Lane 3). No differences were observed when the protein is either present as a soluble form ('UC', Lanes 4 to 6, Fig. 33B) or a membrane-bound form ('Virion', Lanes 7 to 9, Fig. 33B). This result shows that, as expected, the membrane-bound full-length GP and its shed form have complex glycans attached to their GP_1 subunit. At the exception of differences in the amount of glycoproteins present in the different soluble or insoluble fractions, no other differences could be observed between the rVSV-GP and rVSV-GP-HS viruses (Lanes 1 to 9).
In the supernatant of infected cells (Lanes 1 to 3, 'SPNT', Fig. 33B), two distinct GP_2 subunits were again detected, corresponding to the virion-bound GP_2 and the truncated soluble $GP_{2\Delta}$ (Fig. 29). Treatment with Endo H and PNG F lead to a similar change of migration patterns for both proteins. After Endo H treatment, the position of the GP_2 protein is noted by a '*' whereas the position of the $GP_{2\Delta}$ is marked by a '+' (Lane 2, 'SPNT', Fig. 33B). Similarly to what was seen after Endo H, following PNG F digestion, two bands were detected (The position of GP_2 and $GP_{2\Delta}$ after PNG F are noted by '**' and '++' respectively, in the Lane 3, 'SPNT', Fig. 33B). The fact that the two GP_2 forms were both showing to a similar mobility shift and were never co-migrating after treatment with the amidase PNG F that removes almost all N-linked oligosaccharides, demonstrates that the proteins are not differing by their glycosylations but by their amino acid sequences. Analysis of the ultracentrifuged supernatants (Lanes 4 to 6, 'UC', Fig. 33B) and of the pelleted virions (Lanes 7 to 9, 'Virion', Fig. 33B) again confirmed that the higher molecular weight protein that is solely present in the virion fractions, was the insoluble membrane-bound GP_2, as shown by its absence in the UC fraction (Fig. 33B, Lanes 4 to 6 compared to Lanes 7 to 9). Furthermore, as observed for GP_2 in cells, (Fig. 33A), both GP_2 and $GP_{2\Delta}$ were only partially resistant to Endo H treatment. Indeed, proteins digested by Endo H were migrating faster than those that were mock-treated but slower than those digested with PNG F (Fig. 33B, 'SPNT', Lane 2 compared to Lanes 1 and 3 and Fig. 33C). In addition, no $GP_{2\text{-}RES}$ could be observed in the UC and virion fractions after deglycosylation. Interestingly, while similar results were obtained with the rVSV-GP-HS virus, a faint band that migrated in a similar fashion to $GP_{2\Delta}$ present in the clarified ('SPNT') and ultracentrifuged ('UC') supernatants was observed in the virion fraction after Endo H and PNG F treatments (Noted Δ?, Lanes 17 and 18, compared to Lanes 2-3 14-15). Of note, partially digested proteins following PNG F treatment are indicated by a '$' in the figure.

The observation of a form that behaved similarly to $GP_{2\Delta}$ following Endo H and PNG F treatments in viral particles would suggest that $GP_{2\Delta}$ could also in someway be incorporated in the virus. To confirm such observations, rVSV-GP-HS viral particles were first pelleted over a 20% sucrose cushion and were then resuspended and ultracentrifuged over a 20% and 60% sucrose cushion. In those conditions, the virus is present at the interface between the 60% sucrose and the 20% sucrose, preventing contaminations coming from the soluble proteins that cannot penetrate the 20% sucrose cushion. The virus was then collected at the interface

and was analysed as before, alongside the cell culture media ('SPNT') and the ultracentrifuged supernatant ('UC') (Fig. 33D).
In the clarified supernatant, the membrane-bound GP_2 and $GP_{2\Delta}$ were again observed (Lanes 1 to 3, 'SPNT', Fig. 33D) and both forms were partially resistant to Endo H ('*' and '+' respectively in the Figure) and fully sensitive to PNG F ('**' and '++' in the picture). In the virion fraction, in addition to the membrane-bound GP_2 that reacted similarly to Endo H and PNG F treatments as in the previous experiment (see Fig. 33B and Fig. 33D, Lanes 7 to 9, 'Virion'), this $GP_{2\Delta}$-like protein could again be detected. Indeed, in Lanes 8 and 9 ('Virion', Fig. 33D) a protein of lower molecular weight and that migrated at the same position as $GP_{2\Delta}$ in the soluble fraction ('UC') was seen following Endo H and PNG F treatments (marked by a '+' and '++' respectively; Fig. 33D, Lanes 4 and 7). This form presents in the viral particles acted similarly to the $GP_{2\Delta}$ present in the SPNT and the UC fractions after deglycosylation treatments. In this experiment, the amount of GP_2 or $GP_{2\Delta}$ partially digested by PNG F is higher than before (marked by a '$')

Taken together, those results show that (i) in cells, two different $GP_{1,2}$ proteins are produced: A $GP_{1,2}$ protein with a GP_1 subunit that is fully resistant to Endo H treatments and a GP_2 subunit that is partially resistant to Endo H and that then resembles the full-length glycoprotein produced during EBOV infection, and a second $GP_{1,2}$ protein, that has never been observed before this work, that has a mature GP_1 subunit but that has two GP_2 N-glycosylations that have complex N-glycans and that is as such completely resistant to Endo H treatment. We subsequently named this protein form $GP_{2\text{-RES}}$ (Fig. 33C, left panel) (ii) The virion-bound $GP_{1,2}$ and its shed form released from rVSV-GP infected cells are glycosylated similarly to the viral proteins released during *in cellulo* EBOV infection (Fig. 33C, right panel) and (iii) a detectable amount of $GP_{2\Delta}$ can be detected and incorporated into the viral particles in the context of rVSV-GP infection but the $GP_{2\text{-RES}}$ protein detected in cells is neither detected as a soluble form nor present in virus particles.

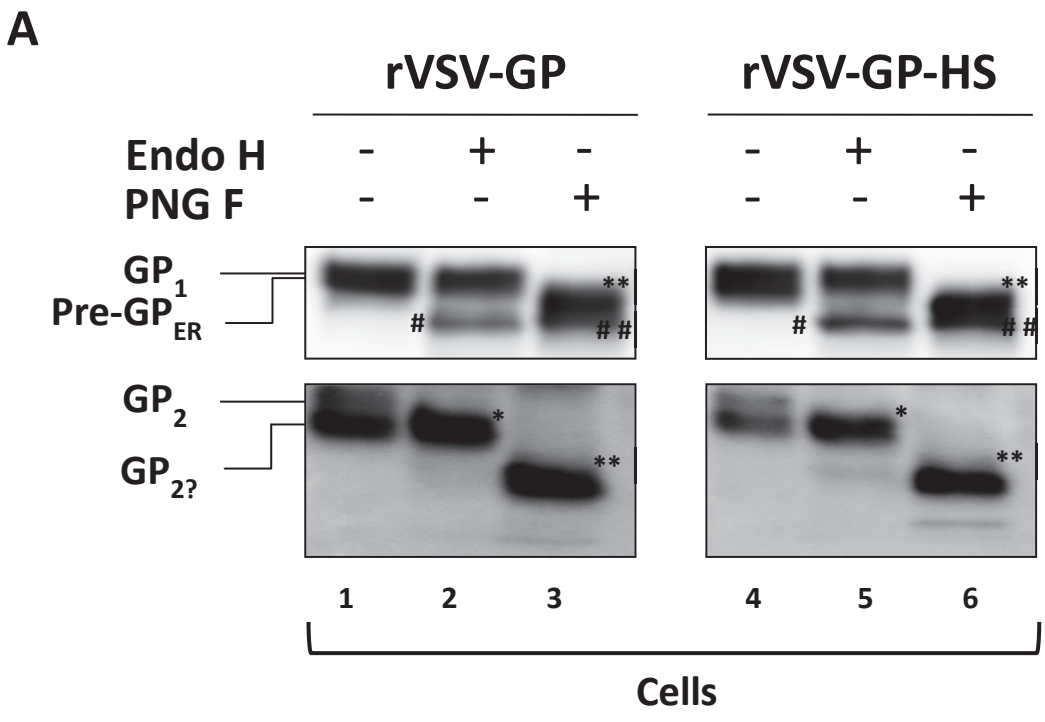

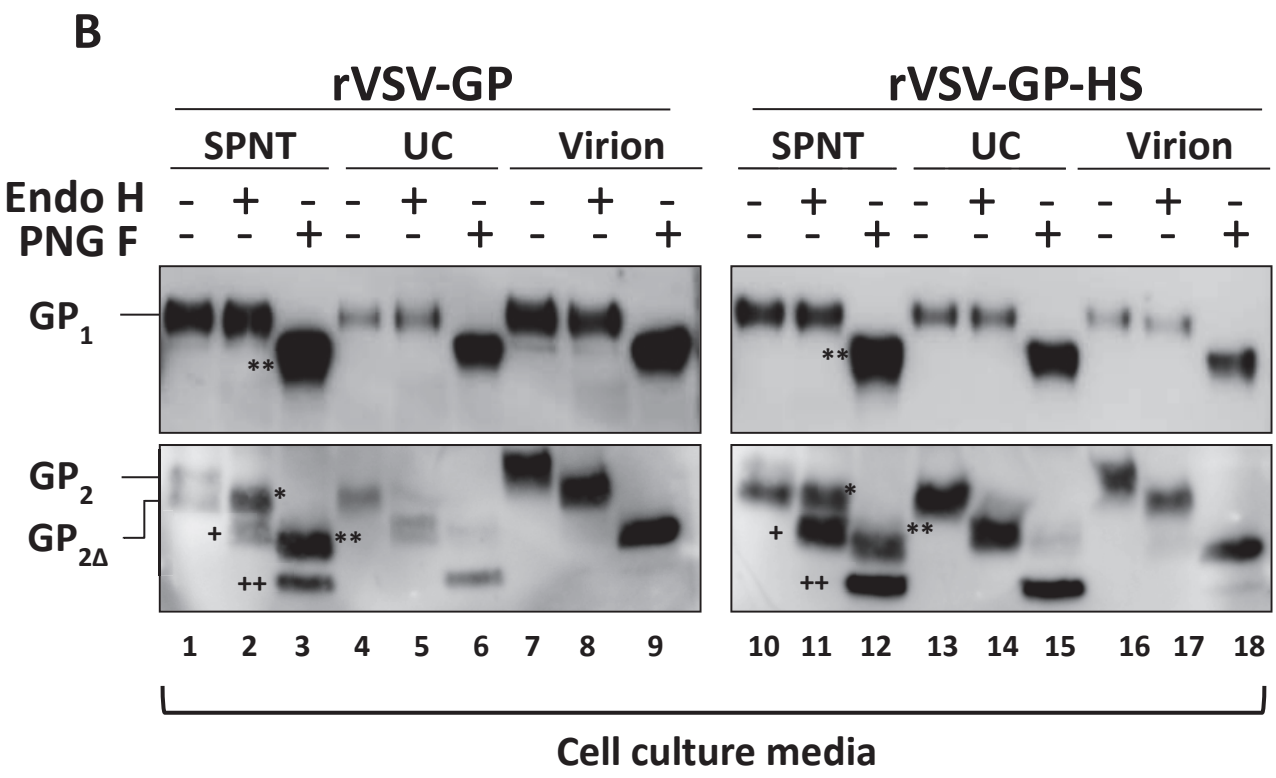
B
rVSV-GP
rVSV-GP-HS
SPNT
UC
Virion
SPNT
UC
Virion
Endo H
PNG F
GP1
GP2
GP2Δ
1 2 3 4 5 6 7 8 9 10 11 12 13 14 15 16 17 18
Cell culture media

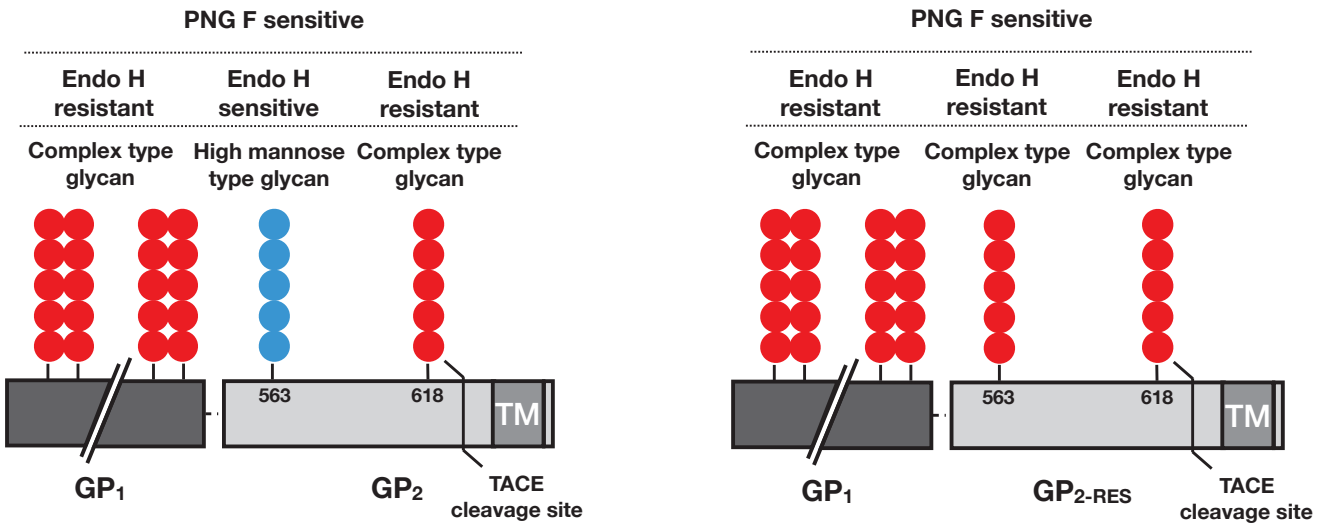
C
PNG F sensitive
Endo H resistant
Endo H sensitive
Endo H resistant
Complex type glycan
High mannose type glycan
Complex type glycan
563
618
TM
GP1
GP2
TACE cleavage site
PNG F sensitive
Endo H resistant
Endo H resistant
Endo H resistant
Complex type glycan
Complex type glycan
Complex type glycan
563
618
TM
GP1
GP2-RES
TACE cleavage site

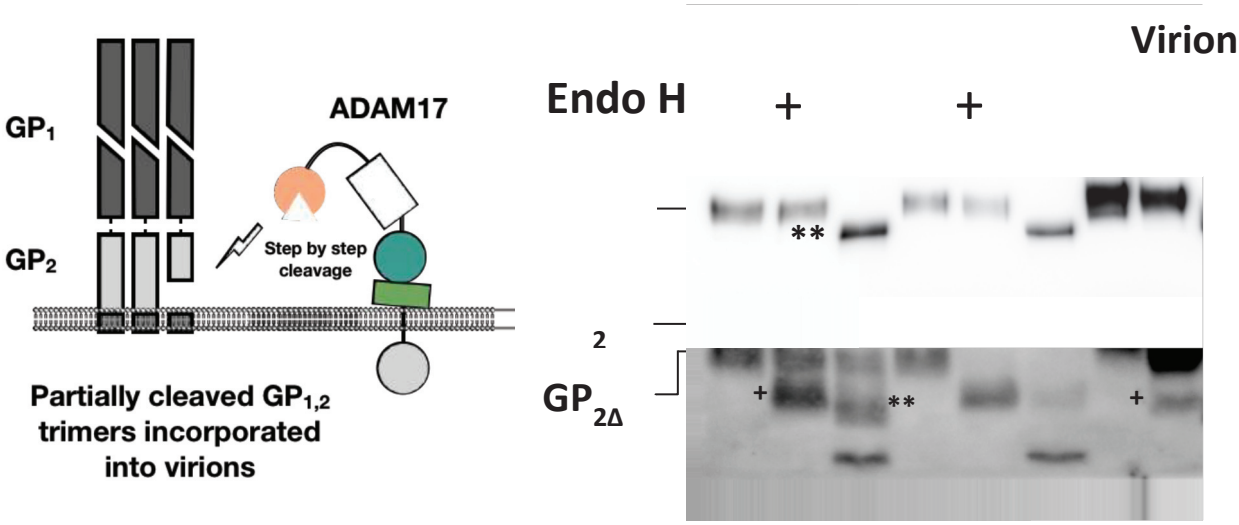

FIGURE 33. GLYCOSYLATION ANALYSIS OF SOLUBLE OR MEMBRANE-BOUND GP RELEASED DURING rVSV-GP INFECTION

VeroE6 cells were infected with rVSV-GP and rVSV-GP-HS at a MOI of 3 and the cells (A) and the cell culture media (I collected as before. Samples were boiled in laemli buffer and then were either mock-treated or incubated with the glyc Endo H or the amidase PNG F for 2 hours 30 at 37°C. Sampels were analysed by western-blotting as before. The scl representation of the N-glycosylations of $GP_{1,2}$ and $GP_{1,2\text{-RES}}$ are shown (C). The model for the incorporation of partially $GP_{1,2}$ molecules is presented (D, left panel). $GP_{2\Delta}$ incoporation into the viral particles was verified by loading the rVSV clarified supernatant on a double 60%-20% sucrose layers and ultracentrifuged. The virion that was at the interfac two sucrose layers was collected. Samples were then analysed by Endo H and PNG F (D, right panel). After deglycos with Endo H and PNG F, the position of Pre-GP_{ER}, GP_1 and GP_2 are indicated by a (#), (*) and after PNG F by a (**), respe $GP_{2\Delta}$ position after Endo H is marked by a (+) and after PNG F by a (++). ($) shows the position of partially d glycoproteins after PNG F treatments.

EXAMINATION OF EBOV $GP_{1,2}$ AND ADAM17 SPATIAL DISTRIBUTION DURING rVSV-GP INFECTION

The incorporation of a pool of partially cleaved $GP_{1,2}$ trimers in rVSV-GP viral particles has never been observed before with EBOV [150]. Considering that both EBOV $GP_{1,2}$ and ADAM17 are colocalised into lipid rafts, it is surprising that this incorporation appears to be limited. Indeed, this aberrant protein can only be detected following Endo H and PNG F treatments, suggesting that a mechanism exists to limit the cleavage of EBOV $GP_{1,2}$ trimers at the plasma membrane (Fig. 33D). In the absence of such mechanisms, the apparition of this partially cleaved glycoprotein into viral particles could be expected to be more important than what was observed here. It was previously shown, that uptake of viral glycoproteins into the budding particles was controlled by a segregation mechanism [322]. As such, we postulated that during the infection EBOV shedding would occur in a separate place than budding allowing to limit the incorporation of aberrant fusion-defective viral glycoproteins into the released virions.

In this respect, A549 cells were infected with rVSV-GP at a MOI of 1 and cells were fixed 24 hours post-infection and stained with anti-EBOV-GP_1 and anti-ADAM17 antibodies. Unpermeabilised cells were then examined by confocal microscopy and the localisation of both proteins at the plasma membrane was visualised following iso-surface 3D surface rendering (Fig. 34). In infected cells, EBOV GP_1 signal (Fig. 34, upper panel, in green) appears to be homogenously distributed at the plasma membrane. On the opposite, ADAM17 (Fig. 34, upper panel, in red) seems to be clustered in specific areas of the cellular membrane. This observation was confirmed following careful analysis of infected cells (Fig. 34, lower panel that shows the cells highlighted by the rectangle in the upper panel), that clearly shows that the cellular sheddase is not uniformly distributed alongside the plasma membrane compared to the viral glycoprotein that covers the surface of the infected cells. A similar result was observed in non-infected cells (Fig. 34, upper panel).

Therefore, this result suggests that ADAM17 is specifically clustered in compartments of the plasma membrane and that it only partially co-localise with EBOV glycoprotein during the infection.

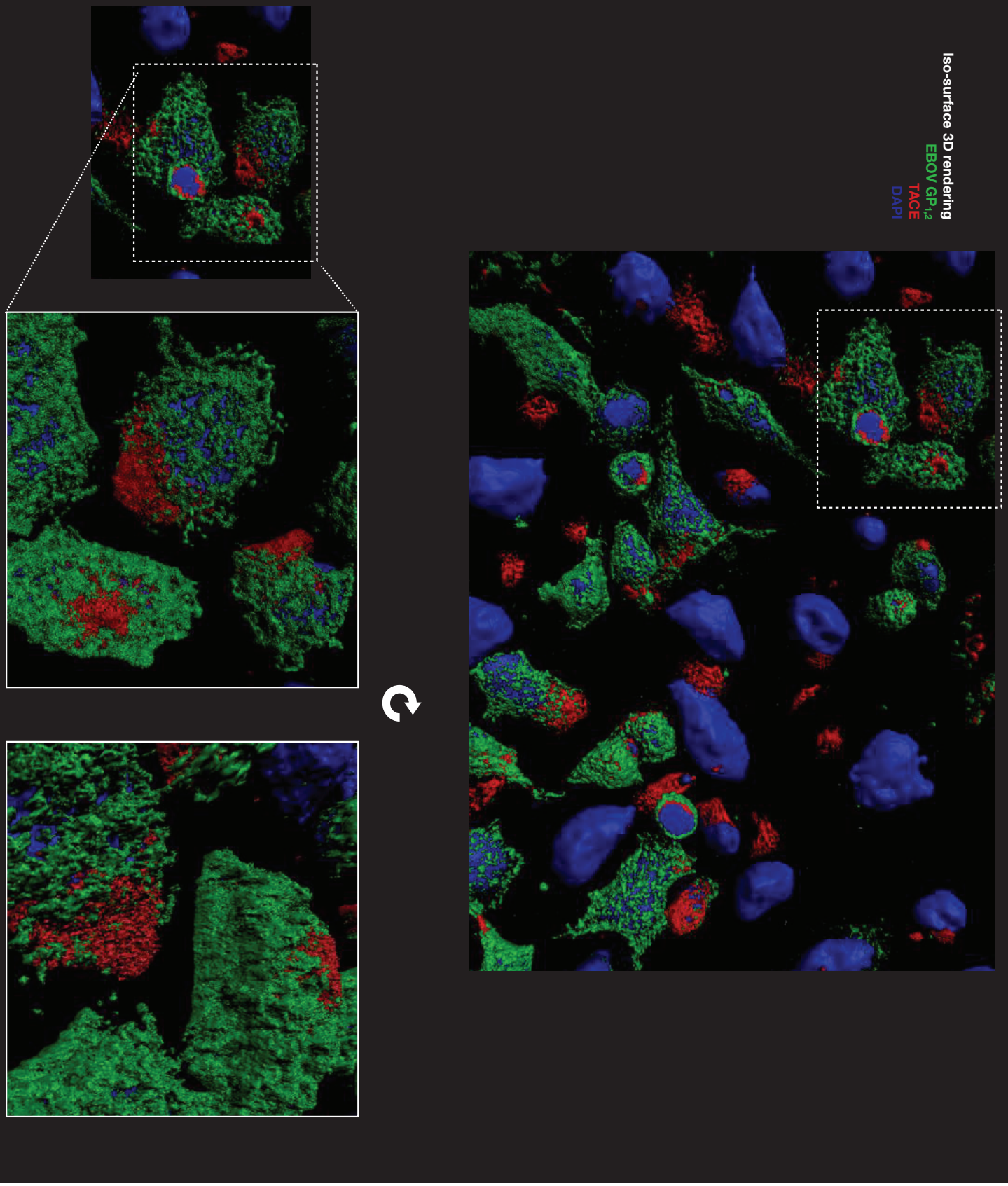

FIGURE 34. SPATIAL DISTRIBUTION OF ADAM17 AND EBOV $GP_{1,2}$ IN rVSV-GP INFECTED CELLS

A549 were infected at a MOI of 1 for 24 hours. Cells were then washed in PBS and fixed with 4% PFA. EBOV GP1 and ADAM17 monoclonal antibodies were used for labelling and imaged on a SP5 Confocal microscope with a Zeiss 1.4 Oil 64x lens. Dapi was used to detect nuclei. 3D reconstruction of cellular membrane was performed using the Imaris Software and the iso-surface rendering option.

The absence of $GP_{1,2\text{-RES}}$ in a soluble form or in viral particles could be due to a defect in its transportation to the plasma membrane. In this case, this protein should be expected to accumulate in the Golgi apparatus of infected cells and be largely absent from the plasma membrane.

To investigate this, rVSV-GP infected cells were collected and lysed in a hypotonic buffer and cellular organelles were separated through a 10%-30% iodixanol gradient by ultracentrifugation. Fractions of equal volumes were collected and analysed by western-blotting (Fig. 35A). ER fractions were revealed using an antibody directed against the ER chaperon-specific protein calreticulin; the plasma membrane and the Golgi-associated membrane proteins were detected with an antibody against Flotillin-2. Both Calreticulin and Flotillin-2 were detected in the first ten fractions and were enriched in some of those fractions. Indeed, Calreticulin was enriched in fractions 5 and 9 whereas Flotillin-2 was more concentrated in fractions 1, 5 and 9. This shows that fractions 1 and 5 contained plasma membrane- and Golgi-associated proteins and fraction 9 ER-associated proteins (Fig. 35A). EBOV GP_1 subunit was detected in all fractions collected but was also enriched in fractions 1, 5 and 9. The GP_2 subunit was only detected in the fractions that contained Golgi and plasma membrane-associated proteins (fractions 1 to 5) while the $GP_{2\text{-RES}}$ protein was also detected in the ER-associated fraction (Fractions 1 to 9). Interestingly, a GP-specific protein of higher molecular weight than GP_2 and $GP_{2\text{-RES}}$ was also observed starting from the fraction 9 and was not detected after the fraction 5 (indicated as '**', Fig. 35A).

To confirm the nature of the different GP proteins present in these three cellular fractions (noted as IO 1, IO 5 and IO 9, respectively, Fig. 35B) and to understand how the different viral glycoproteins are synthesised and transported, samples were treated with the glycosidase Endo H as above and the amounts of the glycoproteins were estimated using ImageJ (See Fig. 32, for the ability of the different GP forms to resist Endo H treatments depending on nature of the attached N-glycosylations and of their cellular localisation). Densitometry quantification of the GP_2 proteins is shown in Fig. 35C.
Unsurprisingly, Pre-GP_{ER} was majoritarily detected in the fractions corresponding to the ER and Golgi (Its position is noted '#', IO 9 and IO 5, Fig. 35B) and was almost undetectable in fraction 1. Whilst the Pre-GP/GP_1 band was still observable in the ER-associated fraction (IO 9), its levels were higher in the fractions associated with the Golgi and the plasma membrane as expected (IO 5 and 1, respectively).
The GP_2 subunit can be only detected as a unique subunit following Furin-dependant cleavage in the Golgi [120]. In this respect, the detection of a GP_2 of higher molecular weight that first appeared in the ER fraction (IO 9) and then accumulated in the Golgi fraction (IO 5, Fig. 35B and densitometry analysis Fig. 35C) was surprising. Following Endo H treatment, a shift in electrophoretic mobility of this product was observed, indicating that this form is Endo H sensitive and contained no mature glycosylations (noted by a '*' in the condition Endo H, fraction IO9). Based on its sensitivity to Endo H and its cellular localisation, this form appears to be the immediate result of the cleavage of Pre-GP_{ER} and it was thus named Pre-GP_2. In the Golgi apparatus/fraction IO5, a protein of lower molecular weight but that is fully Endo H resistant is detected alongside Pre-GP_2 and consequently corresponds to $GP_{2\text{-RES}}$. Of interest,

at the plasma membrane (fraction IO 1), we can detect both the partially sensitive GP_2 (noted '*' in the condition Endo H) and $GP_{2\text{-RES}}$ (Fig. 35B). Interestingly, densitometry analysis reveals that GP_2 represents only 12% of the total GP_2 proteins detected at the plasma membrane suggesting that the complex glycan $GP_{2\text{-RES}}$ form is able to reach and accumulate at the plasma membrane of infected cells (Fig. 35C).

This experiment demonstrates that (i) a non-glycosylated GP_2 precursor can be detected in rVSV-GP infected cells and that (ii) the additional complex glycan attached to GP_2 is not interfering with its transport to the plasma membrane.

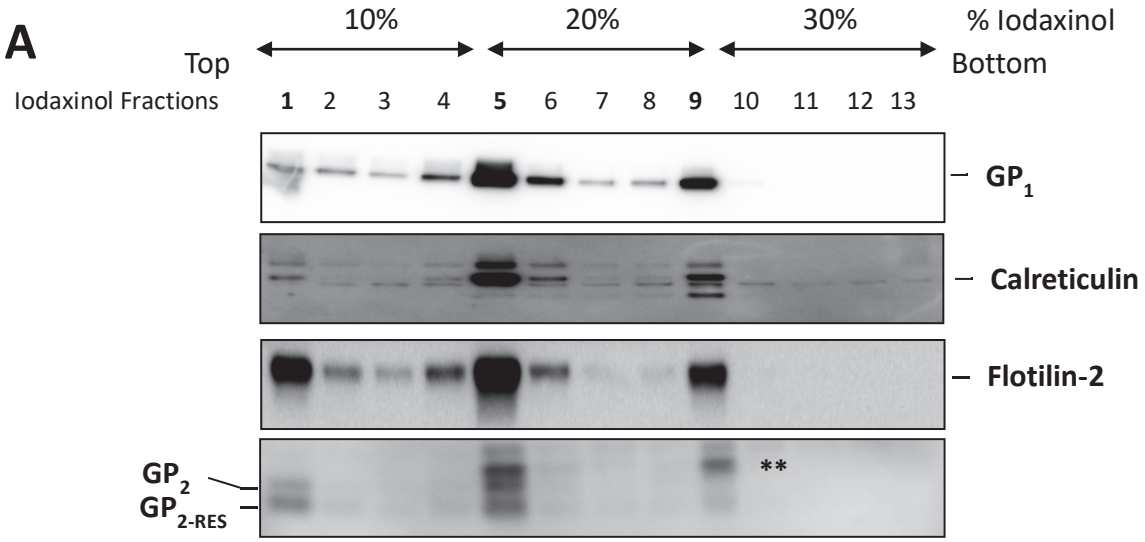

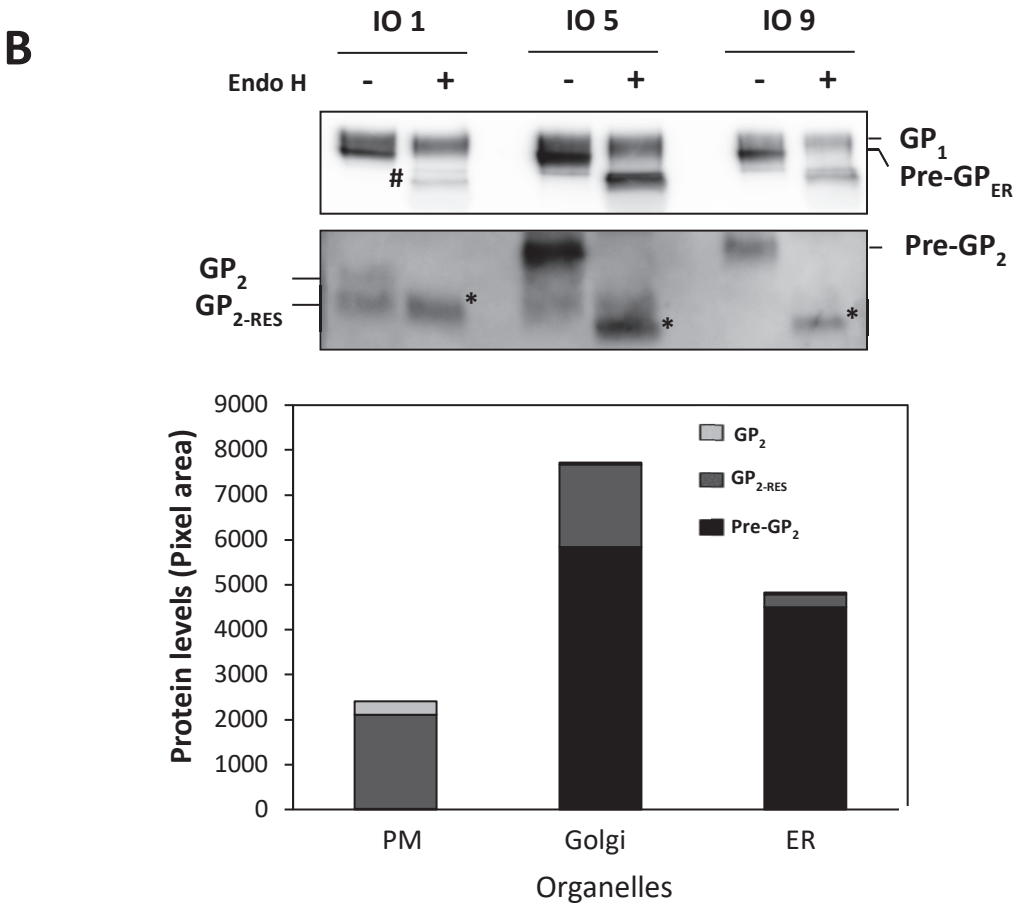

FIGURE 35. ORGANELLES SEPARATION FROM rVSV-GP INFECTED CELLS

rVSV-GP infected cells were collected 24 hours post infection and lysed in a hypotonic buffer for 30 minutes on ice. Nuclei were pelleted and the lysed samples were mixed with OptiPrep™ and organelles were separated by ultracentrifugation. Fractions of equal volumes were collected from the top and analysed as before. To detect GP1 and GP2 rabbit sera were used. Calreticulin and Flotillin-2 were detected with monoclonal antibodies (A). The Iodaxinol fractions 1, 5 and 9 were submitted to Endo H treatments and the amount of the different glycoproteins were quantified by ImageJ (B). After Endo H treatment, (*) indicates the position of GP_2, $GP_{2\text{-RES}}$ and Pre-GP_2, (#) of Pre-GP_{ER}

$GP_{1,2}$ AND $GP_{1,2\text{-RES}}$ LOCALISATION AT THE PLASMA MEMBRANE

The transport of $GP_{1,2\text{-RES}}$ to the plasma membrane but its absence in viral particles and rather its accumulation in cells could be the result of an accumulation of $GP_{1,2\text{-RES}}$ in other plasma membrane compartments than lipid rafts, where rVSV-GP budding and ADAM17 substrate cleavage are supposedly occurring [77,103,155].

To separate the membrane microdomains of rVSV-GP infected cells, cells were lysed in a lysis buffer containing the non-denaturing detergent CHAPS and a floatation assay was performed (Fig. 36) [289]. This protocol allows the separation of detergent-sensitive membranes (DSM) from detergent-resistant membranes (DRM) containing lipid rafts (LR). An antibody against the lipid raft-specific protein Flotillin-2 was used to visualize lipid raft localisation in gradient fractions. GP_1 and the different GP_2 proteins were detected and quantified as above (Fig. 36A). While detected in all fractions, Flotillin-2 was highly enriched in the top fractions 1 and 2. GP_1 was present in all fractions but was also enriched in fractions 1 and 2 and in fractions 7 to 9. GP_2 and $GP_{2\text{-RES}}$ proteins were observed in all fractions (Fig. 36A, upper panel). However, $GP_{2\text{-RES}}$ appeared to be more enriched in fractions 1 and 9 compared to GP_2, as shown by densitometry quantification (Fig 36A, lower panel, red curve).

Similarly to Fig. 35B, the natures of the viral glycoproteins were confirmed by subjecting the proteins from the fraction 1, 2 and 9 to Endo H and PNG F treatments. Treatments of the fractions 1, 2 and 9 revealed that the lipid-raft associated fractions 1 and 2 possess more Endo H-resistant mature Pre-GP/GP_1 than fraction 9, where Pre-GP_{ER} was principally detected (Fig. 36B, fractions 1 and 2 compared to fraction 9; Pre-GP_{ER} is indicated by a '#'). These observations would indicate that, the DSM fractions (fractions 6 to 9) contain Golgi and ER proteins and the fractions 1 and 2 contain majoritarily lipid raft-associated proteins.
The migration patterns of the two GP_2 proteins digested by Endo H and PNG F were identical to what was observed previously (See Fig. 33A). Indeed, after Endo H treatment the GP_2 protein co-migrated with the Endo H-resistant $GP_{2\text{-RES}}$ form. Additionally, both proteins were co-migrating when subjected to PNG F. This demonstrates that $GP_{2\text{-RES}}$ is properly transported to lipid rafts. Of note, following Endo H and PNG F treatments, of the 1 and 2 fractions, no $GP_{2\Delta}$ protein could be observed.

Consequently, it was again possible to confirm that $GP_{2\text{-RES}}$ is transported to the plasma membrane (Fig. 35) and that this complex glycan form of the protein is not excluded from lipid rafts where it appears to be enriched compared to GP_2 (Fig. 36A).

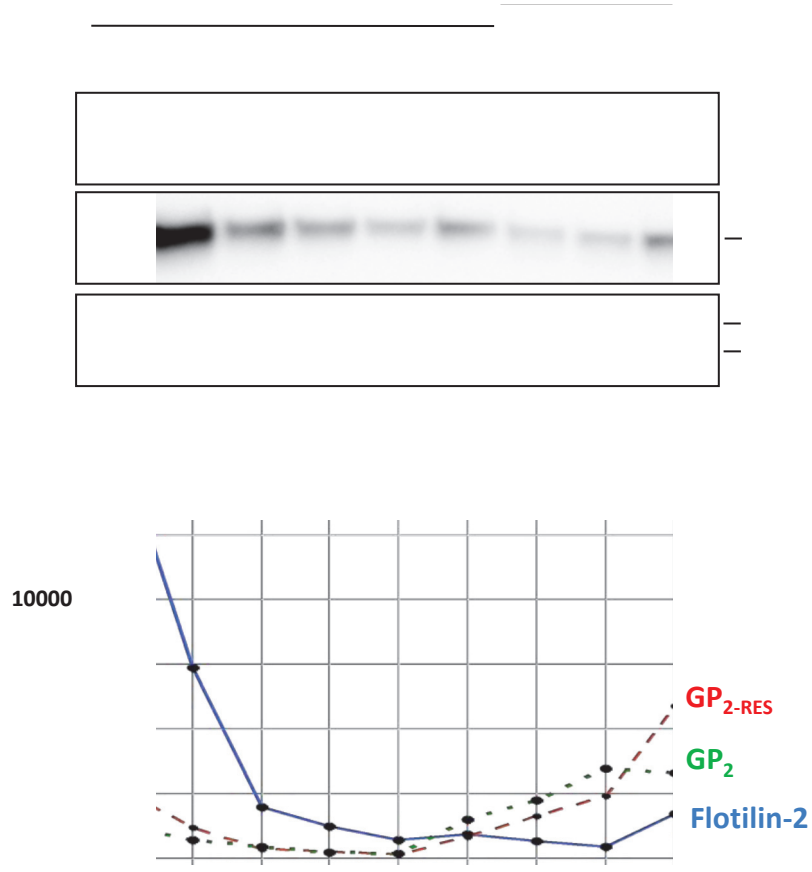

FIGURE 36. DETERGENT-SENSITIVE AND –RESISTANT MEMBRANE SEPARATION FROM RVSV-GP INFECTED CELLS.

After 24 hours of infection, rVSV-GP infected cells were scrapped in ice-cold DMEM 0%FBS, and washed twice in DMEM 0% FBS. Cells were lysed in a buffer containing 20mM of CHAPS for 30 minutes and the membranes were separated by ultracentrifugation. Fractions of equal amount were collected and analysed by western-blotting using an antibody recognising the Flotillin-2 protein or sera detecting EBOV GP1 and GP2. Protein levels were quantified as before (A). The position of the Lipid rafts (LR), the Detergent-resistent membranes (DRM) and the detergent-sensitive membranes (DSM) are indicated. The nature of the different glycoproteins presents in the Lipid rafts (fractions 1 and 2) and in the detergent-sensitive fraction 9 were investigated by Endo H and PNG F treatments and analysed by western-blotting (B). After deglycosylation with Endo H and PNG F, the position of Pre-GP_{ER}, GP_1 and GP_2 are indicated by a (#), (*) and after PNG F by a (**), respecitevly. $GP_{2\Delta}$ position after Endo H is marked by a (+) and after PNG F by a (++). ($) shows the position of partially digested glycoproteins after PNG F treatments.

The results obtained thus far would seemingly suggest that if $GP_{1,2}$ and $GP_{1,2\text{-RES}}$ are both present at the same sites of the plasma membrane but that no $GP_{1,2\text{-RES}}$ is incorporated into the virion, it is likely due to a mechanism that can control the incorporation of correctly glycosylated viral glycoproteins into the virion. $GP_{1,2}$ overexpression is detrimental for cells and its sustained presence at the plasma membrane leads to cellular damage and death [290,291]. Furthermore, it has been shown for other viruses that viral glycoproteins could alter membrane structures and their proper functions [292–294]. Cells infected with a rEBOV virus harbouring the L635V substitution have more glycoprotein incorporated into the viral particles than wild-type EBOV. This comes from the inability of the glycoprotein to be cleaved by ADAM17, leading to its accumulation at the plasma membrane and thus resulting in a more pronounced cytopathic effect [285]. We hypothesised that during the infection by a rVSV-GP virus with a low shedding phenotype (rVSV-GP-LS), the accumulation of the viral glycoprotein at the cell plasma membrane should saturate it, altering membrane structures and rendering the glycoprotein segregation system less efficient, thus leading to the formation of viral particles that contain both the $GP_{1,2}$ and $GP_{1,2\text{-RES}}$ proteins.

To confirm this hypothesis, a rVSV-GP virus with the L635V mutation was rescued as before and the presence of the mutation was confirmed by Sanger sequencing following amplification of the rescued virus on VeroE6 cells (Fig. 37A and 37B) [131,285]. VeroE6 cells were then infected and sedimentation analysis by ultracentrifugation were performed followed by Endo H and PNG F treatment as before to confirm the absence of shedding and the nature of the glycoproteins that were expressed in cells and released in the cell culture supernatant (Fig. 37C). In cells and similarly to before, a single protein was observed for GP_1 (Fig. 37C, upper panel and see Fig. 33). The Pre-GP_1/GP_1 Endo H-resistant form and the Pre-GP_{ER} Endo H-sensitive protein (the only one that was submitted to a change in electrophoretic mobility (noted '#', Fig. 37C, upper panel), were revealed after Endo H treatment. Again, both forms were sensitive to PNG F and were migrating closely following treatment, further demonstrating that Pre-GP_{ER} and Pre-GP/GP_1 are different, based on their glycosylation patterns but also in their protein sequence. For GP_2, two different forms were detected that should correspond to GP_2 and $GP_{2\text{-RES}}$, based on previous results (See Fig. 33). Endo H treatment showed that only the GP_2 protein was partially resistant as it co-migrated with the Endo H-resistant $GP_{2\text{-RES}}$ form (GP_2 position after Endo H is marked by a '*', Fig. 37C, upper panel). Both proteins were again PNG F sensitive and were co-migrating (GP_2 and $GP_{2\text{-RES}}$ PNG F sensitive proteins are noted '**', Fig. 37C, upper panel).

To investigate the incorporation of $GP_{2\text{-RES}}$ in the viral particles under these conditions using the mutant virus, the clarified supernatant ('SPNT') was ultracentrifuged over a 20% sucrose cushion and the ultracentrifuged supernatant ('UC') containing soluble glycoproteins and the pelleted virions ('Virion') containing virion-bound proteins were analysed as before (Fig. 36C, lower panel). In line with previous results, the GP_1 subunit was observed in all fractions as a unique protein that was resistant to Endo H treatments but was PNG F sensitive (GP_1 form after PNG F treatment is noted '**', Fig. 37C, upper panel, Lanes 1 to 9). Despite bearing the L635V mutant, GP_1 was still detected in lower quantity in the soluble fraction (Fig. 37C, 'UC', Lanes 4 to 6).

Interestingly, with the LS mutant two forms of the GP_2 protein were now detectable in the clarified supernatant and could correspond to GP_2 and $GP_{2\text{-RES}}$ (Fig. 37C, lower panel, 'SPNT',

Lanes 1 to 3 and see Fig. 33B for GP_2 and $GP_{2\Delta}$ analysis). Following Endo H and PNG F treatments ('SPNT', Lanes 2 and 3), a single band of high intensity could be detected (The deglycosylated proteins by Endo H or PNG F are noted '*' and '**', respectively). This means that the GP_2 band underwent a mobility shift while the protein of lower molecular weight migrated similarly to how it was already migrating in the mock condition. Furthermore, no $GP_{2\Delta}$ or $GP_{2\text{-RES}}$ proteins could be observed in the soluble fraction, suggesting that neither $GP_{1,2}$ nor $GP_{1,2\text{-RES}}$ are shed during rVSV-GP-LS infection as expected ('UC', Lanes 4 to 6), or are present in a very limited quantity, which cannot be detected with this assay. Notably, in virions, the two GP_2 proteins were observed and were co-migrating following Endo H and PNG F treatment ('Virion', Lanes 6 to 9, compared to 'SPNT', Lanes 1 to 3).

Based on those results, it is possible to conclude that (i) during rVSV-GP-LS infection, viral glycoprotein shedding is significantly reduced, similarly to what was observed with rEBOV-LS [285], and (ii) in a striking difference to rVSV-GP and rVSV-GP-HS viruses, where the 21 kDa $GP_{2\text{-RES}}$ protein was sequestered in infected cells, during rVSV-GP-LS infection, $GP_{1,2\text{-RES}}$ is incorporated into the viral particles and released in a virion-bound form into the supernatant of infected cells.

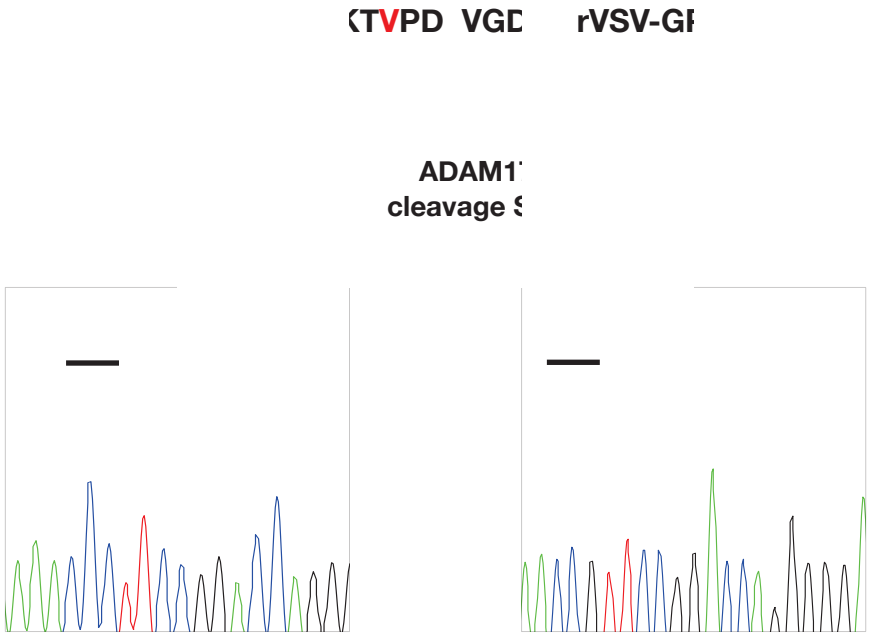

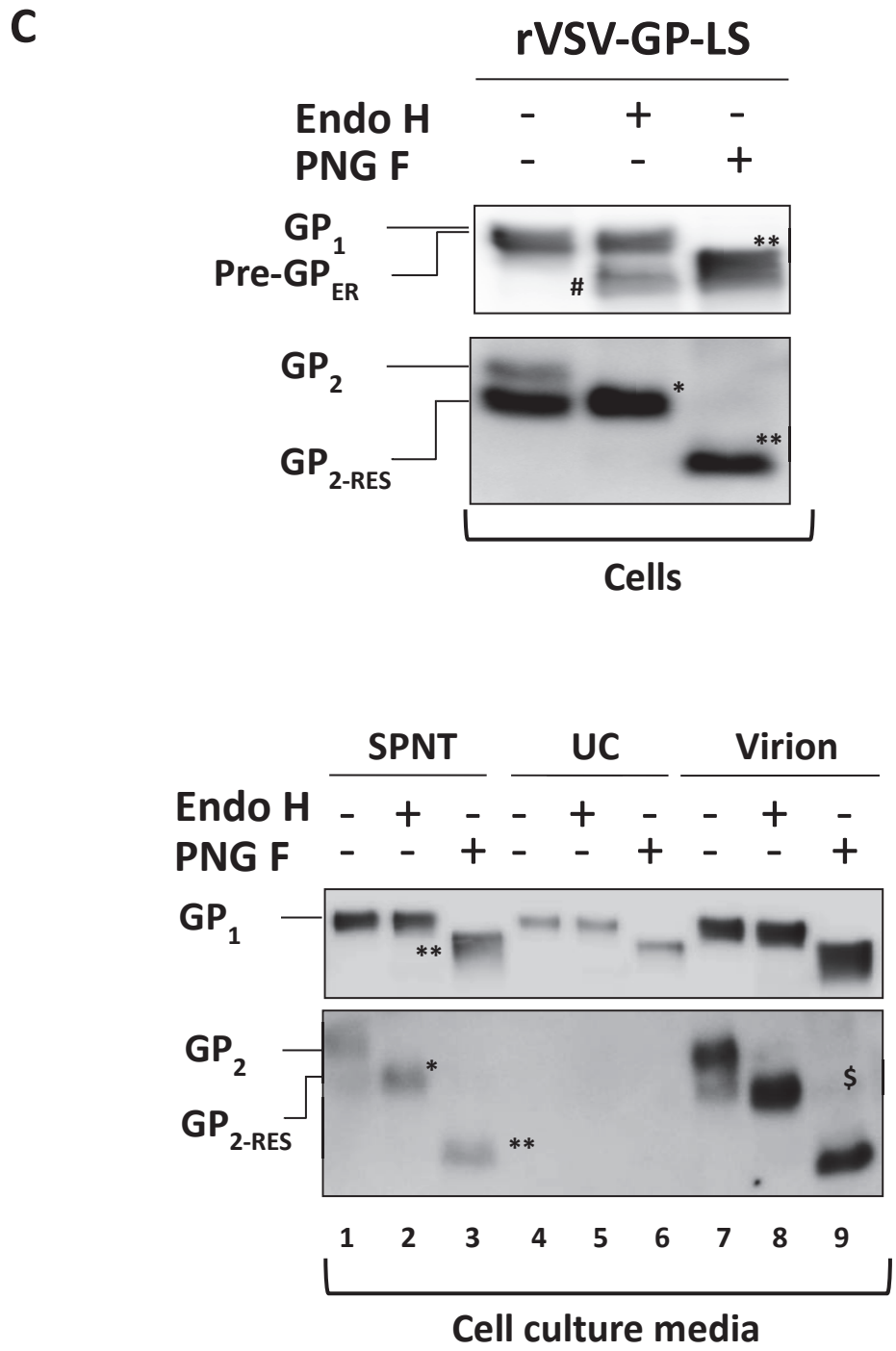

FIGURE 37. GLYCOPROTEIN GLYCOSYLATION PATTERNS ANALYSIS FROM RVSV-GP-LS INFECTED CELLS.

Schematic representation of the GP_2 sequence showing the position of the Low Shedding (LS) mutation (A, in red). After rescue and amplification on VeroE6 cells, the virus was sequenced to confirm the presence of the L635V substitution (B). Cells and supernatants (C) from rVSV-GP-LS were obtained and treated by Endo H and PNG F and the samples were analysed as previously. As before, after deglycosylation with Endo H and PNG F, the position of Pre-GP_{ER}, GP_1 and GP_2 are indicated by a (#), (*) and after PNG F by a (**), respectively. ($) shows the position of partially digested glycoproteins after PNG F treatments.

RELEASE OF sGP OR ssGP-LIKE PRODUCT DURING rVSV-GP INFECTION

During EBOV infection, it was shown that an EBOV virus with an altered editing site that should encode solely for the full-length glycoprotein product (8A genotype, see Fig. 13) was still able to produce sGP through mRNA editing or early termination [58]. Therefore, it was of interest to study if during rVSV-GP infection, the VSV polymerase was able to edit GP mRNA and therefore if similarly, the soluble proteins sGP and ssGP could be synthesised from the vector (Fig. 38 and see Fig. 13, for detailed explanations on sGP and ssGP synthesis).

Similarly to before, VeroE6 were infected with rSV-GP and the cells and supernatant were harvested and the soluble proteins were separated from the membrane-bound proteins by ultracentrifugation. Cells, clarified and ultracentrifuged supernatants ('Cells', 'SPNT' and 'UC' respectively), and the pelleted virions ('Virions') were then analysed for the presence of sGP or ssGP by western-blotting using a GP_1-specific monoclonal antibody in reducing ('+β-Mercaptoethanol) and non-reducing conditions ('-β-Mercaptoethanol'). In denaturing conditions, after a short exposure, only a single GP_1 protein that migrated around 130 kDa and that was present in all analysed fractions was detected (Fig. 38A, upper left panel). An increased exposure revealed an additional GP_1-specific protein of around 50 kDa (marked by a '*'; Fig. 38A, lower left panel). This protein of lower molecular weight appeared to be excluded from the virions but was present in cells and in the clarified and ultracentrifuged supernatant and could therefore represent the soluble viral proteins sGP / ssGP. In non-denaturing condition ('-β-Mercaptoethanol'; Fig. 38A, right panel), both GP precursors and mature proteins should be observed. In cells and as was shown by Volchkov V *et al.* (1998), Pre-GP_{ER} was detected in large quantities and was migrating faster than GP_1. Expectedly, this form was excluded from the clarified and ultracentrifuged supernatant as well as from viral particles (Fig. 37A, upper right panel). In addition, Pre-GP was also detected in small quantities and was also only present in the cellular fraction (Fig. 38A, lower right panel). With the exception of the soluble fraction ('UC'), where the protein was barely detected, the full-length mature 130 kDa $GP_{1,2}$ protein that is incorporated into the virus, was present in all fractions and in large quantities. Interestingly, a protein that migrated between $GP_{1,2}$ and Pre-GP_{ER} (noted '**') was detected in a soluble form, as it was only seen in the clarified and ultracentrifuged supernatants. Considering that it was not detected in cells nor in viral particles this protein could therefore represent $GP_{1,2\Delta}$ (Fig. 38A, lower right panel). Of special interest, a further protein at about 100 kDa could be detected with long exposure (noted '*' in Fig. 38A, lower right panel). It was first detected in cells and in higher quantities in the clarified supernatant. This protein was also present in the ultracentrifuged supernatant but was not incorporated into virions. Consequently, based on its molecular weight and its apparent soluble form, this protein is likely to represent dimers of either sGP or of ssGP.
To confirm the presence of sGP or ssGP during rVSV-GP infection, total RNA was collected from infected cells and mRNA were captured using polystyrene–latex particles that can bind to the mRNA poly(A) tails. The transcriptional editing site was then analysed by cloning and sequencing of GP-specific mRNA and the results are represented as sequencing chromatograms (Fig. 38B, GP editing site is shown). In infected cells, the unedited 8A mRNA (encoding for full-length $GP_{1,2}$) represented 97% of the total sequenced mRNA. Edited mRNA with the addition of one adenine (9A mRNA; encoding for ssGP) was observed in 1% of cases. The last 2% of the GP-specific mRNA sequenced were also edited, with the addition of up to 6 adenines but all mRNA were encoding for the full-length $GP_{1,2}$.

Consequently, it was possible to confirm that the VSV polymerase was able to edit the EBOV GP gene during infection and that a dimeric protein that is migrating at the same size as sGP and ssGP was observed in cells and the cell culture media. It would thus appear that sGP/ssGP forms are indeed able to be produced from infected cells in the context of rVSV-GP infection.

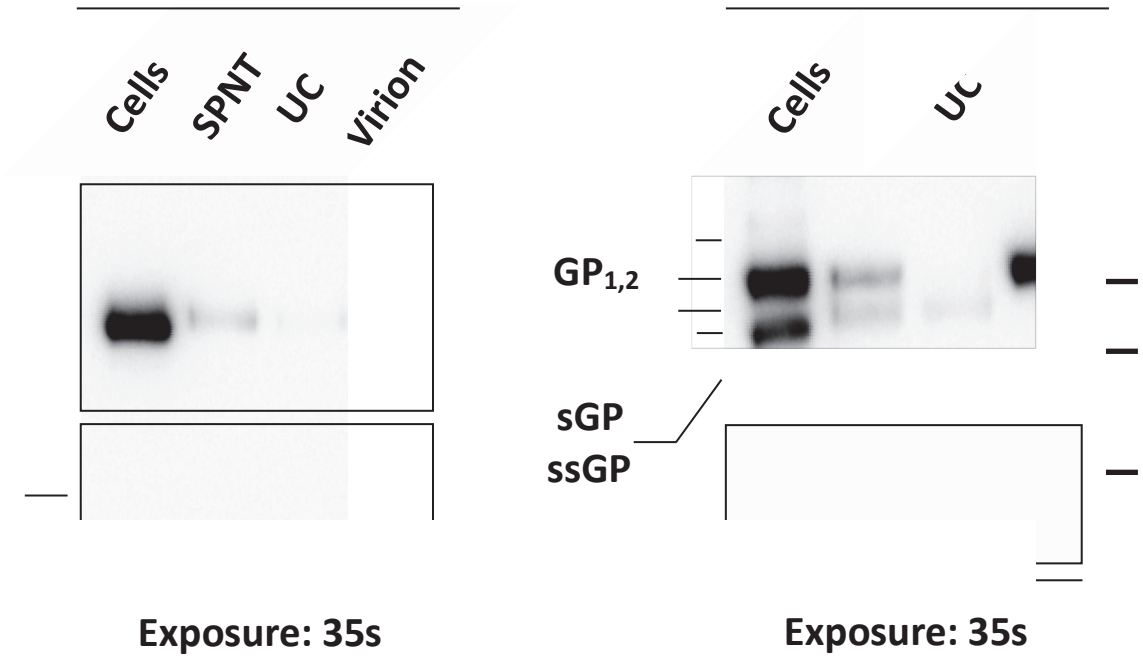

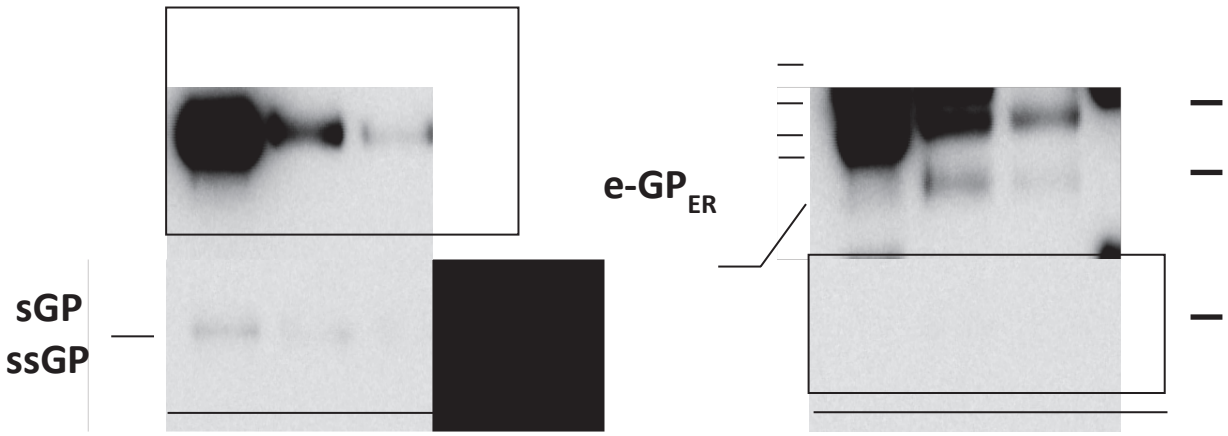

B

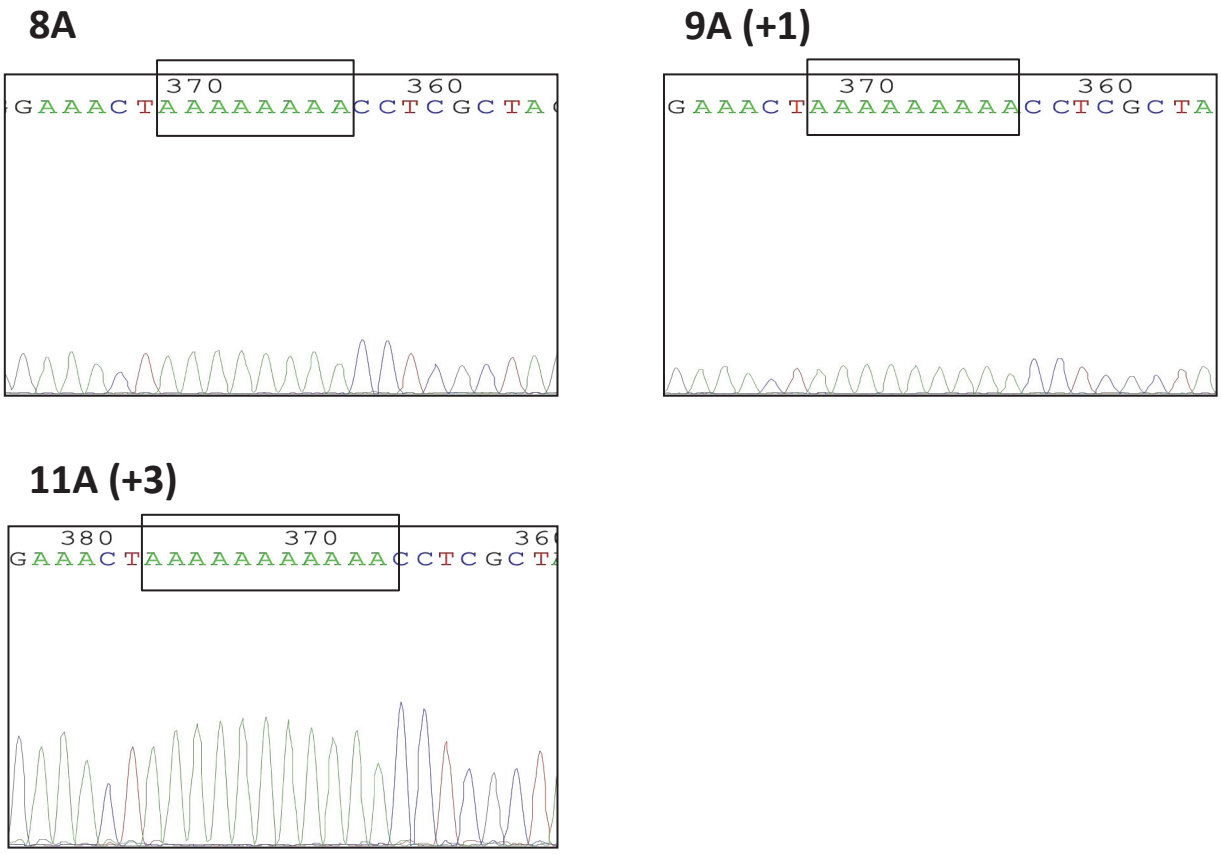

FIGURE 38. EBOV SOLUBLE GLYCOPROTEINS RELEASED THROUGH GP EDITING DURING rVSV-GP INFECTION

Cells were infected with rVSV-GP for twenty-four hours at a MOI of 0.1. Supernatant was collected and analysed as before (A). In parallel, RNA extracted from infected cells and mRNA were isolated, and cloned by RT-PCR into a puc19 plasmid. Single bacteria clones were sequenced using primers allowing sequencing of the editing site (B). Above the chromatogram are represented the total number of adenines observed and the number of adenines that are added compared to the 8A reference sequence.

ADAM17 ACTIVATION DURING rVSV-GP INFECTION

It has been previously demonstrated that during EBOV infection, ADAM17 was responsible for EBOV $GP_{1,2}$ ectodomain shedding [149]. However, the exact molecular mechanisms leading to shedding of the viral glycoprotein are not yet understood. Using rVSV-GP as a surrogate system, the different cellular pathways that could lead to ADAM17 activation and subsequently $GP_{1,2}$ cleavage were investigated.

Initially, the involvement of ADAM17 in EBOV $GP_{1,2\Delta}$ release during rVSV-GP infection was investigated using the metalloproteinase inhibitor marimastat. Briefly, VeroE6 cells were infected with either rVSV-GP or rVSV-GP-HS viruses for one hour, or the inoculum was removed and replaced by fresh media supplemented with FBS and the indicated concentrations of marimastat. As a negative control, an equal amount of DMSO to the lowest dilution of marimastat was used. Thirty-six hours post infection, cells and supernatants were

collected and analysed by western blotting as before. Additionally, samples were treated with Endo H to confirm the presence of $GP_{2\text{-}RES}$ or $GP_{2\Delta}$ (Fig. 39, upper panel) and the different amounts of $GP_{2\Delta}$ were quantified using ImageJ (Fig. 39, lower panel).

As expected, in cells infected with either rVSV-GP or rVSV-GP-HS, the GP_1 subunit was present as a unique band (Fig. 39, upper panel, Lanes 1, 3 and 5). After treatment with Endo H, the Endo H-sensitive Pre-GP_{ER} protein (noted '#') underwent a mobility shift, while Pre-GP/GP_1 were not affected by the deglycosylase (Fig. 39, upper panel, Lanes 2, 4 and 6). In addition, the amount of Pre-GP_{ER} and Pre-GP/GP_1 was similar for all marimastat concentrations, showing that GP_1 synthesis was not affected by the presence of the drug. In the clarified supernatant, the GP_1 subunit was released as a fully Endo H resistant form (Lanes 7 to 12). The presence of the metalloproteinase inhibitor did not seem to impact GP_1 levels (Lanes 7 compared to the lanes 9 and 11). For the different GP_2 subunits, it was possible to observe again two forms in cells. Endo H treatments confirmed that the GP_2 protein of lower molecular weight in cells was $GP_{2\text{-}RES}$ (Lanes 2, 4 and 6). Importantly, blockage of ADAM17 activity with different concentrations of marimastat resulted in an accumulation of GP_2 in infected cells for both viruses, as seen by an increase in GP_2 protein levels compared to the mock condition (Lanes 3 and 5 compared to Lane 1). This suggests that ADAM17 inhibition reduced the viral glycoprotein shedding leading to its accumulation. In agreement with our previous observations (Fig. 30B), cells infected with rVSV-GP or rVSV-GP-HS that were treated with DMSO released about 30% and 60% of $GP_{2\Delta}$ respectively, into the culture supernatants (Fig. 38A, Lanes 7 and 8; $GP_{2\Delta}$ is indicated by a '+' after Endo H treatment and see Fig. 39B for densitometry quantification). Accordingly to what was observed in cells, treatment with marimastat lead to an important reduction in $GP_{1,2}$ shedding. Indeed, $GP_{2\Delta}$ was no longer detected when cells were treated with 20mM or 200mM of marimastat (Fig. 39A, Lanes 11 and 12; Fig. 39B, 99% reduction in $GP_{2\Delta}$ protein levels). In cells infected with rVSV-GP-HS, a similar effect was observed for the highest concentration used, however cells treated with 20mM of Marimastat were still able to shed around 35% of $GP_{2\Delta}$.

Therefore, these results show that during rVSV-GP infection, ADAM17 is also involved in $GP_{1,2}$ shedding.

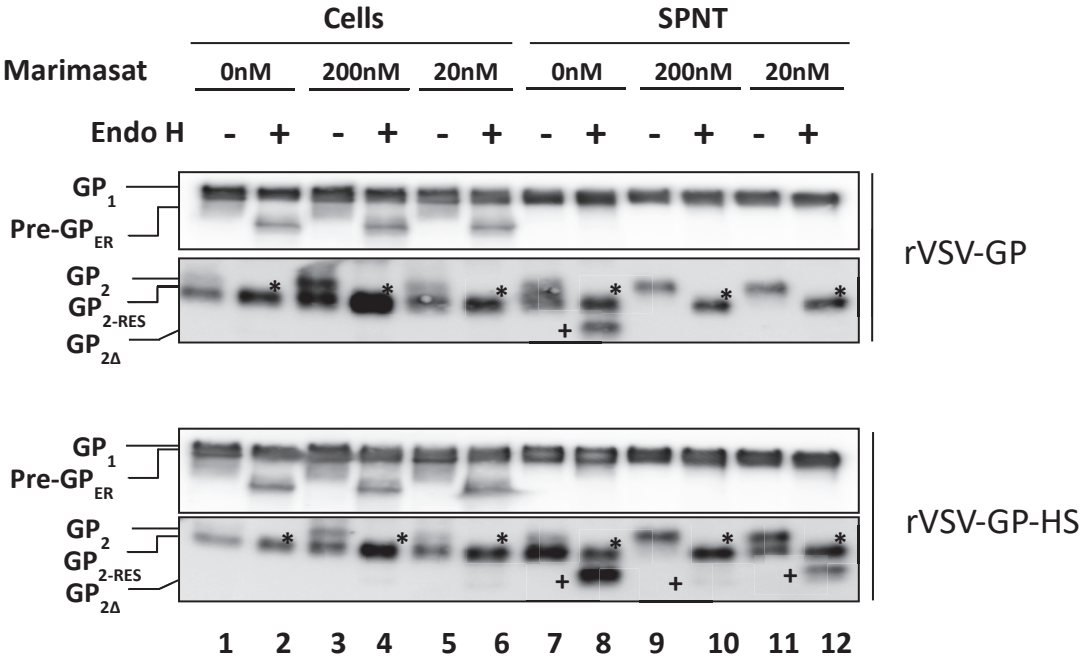

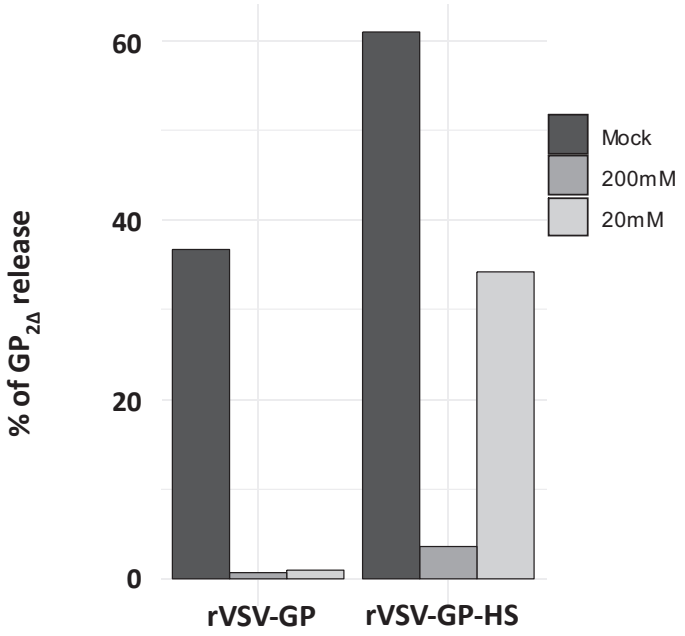

FIGURE 39. ROLE OF ADAM17 IN $GP_{1,2\Delta}$ RELEASE

VeroE6 cells were infected with rVSV-GP and rVSV-GP-HS at a MOI of 3. After one hour of infection, the inoculum was removed and the cells were cultivated in DMEM 3%FBS, in presence or in absence of marimasat. When cells were mock-treated, the same volume of DMSO was added to have the same amount of DMSO used than when cells were treated with the higher concentration of marimasat. For analysis, cells and supernatants were collected thirty-six hours post infection and were either mock treated or treated with Endo H and analysed by western-blotting. The positions of pre-GP_{ER}, GP_2 and $GP_{2\Delta}$ after Endo H treatment are indicated again by (#), (*) and (+) respectively.

To understand how ADAM17 is activated during the infection, the upregulation of several cellular pathways that were identified as key regulators for ADAM17 transport to the plasma membrane and its subsequent activation were studied. In this respect, we decided to investigate ERK1/2 and p38 activation. Indeed, ADAM17-ERK-dependant phosphorylation was shown to participate in its addressing to the plasma membrane and its phosphorylation by p38 prevents its dimerisation and interaction with its plasma membrane-associated inhibitor TIMP3 and therefore is necessary for its activation (See Fig. 19) [153,295] .

In this respect, cells were serum starved for six hours and then infected with VSV and rVSV-GP at a MOI of 5. Cells were then lysed and collected at the indicated time points and the phosphorylation of ERK1/2 and p38 were analysed by western blotting as markers of activation of their respective pathways (Fig. 40A). Following infection with either VSV or rVSV-GP, a rapid phosphorylation of ERK1/2 that peaked after 15 minutes of stimulation was observed. ERK1/2 phosphorylation returned back to its basal level after 60 minutes of infection in the case of VSV and after 120 minutes for rVSV-GP. While the phosphorylation profile of p38 for rVSV-GP stimulated cells was similar to ERK1/2, with a rapid induction followed by a continuous dephosphorylation of the protein, differences are observed for cells stimulated with VSV. Indeed, as for rVSV-GP, p38 is rapidly phosphorylated upon infection, however, no significant decrease in phosphorylation level could be observed in VSV infected cells within the time-course of the experiment.

ADAM17 requires interaction with phosphatidylserines to cleave its targets. This allows the ADAM17 catalytic domain to be brought closer to the membrane and to cleave its target

membrane proximal domains. In addition, it was shown that EBOV leads to phosphatidylserines externalisation in a $GP_{1,2}$-dependant manner. As such, the importance of phosphatidylserine exposure for $GP_{1,2}$ shedding was investigated using different concentrations of O-phospho-L-serine (OPS). OPS are molecules that resemble the phosphatidylserine head group and that was demonstrated to interfere with ADAM17 activity by competing with exposed cellular phosphatidylserines [103,155,225]. In this respect, cells were first infected and incubated with different amounts of OPS and $GP_{1,2\Delta}$ release was investigated by western blotting as before (Fig. 40B).
The GP_1 subunit was present in a single protein in both cells and in clarified supernatants ('SPNT'). No distinguishable effects were observed on GP_1 production or release when cells were treated with different amount of OPS. Analysis of the GP_2 subunit showed the presence of two GP_2 proteins. In cells, the GP_2 subunit of lower molecular weight corresponds to $GP_{2\text{-}RES}$ whereas in the supernatant it corresponds to $GP_{2\Delta}$. In the mock condition, and in accordance to what was observed in Figs. 29, 30 and 39, about 30% of the viral glycoproteins were released in the clarified supernatant as a truncated form (Fig. 39B, upper panel, Lane 6, 'SPNT' and see densitometry quantification, Fig. 40B, lower panel). Unexpectedly, cells treated with 12 mM and 6 mM of OPS were releasing twice more $GP_{2\Delta}$ compared to the mock condition. This increased shedding was associated with a subsequent decrease in GP_2 levels in cells (Lanes 2, 3 and 7 and 8). No effect on shedding was observed following treatment with 3 mM and 1.5 mM of OPS (Lanes 9 and 10, compared to Lane 6). In addition, OPS did not seem to affect $GP_{2\text{-}RES}$ production as no difference could be observed between the mock condition and treated cells.

As a result, in this set of experiments, it was possible to observe a rapid upregulation of the ERK1/2 and p38 pathways following VSV and rVSV-GP infection. Furthermore, contrary to what was previously published, the addition of soluble phosphatidylserine-like molecules increased $GP_{1,2}$ shedding in our hands.

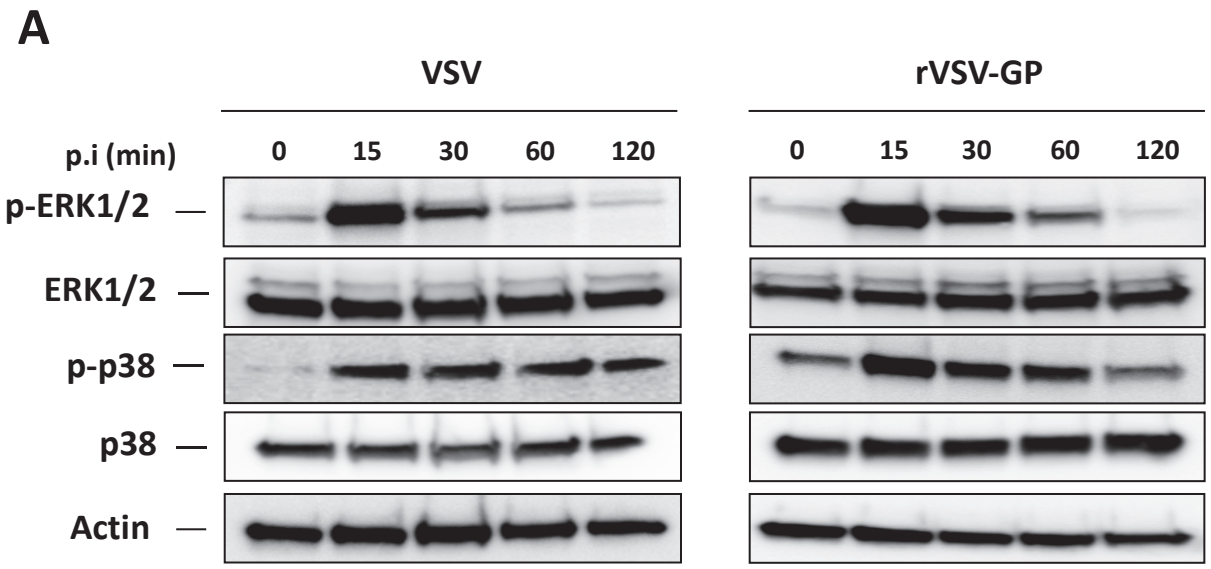

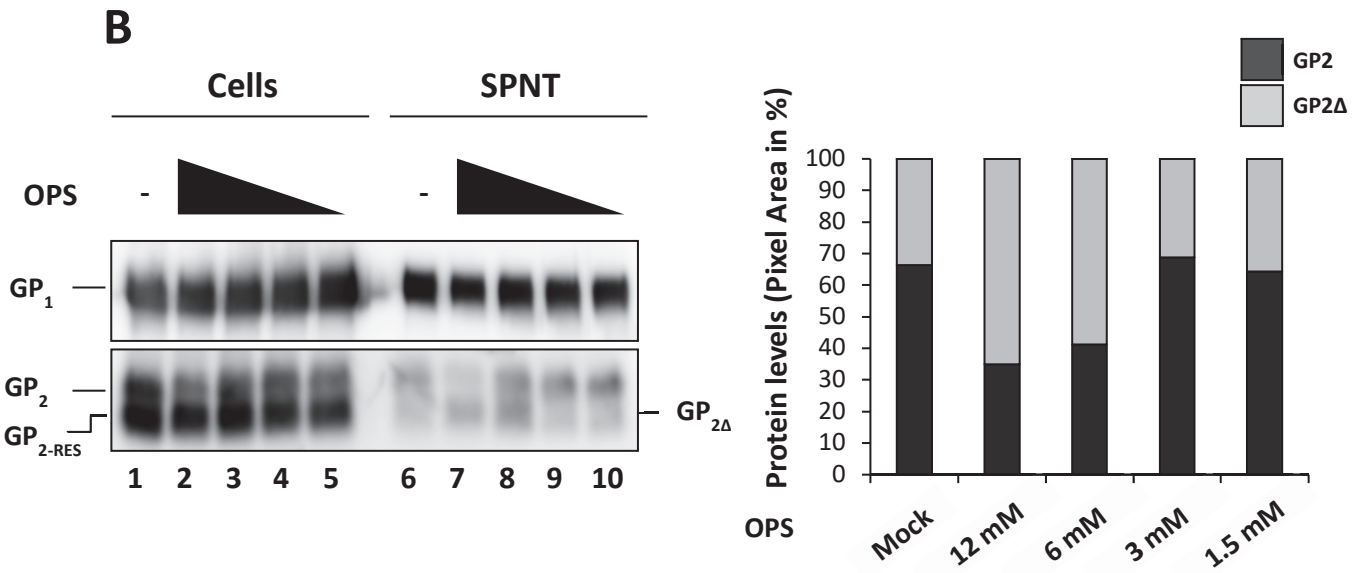

FIGURE 40. ERK1/2 AND P38 UPREGULATION DURING VSV AND rVSV-GP INFECTION AND ROLE OF PHOSPHATIDYLSERINE EXPOSURE IN SHEDDING CONTROL

VeroE6 were serum starved in DMEM 0%FBS for six hours. Cells were then infected in DMEM 0%FBS at a MOI of 5 with VSV and rVSV-GP. At the indicated time points, the supernatants were removed and the cells were lysed and scrapped in a ice-cold lysis buffer containing protease and phosphatase inhibitor cocktails. Cells were analysed by western-blotting and the proteins were revealed using antibodies directed against actin, ERK-1/2, p38 and their respective phosphorylated forms (A). For the analysis of the role of phosphatidylserine in ADAM17 activation, cells were infected with rVSV-GP at a MOI of 3 for one hour and the inoculum was replaced with DMEM 3%FBS. Six hours later, the media was removed and cells were incubated with fresh DMEM 3%FBS that was supplemented with decreasing amount of OPS (see below the densitometry quantification for OPS amount). Thirty-six hours post infection, cells and supernatants were harvested and analysed by western-blot. Protein levels were quantified using the ImageJ software (B).

CHARACTERISATION OF RVSV-GP-LS AND –HS MUTANTS

Recombinant EBOV (rEBOV) bearing either the LS or the HS mutations clearly affected $GP_{1,2}$ shedding as well as rEBOV viral growth and infectivity [239]. The effects of these phenotypes on rVSV-GP infectivity were studied to understand if similarly, differences could be observed during rVSV-GP-LS and -HS infection. Additionally, the molecular characterisation of these viruses could provide information on whether they can be used as BSL-2 model systems to study the role of shed GP in EBOV pathogenesis

In these experiments, VeroE6 cells were infected at a MOI of 0.01 and the supernatants of rVSV-GP (WT), -LS and -HS infected cells were collected at different time points and titrated by TCID50 (Fig. 41A). Distinctly to a rEBOV-GP-HS mutant that grew slower than its WT and LS counterparts, in the case of rVSV viruses, the wild-type grew faster than the other two viruses. This observation was confirmed by plaque assays that demonstrated that rVSV-GP-LS and -HS viruses were forming plaques that were statistically significant smaller than those seen with rVSV-GP. No differences could be observed between plaques formed by the rVSV-GP-LS and -HS viruses (Fig. 41B). To confirm whether $GP_{1,2}$ shedding activity, and by extension, the amount of $GP_{1,2}$ incorporated into viral particles could affect viral growth and infectivity, viruses were spun down by ultracentrifugation, resuspended and titrated. Different amounts of infectious units were then analysed by western blot and the ratio of TCID50/VSV-M was plotted as a measure of viral infectivity. Expectedly, compared to the wild type virus,

the high shed phenotype significantly reduced the amount of $GP_{1,2}$ incorporated into the viral particles whereas the low shed phenotype increased it (Fig. 41C, see GP_1 levels). Surprisingly, it appeared that only rVSV-GP-LS showed reduced infectivity compared to the other two viruses, indicating that the reduction in rVSV-GP-HS titer cannot be linked to a loss in infectivity.

Contrary to what was shown for EBOV, increasing or decreasing GP shedding ability negatively affected rVSV-GP viral growth. Only the low-shedding phenotype was associated with a decrease in rVSV infectivity compared to the other recombinant viruses tested.

A

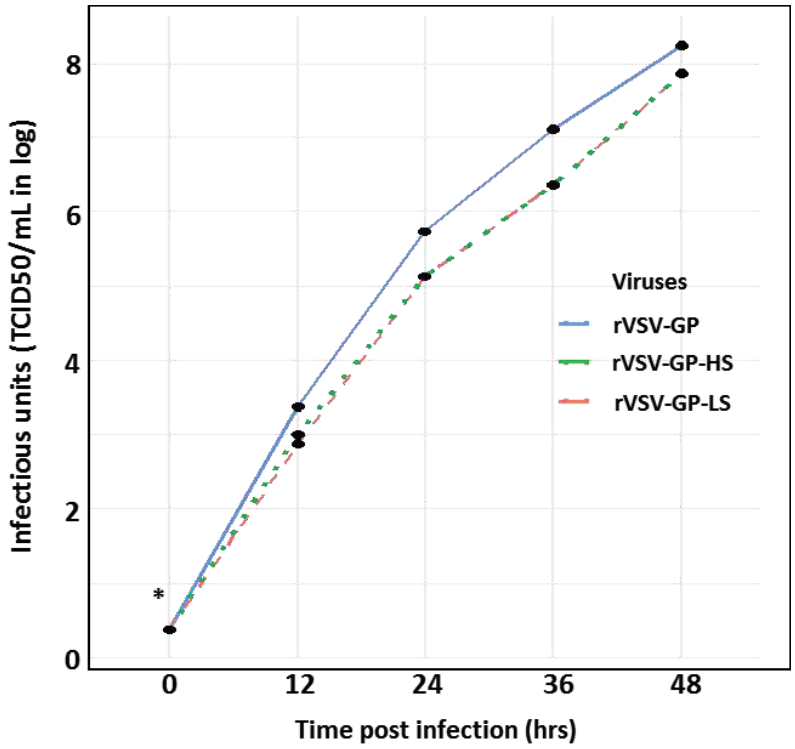

B

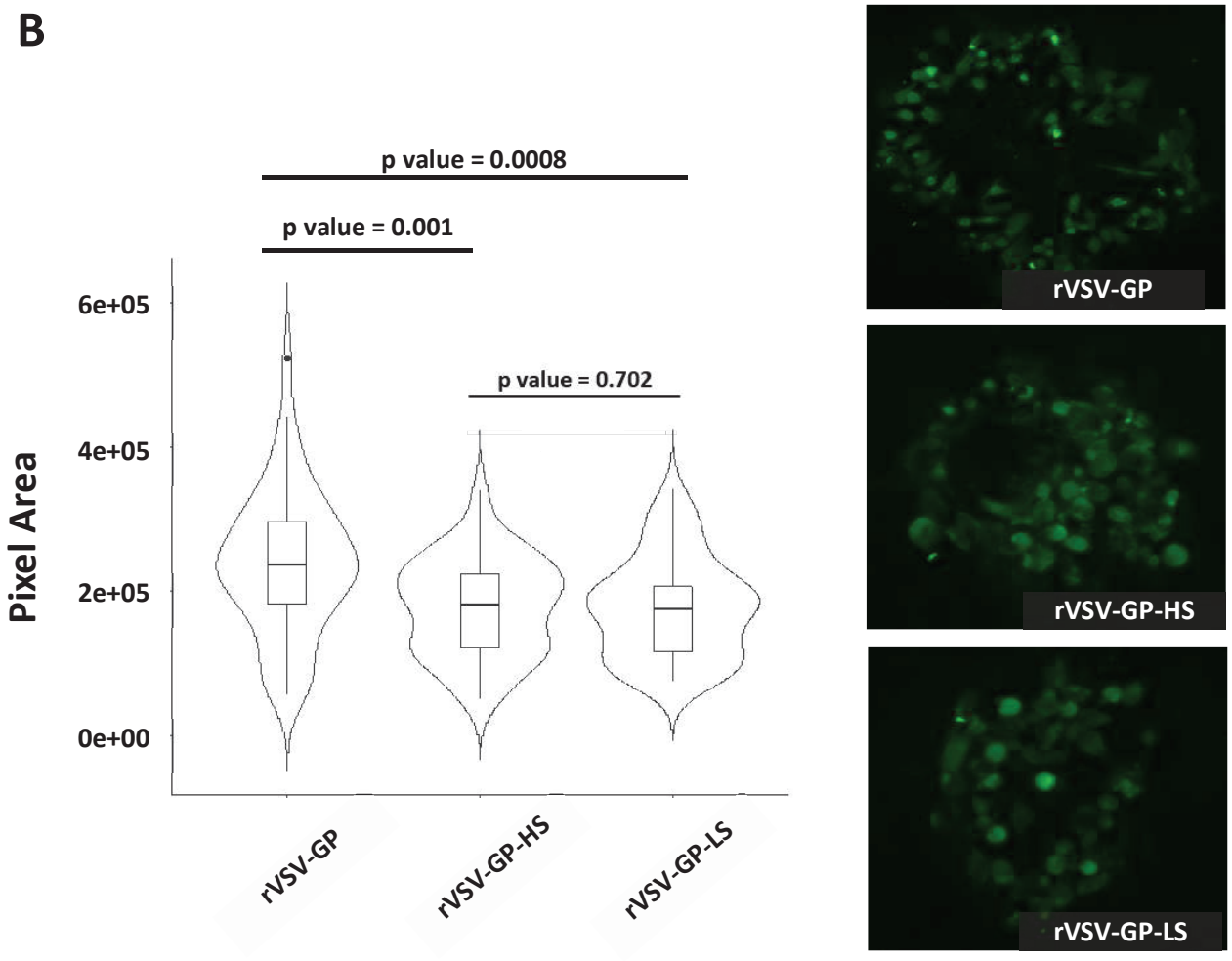
p value = 0.0008
p value = 0.001
p value = 0.702
Pixel Area
6e+05
4e+05
2e+05
0e+00
rVSV-GP
rVSV-GP-HS
rVSV-GP-LS
rVSV-GP
rVSV-GP-HS
rVSV-GP-LS

C

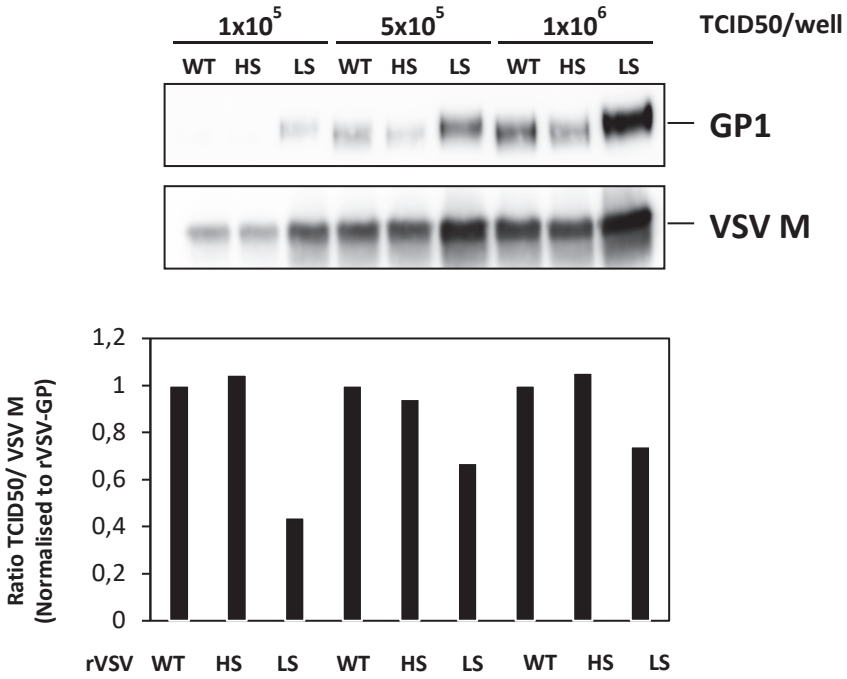
1x10^5
5x10^5
1x10^6
TCID50/well
WT HS LS WT HS LS WT HS LS
GP1
VSV M
Ratio TCID50/ VSV M
(Normalised to rVSV-GP)
1,2
1
0,8
0,6
0,4
0,2
0
rVSV WT HS LS WT HS LS WT HS LS

FIGURE 41. COMPARAISON OF RVSV-GP, -LS AND –HS VIRUSES INFECTIVITY

Cells were infected at a MOI of 0.01 and the virus growth kinetics of rVSV-GP, rVSV-GP-HS and rVSV-GP-LS viruses titrated by TCID50 are shown (A). Plaque assay performed on VeroE6 cells infected with the different rVSV-GP viruses and incubated in presence of Avicel© (B). Plaques were revealed by indirect immunofluorescence using monoclonal antibodies against EBOV GP_1 and VSV M and the size of 50 plaques per viruses are shown as a combined barplot and violin plot. Statistical analysis was performed using the Wilcoxon signed rank test. Pelleted viruses were titrated and similar amounts were loaded per well and analysed by western-blotting (C). The GP_1 and VSV-M proteins were detected using specific antibodies. The infectivity of each virus was calculated as indicated.

* The first timepoint did not fulfil the criteria to calculate the titer by TCID50 and were thus adjusted to the limit of detection of the assay which is of 2.34 TCID50/mL.

Recombinant VSV expressing EBOV $GP_{1,2}$ (rVSV-GP) has been widely used to investigate specific steps of the EBOV life cycle, and is now used as a prototype vaccine, however, so far and as detailed above, the potential release of soluble glycoproteins during rVSV-GP and their characterisation has never been studied even though these soluble forms have clearly been implicated in multiple steps of virus development and pathogenicity mechanisms and may also be crucial in influencing the potential success of a vaccine candidate.

As a first objective, we sought to investigate the potential release of $GP_{1,2\Delta}$ into the cell culture supernatant following inoculation with the rVSV-GP vector (Fig. 29). As the VSV M protein has been shown to stop cellular transcription and translation [306,307], it was uncertain if during rVSV infection, ADAM17 would be activated and allows shedding of the viral glycoprotein in this context. Our results show that in both VeroE6 and 293T cell lines, $GP_{1,2}$ is indeed shed from infected cells and that the truncated soluble $GP_{1,2\Delta}$ form is readily detectable in ultracentrifuged supernatants (Fig. 29A and B). Densitometry quantification showed that between, 10% to 25% of the total viral glycoproteins are released as a shed form and that this phenomenon appears to be cell-type dependant. These numbers are in line with what was previously observed during EBOV infection [285]. However, it should be noted that a higher MOI was used to infect 293T cells compared to VeroE6 in our set-up, as this cell line is known to be less infectable compared to VeroE6 [135], which could in part explain the differences in release of Shed GP between the different cell lines. In reducing conditions, we were able to detect the GP_1 subunit in both a soluble and membrane-bound form (Fig. 29A and B). Interestingly, in non-reducing conditions, it was possible to detect a soluble protein of a lower molecular weight than the membrane-bound $GP_{1,2}$ that could correspond to a $GP_{1,2\Delta}$ form (Fig. 38). These results indicate that the viral glycoproteins, whether they are released as a soluble or membrane-bound form, are all associated with the GP_1 subunit. This observation is, once again, consistent with previous data obtained with WT or rEBOV infection *in cellulo* [120,150]. The existence of $GP_{1,2}$ shedding was further confirmed through the generation of a rVSV-GP virus with a high shedding phenotype (rVSV-GP D637A-Q638V, 'rVSV-GP-HS', Fig. 30A and B). Infection with this mutated GP virus led to an increase of $GP_{1,2}$ shedding of at least three-fold (Fig. 30C). In addition, we were able to rescue a rVSV-GP bearing the mutation L636V, that was previously shown to block GP shedding in both an rEBOV infection and a GP transfection context (rVSV-GP L636V, 'rVSV-GP-LS', Fig. 37) [150,285]. Similarly, with the rVSV-GP-LS virus, no $GP_{1,2\Delta}$ could be observed in cell culture supernatants. Whilst we could observe the GP_1 subunit in the soluble ultracentrifuged fraction from cell culture supernatants, it is most likely to represent the GP_1 subunit of residual viruses that were not spun down in those conditions (Fig. 37C). In addition, we were interested to compare the kinetics of $GP_{1,2\Delta}$ release from rVSV-GP-infected cells to what has been observed in EBOV infected cells. As expected, we observed that viral particles were released exponentially following a latency phase of about 12 hours (Figs. 31 and 41). This latency phase corresponds to the time required for viral RNA synthesis, replication and protein translation, which limit the initial release of virus. On the other hand, $GP_{1,2}$ shedding appeared to be linear, suggesting that the only parameter regulating its release is its recognition at the plasma membrane by the sheddase ADAM17 and subsequent cleavage [308–311]. Furthermore, the unceasing cleavage and release of $GP_{1,2}$ as a truncated form suggests that the cellular enzyme is rapidly and continuously activated during infection (Fig. 31).

It is known that the release of sGP into the extracellular environment from EBOV-infected cells participates in the extreme pathogenicity associated with this virus by preventing antibodies from neutralizing the surface glycoprotein and by limiting GP cytotoxicity during viral replication [58,121,123,126,134,290]. In addition, it was shown that during the infection with a rEBOV with an “8A” genotype, which should encode only for the full-length glycoprotein $GP_{1,2}$ (see Fig. 13. for GP editing), the soluble protein sGP was still detected in significant quantities in the cell culture media [58]. Therefore, it was of interest to investigate if during infection with the rVSV-GP vector, which also has an 8A genotype, we could detect the release of sGP or ssGP from infected cells that could hamper a proper antibody-mediated immune response in a vaccination context. Our results demonstrate that we were able to detect a ~100kDa dimeric protein that could correspond to sGP or ssGP proteins in rVSV-GP infected cells and in their supernatants (Fig. 38A). To confirm our results, we cloned and sequenced GP-specific mRNA from rVSV-GP infected cells to investigate the presence of edited GP-mRNA (Fig. 38B). Indeed, with an 8A genotype virus, the only possibilities to have sGP or ssGP produced are through transcriptional editing (sGP: +2A mRNA; ssGP:+1 mRNA) or through residue skipping (sGP: -1A mRNA; ssGP: -2A mRNA). Our results showed that 97% of the GP-mRNA were non-edited and had the expected 8 adenines at the GP editing site. Of interest, in the remaining 3% of GP-mRNA, editing events were observed and between 1 to 6 additional adenines inserted at the editing site were detected. However, we were not able to observe any “7A” mRNA, suggesting that the polymerase is not able to skip a residue during transcription. These results demonstrate that, similarly to other viruses, the VSV polymerase can edit GP mRNA and this would lead to the production and release of ssGP and/or sGP during the course of the infection [117]. However, VSV’s capacity for editing in this context appears reduced compared to the EBOV polymerase, where up to 20% of edited GP mRNA is commonly detected depending on the cell-type, suggesting differences in polymerase fidelity and the importance of this function for EBOV infection, as already suggested [58,70,125].

In previous studies in our laboratory, during EBOV infection, the LS mutant showed no difference in growth kinetics and infectivity compared to the wild-type virus. On the other hand, the HS mutant was clearly affected by the drastic increase in $GP_{1,2}$ ectodomain cleavage, leading to a lower incorporation of the glycoprotein into viral particles and resulting in slower growth kinetics and infectivity [285]. Considering the differences in growth kinetics that exist between rVSV and EBOV (a complete VSV replication cycle is in the order of 8-10h), we wondered if rVSV-GP viruses with modified shedding sites would also show differences in growth kinetics and viral titers when compared to the wild-type-GP rVSV virus (Fig. 41). As expected, compared to the wild-type GP virus, the high shed phenotype reduced the amount of $GP_{1,2}$ incorporated into the viral particles whereas the low shed phenotype increased it (Fig. 41C). However, in a striking difference to what was observed with rEBOV, both the rVSV-GP-LS and -HS mutants grew to lower titers than the wild-type GP virus (Fig. 41A). Comparable results were obtained with a plaque assay that demonstrated that the mutant viruses were forming statistically significant smaller plaques (Fig. 41B). In addition, a reduction in infectivity was only found for the rVSV-GP-LS virus, as evidenced by the fact that more viral particles were needed to obtain a similar titer to that obtained with rVSV-GP and -HS viruses (Fig. 41C). Of importance, in a previous study Dolnik O *et al.* (2015) measured rEBOV viral infectivity by comparing the amount of VP24 proteins present in the clarified culture supernatant, whilst, here, viral particles were first spun down by ultracentrifugation before being titrated and analysed by western-blotting. The rEBOV-LS phenotype increases GP cytotoxicity due to a

lack of shedding and a subsequent accumulation of the full-length viral glycoprotein at the plasma membrane [134,285,290]. It is therefore possible that, in the context of rEBOV-LS infection, viral proteins are further released in the cell culture media in unpelleted soluble forms, which could have also mask any potential loss of infectivity, as it has been shown for HIV [312]. Nevertheless, in this work, rVSV-GP-HS was also growing to lower titers, whilst being seemingly less cytotoxic and as infectious as rVSV-GP. Interestingly, another study similar results with HIV vectors that were pseudotyped with different amounts of EBOV $GP_{1,2}$ [313]. In this study, the authors showed that pseudotyped viruses lost infectivity when the virions were incorporating more $GP_{1,2}$. Their results alongside ours, suggest that a necessary, fine-tuned balance exists between the amount of $GP_{1,2}$ present in the viral particle and viral infectivity. While rVSV and HIV virions have similar sizes, EBOV is at least 5 times bigger, leading to differences in GP density at the surface of the different viruses. Indeed, when incorporating less $GP_{1,2}$, the density of the glycoproteins presents at the surface of a virus smaller than EBOV would still be more important and appears to be enough to maintain infectivity (Fig. 41C, rVSV-GP and -HS M proteins levels compared to rVSV-GP-LS). However, when more $GP_{1,2}$ are incorporated into a smaller virus, steric hindrance could occur and could prevent the ability of the glycoproteins to interact with cellular receptors reducing its infectivity. As it was observed with a rEBOV system, a high shedding phenotype also appears to reduce growth efficiency in a rVSV context. However, differently to EBOV, no difference in terms of infectivity was observable between rVSV-GP and rVSV-GP-HS viruses. It is not yet known if uptake of $GP_{1,2\Delta}$ in cells occurs and if this process might allow it to interact with intracellular partners of EBOV $GP_{1,2}$ such as Cathepsins or NPC-1. However, as it is known that soluble $GP_{1,2\Delta}$ binding can activate immune cells in a TLR-4 dependant-manner [131], it is likely that this glycoprotein can also compete with the membrane-bound $GP_{1,2}$ for cellular attachment receptors, which could also help to explain why the high shed variant is growing more slowly and is forming smaller plaques than the rVSV-GP virus, while maintaining its infectivity [131].

EBOV $GP_{1,2}$ glycosylations are known to be key elements for correct protein folding and trafficking and are also known to play an important role in EBOV $GP_{1,2}$ functions, especially for its immunogenicity [136,267–269]. Synthesis of the glycoprotein starts in the endoplasmic reticulum as a Pre-GP_{ER} precursor where it will first acquire immature N-glycans (High mannose N-glycosylations), and then be further processed in the Golgi apparatus into Pre-GP where it will be cleaved into the subunits GP_1 and GP_2 by the cellular proprotease Furin. Before cleavage by Furin and before being transported to the plasma membrane as a mature trimeric protein $GP_{1,2}$ that will be inserted into the host-derived viral membrane, pre-GP will acquire mature N-glycans (Complex type N-glycosylations) as well as multiple O-glycans, which are mostly attached to the mucin-like domain. In EBOV infected cells, it was shown that it is possible to discriminate between the Pre-GP_{ER} and the Pre-GP/GP_1 forms based on their resistance to Endoglycosidase H (Endo H) treatment, as detailed above. In this respect, Pre-GP_{ER} is Endo H sensitive, while Pre-GP and the mature GP_1 subunit are all Endo H resistant. In addition, of the two N-glycosylation sites present in GP_2, only one has complex N-glycans rendering GP_2 subunits partially resistant to Endo H treatments. Conversely, $GP_{1,2}$ glycosylations are all removed by treatments with the amidase Peptide N-glycosidase F (PNG F) (Fig. 32) [115,143]. Of important note, it was demonstrated for some vaccine candidates against EBOV, that mutations in the viral glycoprotein could strongly modify the protective nature of the vaccine [248,257]. For instance, and as stated in the introduction (Paragraph ‘Therapeutic approaches against Ebola virus’), animals that were challenged with a Kunjin

virus replicon-based vaccine that expressed a GP-anchorless form, died from subsequent EBOV infection despite developing antibodies against $GP_{1,2}$ following vaccination. On the contrary, animals challenged with a Kunjin-virus that expressed GP with or without this deletion survived. Comparable results were obtained in a recombinant Adenovirus vaccine system [257]. Interestingly, it was shown that the anchorless GP was released as a monomeric form and not as a "natural" trimeric form as is seen with the membrane-bound or soluble shed GP forms [131,150]. These results emphasise the importance to have vaccines that express a GP that highly resembles the ones expressed during EBOV infection for protection. It was therefore of interest to study if the glycoproteins produced during rVSV-GP infection were similar to those evidenced during EBOV infection, which could help to provide further information on the potential ability of the vaccine to provoke efficient neutralizing antibodies against EBOV and to better understand the process by why animals are equipped to survive infection after rVSV-GP vaccination. Furthermore, a better understanding of the nature of the viral glycoproteins that are able to elicit an efficient and protective response can help us to develop better vaccine candidates in the future. The results presented here allow us to confirm that the viral glycoproteins that are either incorporated into the viral particles or shed from cells infected with the rVSV-GP vector indeed have similar glycosylations to the ones produced and released during EBOV infection (Fig. 33). Indeed, for both the virion-bound $GP_{1,2}$ and the Shed GP form, the GP_1 subunit is Endo H-resistant and the GP_2 subunit is partially Endo H-resistant, as expected. While, the proper glycosylation of the two different forms of the full-length glycoprotein is likely to allow the mounting of a proper humoral response against EBOV, it can also potentially have deleterious effects for a vaccine. Indeed, it has been reported numerous times that EBOV $GP_{1,2}$ glycosylations and especially those of its mucin-like domain are essential for the high cytotoxicity of the glycoprotein [131,134,136,141,144,280,281,291]. During vaccination, the release of shed GP, as well as the proper processing of $GP_{1,2}$, could therefore participate as much in the vaccine efficiency as towards its side effects [251,252,314].

Our results demonstrating the presence of a GP_2 product that was accumulating in cells and migrating at the same size as $GP_{2\Delta}$ in the cell culture supernatant were unexpected (Fig. 31). It is known that several metalloproteinases are able to cleave their substrates intracellularly and an early study had even suggested that TNF-α might be cleaved in the Golgi apparatus by ADAM17 [287,288,315]. However, it is now clear that ADAM17 cleaves its substrates only when they are sequestered in lipid rafts and at the plasma membrane [151,154,155]. Therefore, to understand the nature of this unusual protein we decided to compare the electrophoretic mobility of this cellular-associated form to the $GP_{2\Delta}$ present in the cell culture media following different deglycosylation treatments. To our surprise we observed that following Endo H treatment, this $GP_{2\Delta}$-like protein was not undergoing any electrophoretic shift (contrary to what was observed with the partially Endo H-resistant virion-bound GP_2 and $GP_{2\Delta}$), indicating that this GP_2 form is entirely Endo H resistant and that the difference in migration pattern between this form and GP_2 is not due to a difference in amino acid sequence (as is the case with $GP_{2\Delta}$) but to differences in glycosylations (Fig. 33A). In respect to its ability to resist Endo H cleavage, we decided to name this protein $GP_{2\text{-RESISTANT}}$ ($GP_{2\text{-RES}}$). The high-mannose type oligosaccharide, which is Endo H-sensitive in GP_2 and $GP_{2\Delta}$, has been shown to be attached at position 563 of the protein and the complex type oligosaccharide, Endo H-resistant, is bound at position 618 [150]. Consequently, it is possible to conclude that during rVSV-GP infection, the high mannose glycosylation present at position 563 is able to be further

maturated into complex type oligosaccharides. This abnormally glycosylated $GP_{1,2\text{-}RES}$ has never been observed during EBOV infection or with plasmid transfection, suggesting that it is a form specific to rVSV infection. This highlights that, even for possessing of the same gene, differences can exist between the glycoproteins produced during EBOV infection and the ones produced during rVSV-GP infection, arguing in favour of precisely and systematically characterising the different proteins of interest synthesised by different vaccine platforms in order to fully assess the nature of the proteins that could be produced during vaccination.

Surprisingly, however, in the supernatant of infected cells, we failed to detect the presence of the $GP_{2\text{-}RES}$ protein either in a virion-associated or soluble form. To explain such an absence, three possibilities exist: (i) $GP_{1,2\text{-}RES}$ is not transported to the plasma membrane and is retained in the Golgi, (ii) it is present at the plasma membrane but is excluded from the lipid rafts that should contain the normal $GP_{1,2}$ and is not cleaved by ADAM17, or (iii) it is transported to the lipid rafts but the change in glycosylation at position 563 modifies its structure and/or the stability of $GP_{1,2}$ and/or the ability of ADAM17 to properly recognise the viral glycoprotein and to therefore be able to release it as a soluble protein.
To address these points, we first performed organelle fractionation in an iodixanol gradient, that, combined with Endo H treatments, provides insights into $GP_{1,2}$ processing and $GP_{1,2\text{-}RES}$ transport (Fig. 35). As expected, we detected Pre-GP_{ER} in the ER and Golgi-associated fractions and the mature GP_1 in the plasma membrane fraction, in keeping with previous observations [120]. Our results demonstrate that the aberrant $GP_{2\text{-}RES}$ is first detectable in the Golgi, from where it would be transported to the plasma membrane, as observed by its co-migration with GP_2 following Endo H treatment, in corresponding fractions (Fig. 35). Densitometry quantification showed that $GP_{2\text{-}RES}$ was accumulating at the plasma membrane, reinforcing the idea that $GP_{1,2\text{-}RES}$ is neither shed nor incorporated into the viral particles. In addition, it was shown for VSV G, that glycosylations are important for its adressage to the plasma membrane [315]. For EBOV glycoprotein, infectious viruses deleted of most of their GP glycosylations, following removal of their mucin-like domain or modified to be resistant to Furin cleavage, can be produced, suggesting that GP transport is glycosylation-independant [134,316]. However, our results would reason that a mechanism does exist to limit improperly glycosylated GP transport to the plasma membrane. Indeed, while Pre-GP_{ER} was detected in large quantity in the Golgi-associated fraction, very little Pre-GP_{ER} was found in the plasma membrane-associated fraction, suggesting that the different GP precursors are retained in the Golgi apparatus, feasibly to ensure that the viral glycoproteins that are addressed to the plasma membrane are properly glycosylated (Fig. 35). Considering the rapidity of the infection and the massive production of viral proteins, as well as the possible effect of VSV M on protein translation in the context of the rVSV vector [306,307], the transport of immaturely glycosylated proteins to the plasma membrane that we observed here, is likely the result of an exhaustion of the protein synthesis and glycosylation systems. In addition, we were able to detect, in the ER-associated fraction, a GP_2 product of higher molecular weight, which has never been observed previously (Fig. 35, Iodixanol fractions 5 and 9) [120]. To be able detect the subunit GP_2, Pre-GP needs to be cleaved by the cellular proprotease Furin which is only active in the Golgi apparatus [317]. As this GP_2 form of higher molecular weight is completely sensitive to Endo H, we concluded that this protein represents the GP_2 subunit cleaved by Furin that has still its immature N-glycosylations and therefore decided to name it Pre-GP_2. This suggests that Furin cleavage occurs first and only after the GP_2 acquire complex glycans on this subunit. The fact that this form was never observed before in previous studies (Volchkov V *et al.* 1998)

could be due to the inability of the antibodies used to immunoprecipitate the viral proteins prior to fluorography to capture this form [120].

EBOV glycoprotein is believed to be enriched in lipid rafts, which are also its preferred budding sites [105,318]. While it is not known whether rVSV-GP egress is also raft-dependant, we wondered if this $GP_{1,2\text{-RES}}$ form could be excluded from these membrane subdomains, which could explain why we could not observe it in rVSV-GP and rVSV-GP-HS virions. Using a floatation assay, we were able to prove that similarly to GP_2, $GP_{2\text{-RES}}$ was efficiently transported to the lipid rafts (Fig. 36). Interestingly, in addition to confirming that $GP_{2\text{-RES}}$ was transported to lipid rafts, we found that, compared to GP_2, the abnormally glycosylated glycoprotein was enriched in those subdomains, providing further evidence that $GP_{1,2\text{-RES}}$ is not released in any soluble or membrane-bound form.
The immaturely glycosylated aspartate at location 563 on the surface glycoprotein is localised inside of the GP_2 NHR domain that is essential for trimerisation. It was also suggested that this domain controls the production of filamentous-like structures during GP transfection and to participate in EBOV budding [132,319,320]. Furthermore, glycosylation GP_2 mutants, were shown to reduce GP Furin cleavage but also to impair KZ52 neutralizing antibody (a known conformation-dependant antibody) binding to the viral glycoprotein [144,321]. Of interest, Wang B *et al* (2017) suggested in their study that aspartate 563 was involved in $GP_{1,2}$ trimer stabilization and that is was also essential for $GP_{1,2}$ incorporation into VLP and HIV pseudotypes. In line with their results, the presence of $GP_{1,2\text{-RES}}$ in lipid rafts but its absence in pelleted rVSV-GP and -HS virions would suggest that this form is inadequate for viral budding (Fig. 33B). However, when the plasma membrane is saturated with $GP_{1,2}$, as it the case with the rVSV-GP-LS mutant, $GP_{1,2\text{-RES}}$ is incorporated alongside classical $GP_{1,2}$ (Fig. 37C). Therefore, we postulate that during EBOV infection, GP_2 aspartate 563-associated high-mannose type oligosaccharide is not processed into a complex type oligosaccharide to allow proper glycoprotein trimerisation to ensure the production of infectious viral particles. However, during rVSV-GP infection, $GP_{1,2\text{-RES}}$ is someway produced and transported to lipid rafts, where it accumulates due to its structure being less favourable for $GP_{1,2}$ trimerisation and thus release in virions. Furthermore, we could not detect $GP_{1,2\text{-RES}}$ as a shed form despite the fact ADAM17 was shown to be active in lipid rafts [155]. Given the size of the enzyme catalytic domain, it is safe to assume that it is able to cover a large portion of the viral protein. Whilst the additional complex glycan could hamper proper ADAM17 binding and/or cleavage of $GP_{1,2\text{-RES}}$ and therefore block its shedding, it is also possible that ADAM17 is only able to cleave trimeric $GP_{1,2}$ proteins.

Importantly, our results provide real insight into the mechanism that might govern GP incorporation into viral particles. It has been previously postulated that a segregation mechanism controls viral glycoprotein incorporation [322]. In this respect, this study demonstrated that cells co-expressing both HIV and EBOV glycoproteins do not produce pseudotyped particles containing both viral glycoproteins. It was further shown that this is due to the fact that some viruses bud from a single phosphatidylserine-enriched site that only contains a single type of viral glycoprotein [322]. As such and given the absence of $GP_{1,2\text{-RES}}$ incorporation into viral particles in our hands, it is tempting to speculate that during rVSV-GP infection, a similar mechanism controls $GP_{1,2}$ incorporation into viral particles, with $GP_{1,2}$ and $GP_{1,2\text{-RES}}$ both being present at the same time at the plasma membrane but in distinct lipid raft structures. To investigate the existence of an active or passive mechanism that might control

viral glycoprotein segregation, we tried to interfere with the integrity of this system by infecting cells with rVSV-GP-LS. In the absence of sGP and of shedding, there is no way for the virus to regulate the overaccumulation at the plasma membrane of the viral glycoprotein in this context, which could increase the chance of incorporating $GP_{1,2\text{-RES}}$ into viral particles. Of interest, while in virions, $GP_{1,2}$ is still majoritarily present, following rVSV-GP-LS infection, it was indeed possible to observe $GP_{1,2\text{-RES}}$ in the pelleted virion (Fig. 37C).
In addition, when analysing the glycosylations profiles of the released glycoproteins, we detected a protein in rVSV-GP-HS virions that behaved similarly to $GP_{2\Delta}$ in response to Endo H and PNG F treatments (Fig. 33B). To confirm this and to rule out any contaminations coming from the ultracentrifuged supernatant, we purified pelleted rVSV-GP-HS virions on a double 60%-20% sucrose cushion (Fig. 33D). In this experimental setup, we were again able to detect this protein following glycosidase treatment. How exactly ADAM17 cleaves trimeric substrates such as TNF-α is currently unknown. It is admitted that the active form of ADAM17 is monomeric but whether a single molecule of ADAM17 is sufficient to sequentially shed a homotrimer such as TNF-α and $GP_{1,2}$, or if three molecules of ADAM17 are required, is not documented. During EBOV infection, it was shown that Shed GP was released as a trimeric protein [130,148]. We then believe that the protein with the same electrophoretic mobility than the $GP_{2\Delta}$ present in the virion (Fig. 33D) is a partially cleaved $GP_{1,2}$ which is the result of a sequential cleavage of one of the monomers of the membrane-bound trimeric $GP_{1,2}$ by a single ADAM17 monomer. This partially cleaved $GP_{1,2}$ would then still be linked to the trimer but would be detected as $GP_{2\Delta}$ by western-blotting in denaturing conditions (Fig. 33D). Such heterotrimeric forms would be expected to have a partial or complete loss of their ability to perform membrane fusion [132]. The fact that we could observe this solely with the rVSV-GP-HS virus, a virus that has been modified to have a shedding site that is extremely well recognised by ADAM17, could mean that the natural shedding site sequence of EBOV is an evolutionary adaptation by the virus to prevent its glycoprotein from being over targeted by ADAM17 and to avoid the formation of fusion-deficient $GP_{1,2}$ proteins. This limited incorporation of viral glycoproteins also goes in the sense of a mechanism that segregates $GP_{1,2}$, with some portion fated for viral particle formation and the other for shedding (Fig 42). In this regard, our results obtained here demonstrate that, at least in non-infected and infected A549 cells, ADAM17 localisation is controlled at the plasma membrane resulting in clear spatial segregation between areas which are enriched in ADAM17 proteins of areas depleted of ADAM17 (Fig. 34). Such organisations could therefore lead to the protection of a pool of GP protein that would be used for the production of normal viral particles that would never be in danger of being cleaved by the cellular sheddase. It is therefore interesting to postulate that GP is able to take advantage of ADAM17 clustering to ensure the production of highly infectious particles during the infection.

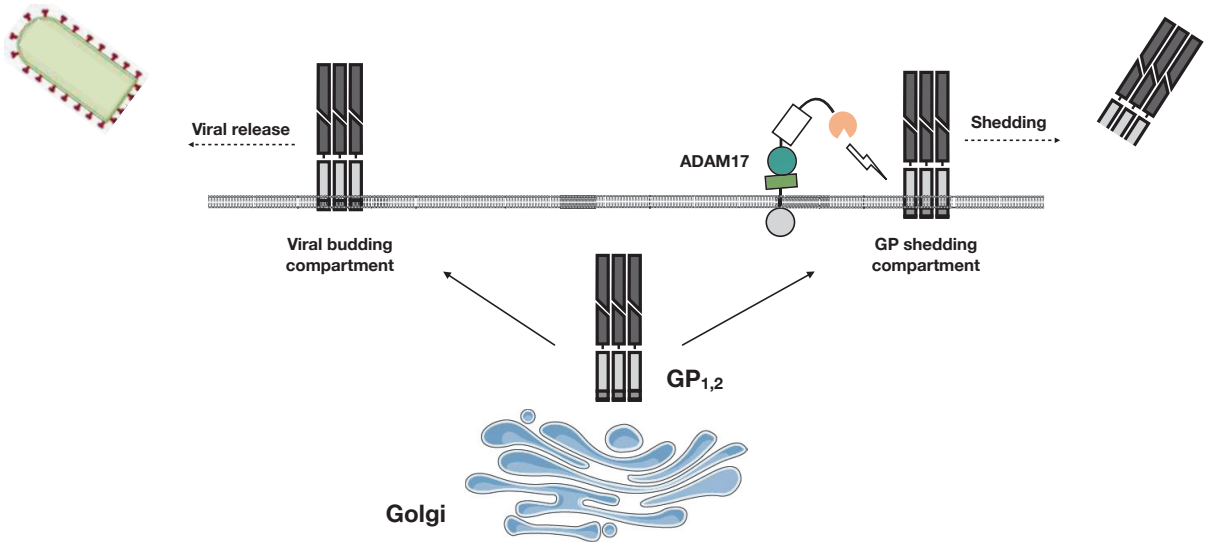

FIGURE 42. MODEL FOR GP SHEDDING CONTROL

In this model, following maturation in the Golgi apparatus, EBOV glycoprotein $GP_{1,2}$ is either addressed to a plasma membrane compartment, specialised in ectodomain shedding (which contains high concentration of ADAM17 proteins) or to a compartment that controls viral egress that is almost completely depleted in ADAM17 proteins.

During this work, we also confirmed that shedding in rVSV-GP infected cells was ADAM17-dependant, similarly to EBOV, as established by the loss of $GP_{1,2\Delta}$ when cells were treated with the inhibitor marimastat (Fig. 39) [306,323]. The fact that differences was observed in the amount of shed GP released in response to marimastat treatment for rVSV-GP and GP-HS viruses is likely linked to differences in affinity between ADAM17 and the wild-type EBOV glycoprotein or its high shed variant. This further illustrates and reinforces the idea that was previously postulated that the wild-type glycoprotein is relatively poorly recognised by the cellular sheddase compared to other proteins shed by ADAM17 [134,285]. We also demonstrated that rVSV infection leads to the activation of two cellular pathways that are required for ADAM17 activity, the ERK1/2 and the p38 MAPK pathways, which were rapidly induced following infection (Fig. 40A). The activation of ERK1/2 has been demonstrated to regulate viral replication of several viruses, including HIV, Coxsackievirus B3, Influenza A but also VSV which requires this pathway to enhance its replication [324–327]. It was therefore not surprising to observe an upregulation of this pathway with VSV infection (Fig. 40A, left panel). The fact that we observed a rapid activation that peaked after 15 minutes of stimulation with both rVSV-GP and VSV viruses implies that the interaction of the viral glycoprotein with one of its attachment receptors is responsible for this upregulation. In this respect, the VSV glycoprotein G was shown to interact with cell surface heparan sulfates that can upon binding upregulate the ERK1/2 pathway [328–330]. The activation of the ERK1/2 pathway during EBOV infection is not yet fully elucidated. It was shown that GP transfection decreased ERK1/2 phosphorylation and ERK2 enzymatic activity but the relevance of this in the context of the viral infection is unknown. Our previous results suggested that in the first steps of EBOV infection, this pathway would be upregulated in a $GP_{1,2}$ -dependant manner [331,332]. It would be however, necessary to confirm those data with infectious, replicating WT EBOV to see if this pathway is not blocked by other viral proteins.

In addition to ERK1/2 activation, we were able to observe the upregulation of the p38 pathway. Interestingly, differences could be observed between VSV and rVSV-GP (Fig. 40A). In VSV infected cells, p38 phosphorylation did not return to its basal level during the time-course of the experiment, whereas during rVSV-GP infection, p38 was dephosphorylated at the end of

the experiment, suggesting differences in the upregulation mechanism. During EBOV infection, it was demonstrated that p38 inhibition reduces EBOV replication by limiting human monocyte-derived dendritic cells macropinocytosis activity and therefore EBOV uptake [333]. However, the mechanisms leading to p38 activation during EBOV infection have thus far not been elucidated. It was shown previously that in human dendritic cells, EBOV VLP produced through transient expression of GP and VP40, upregulated the ERK1/2 pathway (in a GP-dependant manner) but failed to produce a robust activation of the p38 MAPK pathway [334]. On the contrary, our results add contrasting evidence that EBOV glycoprotein binding could help in the initial steps of the infection by increasing its macropinocytosis and therefore its uptake through a rapid induction of the p38 pathway. The discrepancies between the results of Martinez M *et al.* (2007) and ours are likely due to differences in the amount of GP used for stimulation and/or of the cell-type used. Indeed, the authors stimulated their dendritic cells using 10µg/mL of VLP, which was calculated based on the total amount of proteins contained in their VLP while in our study we infected starved VeroE6 cells using a high MOI representing the amount of infectious virus. Therefore, in our experimental setup, it is likely that the amount of GP is more important and enough to activate p38 MAPK pathway, whereas, the amount of GP present in the VLP produced in the 2007 study, which would majoritarily contain VP40 protein, were insufficient to do so. Additional studies using WT EBOV are then clearly necessary to shed light on the role of p38 in EBOV pathogenesis and ADAM17 upregulation. In addition, p38 has been intensively described for its role in the induction of immune genes and notably, it was shown that TLR-4 engagement with LPS leads to p38 phosphorylation [295,335,336]. Interestingly, during EBOV infection, VP24 is able to block p38 phosphorylation. Considering our results and the fact that $GP_{1,2}$ was also shown to interact with TLR-4, this could mean that VP24 is linked to prevention or limiting of the early $GP_{1,2}$-dependant activation of this pathway during EBOV infection to avoid a rapid clearance of the virus [131,190,208,337].

Furthermore, we postulated that exposure of phosphatidylserine during EBOV infection participates in glycoprotein shedding by allowing a better contact between ADAM17 and the $GP_{1,2}$ membrane proximal domain [156,225,338,339]. We hypothesized that preventing ADAM17 interaction with cellular phosphatidylserines would impair $GP_{1,2}$ shedding (Fig.40B). Unexpectedly, our data are showing the opposite phenomenon. Indeed, cells treated with high concentration of OPS (as free phosphatidylserines) show an augmentation of $GP_{1,2\Delta}$ release by about 50%. Additional experiments using cells that are expressing an ADAM17 tagged-substrate could help us to clarify if this effect is specific of $GP_{1,2}$, which would then suggest differences in the mechanism in ADAM17 recognition between the viral glycoprotein and cellular substrates [340].

The 2014-2016 EBOV outbreak helped to accelerate the development of therapeutic approaches against this highly pathogenic virus. So far, the most promising approach is the prototype vaccine rVSV-ΔG-EBOV-GP, also known as rVSV-ZEBOV, and referred to as rVSV-GP throughout this work [251]. While the replicative competent vaccine has now advanced to Phase III human trials, the nature of the viral glycoproteins synthesised during rVSV-GP infection have been so far poorly characterised [253]. This is of special importance as protection during rVSV vaccination is dependent on the development of an appropriate humoral response with neutralizing antibodies against the viral glycoprotein and the nature of the glycoproteins which are synthesised during vaccination has been shown to be key in offering protection in different animal models [206,248,257]. Moreover, during the different vaccine trials, numerous and sometimes severe adverse effects were reported. Here, during this PhD work, we investigated the synthesis and the processing of the full-length $GP_{1,2}$, as well as the release of soluble viral glycoproteins from rVSV-GP infected cells that could feasibly either participate in the successful protection or impair the efficiency and safeness of the vaccine and maybe even cause the adverse effects observed [251–253].

EBOV glycoprotein synthesis is a multi-step mechanism leading to the formation of a highly glycosylated protein packaged at the surface of the virion, and which controls both its cytotoxicity and its immunogenicity. In this work we demonstrated that the glycoprotein which is produced by the rVSV-GP virus highly resembles the $GP_{1,2}$ produced from EBOV infected cells. Indeed, we showed that during rVSV-GP infection, we could detect the precursor Pre-GP_{ER} that has immature glycosylations and that further acquires mature glycosylations following its transport in the Golgi apparatus and its addressage to the plasma membrane. Interestingly, we were also able to identify for the first time, a GP_2 subunit with no mature glycosylation that we named Pre-GP_2 and that would correspond to the immediate product following Pre-GP_{ER} transport to the Golgi and Furin cleavage. The fact that this Pre-GP_2 contains no complex glycan tends to suggest that Furin cleavage precedes GP glycosylations in the Golgi apparatus and offers new insights into the cellular processing and trafficking mechanisms for this important viral protein. Importantly, we also showed that the glycoprotein that is present in the rVSV-GP virion is similarly glycosylated to the one present in EBOV particles. This highly favors the ability of the vaccine to be protective against EBOV infection and that fact that development of $GP_{1,2}$-specific antibodies following rVSV-GP vaccination is linked to the correct synthesis of the viral glycoprotein from the replication-competent vaccine. Furthermore, our results clearly prove that, similarly to EBOV, during infection, soluble viral glycoprotein are released. Indeed, we were able to demonstrate that the viral glycoprotein was readily released in a truncated soluble, shed form, known as $GP_{1,2\Delta}$ and that his release was dependent of ADAM17. Our results prove that this form is similarly glycosylated to the $GP_{1,2\Delta}$ or ‘Shed GP’ produced in EBOV infection or with GP transfection. We also showed that several ADAM17-activating pathways were upregulated during rVSV-GP infection but it would be necessary to repeat similar experiments with EBOV virus to confirm that they are also activated during EBOV infection and that they also control GP shedding. In addition, our data indicate that ssGP is produced following transcriptional editing of the GP gene by the VSV polymerase during rVSV-GP infection. Furthermore, while we did not detect sGP specific mRNA, the ability of VSV L to edit and to insert more than a single adenine at the GP editing site, is evident. In this respect, it is very likely that sGP mRNA is also produced even though we failed to detect

it specifically. However, compared to what was previously observed during EBOV infection, the proportion of edited mRNA is significantly lower and this implies that the release of sGP and ssGP are limited during rVSV infection and is thus unlikely to impair rVSV-ZEBOV vaccine efficiency in this sense.

Of interest, proper processing of GP, its conserved glycosylations as well as its release as a soluble form, that was previously implicated in EBOV pathogenesis, suggest that the cytotoxicity of EBOV $GP_{1,2}$ would to at least some extent be conserved in rVSV-GP infection and that its production could potentially produce some deleterious vaccination-related effects, at least in some individuals. In this respect, and of interest, for this study we successfully generated rVSV viruses with different shedding activities that were attenuated compared to the wild-type rVSV virus. In addition, the use of these mutant viruses as tools for a cost-efficient production of $GP_{1,2\Delta}$ to study its roles in EBOV pathogenesis in animal models, *in vivo* experiments could also shed light on the ability of the rVSV viruses with different shedding abilities to provide similar protection against EBOV while displaying less adverse effects. This is of special importance as a significant part of the immunocompromised population currently cannot be vaccinated with the current rVSV-based vaccine.

We were also able to identify an aberrant form of the GP_2 subunit in the context of rVSV-GP infection that was never observed during EBOV infection or GP transfection and that accumulated in infected cells. We demonstrated that this protein possesses complex, mature glycans on the two GP_2 N-glycosylations sites, rendering it resistant to deglycosylation treatments by the Endo H enzyme, and we therefore decided to name it $GP_{2\text{-RESISTANT}}$ ($GP_{2\text{-RES}}$). Interestingly, the identification of this new GP_2 form helped us to gain a better understanding of $GP_{1,2}$ packaging into rVSV virions. Indeed, during our investigation, we were able to demonstrate that this $GP_{1,2\text{-RES}}$ is not inserted into the viral particles and we were also able to observe a limited pool of partially cleaved $GP_{1,2}$ that can be incorporated into the viral particle. In addition, we showed that ADAM17 localisation appears to be clustered at the plasma membrane. This spatial clustering could be a way for the virus to prevent and limit its glycoprotein ectodomain release and/or partial digestion by the cellular sheddase. Those elements lead us to postulate the existence of a system that allows the segregation of the viral glycoproteins: During the infection, the normal $GP_{1,2}$ is either addressed to lipid rafts microdomains localised in area that are depleted in ADAM17 proteins, those microdomains would therefore ‘specialised’ in viral particle formation and ensure that the viral glycoprotein is protected from ADAM17 cleavage. In parallel, the viral glycoprotein is also addressed to membrane domains that are enriched in ADAM17 where it will be massively released as a shed form and help to limit its cytotoxicity in the infected cell. On the other hand, the abnormal GP1,2-RES is also transported to lipid rafts that are distinct from GP1,2-containing lipid rafts, but as its structure is not suitable for viral release, it is accumulating at the plasma membrane.

Finally, the identification of $GP_{1,2\text{-RES}}$ strongly argues for the importance to continue to properly characterise virus-based vaccines, to assess any differences existing between the antigen that is naturally synthesised by the virus during infection and the one produced by the surrogate virus/vaccine-candidate. Indeed, our results unequivocally demonstrate that while they both have the same GP gene, differences still exist during EBOV and rVSV infection.

In conclusion, this work provides important molecular insights into the rVSV-ZEBOV vaccine (Fig. 43). We give evidence that the viral $GP_{1,2}$ produced by rVSV-GP is similar to the one synthesised by EBOV. We believe that this resemblance is key to allow the production of specific-$GP_{1,2}$ antibodies that are able to offer protection during EBOV infection. The identification of soluble form of $GP_{1,2}$ released during the infection and of the aberrant $GP_{1,2\text{-}RES}$ in rVSV-GP infected cells reinforces the importance of systematically studying the molecular basis of replication-competent based vaccines to recognize factors that could impair vaccine efficiency and safety.

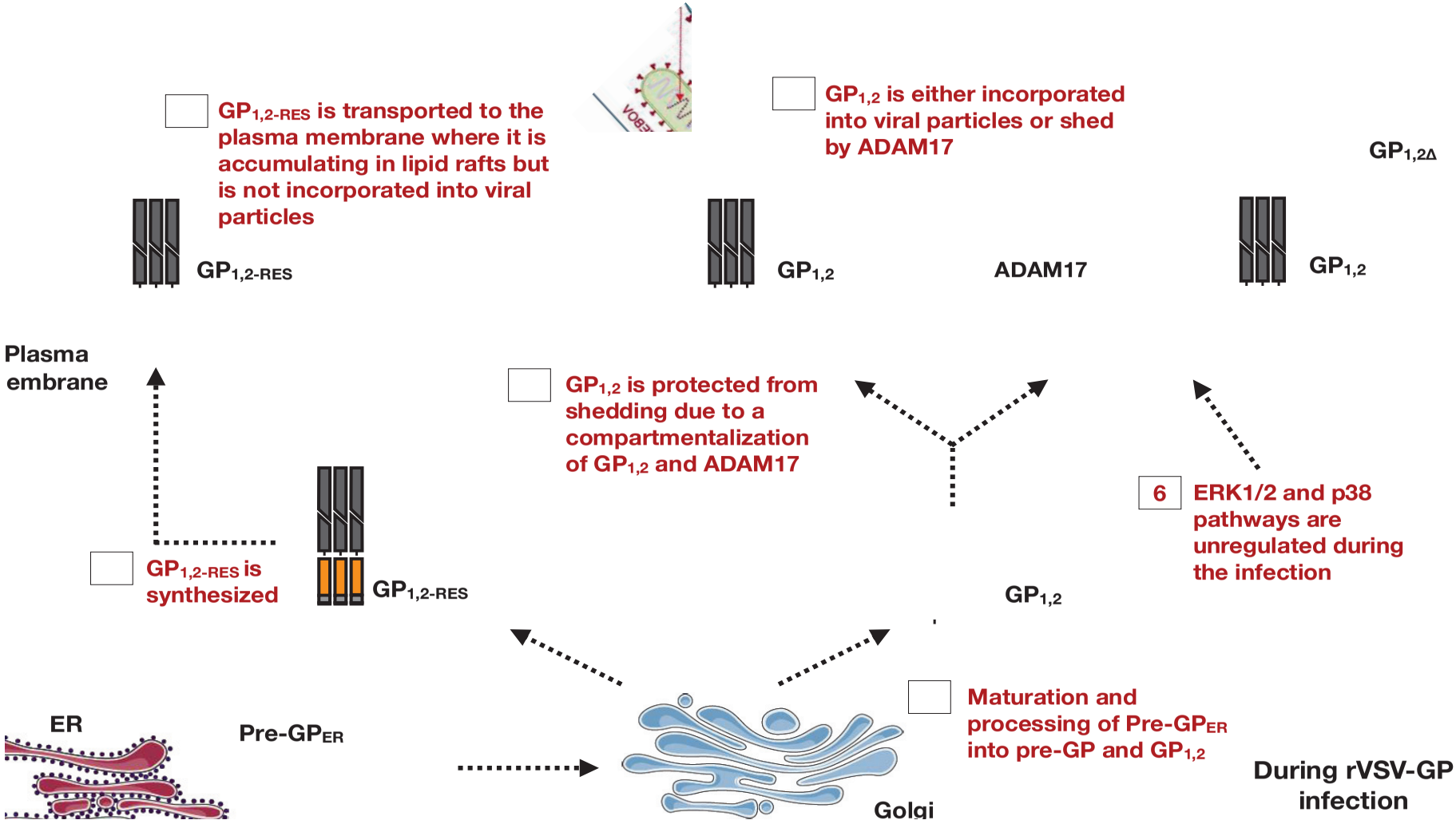

FIGURE 43. EBOV GP SYNTHESIS DURING rVSV-GP INFECTION

During rVSV-GP infection, following synthesis and processing in the Endoplasmic Reticulum (ER) and in the Golgi apparitus (Golgi), the viral glycoprotein $GP_{1,2}$ is cleaved into two subunits GP_1 and GP_2. The GP1 subunit possesses only complex N-glycans, whereas the GP2 subunit has a high-mannose N-glycosylation and a complex type N-glycan which are attached in position 563 and 618, respectively (1). Next, the viral glycoprotein is adressed to the plasma membrane, where it will either be incoroporated into the viral particles or it will be cleaved by the cellular sheddase ADAM17 and released in the infectious supernatant as a truncated soluble glycoprotein $GP_{1,2\Delta}$ (2). In addition, the incoporation of a sufficient amount of glycoproteins into the virions is ensured by the existence of a spatial clustering of ADAM17, which is fully depleted in some areas of the plasma membrane (3). In parralel of GP1,2 synthesis, an aberrant viral glycoprotein is produced in the Golgi. This protein named GP1,2-RES possesses a complex type N-glycan in posiiton 536 (4). GP1,2-RES is transported to the plasma membrane and accumulates in lipid rafts and apepars to not be inserted into the viral host-derived membrane (5). Finally, cellular pathways which

INVESTIGATION OF THE PRESENCE OF FILOVIRUSES IN GHANA, WEST AFRICA

OBJECTIVES

Prior to 2014, all previous EBOV and MARV outbreaks were fairly limited in terms of the number of human cases and transmission events and were restrained to Central and South Africa [9]. As such, the extraordinary scale of the 2014-2016 EBOV outbreak, in regions that were previously largely unaffected by this virus, highlighted the absolute necessity to obtain better insights not only into the ecology but also into the geographical repartition of these highly pathogenic viruses to try to prevent, or to be as best prepared as possible to deal with, any spillover from their natural host and/or accidental hosts into the human population [7,296,297].

Since their discovery, the identification of the natural host for filoviruses has been challenging and as yet has failed to yield many conclusive results [34]. The isolation of Marburg virus (MARV) in 2009 in *R. aegyptiacus* bats, as well as the identification of Lloviu virus (LLOV) and recently of Bombali virus (BOMBV) in different bat species, incriminate bats as the natural reservoir of these viruses and also suggests that they are not restricted to a single bat species [3,39,298]. So far, 26 different bat species were identified as potential hosts for filoviruses in multiple locations in Africa, Asia and Europe [3,5,6,34,54,297]. However, results are mostly based on antibody detection and can be contradictory with molecular data obtained with immortalized bat cell lines or during *in vivo* experiments using captive bats [34,41,44].The absence of positive and negative controls for all of the different bat species tested, as well as the different nature of the techniques or the source of antigens used to detect antibodies, makes it difficult to differentiate between positive results and false positives, rendering it difficult to obtain a clear idea of which bat species could actually transmit and participate in the spillover of filoviruses in the human population.

In Ghana, West Africa, several bat species suspected of being filovirus hosts are present, notably *R. aegyptiacus* (MARV and MARV-related viruses), *E. franqueti* and *H. monstrosus* (EBOV). Despite the fact that antibodies have been detected against filoviruses in Ghanaian bats and that this country is surrounded by several countries that have reported filovirus outbreaks, Ghana has so far not been affected by any suspected outbreak of these viruses [7,9,299,300]. To this end and to further investigate the suspected presence of filovirus species not only in Ghana but also as a tool for future detection and surveillance of potential exposure to these and related viruses, we generated recombinant antigens from known filoviruses that resemble the glycoproteins expressed during filovirus infection and that decorate the surface of theses viruses with the aim of developing a multiplex luminex assay to simultaneously detect the presence of different filovirus glycoproteins in animal (bats and pigs) and human sera [4,5,7,39,45,297,299,301]. In addition, we collected bat and pig organs in Ghana and performed nested RT-PCR using pan-filovirus primers to detect the presence of any putative known or unknown filoviruses.

IDENTIFICATION OF ANTI-LLOV GP ANTIBODIES IN HUMANS AND ANIMAL SERA

Firstly, sera samples from Ghana, obtained from different bat species, domestic pigs and humans notably from bat hunters and pig farmers, that declared no EVD-like disease, were obtained in collaboration with Profs. Andrew Cunningham (Institute of Zoology, London) and James Wood (Cambridge University) and analysed by immunofluorescence for the presence of antibodies against different filovirus glycoproteins to confirm the initial results obtained using a home-made luminex assay with recombinant EBOV and MARV glycoprotein developed by our partners (Fig. 44).

To this end, VeroE6 cells were transfected with a plasmid encoding for EBOV GP that also contained a GFP gene under control of an IRES (Internal Ribosome Entry Site). In such a system, cells that are GFP positive should also express viral GP. Cells were then fixed by acetone:methanol and incubated either with diluted sera or with a specific EBOV GP_1 monoclonal antibody (Fig. 44A). When using GP_1 antibody to reveal the viral glycoprotein, a colocalization of the GP (in red) and of the GFP (in green) signals was observed (Fig. 41A, first panel). However, when using the human sera V123 and V151 as a source of primary antibody, which were previously shown to be positive for EBOV antibodies in the serology assay mentioned above (A.A. Cunningham), no colocalization with GFP positive cells could be observed (Fig. 44A, second and third panels). Similarly, cells transfected with the European Lloviu virus glycoprotein that has, so far, never been detected in Africa were used as an additional study control. Interestingly, cells transfected with LLOV GP, gave a more intense and specific staining compared to cells transfected with EBOV GP and could thus represent a positive signal for LLOV antibodies (Fig. 44B). Of interest, similar results were obtained with pig and bat sera (data not shown).

Therefore, these results suggest that LLOV and/or LLOV-like filoviruses are circulating in Ghana and are able to infect humans, pigs and bats.

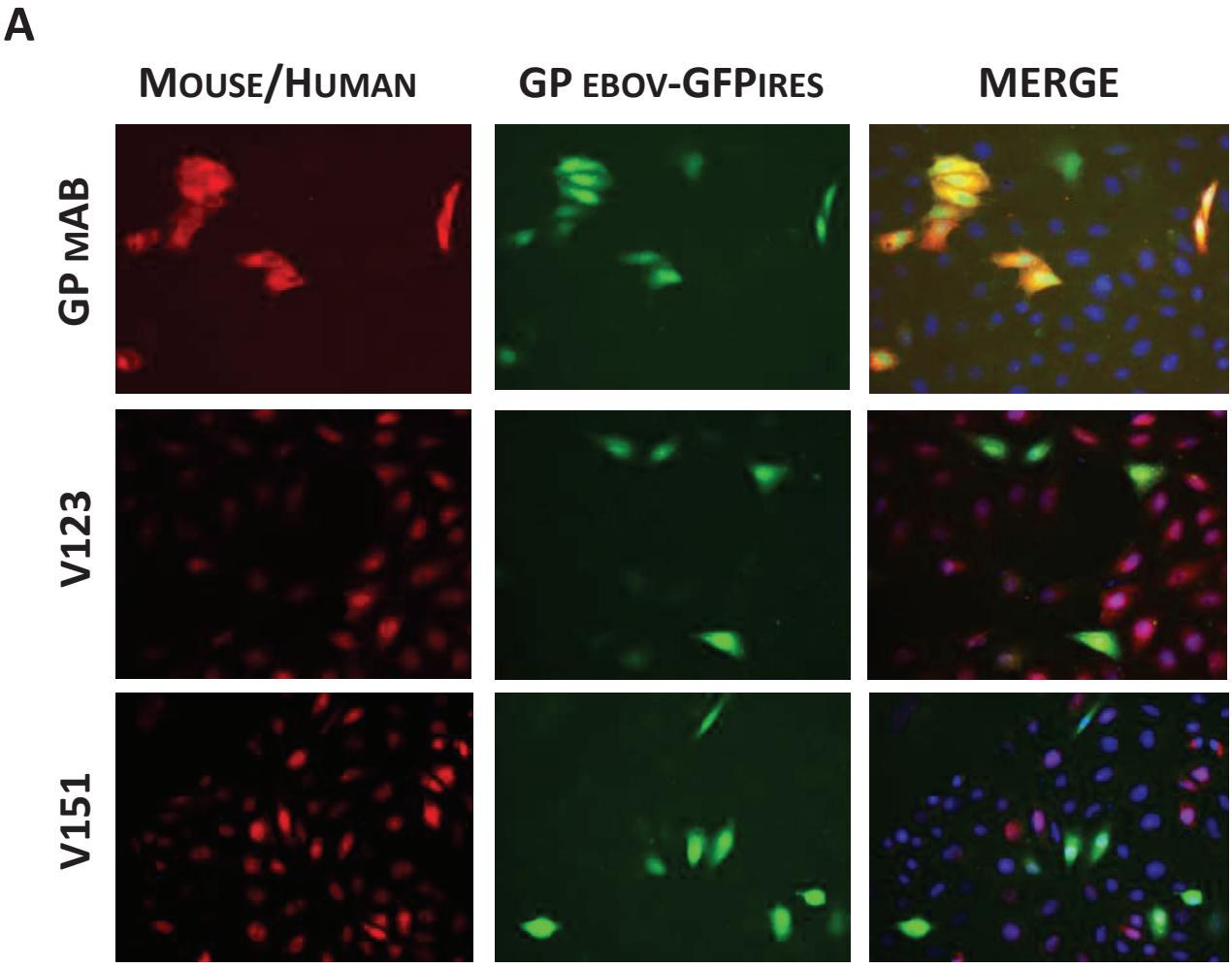
A
MOUSE/HUMAN
GP EBOV-GFPIRES
MERGE
GP MAB
V123
V151

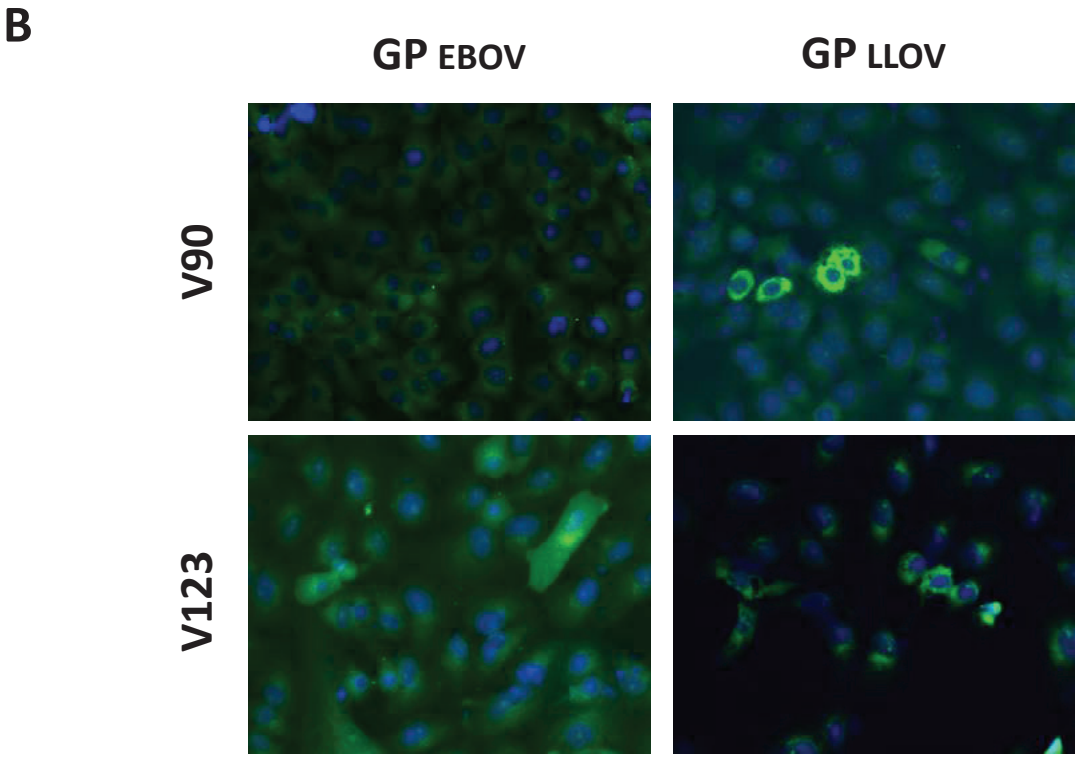
B
GP EBOV
GP LLOV
V90
V123

FIGURE 44. INDIRECT IMMUNOFLUORESCENCE ANALYSIS OF GHANNAIAN HUMAN SERA

VeroE6 cells transfected with either a plasmid encoding for EBOV GP or EBOV GP followed by a GFP under a IRES. Twenty-four hours later, cells were washed and fixed by aceton:methanol and incubated with either Ghanaian human sera or monoclonal antibodies directed against EBOV GP_1 (A). In similar fashion indirect immunofluorescence was performed on VeroE6 cells transfected with EBOV GP or LLOV GP (B).

DEVELOPMENT OF A LLOV AND EBOV-SPECIFIC LUMINEX ASSAY

To confirm the serology results obtained by immunofluorescence shown above, a multiplex bead-based luminex assay using LLOV and EBOV glycoproteins as a source of antigen was developed. To obtain pure antigens to couple to the luminex beads, EBOV $GP_{1,2}$ and LLOV $GP_{1,2}$ chimeric proteins were created. In this respect, a histidine tag was inserted in the C-terminal of the protein upstream of the glycoprotein transmembrane domain (TM) that was thus deleted (EBOV-GPΔTM-His and LLOV-GPΔTM-His). Without their transmembrane anchor, the glycoproteins are released into the cell culture supernatants, with little or no cytotoxicity thus providing a system with which to obtain a readily available source of antigens and to easily purify them through their histidine tag.

As detailed above, glycosylations are known to play a central role in filovirus antigenicity [280]. As such and to verify if the recombinant proteins that are generated possess glycosylations which are similar to the wild-type proteins, 293T cells were transfected with plasmids encoding either for EBOV GP, EBOV GPΔTM-HIS, LLOV GP or LLOV GPΔTM-HIS (Fig. 45A to D). Forty-eight hours post-transfection, cells and supernatants were collected and treated with Endo H and PNG F and analysed by western blotting. Viral glycoproteins were detected using either the 3373 monoclonal antibody that recognises the EBOV GP_1 subunit or the LLO91 rabbit sera obtained from immunization that can recognise both LLOV GP_1 and EBOV GP_1.
In cells, transfected with EBOV GP, in the mock treated condition, two bands of different molecular weights were detected (Fig. 45A, Lane 1). The band with a lower electrophoretic mobility did not undergoing any migration shift following Endo H treatment contrary to the band of lower molecular weight (Fig. 45A, Lane 2). In addition, both forms were sensitive to PNG F and were co-migrating after treatment (Fig. 45A, Lane 3). Those results would indicate that during GP transfection, the protein of higher molecular weight represents Pre-GP/GP_1, which are Endo H resistant (indicated by a '*' after PNG F deglycosylation) and that the band of lower molecular weight is Pre-GP_{ER} that is Endo H sensitive (indicated by a '#') and both are readily detected in transfected cells. In the clarified supernatant, both GP_1 and Pre-GP_{ER} were detected as observed after Endo H and PNG F treatments (Fig. 45A, Lanes 4 to 6). When cells are transfected with an EBOV GPΔTM-His, a single product that was Endo H and PNG F sensitive was observed (Fig. 45B, Lanes 1 to 3). In the supernatant, a unique Endo H-resistant and PNF G-sensitive band corresponding to GP_1 was observed. Furthermore, compared to cells transfected with $GP_{1,2}$ wild-type, the amount of $GP_{1,2}$ released from the cells was higher when cells were transfected with the GPΔTM-His plasmid. Of interest, only the Endo H resistant form was present in the supernatant of cells transfected with the $GP_{1,2}$ mutant plasmid.
When cells were transfected with LLOV GP plasmid, a single protein was observed before Endo H and PNG F treatments (Fig. 45C, Lane 1). However, after Endo H-specific deglycosylation, two bands were detected (Fig. 45C, Lane 2). As the lowest band in the Endo H condition migrated similarly following PNG F treatment (Noted by a '#', Fig. 45C, Lane 3) and the highest band was only sensitive to PNG F (Noted by a '*'), it is possible to conclude

that the band of higher molecular weight is LLOV Pre-GP_1/GP_1 and the other is LLOV Pre-GP_{ER}. Similarly to cells transfected with EBOV GP plasmid, both forms were detected in the supernatant (Fig. 45C, Lanes 4 to 6). Surprisingly, no LLOV specific protein could be detected in cells transfected with a LLOV GPΔTM plasmid (Fig. 45D, Lanes 1 to 3). However, a single protein that was Endo H resistant but PNG F sensitive could be detected in the clarified supernatant (Noted '*', Fig. 45D, Lanes 4 to 6).

Those results show that EBOV GPΔTM- and LLOV GPΔTM-transfected cells release viral glycoproteins that have similar glycosylation profiles to the wild-type and mature glycoproteins and are therefore suitable antigens for the development of a luminex assay with which to detect the presence of potential circulating antibodies against EBOV and LLOV glycoproteins.

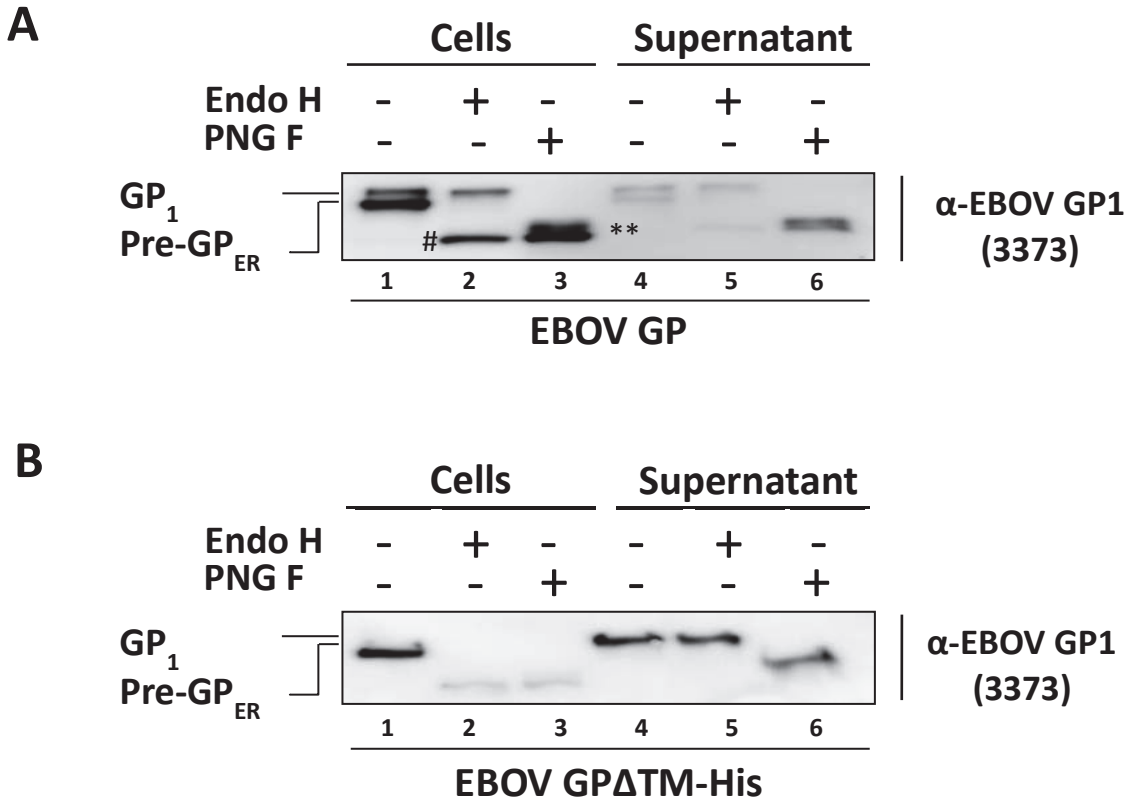

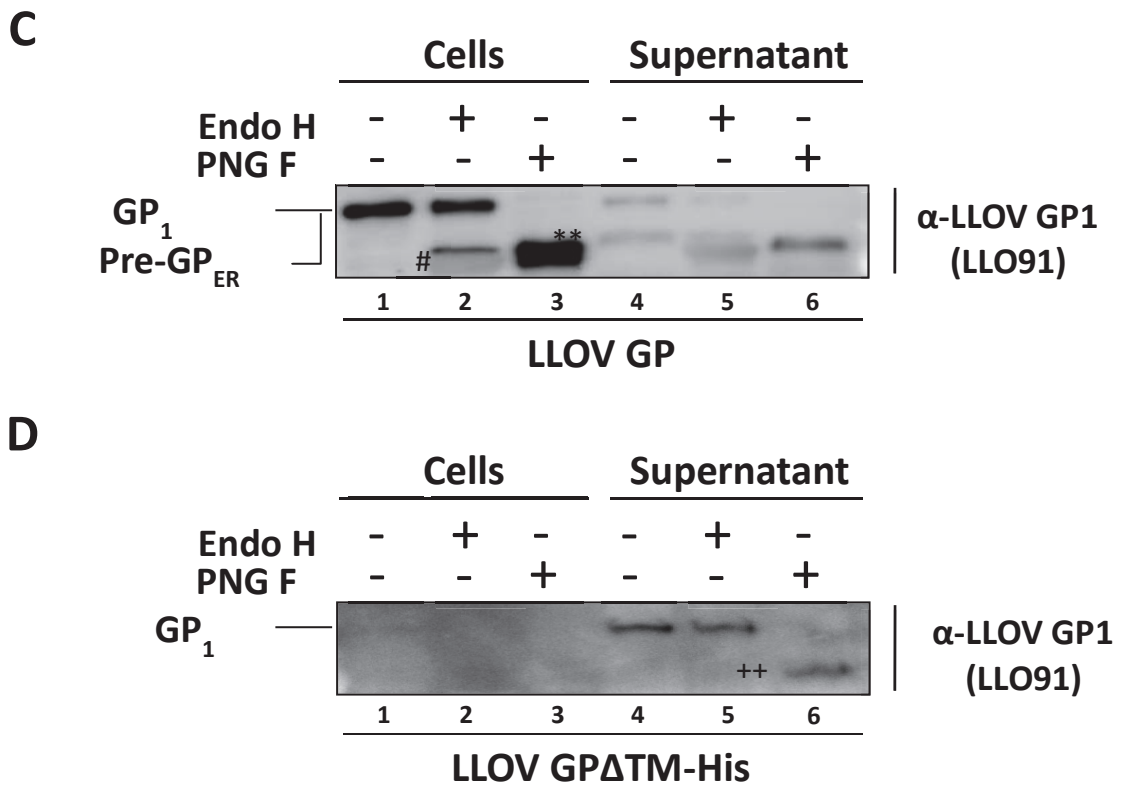

FIGURE 45. EBOV AND LLOV GPΔTM-HIS-TAGGED MUTANTS GLYCOSYLATIONS ANALYSIS

EBOV GP and LLOV GP were modified to generate plasmids encoding GP deleted of their transmembrane domain and fused to a histidine tag (GPΔTM-His). 293T cells were transfected with either plasmid encoding for EBOV GP (A), EBOV-GPΔTM-His (B), LLOV-GP (C) or LLOV-GPΔTM-His (D). Thirty-six hours post-transfection, cells and supernatants were haversted and subjected to Endo H and PNG F treamtents as before. Samples were analysed by western-blotting using an EBOV GP_1 monoclonal antibody or a polyclonal serum recognising LLOV GP1. The position of EBOV GP_1 and Pre-GP_{ER} and of LLOV GP_1 after Endo H and PNG F are indicated by a (**), (#) or a (++) respectively.

For screening purposes, luminex beads were coupled with the purified, characterised EBOV and LLOV antigens described above. Coupling was confirmed by incubating EBOV and LLOV with different amounts of specific antibodies directed either against EBOV or LLOV antigens (Fig. 46). A curve-response is expected if coupling occurred and if the antigens are still available for antibody recognition. In this and following experiments a Hendra virus (HeV) sTAG-coupled G surface glycoprotein, was used as a control. Indeed, HeV G-sTAG proteins coupled to beads were already used to detect the presence of Hendra virus in animals and humans and serve here as a quality control to determine specificity of the assay but also at the same time as an external control to determine the sera background [302–304].

When using the same antibodies that was used for EBOV GP_1 detection by western blotting (Antibody 3373; Figs. 46, 45A and 45B a dose response curve was obtained. Indeed, in response to increasing amounts of antibodies, the signal obtained for the beads coupled with EBOV $GP_{1,2}\Delta TM$ increased (signals are given as Median Fluorescence Intensity (MFI); Fig. 46, upper left, black curve). A plateau was reached when the beads were incubated with 0.75 to 1.5mg/mL of antibodies. Expectedly, no signals were observed for beads coupled with HeV

or LLOV antigens, demonstrating the specificity of 3373 binding to EBOV glycoprotein (Fig. 46, upper left, green and red curves respectively). However, while a response curve was observed, the intensity of the Median Fluorescence Intensity (MFI) was very low (<200 MFI), even for the highest concentrations of antibody used. Therefore, to further confirm antigen coupling, another GP_1 monoclonal antibody (Antibody 3327) was used (Fig. 46, upper right). Of interest, this antibody was shown to be able to neutralize EBOV and VSV-pseudotyped particles and bind to a different epitope than the non-neutralizing antibody 3373 [305]. Following incubation of the EBOV, LLOV and HeV beads with different quantities of the 3327 antibody, a strong and increasing MFI was observed for EBOV while no signal was measured for HeV and LLOV, allowing confirmation of EBOV antigen coupling (Fig. 46, upper right, black curve against red and green curves).
Similarly to what was obtained with the 3373 antibody, a weak dose response curve was observed in response to the purified sera LLO91 (Fig. 46, lower left, red curve). In addition, a non-negligible background for HeV and EBOV was obtained (Fig. 46, lower left, green and black curves respectively). In the absence of other available LLOV GP-specific antibodies, a his-tag antibody was used to confirm coupling. Unsurprisingly, no signal was observed for the HeV G protein that was tagged with a sTAG, while strong signals were detected for EBOV and LLOV antigens. The dose response curves obtained were different for the two filovirus glycoproteins. Indeed, a plateau was reached when beads were incubated with 0.1 mg/mL of His-Tag antibody for EBOV (Fig. 46, lower right, black curve) and with 0.25 mg/mL for LLOV (Fig. 46, lower right, red curve), suggesting either differences in epitope availability or in coupling efficiency.

Consequently, these results confirm (i) that EBOV and LLOV antigens were successfully coupled to the polystyrene beads, (ii) that differences exist in terms of antigen recognition as observed by the differences in the MFI obtained when using two different monoclonal EBOV GP_1 antibodies and (iii) that differences in coupling efficiency could also exist resulting in reduced MFI for a specific antigen.

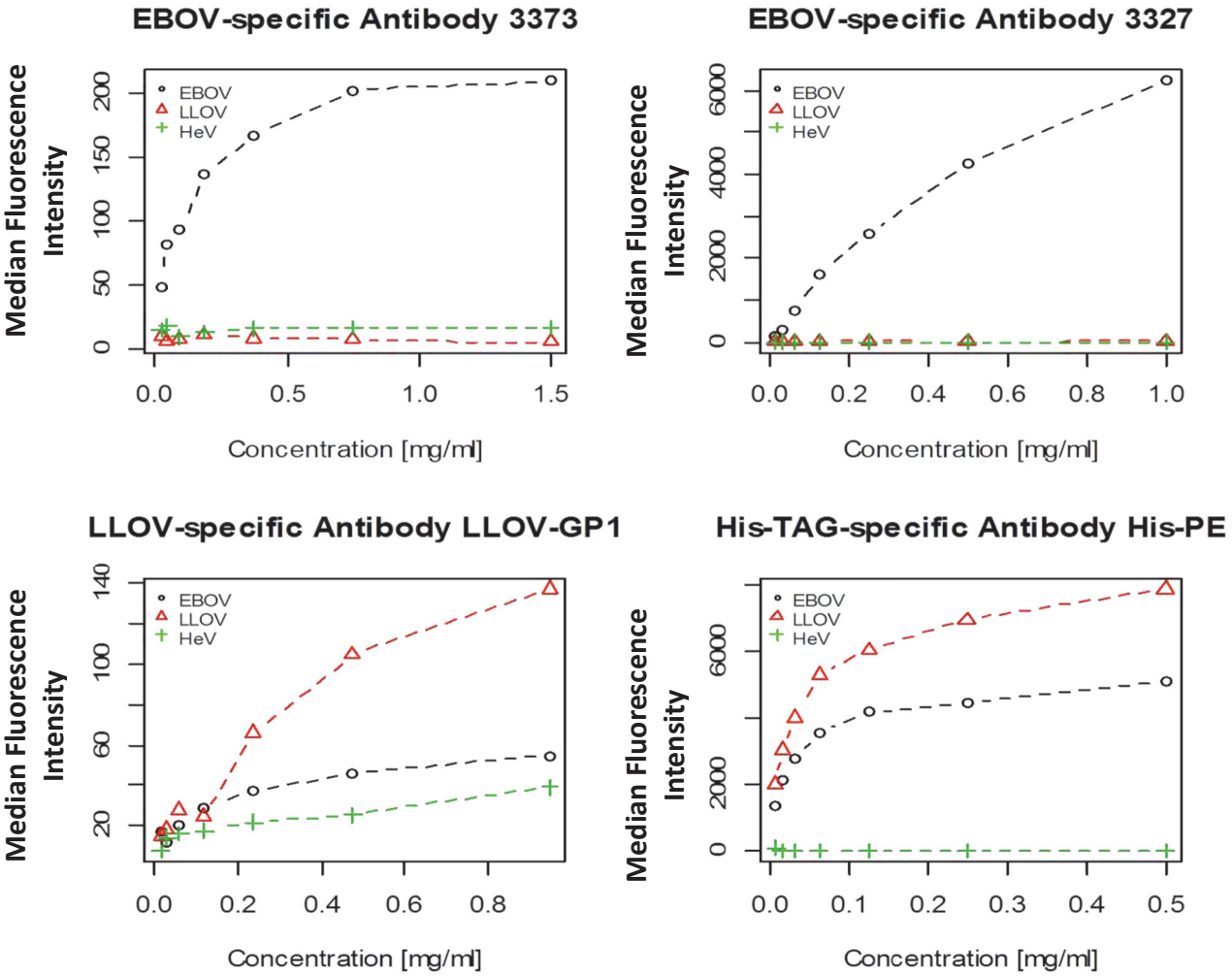

FIGURE 46. ANTIGENS COUPLING CONFIRMATION

His-tagged purified EBOV and LLOV $GP_{1,2}$ and sTAG purified HeV G antigens were coupled to bio-plex microsphere beads. Antigens coupling were confirmed by incubating 3700 beads of each analytes per well for one hour at room temperature with the indicated amount of either EBOV GP_1 monoclonal antibodies (3373 and 3327), LLOV-GP_1 purified polyclonal sera or monoclonal his-tag antibody. The binding of the antibodies to the microspheres was detected by incubating beads with Protein A/G and then with SAPE. The median fluorescence intensities (MFI) of the three analytes in each well were then read on a Flexmap 3D instrument.

GHANA SERA SAMPLE SCREENING

In the absence of positive and negative controls for the tested animal species (pigs and bats) and for the human samples, it is technically difficult to set up a cut-off value that would allow us to discriminate between a positive and a negative sample. As such, a value of 1000 MFI was arbitrarily chosen as an initial cut-off. All samples beyond this value were considered as positive and were chosen for further confirmations by immunofluorescence. Furthermore, by comparing the MFI obtained for one analyte to the other analytes it is possible to obtained information on the background signals. The results of the sample screening by luminex with EBOV, LLOV and HeV antigens for human, bats and pigs are shown Figs. 47A, 47B and 47C respectively.

As can be observed, for majority of the samples the MFI were below the decided cut-off (indicated by a black line, Figs. 47A to C). In humans, four samples were above the 1000 MFI cut-off for EBOV and LLOV antigens (Fig. 47A), whilst seven samples showed a strong reactivity for HeV antigen. Of interest, the V123 human sera that appeared positive by immunofluorescence for LLOV gave a signal close to 1000 MFI (980 MFI) in this assay. On the opposite side, the V26 serum that was apparently positive by immunofluorescence for LLOV gave an MFI value for this antigen that couldn't be disassociated for background signals, whilst giving strong MFI values for EBOV and HeV antigens (243.50 LLOV MFI, 4327.50 EBOV MFI, 3261.75 HeV MFI).
In bats, samples from *M. daubentonii* that were sampled in the United Kingdom were included and considered as naive for any Filo-like virus and helped to obtain information on the background signals (Fig. 47B; the symbols on the Figure are associated to different bat species). Of special interest, for other bat species several sera appeared to possess antibodies that bound strongly LLOV and EBOV antigens, especially the 5510 sera obtained from a *E. franqueti* bat that resulted in a very strong signal for EBOV (10490 MFI) with no or very little signal for LLOV and HeV (107.25 MFI and 83.25 MFI, respectively).
For pig samples, sera from a hyper-immune pig that was obtained both before and after immunisation with EBOV virus-like particles served as a negative and positive control respectively (Fig. 47C; EBOV-VLP- and EBOV-VLP+). Before immunisation, for all antigens, the MFI obtained were ranged from 300-500 (LLOV and EBOV) to 2000 (HeV). The high signal that was obtained using the post-immunisation sera and that only increased for EBOV confirmed the specificity of the assay (23143.33 for EBOV MFI against 947.67 for LLOV MFI and 2178.66 for HeV MFI). Interestingly, several pig sera showed a strong reactivity to the two filovirus glycoproteins, especially the P33 and P49 sera that gave respectively MFI values of 9897.75 and 4239 for LLOV antigens. Those values were at least 10 times above the value obtained when the LLOV beads were incubated with the negative pig control (484 MFI) and were at least 4 times above the values obtained for EBOV and HeV analytes with the same sera samples. The P90 sera also gave a strong MFI for EBOV (7200.75 MFI) that was also 4 times above the values obtained for LLOV and HeV beads (1081.75 LLOV MFI and 1667.00 HeV MFI). Overall, our results show that the same proportion of humans positive for EBOV and LLOV antibodies was obtained in this assay (2.9% of the sera above 1000 MFI). For pigs appear to have more antibodies against a LLOV-like virus than against the EBOV-like virus (41% and 17%, respectively), while bats had more antibodies against an EBOV-like virus than a LLOV-like virus (2.8% for LLOV-GP against 5.7% EBOV-GP).

As of a result, using the Luminex® technology and a home-made assay, it was possible to detect the presence of antibodies in the sera of humans, domestic pigs and different bat species against potential EBOV and LLOV-like virus(es) circulating in Ghana.

A

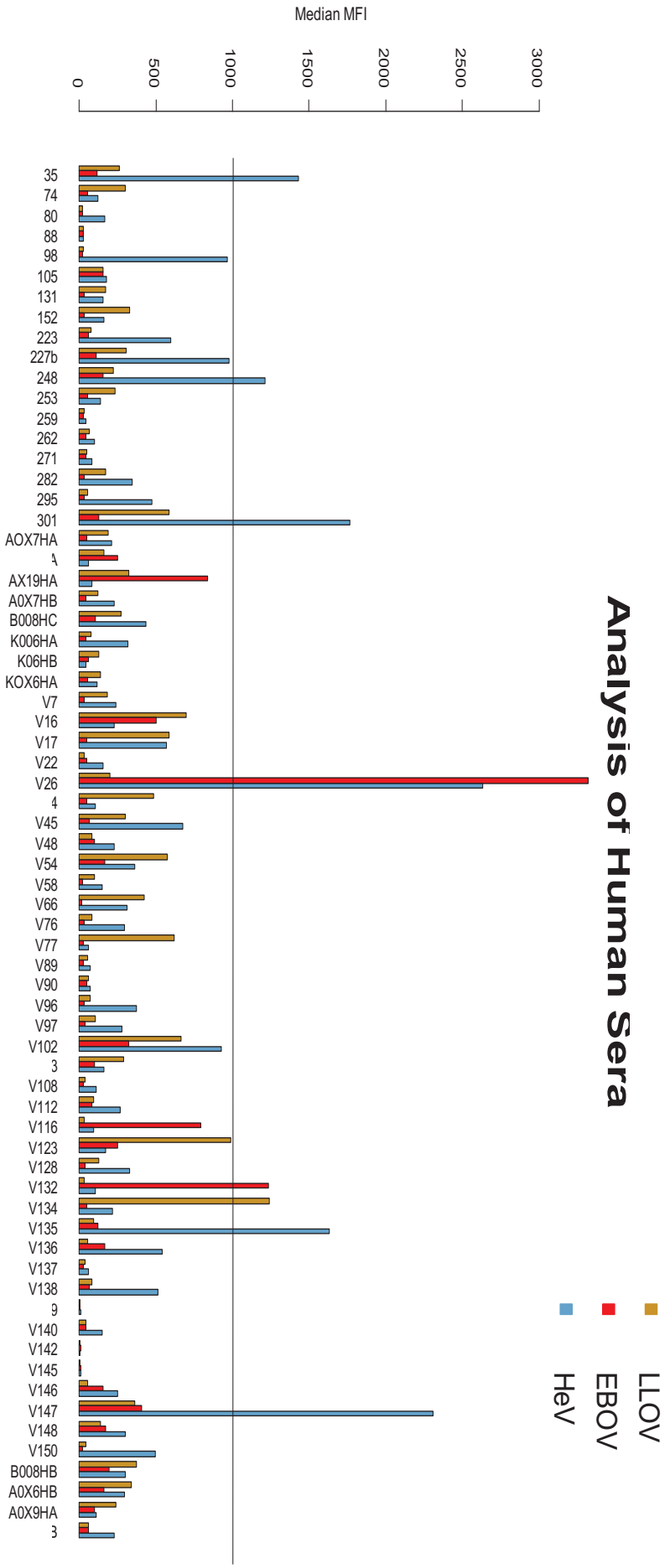
Analysis of Human Sera
Median MFI
0
500
1000
1500
2000
2500
3000
35
74
80
88
98
105
131
152
223
227b
248
253
259
262
271
282
295
301
AOX7HA
AX19HA
A0X7HB
B008HC
K006HA
K06HB
KOX6HA
V7
V16
V17
V22
V26
4
V45
V48
V54
V58
V66
V76
V77
V89
V90
V96
V97
V102
3
V108
V112
V116
V123
V128
V132
V134
V135
V136
V137
V138
9
V140
V142
V145
V146
V147
V148
V150
B008HB
A0X6HB
A0X9HA
3
LLOV
EBOV
HeV

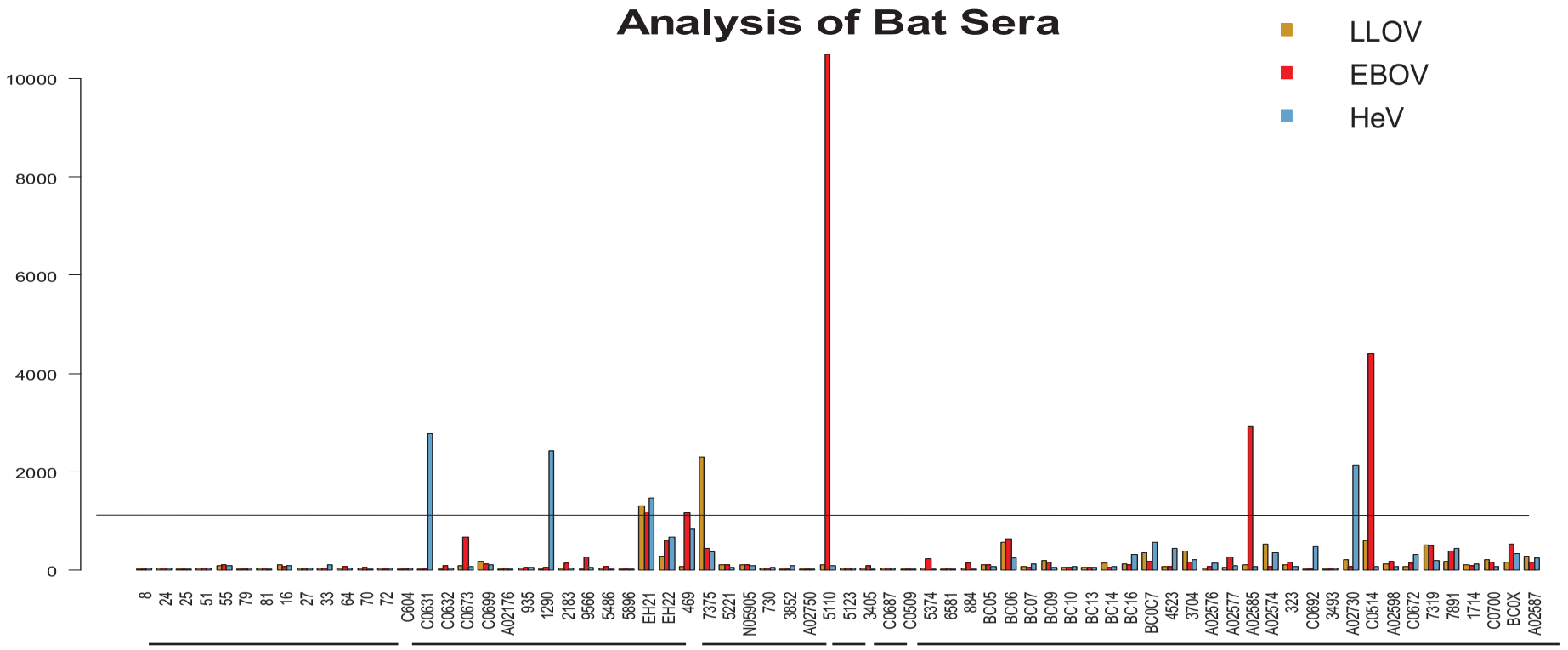
Analysis of Bat Sera
LLOV
EBOV
HeV
10000
8000
6000
4000
2000
0
8
24
25
51
55
79
81
16
27
33
64
70
72
C604
C0631
C0632
C0673
C0699
A02176
935
1290
2183
9566
5486
5896
EH21
EH22
469
7375
5221
N05905
730
3852
A02750
5110
5123
3405
C0687
C0509
5374
6581
884
BC05
BC06
BC07
BC09
BC10
BC13
BC14
BC16
BC0C7
4523
3704
A02576
A02577
A02585
A02574
323
C0692
3493
A02730
C0514
A02598
C0672
7319
7891
1714
C0700
BC0X
A02587

C

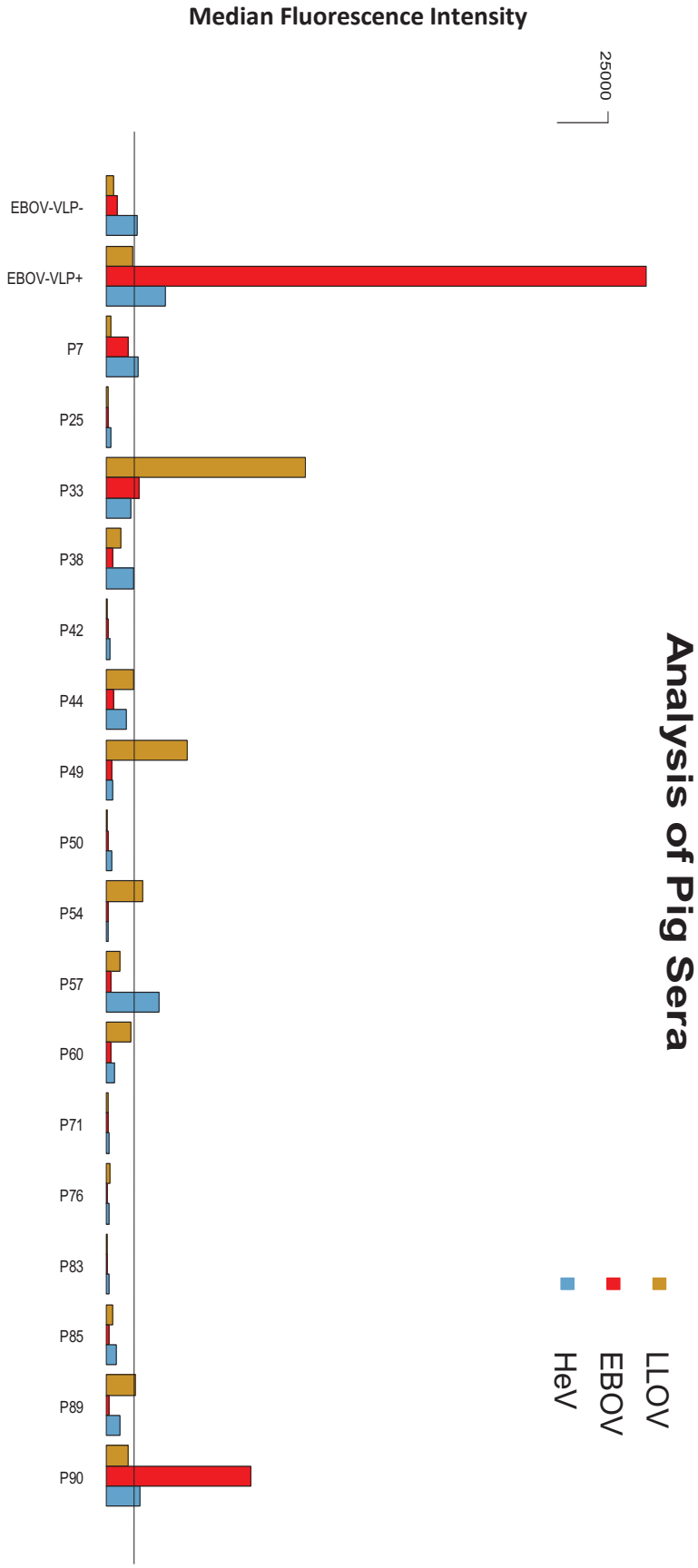
Median Fluorescence Intensity
25000
EBOV-VLP-
EBOV-VLP+
P7
P25
P33
P38
P42
P44
P49
P50
P54
P57
P60
P71
P76
P83
P85
P89
P90
Analysis of Pig Sera
LLOV
EBOV
HeV

FIGURE 47. GHANIAN SERA SCREENNING

Human (A), bat (B) and pig (C) ghanian sera were collected and analysed by luminex using microsphere beads coupled with EBOV GP, LLOV GP and HeV G antigens that were generated before. The horizonal line representes the chosen cut-off of 1000 MFI. For the bat samples, the names of the species are indicated below the figure. In the case of the *M. daubentonii* species, the samples were collected in England as part of a surveillance program for Rabies virus.

LUMINEX DATA CONFIRMATION BY INDIRECT IMMUNFLUORESCENCE ASSAY

To confirm the luminex results presented above, the sera that gave the strongest MFI were selected and analysed by immunofluorescence as before. In this respect, VeroE6 cells were transfected either with plasmids encoding EBOV GP, LLOV GP or an empty plasmid as control. Cells were then fixed and incubated with diluted sera (Fig. 48). In a similar fashion than what was observed in Fig. 44), when a serum does not contain any specific antibodies against one of the expressed viral glycoproteins, the observed staining is either very diffused or almost indistinguishable (see Fig 48. 'Empty' row; LLOV GP in Lanes 1 and 5 and EBOV GP, Lanes 3 and 4). Conversely, positive sera gave a distinct staining pattern in transfected cells (Fig. 48, cells considered positive are marked by a white arrow). Generally, an accordance was observed between sera that gave positive, specific signals in this assay and the sera that had an MFI >1000 by luminex assay. One exception was observed for the human sera V132 for which we obtained an MFI of 1232.75 for EBOV and 34.75 for LLOV by Luminex but that seemed to give positive signals for antibodies against LLOV glycoprotein instead of EBOV in this assay. Indeed, and as expected, positive cells were found when EBOV GP transfected cells were incubated with the positive pig sera control, while no staining or nonspecific staining was observed following incubation with cells transfected with LLOV GP plasmid or an empty plasmid (Fig. 48, Lane 1). Of special interest, similarly stained EBOV GP transfected cells were found with the highly reactive bat sera 5510. On the other side, the staining obtained for LLOV with this serum was similar to what was observed for the empty plasmid, demonstrating the detection of specific EBOV GP antibodies in those two sera (Fig. 48, Lanes 1 and 5). For LLOV, using the pig sera P33, comparable results to what was obtained for EBOV and the bat sera 5510 were observed (Fig. 48, Lane 3). Interestingly, the pig P90 sera had MFI above for 1000 for both EBOV and LLOV and appeared to be both also positive for antibodies directed against EBOV and LLOV antibodies by immunofluorescence, with positive cells that were found in both conditions, suggesting the presence of cross-reacting antibodies in this serum (Fig. 48, Lane 2).

Consequently, and at the exception of one human serum, it was possible to confirm the results obtained by Luminex using an indirect immunofluorescence approach. Of interest, the sera obtained from an *E. franqueti bat*, for which RNA against EBOV has been detected (see paragraph 'Natural and accidental hosts of Filoviruses) was positive for EBOV in both techniques. In a similar fashion, the pig sera P33 was also positive by Luminex and indirect immunofluorescence. Taken together, those results are strongly suggesting that at least one EBOV and/or LLOV-like viruses are circulating in Ghana, West Africa.

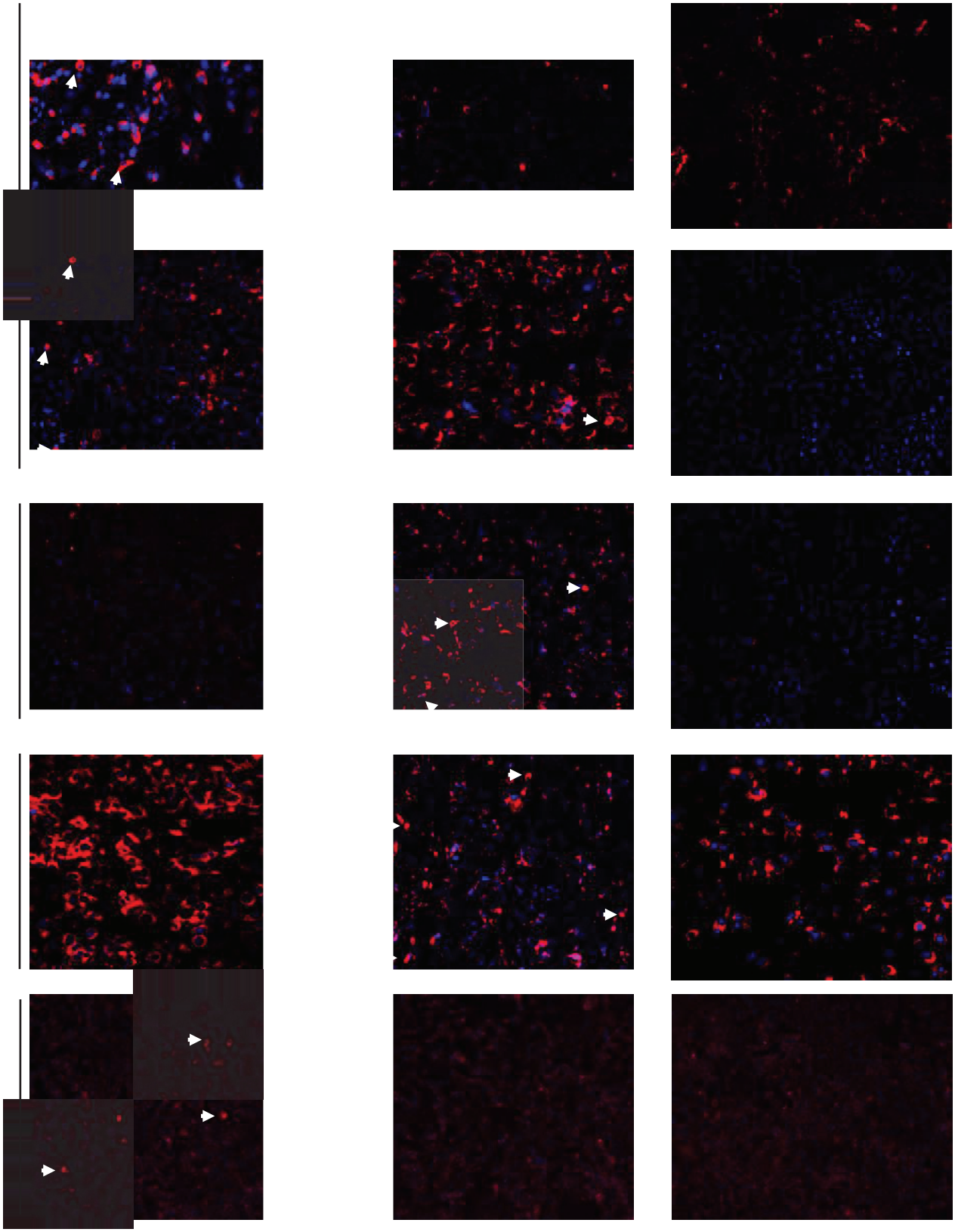

FIGURE 48. CONFIRMATION OF LUMINEX RESULTS BY INDIRECT IMMUNOFLUORESCENCE ANALYSI

Similarly to before, sera showing the highest reactivity by luminex were chosen for confirmation by in immunofluorescence using cells transfected with EBOV GP, LLOV GP or an empty plasmid. The white arrows indica position of positive cells. The values obtained by luminex are indicatecd.

The results obtained so far lead to believe that in Ghana, one or several filo-like viruses are circulating in different animal species and that these viruses can infect humans. To confirm those results, animal tissues were collected to obtain samples for RNA extraction, histology analysis as well as for as viral isolation attempts in cases where samples were found positive by RT-PCR.

During this mission, 76 *E. gambianus* bats, 67 *R. aegyptiacus* bats and 73 *S. domesticus* (domestic pigs) were sampled. Bat and pig samples were collected at two different localisations (Fig. 49A): *E. gambianus* samples were obtained in the Ghanaian capital Accra from bats roosting in the trees of the 37th Military hospital while *R. aegyptiacus* tissues were collected from bats nesting in the Buoyem caves, near Techiman further north (Fig. 49B and C). All bats were captured by skilled bat hunters using nets that were set up near their resting trees or at the exit of the cave (Fig. 49E and C). After capture, bats were transported in cotton bags to the sites of necropsy (Fig. 49B and D) and were kept and feed in a cage (Fig. 50A and B, upper panel) prior to being euthanized for sampling. For the bats, the brain, lungs, kidneys, liver, spleen, intestines, lymph nodes and gonads, as well as rectal and oral swabs were collected and stored in RNAlater prior to RNA extraction. The canines were also extracted and used for cementum age determination (Fig. 50B, left panel). Bats were also weighed and measured (Fig. 50B, right panel). For pigs, samples were collected in different farms in Techiman and in Accra. When possible, lungs, liver, spleen, intestines, lymph nodes and kidneys were collected. Samples were kept on ice before being processed similarly to the bat tissues. During the necropsy, a report of all observed signs of infection, including for example the presence of lesions or lymph nodes enlargements, was kept for both pigs and bats.

In total, excluding the oral and rectal swabs, 1245 samples were collected and used for total RNA isolation (Fig. 51A). RNA analysis showed a clear difference in total RNA yield obtained for the different organs, with the livers, the spleens and the lymph nodes giving more RNA than the brain, gonads, intestines and lungs, for the three species (Fig. 51B). Northern blot analyses of the 28S and 18S rRNA subunits for RNA extracted from bat tissues (gonads and intestines) were performed to verify RNA integrity (Fig. 51C). As can be observed, the two rRNA subunits are visible for all samples and no degradation was observed. In addition, RNA from *R. aegyptiacus* and *E. gambianus* were successfully used to amplify the NPC1 gene as a quality control (data not shown).

Therefore, those data demonstrate that RNA was not degraded during the different steps that lead to its isolation and that it is suitable to perform nested RT-PCR.

FIGURE 49. SAMPLING LOCALISATION AND LABORATORIES INSTALLATION

Map of Ghana (A) showing the cities where the different bat and pig samples were collected. The R. aegyptiacus were collected, near Techiman (B), in the Bouyem Caves (C, the exit of the cave is shown). The E. gambianus were sampled in Accra (D) in the fields of the 37 Military Hospitals (E). Pigs were sampled from local farms in Techiman or from the great Accra region.

A

E. gambianus

R. aegyptiacus

B

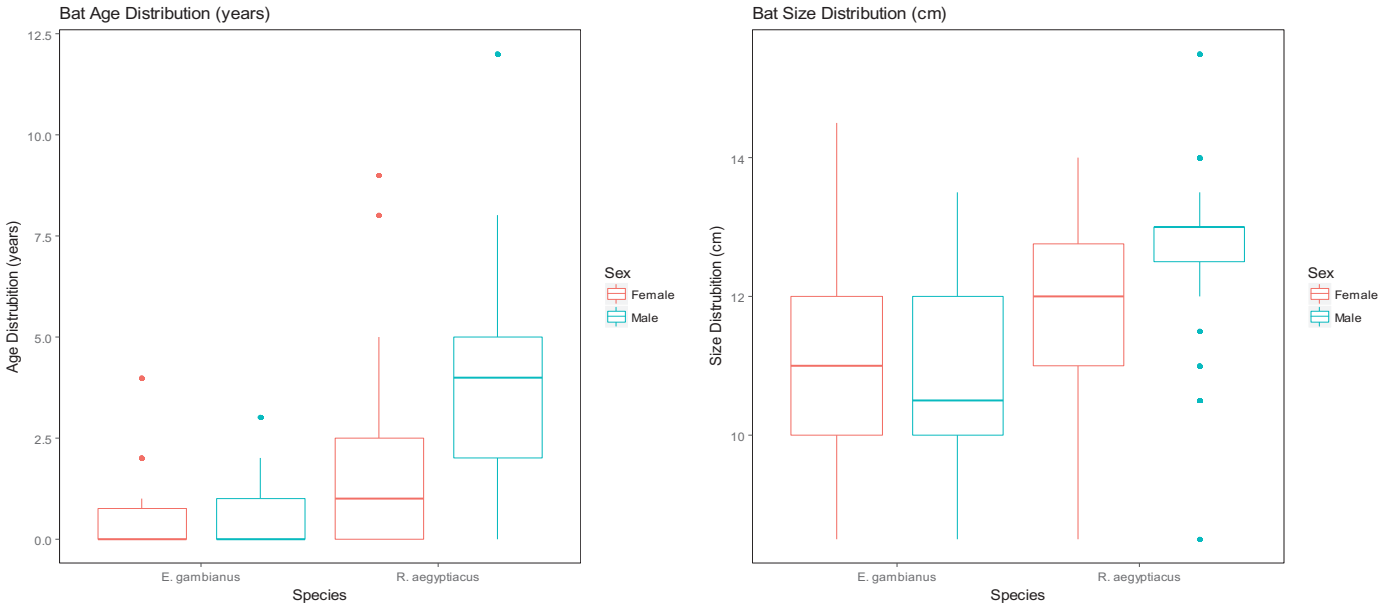

FIGURE 50. AGE AND SIZE DISTRIBUTION OF *E. GAMBIANUS* AND *R. AEGYPTIACUS* SAMPLED BATS

Representative pictures of each bat species are shown (A). Canines were extracted for cementuum aging (B, left panel) and the size of each animal was measured (right panel).

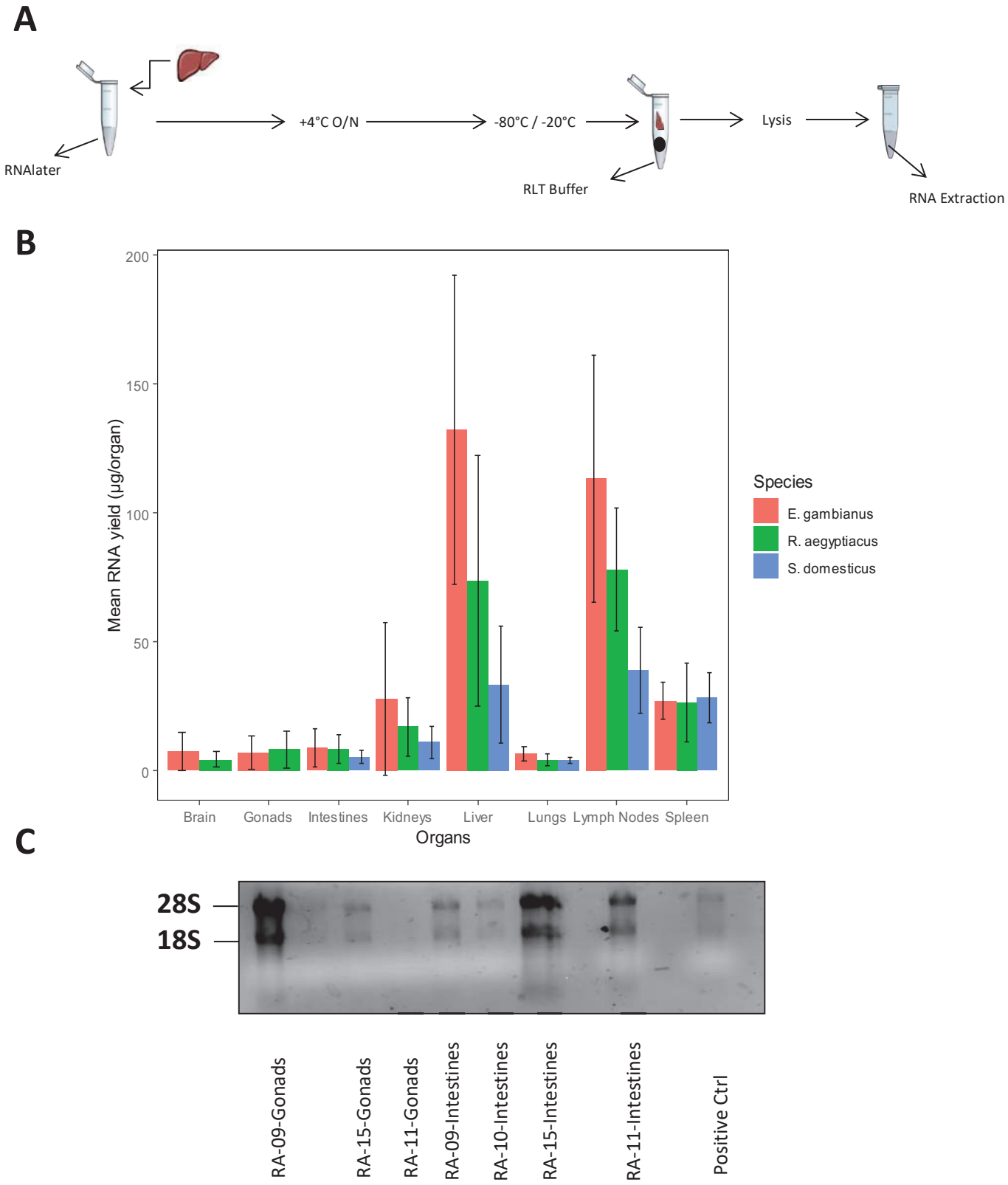

FIGURE 51. RNA EXTRACTION ANALYSIS FROM GHANAIAN ORGANS STORED IN RNALATER

The protocol outlines used for storing samples before RNA extraction is shown in (A). For RNA extraction, samples were removed from the RNAlater and the organs were destroyed in a RLT buffer. RNA extraction was performed as per the manufacturer's instructions and the amount in µg per organ is shown in (B). Several samples were used to verify the RNA integrity by northern-blot and the position of the rRNA 28S and 18S are shown (C). RA: R. aegyptiacus; Ctrl: Control (cellular extract)

To detect any putative new or already existing Filovirus in the collected samples, primers directed against a highly conserved region of the Filovirus polymerase L were used to perform nested RT-PCR. Samples that showed an amplicon of the correct, predicted size after the nested PCR (270 nucleotides) were sent for Sanger sequencing.

For all of the samples analysed following nested RT-PCR, only a few gave an amplicon with a correct size (Fig. 52A, within the white rectangle). From all of the sequences obtained, three samples corresponding to the *R. aegyptiacus* bats #1 (lymph nodes, '***', Fig. 52A), #6 (spleen, '*', Fig. 52A) and #12 (lymph nodes, '**', Fig. 49A) were purified and sent for sequencing. The DNA chromatograms obtained after sequencing are shown (Fig. 52B) and demonstrate the high quality of the sequences obtained that contained no (Fig. 52B, *R. aegyptiacus* bats #1 and #6) or very little parasite sequences (Fig. 52B, *R. aegyptiacus bat* #12). Following sequencing, similarity searches between the newly obtained sequences and known filoviruses were performed using the Megablast algorithm. Of particular interest for our study, it was found that the three sequences amplified from the different bats indeed aligned with existing MARV natural isolate sequences already present in the database (Fig. 52C). For convenience, only the first result of the Megablast analysis is presented and all substitutions are highlighted by black rectangles. Of note, for the three different animals, between 9 and 11 substitutions (95% to 96% identity) were found compared to published MARV sequences. Importantly, expectation values (E-value[6]; 'Expect' in Fig. 52C) ranged from $2x10^{-96}$ to $4x10^{-98}$, confirming the specificity of the blast results and allowing us to affirm that those animals were indeed infected with a MARV-related virus.
Multiple sequence analysis (Fig. 52D) and phylogenetic tree reconstruction (Fig. 52E) showed that the three newly-identified sequences were more related to the Angola strain of MARV than to RAVV strains (2009 bat isolate and 1987 human isolate). Interestingly, the sequence found in the *R. aegyptiacus* bat #12 did not cluster with the other two bat sample results in the phylogenetic trees, suggesting that at least two different MARV-like viruses are circulating in *R. aegyptiacus* bats in Ghana.

Through the collection of different bat and pig tissues, we were able to identify sequences of at least one unknown Filovirus that appeared to be closely related to MARV-Angola. This is the first identification of filoviruses sequences that are closely related to a highly pathogenic Filovirus for humans in an area where no filovirus outbreak has yet been reported.

[6] E-value: The lowest this value is, the lower the chance of two sequences aligning by chance.

A

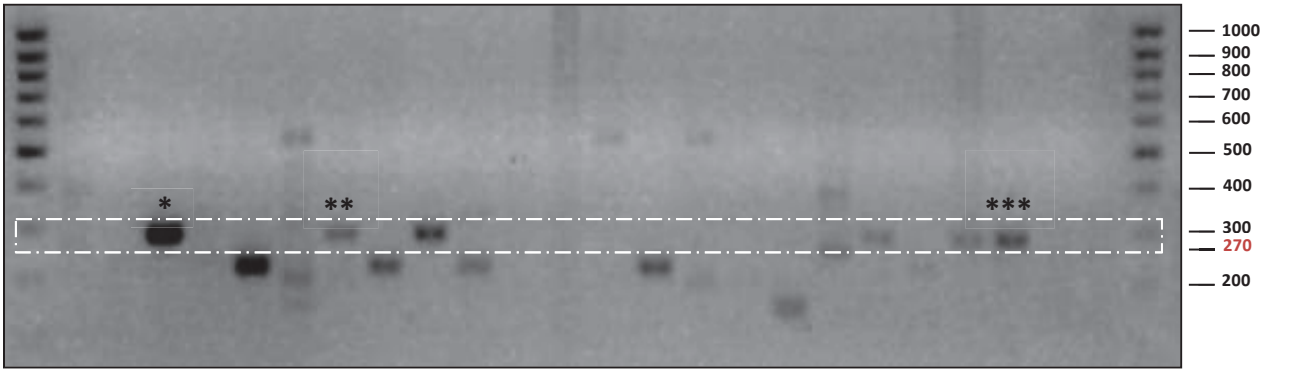

B

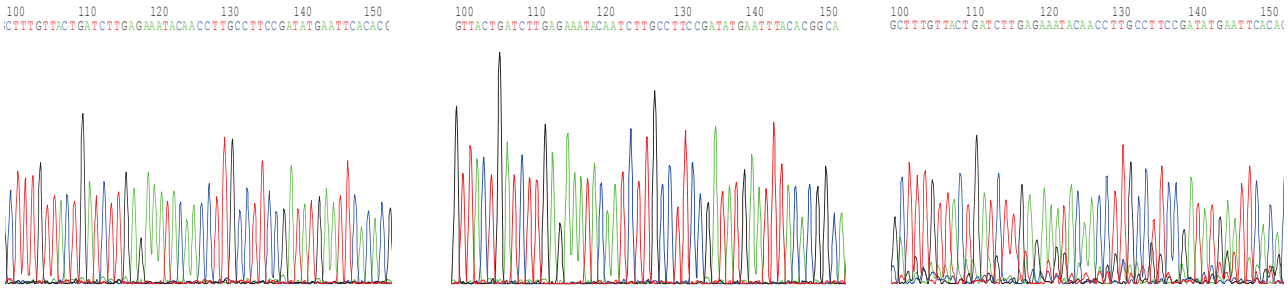

C

***R. aegyptiacus* #01 Lymph nodes**

Score	Expect	Identities	Gaps	Strand
368 bits(199)	4e-98	221/232(95%)	0/232(0%)	Plus/Plus

```
Query  1      GCATTATTGCATCAGGCCTCTTGGCACCATAATTCAGCAAGCATAGGGGAAAACGCTATA  60
Sbjct  13283  GCTTTATTGCATCAGGCTTCTTGGCACCACAATTCAGCAAGCATAGGGGAAAACGCCATA  13342
Query  61     GTGAGAGGTGCGAGCTTTGTTACTGATCTTGAGAAATACAACCTTGCCTTCCGATATGAA  120
Sbjct  13343  GTGAGGGGTGCGAGTTTTGTTACTGATCTTGAGAAATACAACCTTGCCTTCCGATATGAA  13402
Query  121    TTCACACGGCATTTCATAGACTACTGTAATCGATGTTATGGTGTTAAGAATTTATTCGAT  180
Sbjct  13403  TTTACACGGCATTTCATAAACTACTGTAATCGATGTTATGGTGTGAAGAATTTATTCGAT  13462
Query  181    TGGATGCACTTTTTAATACCACTATGTTATATGCATGTGAGTGATTATTATA  232
Sbjct  13463  TGGATGCACTTTTTAATACCACTATGTTATATGCATGTCAGTGATTTTTATA  13514
```

***R. aegyptiacus* #06 Spleen**

Score	Expect	Identities	Gaps	Strand
364 bits(197)	5e-97	215/224(96%)	0/224(0%)	Plus/Plus

```
Query  5      GCATCAAGCCTCTTGGCACCATAATTCAGCAAGCATAGGGGAAAACGCTATAGTGAGAGG  64
Sbjct  13307  GCATCAAGCTTCTTGGCACCACAATTCAGCAAGCATAGGGGAAAACGCCATAGTGAGGGG  13366
Query  65     TGCGAGTTTTGTTACTGATCTTGAGAAATACAATCTTGCCTTCCGATATGAATTTACACG  124
Sbjct  13367  TGCGAGTTTTGTTACTGATCTTGAGAAATACAACCTTGCCTTCCGATATGAATTTACACG  13426
Query  125    GCATTTTATAGACTACTGTAATCGATGTTATGGTGTGAAGAATTTATTCGATTGGATGCA  184
Sbjct  13427  GCATTTCATAAACTACTGTAATCGATGTTATGGTGTGAAGAATTTATTCGATTGGATGCA  13486
Query  185    CTTTTTAATACCACTATGTTATATGCATGTGAGTGATTATTATA  228
Sbjct  13487  CTTTTTAATACCACTATGTTATATGCATGTCAGTGATTTTTATA  13530
```

***R. aegyptiacus* #12 Lymph Nodes**

Score	Expect	Identities	Gaps	Strand
363 bits(196)	2e-96	220/232(95%)	0/232(0%)	Plus/Plus

```
Query  1      GCATTATTGCATCAGGCCTCTTGGCACCATAATTCAGCAAGCATAGGGGAAAACGCTATA  60
Sbjct  13283  GCTTTATTGCATCAGGCTTCTTGGCACCACAATTCAGCAAGCATAGGGGAAAACGCCATA  13342
Query  61     GTGAGAGGTGCGAGCTTTGTTACTGATCTTGAGAAATACAACCTTGCCTTCCGATATGAA  120
Sbjct  13343  GTGAGGGGTGCGAGTTTTGTTACTGATCTTGAGAAATACAACCTTGCCTTCCGATATGAA  13402
Query  121    TTCACACGGCATTTCATAGACTACAGTAATCGATGTTATGGTGTTAAGAATTTATTCGAT  180
Sbjct  13403  TTTACACGGCATTTCATAAACTACTGTAATCGATGTTATGGTGTGAAGAATTTATTCGAT  13462
Query  181    TGGATGCACTTTTTAATACCACTATGTTATATGCATGTGAGTGATTATTATA  232
Sbjct  13463  TGGATGCACTTTTTAATACCACTATGTTATATGCATGTCAGTGATTTTTATA  13514
```

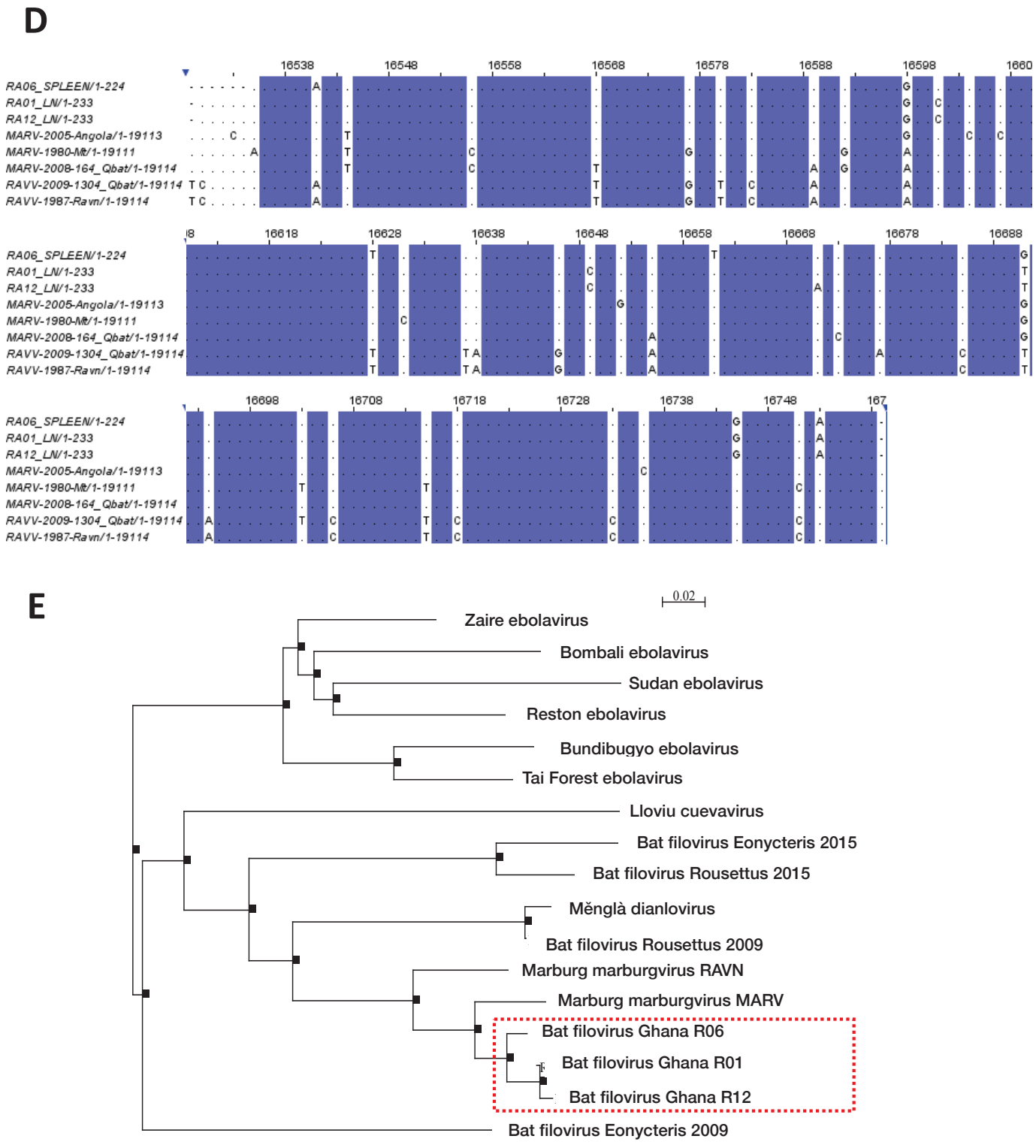

FIGURE 52. MARBURGVIRUS-LIKE SEQUENCES IDENTIFICATION AND ANALYSIS

Nested RT-PCR using pan-filovirus primers, recognising both EBOV and MARV viruses, were performed (A). Organs that had amplicon matching the expected amplicon size (highlighted by a white rectangle in A) were sequenced. The sequencing DNA chromatograms (B) and the results of the blast analysis (C; only the first result of the analysis) are shown. Using the Muscle program for multiple sequence alignment, the ghanian sequences were aligned with sequences of known MARV and RAVV strains (D) and a phylogeetic analysis was performed (E). For those analysis the JalView program was used and the position of the MARV-like viruses are shown by a red rectangle. In D, the dots are showing non-conserved regions and only the nucleotides that are conserved between few sequences are shown. The regions which are highlighted in blue are regions conserved between all sequences. RA: *Rousettus aegyptiacus*; LN: Lymph nodes

The discovery of potential new circulating viruses and their natural hosts and the identification of regions where such highly pathogenic viruses are present is essential in limiting, as much as possible, spillover events into the human population and to prevent new epidemies. In this part of our work, we aimed to detect potential, new or already known filoviruses in Ghana, West Africa, a region which has been so far been spared from any recognized filovirus outbreak, despite being surrounded by countries that were recently affected by EBOV.

In a first series of experiments, we tried to confirm serology results using indirect immunofluorescence (IFA), obtained previously for EBOV and MARV antibodies by Profs. A. Cunningham and J. Wood, and obtained with an in-house multiplex luminex assay, which they were developing using different EBOV and MARV GP mutants. Whilst we were unable to confirm their results, we were able to detect antibodies directed against the LLOV glycoprotein in both human and animal sera samples they provided, suggesting that at least one filovirus (either LLOV or a LLOV-like virus) is circulating in Ghana (Fig. 44). The discrepancy between their bead-based assay and our results obtained by indirect immunofluorescence could come from the nature of the antigens used. In our assay (IFA) the antigens used were well characterized proteins expressed from native EBOV and LLOV GP genes whereas for the luminex assay, the antigens used were sTAG-ged proteins that were released into the cell culture supernatant through the deletion of the glycoprotein transmembrane domains and protein trimerisation was forced through the addition of a GCN trimerisation peptide [341]. In this context, the actual structures of the glycoproteins which were bound to the beads to perform the luminex assay in their hands are unknown and could have provided false positives. Technique dependent-differences in antibody detection of viral proteins by IFA or ELISA (or similar techniques, such as Luminex) are well documented, with the latter being less sensitive and more incline to provide false positives [342–344].

Therefore, to confirm our IFA results and to compensate for the little amount of sera that were available for the experiments that made it impossible to perform sera-neutralizing assays, which is considered as a gold standard for serology, we also decided to develop our own multiplex bead-based assay. The advantage of this system is that, compared to ELISA, it allows the simultaneous detection of antibodies against several viruses in a single well. In this respect and as a source of antigens, we chose to generate EBOV and LLOVΔTM-His-tagged mutants, which are commonly used to detect filovirus antigens [345,346] (Fig. 45). In the absence of their transmembrane anchor, the viral glycoproteins are continuously secreted into the cell culture supernatant, with no sign of cytotoxicity compared to the anchored glycoproteins, providing a reliable and single source of antigens, which can also be easily purified by their histidine tag. As stated above, the choice of the source of antigens and even the expression system used is vital and can severely affect the results obtained for the detection of antibodies against a specific pathogen. It is therefore essential to choose a protein that resembles as much as possible the native surface proteins of the pathogen of interest. In this respect, deglycosylation treatments proved to be a powerful tool to assess the conserved structure of filovirus glycoproteins (See, Part. 1). Expectedly, we were able to observe a significant increase in release of these mutated viral glycoproteins into the cell culture supernatants, compared to their wild-type counterparts (Fig. 45). Furthermore, our analysis showed that the $GP_{1,2}\Delta$TM-His proteins that were released into the culture media were

resistant to Endo H treatments but sensible to PNG F, and were, as such, resembling the wild-type viral glycoproteins which are present in viral particles (Figs. 45 and 33B of Part 1). The fact that our constructs have similar glycosylations to the wild-type glycoproteins is essential as it was demonstrated multiples times that changes in EBOV glycosylations were able to impact its immunogenicity and to interfere with the protein structure [34,141,144,280,282] (see also $GP_{2\text{-}RES}$ results from Part 1). Interestingly, and of note, during our glycosylation analysis, we were able to observe that the levels of Pre-GP_{ER} are lower in LLOV GP transfected cells compared to EBOV transfected cells, suggesting that LLOV $GP_{1,2}$ is processed and glycosylated faster than EBOV $GP_{1,2}$ (Fig. 45).

Using different amounts of EBOV GP_1, LLOV GP_1 and His-tag antibodies we were able to confirm coupling of our purified antigens on luminex microspheres (Fig. 46). Of importance, in these experiments, we were able to observe differences in the ability of different EBOV GP_1 monoclonal antibodies to detect the coupled $GP_{1,2}\Delta TM$ antigens. Indeed, when using the non-neutralizing EBOV GP_1 3373 antibody, despite observing a response curve to antibodies, the MFI obtained were significantly lower than those obtained with the neutralizing EBOV GP_1 3327 antibody [305] (Fig. 46 upper panel). Similar results were obtained with the only anti-LLOV GP sera available in our laboratory, which lead us to use an anti-His-tag antibody to confirm LLOV $GP_{1,2}\Delta TM$-His coupling (Fig. 46, lower panel). Of importance, the 3327 antibody was shown to recognize a conformational epitope, suggesting that the EBOV anchorless-mutant has a structure that would be conserved with the virion-bound $GP_{1,2}$ protein and that we are likely to be able to successfully detect antibodies against filovirus using the tools we have developed.

Using this novel assay, we investigated the presence of EBOV and LLOV antibodies in different animals and human sera (Fig. 47). To determine the limit of positivity in a serology assay, a cut-off is usually determined using positive and negative sera or is calculated by comparison with more robust methods such as sera neutralizing assays [302]. In our case, in the absence of both controls for humans and for each bat species, as well as a limited volume of sera that limited the possibility of performing cross-reactive serological assays, we decided to set our cut-off as 1000 MFI.
Several sera provided positive results in our screening. For instance, *E. franqueti* bat sera 5510 was highly reactive for EBOV glycoprotein whilst giving very little signal for LLOV and HeV glycoproteins, suggesting the presence of specific antibodies against EBOV. Similar conclusions can be made for LLOV and the *E. gambianus* sera 7375 or with the pig sera P33. In addition, the detection of antibodies directed against filoviruses in *R. aegyptiacus* and *E. franqueti* bats, but also in pigs, is consistent with data obtained previously by others [34,45,296,299,347]. Of interest, our results showed that for most of the sera, there was very little cross-reactivity between the different glycoproteins used from the same or for a different virus family (e.g 5510 or P33), highlighting the possibility to further multiplex this assay and to include all filoviruses known so far to obtain a full spectrum of the different filovirus circulating in this area. Similarly to before, we aimed to confirm our luminex results by IFA (Fig. 48). Remarkably, compared to the first results obtained by luminex (Fig. 47), with the exception of one serum, we were able to find a good correlation between the samples that reacted strongly in our luminex assay and those that appeared positive by IFA. The inability to confirm the presence of antibodies for one of the samples that had a high MFI by luminex by IFA could be

again explained by differences in protein structures and their presentation and therefore epitope availabilities, as explained above.
Taken together, our results strongly suggest that one or several filoviruses are circulating in Ghana. The detection of antibodies against EBOV in humans is also not surprising. However, it is the first time that in humans, antibodies against one or several filoviruses were detected in this country, which has never reported any EBOV cases [9]. LLOV has never been isolated and in the absence of any outbreak in humans thus far is believed to be non-pathogenic for mankind [3,6]. To our knowledge, it is also the first time that antibodies that can bind LLOV glycoprotein have (i) ever been detected in Africa, and (ii) that humans as well as pigs, showed antibodies against this virus [34]. While antibodies against EBOV in humans, that otherwise declared no apparent Filovirus-like associated-disease, have already been documented, those data were obtained from countries which have previously been affected by the virus or were undergoing an outbreak, and are therefore thought to be the result of asymptomatic EBOV infection [348,349]. However, in this case, we believe that the detection of antibodies against EBOV or LLOV are more likely to be the result of an infection with a closely related but non- or mildly-pathogenic filovirus. The idea that a sub-lethal virus could be circulating in specific regions and that it could then confer protection against a more pathogenic virus of the same family has been suggested to explain the relatively high seroprevalence observed in some studies for lethal viruses such has EBOV, while having, in the end, only a limited number of outbreaks [350,351]. The recent discovery of *Bombali ebolavirus* — whilst its pathogenicity remains unknown for humans — and the high seroprevalence in the Bombali District for EBOV antibodies could actually fit this hypothesis [298,352].

To confirm our serology analysis, we attempted to detect any potential circulating filovirus by sampling organs from two bat species (*E. gambianus* and *R. aegyptiacus*), as well as domestic pigs, by sampling in two different regions of Ghana (Fig. 49). The organs and the bat species sampled were chosen based on our serology results and the fact that Rousettus spp. have been shown to be the host of several MARV and MARV-related virus [4,5,34,39,44,53]. In this project, we sampled more than 67 animals for each species (75 *E. gambianus*, 67 *R. aegyptiacus* and 73 *S. domesticus*). The number of animals were selected based on our serological data and previous publications. Indeed, we evaluated that, if the virus would be circulating in these animal species in this region and at this time of the year, it is the necessary number of animals to have at least one positive sample (estimations made with Sampsize V0.6.0). Furthermore, it has been shown for MARV that the infection prevalence increased during the weeks preceding the twice-yearly birthing season for the sampled bat species [353]. Therefore, the good quality of our RNA after storage and extraction and the fact that the sampling mission occurred in the window that was suggested to be favourable for the detection of MARV [353], gave us confidence that this should not interfere with our assay sensitivity and that we should be able to detect a filovirus if it is present in our samples (Fig. 51).

Nested RT-PCR screening on *E. gambianus* and *S. domesticus* samples failed to provide any positive samples. Domestic pig sampling was performed in different pig farms that were in or around Techiman and Accra, but in most of the cases we were not able to obtain the exact origin of the animals and to know if they were housed together. It is thus very unlikely that we sampled the required number of animals from the same population. Therefore, in the absence of a clearly defined population, we cannot apply our initial estimation on the number of animals

necessary to get a single positive sample and this could explain why we failed to detect any virus in our samples for these species.
For *E. gambianus* bats, with the exception of antibodies against EBOV and RESTV, no filovirus or RNA sequences of filo-like viruses have been detected [34,300]. *R. aegyptiacus* and *E. gambianus* habitats are incomparable, one living in caves and the other one roosting in trees. Furthermore, our observations showed that the two species do not have the same behaviour in cages. Indeed, clear social behavioural differences between the two bat species could be observed and could provide hints on how the viruses can be maintained in the population (Fig. 50). In the cages, *E. gambianus* bats were always separated from each other's, except when feeding on the same fruit, whereas the *R. aegyptiacus* bats were always seen packed together. It can thus tempting to speculate that for *E. gambianus* bats, the horizontal transmission of different viruses is more likely occurring through fomites than through direct individual contacts, as already described for MARV transmission in *R. aegyptiacus* bats [43]. Those differences could play a substantial role in viral dynamic transmission and maintenance and as our experimental design was made according to data obtained on the relationship between MARV and *R. aegyptiacus*, it could also explain the absence of positive samples in this population.

While we were not able to detect any filovirus in *E. gambianus* and *S. domesticus*, three of our *R. aegyptiacus* bats were positive for a MARV-like virus in organs that are known to be the main targets for filovirus replication (Fig. 52A) [25,39,41]. Based on the number of *R. aegyptiacus* that were sampled, we estimated the rate of infection to be of 4% at that time and in this population. Those results are in line with what has already been observed previously [353]. Sequence analysis showed that our sequences have 95% identity at the nucleotide level and that they have 99% identity at the protein level, with one mutation that is not silent (F>Y), with all known MARV and RAVV strains. The high number of mutations (between 9 to 11 nucleotides substitutions for sequences of about 220 to 230 nucleotides) and the quality of the sequencing data allow us to fully exclude any contamination coming from our different positive controls used during the nested RT-PCR or sequencing issues and to be certain of the identification of new MARV sequences (Fig. 52B). Phylogenetic analysis showed that our sequences are more closely related to MARV and especially the Angola strain, which is considered to be the most pathogenic MARV strain (Fig. 52C and D). This result is highly surprising considering that no outbreak has ever been reported in Ghana and that no EVD-like disease was reported from people living in close proximity to the cave. Of note, necrosis analysis showed that animals were seemingly healthy, with only one of the animals that showing enlarged lymph nodes, supporting the idea that *R. aegyptiacus* bats are able to replicate the virus with no signs of disease and that they are indeed the natural reservoir of *Marburg marburgvirus*. Finally, divergences could be observed between the three MARV positive samples obtained, and the *R. aegyptiacus* #6 MARV sequence, with 3 additional differences compared to the other two samples, did not cluster with the other two sequences obtained (that were diverging between each other at a single position) in the phylogenetic analysis (Fig. 52D). Co-infection and co-circulation of MARV-like viruses in the same bat population have already been documented [5]. Further data and analysis will be required to determine the exact nature of these circulating Ghanaian strains.

Since its discovery in 1976, the scientific community has been able to obtain a better understanding of the molecular basis of EBOV pathogenesis. However, whilst numerous studies and attempts were made to try to discover the natural hosts of the different filoviruses and especially of EBOV, our knowledge in this respect is terribly limited and constitutes an important obstacle in our ability to predict and to limit filovirus outbreaks in susceptible wild animals and in humans.

In this project, we strove to identify the regions and also the natural hosts in which filoviruses are currently circulating. This work is of special importance as the identification of the filovirus natural reservoirs and the different areas housing filoviruses could help to prevent spillover events into the human population and to prevent new deadly outbreaks. Previous published results identified antibodies in bats obtained in Ghana, but so far, no viruses were ever detected despite intensive efforts and sample collection.

The identification of specific antibodies against one or several pathogens is challenging and is highly dependent on the antigen used to capture the antibodies. In this work, we decided to use transmembrane-truncated, trimeric EBOV and LLOV as a source of antigens for the development of a multiplex bead-based assay. We demonstrated that those antigens were similar to the full-length glycoproteins and were suitable as EBOV and LLOV antigens. We managed to successfully detect antibodies circulating in the sera of several bats and pigs as well as in humans, against both viruses. It would be of interest to further multiplex this assay to include all known filovirus species to get a better understanding of the filoviruses circulating in this country. In addition, the obtention of samples from bats and pigs infected with different filoviruses in a laboratory setting and sera from human survivors would help us to establish an appropriate cut-off value and to fully validate our assay.

Of special interest, we were able to obtain three new MARV sequences which are closely related to the most pathogenic MARV strain, MARV-Angola. Further analysis of the complete genome will be key to fully assess the relationship between the newly identified MARV and the other strains. The fact that no outbreak was ever reported in Ghana, while our data demonstrate that filoviruses are present in this country is puzzling. In this respect, viral isolation and characterisation will provide us the opportunity to evaluate the pathogenicity of this(these) new virus(es) for humans. In the case that the virus is less pathogenic, it will help us to improve our comprehension of MARV pathogenicity, which is thus far poorly understood.

In summary, we managed to detect antibodies against different filoviruses and were able to identify for the first time the presence of MARV-like virus(es) in Ghana. This is the first identification of a strain/strains that is/are closely related to a pathogenic filovirus in a country that has never been affected by any filovirus outbreaks.

Cell lines and cell culture: VeroE6 cells (African green monkey kidney epithelial cell line), 293T (human embryonic kidney cell line) and A549 (Adenocarcinomic human alveolar basal epithelial cells) were grown in DMEM, Glutamax 1X medium (Dulbecco's Modified Eagle's medium, Life Technologies, Cat #61965-059) supplemented with 10% heat inactivated foetal bovine serum (FBS, PerbioHyclone), 50U/mL of Penicillin and 50µg/mL of Streptomycin (Pen Strep, Gibco, Cat #15070-063). BHK-21 cells stably expressing the T7 polymerase (Baby Hamster Kidney-21 T7 cell lines) were grown in G-MEM BHK21 media (Glasgow MEM BHK-21 media, Gibco, Cat #21710-025) supplemented with MEM Non-Essential Amino Acids (MEM NEAA, Life Technologies, Cat #11140035), Tryptose Phosphate Broth (Sigma-Aldrich, Cat #T8159), 10% FBS and 500µg/mL of geneticin (Sigma-Aldrich, Cat #A1720). Cells were maintained at 37°C with 5% CO2 in a humidified incubator.

Transfection and rescue of recombinant VSV: $8x10^5$ BHK-T7 cells were seeded in T25 flasks the day before transfection. The cells were washed and starved for 1 hour with G-MEM BHK21 0% FBS before being transfected with the following plasmids: 1.5µg of pBS-N, 2.5µg of pBS-P, 1µg of pBS-L and 0.5µg of T7 and 5µg of pVSV-FL encoding either for the wild-type EBOV $GP_{1,2}$ or for a HS EBOV $GP_{1,2}$ mutant (both derived from Zaire Ebola virus, strain Mayinga), which has been described elsewhere [131]. In the case of rVSV-GP-LS rescue, cells were plated in a 10 cm dishes, in a similar fashion, however, cells were transfected with 3µg of pCAACS-N, 5µg of pCAACS-P, 2µg of pCAACS-L, 1µg of T7 and 10µg of pVSV-FL. For transfection, Fugene 6 (Promega, Cat #E2691) was used following the manufacturer's instructions with a ratio plasmids:reagent of 1:3. Six hours post-transfection, the transfection mix was replaced with fresh G-MEM BHK21 media supplemented with 3% FBS and antibiotics. Up to 7 days, supernatants were collected and passaged on VeroE6 cells for amplification. Cytopathic effects and rescues were confirmed by microscopy and western-blot analysis.

Virus stocks and virus infection: For infection with rVSV-ΔG-GP, rVSV-ΔG-GP-HS, rVSV-ΔG-GP-LS viruses, VeroE6 or 293T cells were washed once with DMEM 0% FBS and infected with the different amount of viruses in DMEM 0% FBS for 1 hour. After, the inoculum was removed and fresh DMEM 3% FBS was added for cell maintenance. Virus stocks were titrated using the TCID50 technique. At the appropriate time points, supernatants were harvested and clarified by low-speed centrifugation (1200 rpm, 15 minutes). For separation of the soluble viral proteins from the virion-bound proteins, clarified supernatants were loaded on a 20% sucrose cushion and viruses were pelleted by ultracentrifugation using a Beckman SW60 rotor (58 000 rpm, 50 minutes, 4°C) with a Beckman Optima L-70K ultracentrifuge. Of note, infected cells were resuspended in the same amount of DMEM 3% FBS than the volume used for cultivating cells while virions were concentrated 5 times in DMEM 3% FBS. In one experiment, pelleted virion was washed in 1mL of DMEM 3%FBS and loaded on a double sucrose cushion with one layer of 20% sucrose layered on top of a 60% sucrose cushion. The resuspended virion was spin down by ultracentrifugation as before and was isolated by inserting a needle at the interface of the 60% sucrose and a single fraction containing the virion was collected.

Analysis of DRM in rVSV-infected cells: In a T75 flask, $6x10^6$ cells were plated and infected on the same day with rVSV-GP and rVSV-GP-HS viruses at a MOI of 3 for one hour. Cells were then cultivated in DMEM 3%FBS. Twenty-four hours later, cell culture supernatant was removed and cells were scrapped in ice-cold DMEM 0%FBS. Cells were spun down for 10 minutes at 1200 rpm and washed two more times in ice-cold media. Cells were then resuspended in 600µL of CHAPS lysis buffer (20mM CHAPS, 50mM TrisHCl pH 7.4, 150mM NaCl, 5mM EDTA and 1mM PMSF) on ice, followed by mechanical disruption using a syringe and a needle. After 30 minutes, 600µL of 80% sucrose prepared in 50mM TrisHCl pH 7.4, 150mM NaCl, 5mM EDTA, 1mM PMSF to the lysed cells. To this mixture was overlaid 2200µL of 30% sucrose and 700µL of 5% sucrose, prepared in the same buffer than the 80% sucrose. Lysed cells were then submitted to ultracentrifugation for 120 minutes (48000 rpm, 4°C, no brake). 10 fractions of equal volumes were collected and analysed by western-blotting.

Organelles separation of rVSV-infected cells: As before, $6x10^6$ VeroE6 cells were plated in a T75 flask and infected with rVSV-GP. Twenty-four hours later, cells were detached using Versene and lysed on ice for 30 minutes in 1.6mL of hypotonic buffer (10mM TrisHCl pH 7.5, 1mM EDTA, and 0.25M saccharose). Cells were further disrupted by mechanical disruption using a syringe and a needle. Nuclei were pelleted by centrifugation (600xg, 10 minutes) and the lysed cells were separated in three fractions equal volumes. Fractions were then diluted with OptiPrep™ 60% (Sigma Aldrich, Cat #D1556-250ML) to obtain three fractions of identical volume with a final concentration of OptiPrep™ of 30%, 20% and 10% respectively. Lysed cells mixed with OptiPrep™ were then overlaid in an ultracentrifuge tube and samples were ultracentrifuged for 1.5 hour, 60000rpm, 4°C, on a SW60 rotor, without brake. Fractions of equal volume were then obtained from the top and analysed by western-blotting.

ADAM17 inhibition analysis: To confirm the role of ADAM17, the metalloproteinase inhibitor marimastat (Sigma-Aldrich, Cat #M2699-5MG) or DMSO, was added to the cells after removing the viral inoculum. EBOV $GP_{1,2}$ shedding was analysed by western-blotting as presented below. For phosphatidylserine competition assay, cells were incubated with different amount of O-phospho-L-serine (Sigma-Aldrich, Cat #P0878-10mg) after 6 hours of infection in DMEM 3% FBS. Importantly, all pH of the inhibitors were adjusted to 7.2.

Deglycosylation assays: N- and O-Glycosylations analyses were performed using Endo H and PNG F enzymes from New England Biolabs (Cat #P0702S and #P0704S). Briefly, 45µL of samples were first denatured for 10 minutes at 95°C in a supplied buffer and then 5µL of either Endo H or PNG F enzymes were used for deglycosylation of the different samples with their appropriate buffers and when necessary NP-40 was added. Deglycosylation occurred for 2h30 at 37°C. Samples were then analysed by western-blotting. In the case that samples were already in loading buffer and denatured, samples were incubated with their specific buffers and enzymes, but the denaturation step and NP-40 were omitted.

Antibodies and western-blot analysis: For western-blot analysis, samples were prepared using a 4X-gel loading buffer (SDS 8%, Glycerin 40%, 2-mercaptoethanol 20%, 0.4% Bromophenol blue) and boiled for 10 minutes at 95°C. Protein separation was performed by SDS-PAGE using 12% Mini-PROTEAN® TGX precast gels (BioRad, Cat #4561045**)** and transferred to

PVDF membranes (BioRad, Cat #1704157) using the semi-dry transfer from BioRad and the pre-saved Low MW program (Trans-Blot® TurboTM Transfer system; 1.3A, 25V for 5 minutes). Unspecific binding was blocked by incubating membranes in Milk 1%-PBS 1X, for 30 minutes at room temperatures. Membranes were then incubated with either anti-GP sera recognizing both GP_1 and GP_2 subunits or monoclonal anti-GP_1 antibody diluted in Milk 1%-PBS 1X-Tween 0.1% for 2 hours at room temperature. Following washing steps with PBS 1X-Tween 0.1%, membranes were incubated for 45 minutes with horseradish peroxidase conjugated antibodies purchased from Dako (Polyclonal Rabbit anti-Goat Cat #P0049; Polyclonal Goat anti-Mouse Cat #P0047). Finally, protein detections were performed by the ECL technique (Bio-Rad, ClarityTM Western ECL Substrate; Cat #170-5060). Membranes were read using the ImageQuantTM Las 4000 (GE, Cat #28-9558-10) equipped with a CCD camera cooled at -25°C driven by the ImageQuantTM Las 4000 software. For the detection of phosphoproteins, the same protocol was followed except that membranes were blocked in BSA 5%-PBS1X and primary and secondary antibodies were diluted in BSA 5%-PBS 1X-Tween 0.1%. Images were analysed afterward using ImageJ [340]. In this work, the following antibodies were used ERK-1 (Santa Cruz, #sc-271270), phospho-p38 MAPK (Cell Signalling Technology, #4511S), p38 (Cell Signaling Technology, #8690S) and ERK1/2 (Cell Signalling Technology, #9120S).

3D reconstruction of rVSV-GP infected cells: The day before infection, A549 cells were plated on coverslip in a 6 well plate to obtain about 50% confluence at the time of infection. For infection, cells were washed once with DMEM 0%FBS and infected with rVSV-GP at a MOI of 1 for 1 hour. Twenty-four hours post infection, supernatant was removed and cells were washed three time in PBS 1X and fixed with Paraformaldehyde 4% (PFA 4%) for 10 minutes. Next, cells were washed three times in PBS 1X and blocked in BSA 2%-PBS 1X for 15 minutes at room temperature. Cells were then incubated with EBOV GP_1 3373 monoclonal antibody (1:1000 dilution) and ADAM17 antibody (20µg/mL; Abcam, # ab39162) for 1 hour, on ice. Cells were washed three times in PBS 1X and incubated with appropriate secondary antibodies at room-temperature (Anti-mouse Alexa 488 and Anti-rabbit Alexa 555 antibodies, respectively; 1:2000 dilution). Both primary and secondary antibodies were diluted in BSA 0.2%-PBS 1X. Slides were then washed twice in PBS 1X and three times in ddH_2O and mounted using a mounting medium containing DAPI. For imaging, a Leica SP5 Confocal microscope was used equipped with the Las AF software. Pictures were obtained with a 63 x 1.4-0.6 oil DIC wd 0.1 mm lens (Leica # 11506192) leading to a xy pixel size of 0.246µm (Laser argon 488nm) and of 0.225µm (Laser DPSS 561nm). To capture multi-wavelength 3D images, the sequential imaging mode was used with the following parameters: Pinhole: 1 Airy unit; zoom factor: 1; scan format 2048x2048; scan speed: 400 Hz and with a frame averaging of 8 (only for the Laser argon 488nm and DPSS 561nm) and a smart gain of 1047.0V. In total, 69 pictures for each colour were acquired. For the 3D reconstruction, the Imaris software V9 (Bitplane) and its iso-surface rendering function was used.

Fluorescence analysis of human and animal sera: The day before transfection, VeroE6 cells $2.2x10^4$ were plated in a 12 well plate on glass slide that were coated with FBS for 30 minutes. Cells were then transfected with 500ng of plasmids encoding for EBOV or LLOV $GP_{1,2}$ per well using turbofect at a ratio of 1:5. Twenty-four hours later, cell culture media was removed and cells were washed with D-PBS 1X Ca^{2+} Mg^{2+}. Cells were then fixed and permeabilized on ice with a 1:1 Methanol:Acetone solution for 10 minutes. The fixation solution was removed and its complete removal was ensured by drying the plate at room temperature. Wells were then blocked with using PBS-BSA 2% for 15 minutes at room temperature. Specific GP antibodies

and sera were diluted in PBS-BSA 0.2% and put in contact with the glass slides for 1h, on ice. For sera, dilution between 1:100 and 1:300 were used. Next, glass slides were washed three times with PBS 1X and the secondary antibody was added. Anti-mouse and anti-rabbit Alexa Fluor 555 conjugated antibodies were diluted in PBS-BSA 0.2% at a dilution of 1:2000. Anti-pig-FITC was diluted 1:50 and anti-human 1:400. Staining was performed at +4°C, for 45 minutes, in the dark. Finally, cells were washed twice in PBS 1X and three times in ddH20 and slides were mounted using a mounting medium containing DAPI. For bat antibodies detection, goat anti-bat Ig were used followed by incubation with anti-goat Alexa Fluor 555.

Luminex beads coupling: For coupling, Bio-plex COOH luminex beads (Bio-rad, Cat #171506027 and #171506033), were resuspended and $1.5x10^6$ in a Lobind microcentrifuge tube (Sigma Aldrich, Cat #Z666505-100EA) and spin down for 4 minutes at 12500 rpm. Supernatant was discarded and the beads were resuspended in 100µL of dH20 by vortex and sonication for 20 seconds. Beads were again pelleted and the washed microspheres were resuspended in 80µL of 100mM Monobasic Sodium Phosphate (Sigma Aldrich, Cat #S3139-250g) pH 6.2 by vortex and sonication for 20 seconds. 10µL of a 50mg/mL Sulfo-NHS (Pierce, Cat #S3139-250g) solution prepared in dH20 was added to the beads, followed by gentle mixing by vortexing. Beads were incubated for 20 minutes at room temperature. After the incubation, microspheres were spun down as before and washed two times in 250µL of 50mM MES (Sigma Aldrich, Cat #M2933-100g), pH 5.0. For each washing steps, beads were resuspended by vortexing and sonication for 20 seconds. Before incubating the activated microspheres with the LLOV and EBOV antigens, microspheres were spin down and resuspended as before in 100µL of 50mM MES, pH 5.0. Microspheres were then incubated for 2 hours with 5µg of protein, in a final volume of 500µL of 50mM MES, pH 5.0, for two hours on a rotating wheel at room temperature. After two hours, the microspheres were spun down and resuspended in 500µL of PBS-TBN (PBS-BSA 0,1%-0,002%Tween-20-0,05% sodium azide). Coupled microspheres were washed for an additional two times with 1mL of PBS-TBN and then were resuspended in 250µL of PBS-TBN. Recovered beads were then counted by microscopy.

Antigen coupling confirmation and sera screening: A 96 well filter plate (Millipore, Cat #MSBVN1210), was pre-wet with 100µL of PBS-TBN. Beads were resuspended by vortex and sonification and diluted in PBS-TBN to obtain a final concentration of 70 microspheres/µL. The PBS-TBN was removed from the plate and 3500 beads (50µL) were added per well. In the case of antigen coupling confirmation, 50µL of diluted antibodies in PBS-TBN or negative control, were added to the plate. For human and animal sera screening, sera were diluted 1:50 and 50µL of this dilution were added to the plate. Each time the antibodies or the sera were added, the samples were mixed by pipetting several times, while taking care to not damage the plate filter. The plate was then covered with a film and a lid and incubated in the dark at room temperature for 1 hour on a plate shaker. The plate was then emptied and washed three times with 100µL of PBS-TBN and incubated with 100µL of 2µg/mL solution of Protein A/G (Pierce, Cat #32490), for 30 minutes at room temperature, in the dark, on a plate shaker. Plate was washed as before and 100µL of SAPE (Thermo Fisher, Cat #S866) at a concentration of 1µg/mL was added in each well. The plate was incubated again for 30 minutes as before and washed for two times, before resuspended the beads in 100µL of PBS-TBN. For analysis, 75µL were used to be read on a Flexmap 3D.

Animals sampling and autopsies: All procedures were approved by the Zoological Society of London Ethics Committee and the Ghanaian Council for Scientific and industrial Research. Experiments were performed with the help of the Wildlife Division, Forestry Commission. Animals were captured by experienced bat hunters using mist netting and were euthanized by intravenous lethal injections of Pentobarbitone. Before, blood was withdrawn by intracardiac puncture and plasma was prepared by centrifugation and bats were scanned for the presence of microchips. For all bats, pictures of the animals were taken before the autopsy to observe all lesions that could have occurred during their capture. For pig sampling, animals were obtained in the pig farm of Accra that obtained their pigs from local farmers coming from the region Great Accra. In Tachimen, pigs were obtained from local farmer directly. Organs were extracted from the animals and their processing was performed later the day. Between, the organs were kept on ice blocks to try to preserve RNA integrity.

Bat and pig tissues extraction: During the animal necrosis, the organs were sampled and placed directly into an eppendorf tube containing RNAlater™ (Thermo Fisher, #AM7021), and the tube were placed at the end of the day at +4°C overnight. When possible, the tubes were transferred at -20°C or -80°C or were otherwise kept at °4C until shipment. For RNA extraction, the tissues were removed from their tubes and the excess of RNAlater™ was removed by patting the tissue onto an absorbent paper. The piece of tissues was then placed into a 2mL sterile Eppendorf tubes containing a stainless bead and RLT buffer (Qiagen, Cat #79216) supplemented with 2-mercaptoethanol (Sigma Aldrich, Cat #M6250-250mL). The tissues were destroyed using a TissueLyser II (Qiagen, Cat #85300), for 1 minute, 30Hz, twice. Samples were then spun down and the tissue lysates were transferred onto a NucleoSpin® RNA Filter Plate (Macherey-Nagel, #740711) for further clarification. RNA was extracted from the lysed tissue using the NucleoSpin® RNA 96 (Macherey-Nagel, Cat #740709.24) isolation kit following the manufacturer's instructions. Elution was performed in two steps. First 75µL of RNAse-free H_2O were used to elute the RNA from the columns. In a second time, 50µL of the eluted RNA were loaded again to ensure total RNA elution without diluting the samples. RNA was then aliquoted and stored at -80°C until RT-PCR and nested analysis. Aliquots were kept for RNA quantification.

Nested RT-PCR: For RT-PCR, 5µL of RNA and the primers described in [342] were used: FiloA 5'-ATCGGAATTTTTCTTTCTCATT (FW) and FiloB 5'-ATGTGGTGGGTTATAATAATCACTGACATG (RV) with the SuperScript™ III One-Step RT-PCR System with Platinum™ Taq DNA Polymerase (#12574018, Thermo Fisher). For the nested PCR, 1µL of the first round RT-PCR was used using the subsequent primers FiloC 5'-AAAGCATTTCCTAGCAACATGATGG (FW) and FiloD 5'-ATAATAATCACTCACATGCATATAACA (RV). For the RT-PCR and the nested PCR, the conditions are indicated in Table 3 (A: RT-PCR and B: Nested PCR).

A

Temperature	Duration	Cycles
42°C	30'	
94°C	3'	
94°C	30"	3
37°C	30"	
72°C	2'	
94°C	30"	30
45°C	30"	
72°C	1'	

B

Temperature	Duration	Cycles
94°C	1'	
94°C	1'	3
37°C	2'	
74°C	1'	
94°C	1'	35
45°C	2'	
74°C	1'	
72°C	2'	

TABLE 4. RT- AND NESTED PCR CONDITIONS

Virus filtration: VeroE6-infected supernatants were prepared in DMEM 3% FBS as previously described and stored at 4°C until filtration. For filtration, a Planova 35N 0.001m^2 (AK-bio, Cat #35NZ-001) filter was used. Before filtrating the infectious supernatants, filters were visually checked for any defaults and emptied from the water that protects the straw-shaped hollow fibers. The filters were then washed with ultra-pure water and once with DMEM 0%FBS. Air bubbles were removed by tapping the filter. Filtrated supernatants were collected directly from the filter into an empty reservoir. The Planova 35N filter was connected to a peristaltic pump with a PVDF cable of 2.7mm of diameter and a manometer was used to constantly monitor the pressure. The speed of the peristaltic pump was adjusted to be sure that the pressure never exceeded 98 kPa and that the speed was of around 2mL/min. Virus removal was confirmed by the TCID50 technique.

Platelet preparations and stimulations: Peripheral blood was collected from healthy donors in endotoxin-free tubes supplemented with 3.2% sodium citrate. All donors were informed and gave written consent that their blood could be used for non-therapeutic purposes. Platelet-Rich Plasma (PRP) was prepared by low-speed centrifugation (150xg, 10 minutes, 22°C) and collected into endotoxin-free Eppendorf tubes. For stimulation, PRP were either left unstimulated or were incubated with 50µg/mL of thrombin receptor activator peptide (Sigma-Aldrich, Cat #S7152-1MG). For viral stimulation, 50µL of PRP were stimulated with different amount of either rVSV-GP or VSV Indiana viruses. All incubations were performed at 37°C for 30 minutes. Before flow cytometry analysis, platelets were fixed using Thrombofix™ Platelet Stabilizer (Beckman-Dickinson, #6607130). Washed platelets were prepared as described in [341]. PRP was prepared and diluted with Citrate-dextrose anticoagulant solution (Sigma Aldrich, Cat #C3821-50mL, v/v, 1:5). EDTA was added to a final concentration of 10mM and the diluted PRP was centrifuged for 5 minutes at 600xg to remove remaining red blood cells. The supernatant was further centrifuged to pellet platelets for 10 minutes at 1000xg. The pellet was then resuspended in 500µL of Tyrode's buffer (Sigma Aldrich, Cat #T2397-500mL) pH6.5 and 9.5mL of Tyrode's buffer pH7.4. Platelets were centrifuged one last time at 1300xg for 5 minutes and resuspended in Tyrode's buffer pH 7.4 supplemented with 5mM $CaCl_2$. Stimulation was then performed as previously.

Available online at www.sciencedirect.com

ScienceDirect

Current Opinion in Virology

Human transmission of Ebola virus

Philip Lawrence [1,2], Nicolas Danet [1], Olivier Reynard [1], Valentina Volchkova [1] and Viktor Volchkov [1]

Ever since the first recognised outbreak of Ebolavirus in 1976, retrospective epidemiological analyses and extensive studies with animal models have given us insight into the nature of the pathology and transmission mechanisms of this virus. In this review focusing on Ebolavirus, we present an outline of our current understanding of filovirus human-to-human transmission and of our knowledge concerning the molecular basis of viral transmission and potential for adaptation, with particular focus on what we have learnt from the 2014 outbreak in West Africa. We identify knowledge gaps relating to transmission and pathogenicity mechanisms, molecular adaptation and filovirus ecology.

Addresses
[1] Molecular Basis of Viral Pathogenicity, International Centre for Research in Infectiology (CIRI), INSERM U1111 – CNRS UMR5308, Universite´ Lyon 1, Ecole Normale Supe´rieure de Lyon, Lyon 69007, France
[2] Universite´ de Lyon, UMRS 449, Laboratoire de Biologie Ge´nérale, Universite´ Catholique de Lyon – EPHE, Lyon 69288, France

Corresponding author: Volchkov, Viktor (viktor.volchkov@inserm.fr)

Current Opinion in Virology 2017, 22:51–58

This review comes from a themed issue on Emerging viruses: intraspecies transmission

Edited by Ron A.M Fouchier and Lin-Fa Wang

For a complete overview see the Issue and the Editorial

Available online 22nd December 2016

http://dx.doi.org/10.1016/j.coviro.2016.11.013

Introduction

Filoviruses are enveloped, non-segmented, negative-strand RNA viruses, composed of three genera: Ebolavirus, Marburgvirus and Cuevavirus (Figure 1) [1–3]. Ebolavirus and Marburgvirus are together the causative agents of severe disease in human and non-human primates (NHPs) displaying fatality rates reaching 90% [1] (Table 1). There are currently five known, genetically distinct species of Ebolavirus — Zaire ebolavirus (EBOV), Sudan ebolavirus (SUDV), Taı¨ Forest ebolavirus (TAFV), Bundibugyo ebolavirus (BDBV) and the Asian filovirus; Reston ebolavirus (RESTV) [2]. Almost all human cases are due to the emergence or re-emergence of EBOV in Gabon, Republic of the Congo, Democratic Republic of Congo (DRC), and most recently in West Africa [4], and of SUDV in Sudan and Uganda [5] (Table 1).

The increase in the number of outbreaks of Ebola virus disease (EVD) in Africa since 2000 (Table 1) has been postulated to result from increased contact between wildlife and humans [6]. The ever increasing encroachment of mankind into previously uninhabited areas will continue to bring not only humans but also potentially susceptible, domesticated animals into contact with unknown pathogens and their reservoir species [7]. Deforestation and climate change can also be expected to cause certain species to modify their geographic and ecological distribution and potentially into greater proximity to human agricultural exploits or settlements. It appears thus urgent to better understand both filovirus ecology and the mechanisms involved in viral transmission from their natural hosts and between humans.

Retrospective analysis of human outbreaks since the first EBOV epidemic in 1976 and intensive studies performed on animal models have helped to understand both the nature of EBOV pathology and its transmission. However, the 2014 outbreak has again shown that a complete knowledge of EBOV human-to-human transmission mechanisms is still lacking and is in many cases based only on retrospective observations rather than empirical data. Here, focusing on EBOV, we present an overview of our current understanding of filovirus transmission in humans. We also summarise our current knowledge concerning the molecular basis of viral transmission and potential adaptation including that gained from the recent outbreak, together with our opinions on knowledge gaps and future directions for research.

Transmission routes

In humans, EBOV has been evidenced either directly or via detection of viral RNA in a range of bodily fluids including blood, stool, semen, breast milk and saliva as well as sweat and tears [8,9]. It is generally accepted that contact with such fluids/fomites from an infected and symptomatic, or deceased person is the most likely route of transmission of EBOV. Other than direct or close contact with these fluids, transmission routes proposed for EBOV involve the presence of infectious virus in fomites, droplets and aerosols [10••]. Experiments using NHPs have shown that EBOV is both highly infectious and contagious [11–13]. Evidence from NHP studies has confirmed viral infection associated with a variety of administration routes including oral, conjunctival,

Figure 1

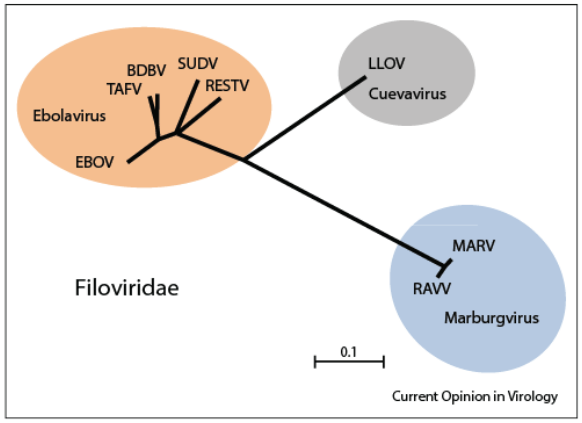

Phylogenetic relationship for the viral famiy Filoviridae. The family Filoviridae are enveloped, non-segmented, negative-strand RNA viruses of the order Mononegavirales, composed of three major genera: Ebolavirus, Marburgvirus and Cuevavirus. There are currently five known, genetically distinct species of Ebolavirus — Zaire ebolavirus (EBOV), Sudan ebolavirus (SUDV), Tai¨Forest ebolavirus (TAFV), Bundibugyo ebolavirus (BDBV) and Reston ebolavirus (RESTV). The genus Marburgvirus comprises one viral species; Marburg marburgvirus with two current viral members Marburg virus (MARV) and Ravn virus (RAVV). The genus Cuevavirus currently has one species member Lloviu cuevavirus (LLOV). 29 filovirus L protein sequences for the illustrated virus species were obtained from the ViPR database and aligned using the muscle algorithm. The aligned sequences served to generate the phylogenetic tree using the distance method in the Seaview software [80]. The scale bar indicates evolutionary distance between each node.

submucosal and respiratory routes amongst others. Based on detailed analysis of available data [10••,14] the transmission routes for EBOV can be summarised as follows.

Direct contact

As stated above, evidence from outbreaks, epidemiological data and NHP models have all confirmed direct contact of an individual with contaminated bodily fluids from a symptomatic patient or from a disease victim as the most likely interhuman transmission route. It is interesting to note that recent data from an NHP study using the West African outbreak EBOV Makona variant suggest that more natural routes ofi nfection via oral or conjunctiva mucosa may require higher doses of EBOV to produce disease [13], although further studies are required in comparison to other EBOV variants to confirm such observations. Since the recent epidemic however it has also become clear that sexual transmission of EBOV presents a certain risk even with patients that are no longer symptomatic for EVD and this many months after remission [15,16••,17,18]. Indeed, infectious EBOV can be detected in semen of survivors at least up to around 500 days [19,20] and sexual transmission has already been linked to the start of new chains of transmission [21,22].

Droplet transmission

By common definition [23] droplet transmission is thought to occur up to a metre from an infected individual depending on the stability of the virus in question and specific environmental conditions. Cases of droplet transmission are suspected from epidemiological data for patients where no direct contact was reported [24]. In the case of EBOV, the presence of virus in droplets might arise from a range ofi nfected fluids, including blood, vomit, saliva or diarrhoea or be produced by coughing or during medical intervention.

Fomites

Transmission from fomites involves viral deposition on surfaces that have been in contact with contaminated secretions including disposed medical waste or corpses [10••,14]. Indeed, contamination from disease victims appears common and has been linked to many cases of transmission, highlighting funerals and burial practices as key transmission events [25•]. Viable virus has been detected on solid surfaces and liquids several days to several weeks after contamination and infectious virus has been retrieved from EBOV infected monkeys seven days after death and RNA detected up to 10 weeks [26]. Data is however often lacking concerning the stability of virus on surfaces and in secretions not typically associated with transmission of enveloped RNA viruses, including vomit and diarrhoea.

Aerosols

Experimental data from NHPs have shown that mechanical aerosolisation of virus particles can cause disease with even low infectious doses [27] but the relevance of such findings in a natural setting is unclear [10••]. Stability studies would also suggest that aerosolised particles produced in this way are relatively unstable (loss of 99% of particles after 100 min at room temperature and humidity) [28]. As stated above, the majority of transmission cases arise from direct contact and in outbreak settings containment is possible without strict precautions against airborne transmission [10••,14].

EBOV transmission and molecular potential for virus adaptation/evolution

Pathogens such as EBOV would appear already intrinsically able to break the interspecies barrier and both the intrahuman and interhuman barriers, allowing the virus to propagate within the human population. However, as the specific natural host of Ebolavirus is yet to be discovered it is difficult to clearly assess whether EBOV needs any adaptation to successfully infect humans or other species. Nevertheless, evidence of EBOV infection has been reported in various wild species including primates, bats, duikers or domestic pigs [29–32], and thus far, similarly to Marburgvirus, bats are thought to be the most likely natural reservoir for this virus [33•].

Figure 2

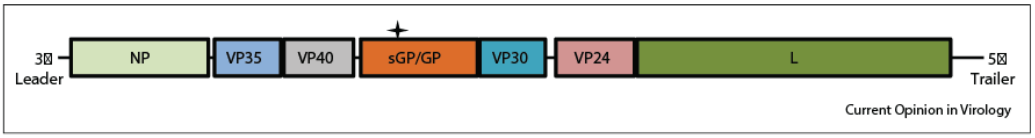

Schematic representation of Ebola virus genome. The 19 kb negative-sense RNA genome of EBOV and its seven genes give rise to the individual viral structural and non-structural proteins. The central core of the virion is formed by the genomic RNA molecule encapsulated by nucleoprotein (NP) and linked to viral inner capsid proteins 30 (VP30) and 35 (VP35) and the RNA-dependent RNA polymerase (L), together with VP24 forming the viral ribonucleoprotein complex (RNP) that is essential for viral transcription, replication and encapsidation. The two remaining viral proteins, surface glycoprotein (GP) and VP40 are membrane-associated; VP40 is displayed at the inner surface of the lipid bilayer of the viral envelope and is linked to the RNP. Through transcriptional RNA editing, three GP gene specific mRNA products are expressed from the GP gene of EBOV, coding for full-length transmembrane surface GP and the soluble, non-structural proteins sGP and ssGP. Star indicates the position of the GP gene editing site.

able to evolve more rapidly [44], the whole genome mutation rate for EBOV Makona now appears to be comparable with that observed during other EBOV outbreaks, with a substitution rate estimated at $\sim 1.3 \times 10^{-3}$ nucleotides/site/year [45–48]. Indeed, the molecular data, as well as the epidemiological analysis allowing estimation of parameters such as the basic reproduction number R0, so far obtained cannot discriminate EBOV Makona from previous outbreak variants [25•,44,52–55]. In general, EBOV Makona would appear however to have a longer incubation time than most previous EBOV outbreaks, potentially allowing a longer period of dissemination from infected persons between different regions, facilitating propagation of the virus [25•,44,52].

Although both synonymous and non-synonymous mutations are detected in all viral genes, the most frequent gene mutations observed during the outbreak were located in GP, NP, and L [44,45,47,48,49•,56], and interestingly this tendency appears conserved between previous outbreaks when such data is available [49•,57,58•]. Analysis of the EBOV Makona GP mucin-like domain has shown it to be more subject to positive selection in several studies, with an acquisition of mutations in B and T cell epitopes [50,54,57,58•]. Additionally for GP, a non-synonymous mutation at amino acid 82 (A82V) appeared to be selected in a region containing the receptor-binding domain [47,49•]. Indeed, recent analyses of this A82V mutation in pseudovirus or reverse genetics systems have highlighted the role of this mutation in adaptation to a human host through a certain refining of receptor binding affinity and associated increase in viral fitness in human cells [59••,60,61]. Whilst GP mutations probably reflect the arms race between the immune system and the virus or differences in receptor binding affinity [57,59••,60–62], mutations in NP, VP30, VP35 and L, the four proteins forming the viral ribonucleoprotein replication complex, might play a role in viral adaptation in the human population in the processes of viral transcription, replication or encapsidation or in facilitating the interaction of cellular factors with viral proteins and RNA in a new host environment, as already shown for Influenza [63]. For EBOV, mutations in L have already been speculated to play a role in both GP editing and viral replication rates [64], although experimental evidence for this is currently lacking. Several recent studies based on the genetic analysis of Makona variants arising during the recent outbreak have shown that mutations in VP30 and in L [65] or in NP and L [59••] can have implications for virus adaptation and fitness.

As single mutations often occur at the cost of viral fitness, which need to be compensated by other co-mutations, it appears essential to continue to analyse co-occurring mutations to fully understand viral evolution and adaptation [59••,65–67]. EBOV co-mutation network analysis shows strong evidence of selection for GP, NP, L and VP40, especially for EBOV Makona, with mutations occurring more frequently in protein interaction domains [58•]. This study suggests that a still understudied cooperation between viral proteins exists and could play a role in viral adaptation to humans. In addition, several studies reported serial T > C substitutions in viral genomes, suggested to be due to specific cellular Adenosine Deaminase Acting on RNA (ADAR) enzymes [45,46,68]. The role of these substitutions is currently unknown but ADAR modifications have been shown to be involved in replication and pathogenesis for several other viruses including influenza and measles virus and therefore merit further investigation [69].

Another major discovery of sequence analyses was the low percentage (∼1%) of viral GP gene specific mRNA encoding for the full-length, transmembrane, surface GP [44]. In fact Ebolavirus is somewhat unique in this respect in that synthesis ofi ts surface GP is dependent on transcriptional RNA editing at a site constituting seven consecutive U residues (editing site) present within the GP gene (Figure 2). Direct expression of the GP gene however results in synthesis of a nonstructural secreted glycoprotein termed sGP [70], which has been proposed

Table 1

List of Ebolavirus outbreaks (1976 –present day)

Year(s)	Country	Ebola subtype	Reported number of human cases	Reported number of fatalities	Case fatality rate
August–November 2014	Democratic Republic of the Congo	Ebola virus	66	49	74
March 2014 –Present	Guinea, Sierra Leone, Liberia and others *	Ebola virus	28 616 *	11 310 *	~70 **
November 2012 –January 2013	Uganda	Sudan virus	6	3	50
June–November 2012	Democratic Republic of the Congo	Bundibugyo virus	36	13	36
June–October 2012	Uganda	Sudan virus	11	4	36
May 2011	Uganda	Sudan virus	1	1	100
December 2008 –February 2009	Democratic Republic of the Congo	Ebola virus	32	15	47
November 2008	Philippines	Reston virus	6 (asymptomatic)	0	0
December 2007 –January 2008	Uganda	Bundibugyo virus	149	37	25
2007	Democratic Republic of the Congo	Ebola virus	264	187	71
2005	Republic of the Congo	Ebola virus	12	10	83
2004	Sudan (South Sudan)	Sudan virus	17	7	41
November–December 2003	Republic of the Congo	Ebola virus	35	29	83
December 2002 –April 2003	Republic of the Congo	Ebola virus	143	128	89
October 2001 –March 2002	Republic of the Congo	Ebola virus	57	43	75
October 2001 –March 2002	Gabon	Ebola virus	65	53	82
2000–2001	Gulu, Uganda	Sudan virus	425	224	53
1996	South Africa	Ebola virus	2	1	50
1996–1997 (July –January)	Gabon	Ebola virus	60	45	74
1996 (January –April)	Gabon	Ebola virus	37	21	57
1995	Democratic Republic of the Congo	Ebola virus	315	250	81
1994	Côte d'Ivoire (Ivory Coast)	Taı ¨Forest virus	1	0	0
1994	Gabon	Ebola virus	52	31	60
1989–1990	Philippines	Reston virus	3 (asymptomatic)	0	0
1990	USA	Reston virus	4 (asymptomatic)	0	0
1979	Sudan (South Sudan)	Sudan virus	34	22	65
1977	Ebola	Ebola virus	1	1	100
1976	Sudan (South Sudan)	Sudan virus	284	151	53
1976	Democratic Republic of the Congo	Ebola virus	318	280	88

Adapted from [5,79]

* Includes cases from Guinea, Sierra Leone and Liberia only.
** Estimated.

In terms of susceptibility to infection and species tropism, filoviruses have one surface glycoprotein (GP) (Figure 2) that drives binding and entry of the virus through interaction with multiple cellular surface molecules [34,35]. The cellular endosomal receptor Niemann-Pick C1 (NPC1) has been identified as playing a key role in the fusion process through binding the proteolytically-primed GP. Mapping of the key positions on NPC-1 and EBOV GP responsible for EBOV tropism shows that these residues are shared between both susceptible bat and human cell lines [36•,37]. Such data suggest that EBOV would not require specific adaptation for successful entry into human cells. Likewise, molecular studies performed on human macrophages and aMarburgvirus bat isolate suggest that no further adaptation is necessary for spillover from bats to the human population [38]. In rodent models however, Ebolavirus infection with wild-type EBOV virus results in an asymptomatic illness [39–41]. Importantly, sequential passaging of wild-type virus in these small animal models can lead to the generation of highly pathogenic variants of the virus that display mutations in three viral genes: polymerase (L), nucleoprotein (NP) and viral protein VP24, when compared to the initial, wild-type viral sequence [40,42,43]. By generating recombinant viruses containing different combinations of these mutations, it was subsequently shown that a single mutation in VP24 was sufficient for the virus to acquire virulence in Guinea pigs [40,42]. Similarly, an adapted EBOV strain containing mutations in VP24 and NP genes is lethal in immunocompetent mice and hamsters [39,40].

The recent epidemic is the first time that such an outbreak has been described in terms of the genetic evolution of the viral genome over the course of an epidemic. Systematic deep sequencing of EBOV positive patients has thus provided new insights into viral spread and transmission chains [4,44–48,49•]. The extent of the 2014 West Africa outbreak lead to numerous concerns about the ability of the EBOV Makona variant to evolve in terms of pathogenicity and/or transmissibility in the human population [44,50]. The emergence of variants with a lower pathogenicity was also feared; as such viruses can potentially establish a long-term endemic presence of the virus in afflicted countries [51]. Initially thought to be

to participate in the immune evasion of EBOV by capturing certain antibodies directed against GP [71]. Early reports based on cell culture experiments had indicated a figure of around 1:4 for the ratio of surface GP versus sGP transcripts [70,72]. Discovery of a much lower percentage in patients during the outbreak corroborates recent findings indicating that the editing site is also a transcription termination signal and highlights the necessity for a productive viral cycle to minimize surface GP expression, as recently demonstrated [73,74]. Interestingly, these observations resemble those seen in experimental animal models of adaptation in which it was demonstrated that control over surface GP expression is also exerted at the GP editing site at the genomic level [75,76]. On the other hand, the maintenance of the wild-type editing site may indicate that a well-balanced, rationally minimal expression of surface GP vs. synthesis of secreted sGP offers a selective advantage and that this feature is an essential element in the replication and spread of EBOV, playing a role in viral pathogenicity and in counteracting the immune system [71,73,77]. In keeping with this idea, another mutation hotspot that was identified during the 2014 outbreak is near the GP tumour necrosis factor-alpha converting enzyme (TACE) cleavage site (Q638R/L) [49•]. This cleavage site is responsible for an additional decrease in expressed membrane-bound GP via its removal from the cell surface as a shed form that is proposed to play a role in virus dissemination and pathogenesis [77,78]. However, the biological significance of this mutation remains to be tested.

Conclusions and areas for future study

Coupled with data from animal models, the outbreak in West Africa has again highlighted the importance of contact with bodily fluids for a successful transmission. However, further characterisation of which fluids are most likely to lead to infection needs to be performed in terms of virus loads and survival rates. In the same vein there is currently very little experimental data on how the virus physically penetrates into the body. Likewise the relative impact and risk associated with the potential of sexual transmission of EBOV should be thoroughly investigated. Based on everything that we have learnt concerning the genomics of the latest outbreak it will be vital to continue to perform molecular studies to assess the importance of the various mutations and polymorphisms consistently detected from epidemiological data in terms of their impact on virus immune escape, receptor binding affinities, pathogenicity and transmissibility. In light of recent molecular data based on 2014 EBOV outbreak isolates [59••,60,61,65], it will be ofi nterest to further study and to model such mutations through consecutive passages of initial/early outbreak variants in human cells. It also remains to be seen whether adaptation mutations seen over the course of an outbreak can be in some way preserved, given the unprecedented scale of the epidemic and multiple contacts between infected patients, disease victims and the environment.

A surprising feature of some of the recent outbreaks has been the appearance of Ebolavirus species in new locations, including BDBV in DRC and more recently and more devastatingly, EBOV in West Africa [4]. In this respect it seems vital that future studies cover the identification of risk factors linked to the emergence of zoonotic pathogens and include continuing studies of the molecular basis of transmission events that allow such breaches of the animal to human species barrier or that promote efficient human-to-human transfer. Although we are just beginning to understand filovirus ecology, it seems clear given the absence of any current vaccine or proven treatment for EVD and the difficulty in containing outbreaks in countries where access to adapted medical and containment facilities is rare, that for the moment any increased understanding of filovirus ecology and surveillance may help to minimize the risk off uture outbreaks.

Acknowledgements

This work was supported by the European Commission (FP7 programme in the framework of the project 'Antigone — ANTIcipating the Global Onset of Novel Epidemics', project number 278976) and by Agence Nationale de la Recherche (ANR-14-EBOL-002-01). The sponsor had no role in the collection, analysis and interpretation of data, in the writing of this review; nor in the decision to submit for publication.

References and recommended reading

Papers of particular interest, published within the period of review, have been highlighted as:

- • of special interest
- •• of outstanding interest

1. Groseth A, Eickmann M, Ebihara H, Becker S, Hoenen T: Filoviruses: Ebola, Marburg and Disease . eLS . John Wiley & Sons, Ltd.; 2015 http://dx.doi.org/10.1002/9780470015902.a0002232.pub3 http://www.els.net.

2. Kuhn JH, Yiming B, Sina B, Stephan B, Steven B, Rodney Brister J, Bukreyev AA, Yı´ngyún C, Kartik C, Davey RA et al.: Virus nomenclature below the species level: a standardized nomenclature for laboratory animal-adapted strains and variants of viruses assigned to the family Filoviridae . Arch Virol 2013, 158:1425-1432.

3. Negredo A, Palacios G, Va´zquez-Moro´n S, Gonza´lez F, Dopazo H, Molero F, Juste J, Quetglas J, Savji N, de la Cruz Martı´nez M et al.: Discovery of an ebolavirus-like filovirus in Europe . PLoS Pathog 2011, 7:e1002304.

4. Baize S, Pannetier D, Oestereich L, Rieger T, Koivogui L, Magassouba N, Soropogui B, Sow MS, Keı¨ta S, De Clerck H et al.: Emergence of Zaire Ebola virus disease in Guinea . N Engl J Med 2014, 371:1418-1425.

5. Centers for Disease Control and Prevention. Outbreaks Chronology: Ebola Virus Disease (accessed on 05.09.16); Available online: http://www.cdc.gov.gate2.inist.fr/vhf/ebola/outbreaks/history/chronology.html .

6. Plowright RK, Foley P, Field HE, Dobson AP, Foley JE, Eby P, Daszak P: Urban habituation, ecological connectivity and epidemic dampening: the emergence of Hendra virus from flying foxes (Pteropus spp.) . Proc Biol Sci 2011, 278:3703-3712.

7. Patz JA, Olson SH: Climate change and health: global to local influences on disease risk . Ann Trop Med Parasitol 2006, 100:535-549.

8. Bausch DG, Towner JS, Dowell SF, Kaducu F, Lukwiya M, Sanchez A, Nichol ST, Ksiazek TG, Rollin PE: Assessment of the risk of Ebola virus transmission from bodily fluids and fomites . J Infect Dis 2007, 196(Suppl. 2) :S142-S147.

9. Centers for Disease Control and Prevention. Transmission: Ebola Virus Disease (accessed on 03.09.16): Available online: http://www.cdc.gov.gate2.inist.fr/vhf/ebola/transmission/ .

10. •• Judson S, Prescott J, Munster V: Understanding ebola virus transmission . Viruses 2015, 7:511-521.
Authors present a thorough overview of our current understanding of filovirus transmission and discuss important knowledge gaps for future research.

11. Alfson KJ, Avena LE, Beadles MW, Staples H, Nunneley JW, Ticer A, Dick EJ Jr, Owston MA, Reed C, Patterson JL et al.: Particle-to-PFU ratio of Ebola virus influences disease course and survival in cynomolgus macaques . J Virol 2015, 89:6773-6781.

12. Jaax N, Jahrling P, Geisbert T, Geisbert J, Steele K, McKee K, Nagley D, Johnson E, Jaax G, Peters C: Transmission of Ebola virus (Zaire strain) to uninfected control monkeys in a biocontainment laboratory . Lancet 1995, 346:1669-1671.

13. Mire CE, Geisbert JB, Agans KN, Deer DJ, Fenton KA, Geisbert TW: Oral and conjunctival exposure of nonhuman primates to low doses of Ebola Makona virus . J Infect Dis 2016, 214:S263-S267.

14. Vetter P, Fischer WA II, Schibler M, Jacobs M, Bausch DG, Kaiser L: Ebola virus shedding and transmission: review of current evidence . J Infect Dis 2016 http://dx.doi.org/10.1093/infdis/jiw254 .

15. Thorson A, Formenty P, Lofthouse C, Broutet N: Systematic review of the literature on viral persistence and sexual transmission from recovered Ebola survivors: evidence and recommendations . BMJ Open 2016, 6:e008859.

16. •• Mate SE, Kugelman JR, Nyenswah TG, Ladner JT, Wiley MR, Thierry C-L, Athalia C, Schroth GP, Gross SM, Davies-Wayne GJ et al.: Molecular evidence of sexual transmission of Ebola virus . N Engl J Med 2015, 373:2448-2454.
This paper shows for the first time that EBOV can be considered as sexually transmitted disease and emphasises the need to monitor EBOV persistence in semen in survivors to successful control an epidemic of this size.

17. Uyeki TM, Erickson BR, Brown S, McElroy AK, Cannon D, Gibbons A, Sealy T, Kainulainen MH, Schuh AJ, Kraft CS et al.: Ebola virus persistence in semen of male survivors . Clin Infect Dis 2016, 62:1552-1555.

18. Sow MS, Etard J-F, Baize S, Magassouba N'fally, Faye O, Msellati P, Toure´ Al, Savane I, Barry M, Delaporte E et al.: New evidence ofl ong-lasting persistence of Ebola virus genetic material in semen of survivors . J Infect Dis 2016 http://dx.doi.org/10.1093/infdis/jiw078 .

19. Chughtai AA, Barnes M, Macintyre CR: Persistence of Ebola virus in various body fluids during convalescence: evidence and implications for disease transmission and control . Epidemiol Infect 2016, 144:1652-1660.

20. Diallo B, Sissoko D, Loman NJ, Bah HA, Bah H, Worrell MC, Conde LS, Sacko R, Mesfin S, Loua A et al.: Resurgence of Ebola virus disease in Guinea linked to a survivor with virus persistence in seminal fluid for more than 500 days . Clin Infect Dis 2016 http://dx.doi.org/10.1093/cid/ciw601 .

21. Arias A, Armando A, Watson SJ, Danny A, Tobin EA, Jia L, Phan MVT, Umaru J, Wadoum REG, Luke M et al.: Rapid outbreak sequencing of Ebola virus in Sierra Leone identifies transmission chains linked to sporadic cases . Virus Evol 2016, 2:vew016.

22. Abbate JL, Murall CL, Richner H, Althaus CL: Potential impact of sexual transmission on Ebola virus epidemiology: Sierra Leone as a case study . PLoS Negl Trop Dis 2016, 10:e0004676.

23. Darquenne C: Aerosol deposition in health and disease . J Aerosol Med Pulm Drug Deliv 2012, 25:140-147.

24. Roels TH, Bloom AS, Buffington J, Muhungu GL, Mac Kenzie WR, Khan AS, Ndambi R, Noah DL, Rolka HR, Peters CJ et al.: Ebola hemorrhagic fever, Kikwit, Democratic Republic of the Congo, 1995: risk factors for patients without a reported exposure . J Infect Dis 1999, 179(Suppl. 1) :S92-S97.

25. • Van Kerkhove MD, Bento AI, Mills HL, Ferguson NM, Donnelly CA: A review of epidemiological parameters from Ebola outbreaks to inform early public health decision-making . Sci Data 2015, 2:150019.
The authors present a very detailed analysis off actors driving transmission, highlighting differences between the West Africa 2014 epidemic and previous outbreaks.

26. Prescott J, Joseph P, Trenton B, Robert F, Kerri M, Seth J, Munster VJ: Postmortem stability of Ebola virus . Emerg Infect Dis 2015, 21:856-859.

27. Reed DS, Lackemeyer MG, Garza NL, Sullivan LJ, Nichols DK: Aerosol exposure to Zaire ebolavirus in three nonhuman primate species: differences in disease course and clinical pathology . Microbes Infect 2011, 13:930-936.

28. Piercy TJ, Smither SJ, Steward JA, Eastaugh L, Lever MS: The survival of filoviruses in liquids, on solid substrates and in a dynamic aerosol . J Appl Microbiol 2010, 109:1531-1539.

29. Olival KJ, Hayman DTS: Filoviruses in bats: current knowledge and future directions . Viruses 2014, 6:1759-1788.

30. Nkoghe D, Formenty P, Leroy EM, Nnegue S, Edou SYO, Ba JI, Allarangar Y, Cabore J, Bachy C, Andraghetti R et al.: Multiple Ebola virus haemorrhagic fever outbreaks in Gabon, from October 2001 to April 2002 . Bull Soc Pathol Exot 2005, 98:224-229.

31. Nfon CK, Leung A, Smith G, Embury-Hyatt C, Kobinger G, Weingartl HM: Immunopathogenesis of severe acute respiratory disease in Zaire ebolavirus-infected pigs . PLoS ONE 2013, 8:e61904.

32. Genton C, Cristescu R, Gatti S, Levre´ro F, Bigot E, Caillaud D, Pierre J-S, Me´nard N: Recovery potential of a western lowland gorilla population following a major Ebola outbreak: results from a ten year study . PLoS ONE 2012, 7:e37106.

33. • Leroy EM, Kumulungui B, Pourrut X, Rouquet P, Hassanin A, Yaba P, De´licat A, Paweska JT, Gonzalez J-P, Swanepoel R: Fruit bats as reservoirs of Ebola virus . Nature 2005, 438:575-576.
After years of supposition as to the EBOV natural host, the authors detect for the first time EBOV RNA in three different species.

34. Moller-Tank S, Maury W: Ebola virus entry: a curious and complex series of events . PLoS Pathog 2015, 11:e1004731.

35. Simmons G, Graham S: Filovirus entry . Adv Exp Med Biol 2013:83-94.

36. • Ng M, Ndungo E, Kaczmarek ME, Herbert AS, Binger T, Kuehne AI, Jangra RK, Hawkins JA, Gifford RJ, Biswas R et al.: Filovirus receptor NPC1 contributes to species-specific patterns of ebolavirus susceptibility in bats . Elife 2015, 4.
In this study, the authors show the molecular factors driving EBOV tropism using VSV recombinant viruses. The identification of key residues for EBOV interaction with NPC-1 could help to determine which bat species are potential hosts for EBOV.

37. Carette JE, Matthijs R, Wong AC, Herbert AS, Gregor O, Nirupama M, Kuehne AI, Kranzusch PJ, Griffin AM, Gordon R et al.: Ebola virus entry requires the cholesterol transporter Niemann-Pick C1 . Nature 2011, 477:340-343.

38. Albariño CG, Uebelhoer LS, Vincent JP, Khristova ML, Chakrabarti AK, McElroy A, Nichol ST, Towner JS: Development of a reverse genetics system to generate recombinant Marburg virus derived from a bat isolate . Virology 2013, 446:230-237.

39. Bray M, Davis K, Geisbert T, Schmaljohn C, Huggins J: A mouse model for evaluation of prophylaxis and therapy of Ebola hemorrhagic fever . J Infect Dis 1999, 179(Suppl. 1) :S248-S258.

40. Volchkov VE, Chepurnov AA, Volchkova VA, Ternovoj VA, Klenk HD: Molecular characterization of Guinea pig-adapted variants of Ebola virus . Virology 2000, 277:147-155.

41. Ebihara H, Zivcec M, Gardner D, Falzarano D, LaCasse R, Rosenke R, Long D, Haddock E, Fischer E, Kawaoka Y et al.: A Syrian golden hamster model recapitulating Ebola hemorrhagic fever . J Infect Dis 2013, 207:306-318.

42. Mateo M, Carbonnelle C, Reynard O, Kolesnikova L, Nemirov K, Page A, Volchkova VA, Volchkov VE: VP24 is a molecular determinant of Ebola virus virulence in Guinea pigs . J Infect Dis 2011, 204:S1011-S1020.

43. Geisbert TW, Hensley LE, Kagan E, Yu EZ, Geisbert JB, Daddario-DiCaprio K, Fritz EA, Jahrling PB, McClintock K, Phelps JR et al.: Postexposure protection of Guinea pigs against a lethal Ebola virus challenge is conferred by RNA interference . J Infect Dis 2006, 193:1650-1657.

44. Gire SK, Goba A, Andersen KG, Sealfon RSG, Park DJ, Kanneh L, Jalloh S, Momoh M, Fullah M, Dudas G et al.: Genomic surveillance elucidates Ebola virus origin and transmission during the 2014 outbreak . Science 2014, 345:1369-1372.

45. Tong Y-G, Shi W-F, Liu D, Qian J, Liang L, Bo X-C, Liu J, Ren H-G, Fan H, Ni M et al.: Genetic diversity and evolutionary dynamics of Ebola virus in Sierra Leone . Nature 2015, 526:595.

46. Park DJ, Dudas G, Wohl S, Goba A, Whitmer SLM, Andersen KG, Sealfon RS, Ladner JT, Kugelman JR, Matranga CB et al.: Ebola virus epidemiology, transmission, and evolution during seven months in Sierra Leone . Cell 2015, 161:1516-1526.

47. Carroll MW, Matthews DA, Hiscox JA, Elmore MJ, Pollakis G, Rambaut A, Hewson R, Garcı ´a-Dorival I, Bore JA, Koundouno R et al.: Temporal and spatial analysis of the 2014 –2015 Ebola virus outbreak in West Africa . Nature 2015, 524:97-101.

48. Hoenen T, Safronetz D, Groseth A, Wollenberg KR, Koita OA, Diarra B, Fall IS, Haidara FC, Diallo F, Sanogo M et al.: Virology. Mutation rate and genotype variation of Ebola virus from Mali case sequences . Science 2015, 348:117-119.

49. • Ladner JT, Wiley MR, Mate S, Dudas G, Prieto K, Lovett S, Nagle ER, Beitzel B, Gilbert ML, Fakoli L et al.: Evolution and spread of Ebola virus in Liberia, 2014 –2015. Cell Host Microbe 2015, 18:659-669.

An interesting, in-depth analysis of virus evolution during the recent outbreak in Liberia, including a discussion on the selection of mutations and patterns of divergence.

50. Kugelman JR, Wiley MR, Mate S, Ladner JT, Beitzel B, Fakoli L, Taweh F, Prieto K, Diclaro JW, Minogue T et al.: Monitoring of Ebola Virus Makona evolution through establishment of advanced genomic capability in Liberia . Emerg Infect Dis 2015, 21:1135-1143.

51. Blackley DJ, Wiley MR, Ladner JT, Fallah M, Lo T, Gilbert ML, Gregory C, D'ambrozio J, Coulter S, Mate S et al.: Reduced evolutionary rate in reemerged Ebola virus transmission chains . Sci Adv 2016, 2:e1600378.

52. Pigott DM, Golding N, Mylne A, Huang Z, Henry AJ, Weiss DJ, Brady OJ, Kraemer MUG, Smith DL, Moyes CL et al.: Mapping the zoonotic niche of Ebola virus disease in Africa . Elife 2014, 3:e04395.

53. Althaus CL: Estimating the reproduction number of Ebola Virus (EBOV) during the 2014 outbreak in West Africa . PLoS Curr 2014, 6.

54. Olabode AS, Xiaowei J, Robertson DL, Lovell SC: Ebola virus is evolving but not changing: no evidence for functional change in EBOV from 1976 to the 2014 outbreak . Virology 2015, 482:202-207.

55. Gatherer D, Derek G: The unprecedented scale of the West African Ebola virus disease outbreak is due to environmental and sociological factors, not special attributes of the currently circulating strain of the virus . Evid Based Med 2014, 20:28.

56. de La Vega M-A, Stein D, Kobinger GP: Ebolavirus evolution: past and present . PLoS Pathog 2015, 11:e1005221.

57. Liu S-Q, Deng C-L, Yuan Z-M, Rayner S, Zhang B: Identifying the pattern of molecular evolution for Zaire ebolavirus in the 2014 outbreak in West Africa . Infect Genet Evol 2015, 32:51-59.

58. • Deng L, Lizong D, Mi L, Sha H, Yousong P, Aiping W, Xiao-Feng Qin F, Genhong C, Taijiao J: Network of co-mutations in Ebola virus genome predicts the disease lethality . Cell Res 2015, 25:753-756.

The authors show the importance of studying mutations in a virus genome not individually but as a whole, to detect protein interactions that are currently not known to participate in viral replication.

59. •• Dietzel E, Schudt G, Kra ¨hling V, Matrosovich M, Becker S: Functional characterization of adaptive mutations during the West African Ebola virus outbreak . J Virol 2016 http://dx.doi.org/10.1128/JVI. 01913-16 .

This paper presents a detailed, functional analysis of commonly occurring virus variants from the West African EBOV outbreak using a series of VLP and reverse genetics approaches and show that these mutations can enhance viral fitness in cell culture.

60. Diehl WE, Lin AE, Grubaugh ND, Carvalho LM, Kim K, Kyawe PP, McCauley SM, Donnard E, Kucukural A, McDonel P et al.: Ebola virus glycoprotein with increased infectivity dominated the 2013–2016 epidemic . Cell 2016, 167 1088–1098.e6.

61. Urbanowicz RA, McClure CP, Sakuntabhai A, Sall AA, Kobinger G, Müller MA, Holmes EC, Rey FA, Simon-Loriere E, Ball JK: Human adaptation of Ebola virus during the West African Outbreak . Cell 2016, 167:1079-1087 e5.

62. Mahale KN, Patole MS: The crux and crust of ebolavirus: analysis of genome sequences and glycoprotein gene . Biochem Biophys Res Commun 2015, 463:756-761.

63. Mä nz B, de Graaf M, Mo ¨gling R, Richard M, Bestebroer TM, Rimmelzwaan GF, Fouchier RAM: Multiple natural substitutions in avian influenza A virus PB2 facilitate efficient replication in human cells . J Virol 2016, 90:5928-5938.

64. Dowall SD, Matthews DA, Garcia-Dorival I, Taylor I, Kenny J, Hertz-Fowler C, Hall N, Corbin-Lickfett K, Empig C, Schlunegger K et al.: Elucidating variations in the nucleotide sequence of Ebola virus associated with increasing pathogenicity . Genome Biol 2014, 15:540.

65. Albariño CG, Guerrero LW, Chakrabarti AK, Kainulainen MH, Whitmer SLM, Welch SR, Nichol ST: Virus fitness differences observed between two naturally occurring isolates of Ebola virus Makona variant using a reverse genetics approach . Virology 2016, 496:237-243.

66. Du X, Wang Z, Wu A, Song L, Cao Y, Hang H, Jiang T: Networks of genomic co-occurrence capture characteristics of human influenza A (H3N2) evolution . Genome Res 2007, 18:178-187.

67. Rimmelzwaan GF, BerkhoffEGM, Nieuwkoop NJ, Smith DJ, Fouchier RAM, Osterhaus ADME: Full restoration of viral fitness by multiple compensatory co-mutations in the nucleoprotein ofi nfluenza A virus cytotoxic T-lymphocyte escape mutants . J Gen Virol 2005, 86:1801-1805.

68. Shabman RS, Jabado OJ, Mire CE, Stockwell TB, Edwards M, Mahajan M, Geisbert TW, Basler CF: Deep sequencing identifies noncanonical editing of Ebola and Marburg virus RNAs in infected cells . MBio 2014, 5:e02011.

69. Samuel CE: Adenosine deaminases acting on RNA (ADARs) are both antiviral and proviral . Virology 2011, 411:180-193.

70. Volchkov VE, Becker S, Volchkova VA, Ternovoj VA, Kotov AN, Netesov SV, Klenk HD: GP mRNA of Ebola virus is edited by the Ebola virus polymerase and by T7 and vaccinia virus polymerases . Virology 1995, 214:421-430.

71. Mohan GS, Li W, Ye L, Compans RW, Yang C: Antigenic subversion: a novel mechanism of host immune evasion by Ebola virus . PLoS Pathog 2012, 8:e1003065.

72. Volchkov VE, Volchkova VA, Muhlberger E, Kolesnikova LV, Weik M, Dolnik O, Klenk HD: Recovery ofi nfectious Ebola virus from complementary DNA: RNA editing of the GP gene and viral cytotoxicity . Science 2001, 291:1965-1969.

73. Volchkova VA, Dolnik O, Martinez MJ, Reynard O, Volchkov VE: RNA editing of the GP gene of Ebola virus is an important pathogenicity factor . J Infect Dis 2015, 212(Suppl. 2) :S226-S233.

74. Volchkova VA, Vorac J, Repiquet-Paire L, Lawrence P, Volchkov VE: Ebola virus GP gene polyadenylation versus RNA editing . J Infect Dis 2015, 212(Suppl. 2) :S191-S198.

75. Volchkova VA, Dolnik O, Martinez MJ, Reynard O, Volchkov VE: Genomic RNA editing and its impact on Ebola virus adaptation during serial passages in cell culture and infection of guinea pigs . J Infect Dis 2011, 204(Suppl. 3) :S941-S946.

76. Trefry JC, Wollen SE, Nasar F, Shamblin JD, Kern SJ, Bearss JJ, Jefferson MA, Chance TB, Kugelman JR, Ladner JT et al.: Ebola virus infections in nonhuman primates are temporally influenced by glycoprotein poly-U editing site populations in the exposure material . Viruses 2015, 7:6739-6754.

77. Dolnik O, Volchkova VA, Escudero-Perez B, Lawrence P, Klenk H-D, Volchkov VE: Shedding of Ebola virus surface glycoprotein is a mechanism of self-regulation of cellular cytotoxicity and has a direct effect on virus infectivity . J Infect Dis 2015, 212(Suppl. 2) :S322-S328.

78. Escudero-Pe´rez B, Volchkova VA, Dolnik O, Lawrence P, Volchkov VE: Shed GP of Ebola virus triggers immune activation and increased vascular permeability . PLoS Pathog 2014, 10:e1004509.

79. Singh SK, Ruzek D: Viral Hemorrhagic Fevers . CRC Press; 2016.

80. Gouy M, Guindon S, Gascuel O: SeaView version 4: a multiplatform graphical user interface for sequence alignment and phylogenetic tree building . Mol Biol Evol 2010, 27:221-224.

ANNEXES

rVSV-GP-HS AS A TOOL TO INVESTIGATE THE ROLE OF $GP_{1,2\Delta}$ IN INNATE IMMUNITY AND COAGULATION DISORDERS

EBOV shed GP was shown to be able to bind and to activate monocytes-derived dendritic cells and monocytes-derived macrophages that in response released anti- and pro-inflammatory mediators [131]. However, $GP_{2\Delta}$ production through transfection is laborious, expensive and time-consuming and requires concentrating the cell culture supernatant using protein concentrators [131]. In this part, we aimed to use the rVSV-GP-HS virus as a platform for $GP_{1,2\Delta}$ production to be able to obtain a reliable source of Shed GP to further characterise its role in immune dysregulations.
To study the role of $GP_{1,2\Delta}$, it is necessary to be able to remove the remaining infectious viral particles from the cell culture supernatant. The difference between the virion-bound GP_2 and $GP_{2\Delta}$ is of only 13 amino acids. It is therefore, impossible to purify $GP_{1,2\Delta}$ using EBOV GP antibodies. As a consequence, several viral removal methods were tried to be able to remove the infectious virus to obtain a virus-free $GP_{1,2\Delta}$.

In a first time, a multiple steps approach that involved the infectious supernatant to be ultracentrifuged and ultrafiltrated was attempted to try completely remove the rVSV-GP-HS virus (Fig. 53A, upper part). For each step, supernatants were titrated by the TCID50 technique (Fig. 53B, lower part). After ultracentrifugation, the amount of residual virus in the ultracentrifuged supernatant was titrated at $1.58x10^5$ TCID50/mL. To further remove the residual amount of viruses, ultrafiltration centrifugal columns with a polyethersulfone membrane with a specific molecular weight (MW) cut-off (MWCO) were used. VSV MW is superior to 1 MkDa while $GP_{1,2\Delta}$ MW is around 350 kDa. When passing the ultracentrifuged supernatant on an ultrafiltration columns with a MWCO of 1000 kDa, the virus should be retained in the upper chamber of the column whereas the viral glycoprotein should be able to pass the polyethersulfone membrane [358]. However, as shown in Fig. 53B, in this setup, the viral titer in the supposed virus free flow through, was of $3.74x10^4$ TCID50/mL, indicating that a virus logarithmic reduction value (LRV) of 1 was achieved. Passing the ultrafiltrated supernatant on a second 1000 kDa MWCO column did not improve viral removal (Fig. 53B, $2.81x10^4$, LRV < 1). When the two time ultrafiltrated supernatant was passed on a 300 kDa ultrafiltration centrifugal columns, the vast majority of the infectious virus was retained in the upper chamber that titrated at $1.19x10^4$ TCID50/mL while in the flow through the titer was of $1.19x10^1$. This shows that using a 300 kDa MWCO, it was possible to obtain a LRV of 3 (see point 'Flow Through Column 300 kDa' to compare to 'Concentrated SPNT 300 kDa'). However, while proteins levels were similar after ultracentrifugation and the passages on the different 1000 kDa MWCO columns, with the 300 kDa MWCO column a non-negligible amount of GP_2 was retained in the upper chamber as observed by GP_2 decreased levels in the western-blot analysis (data not shown).

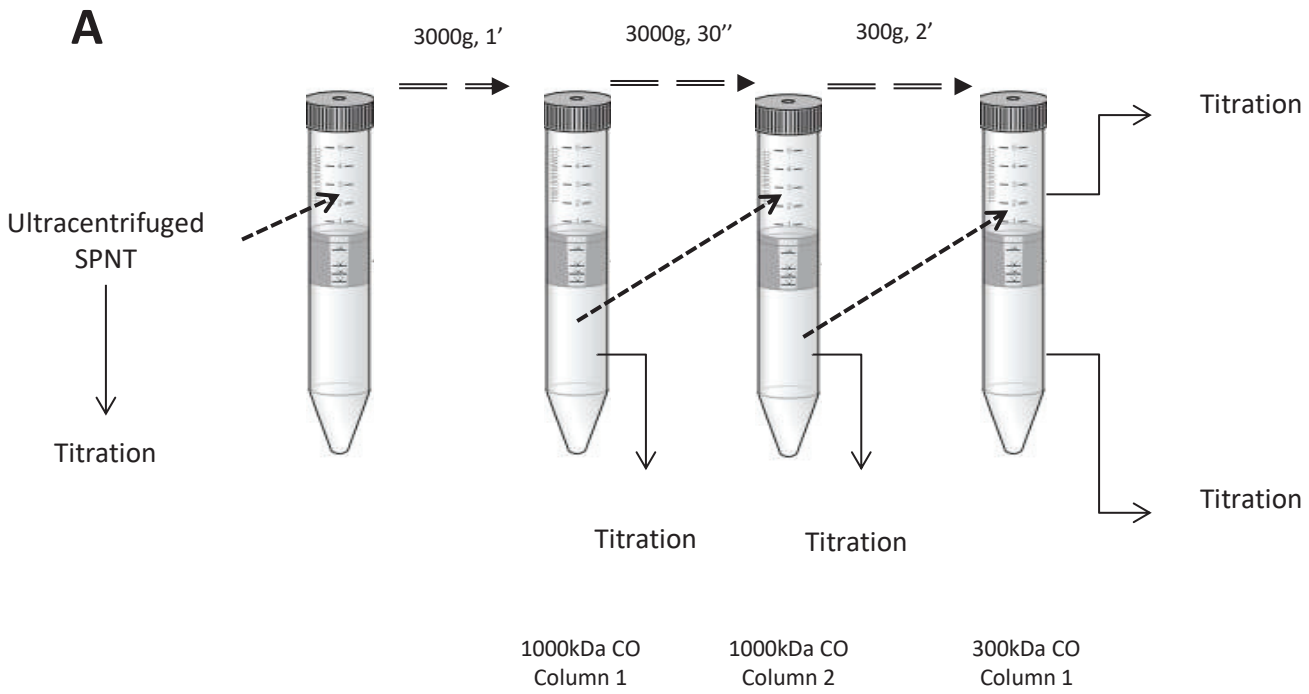

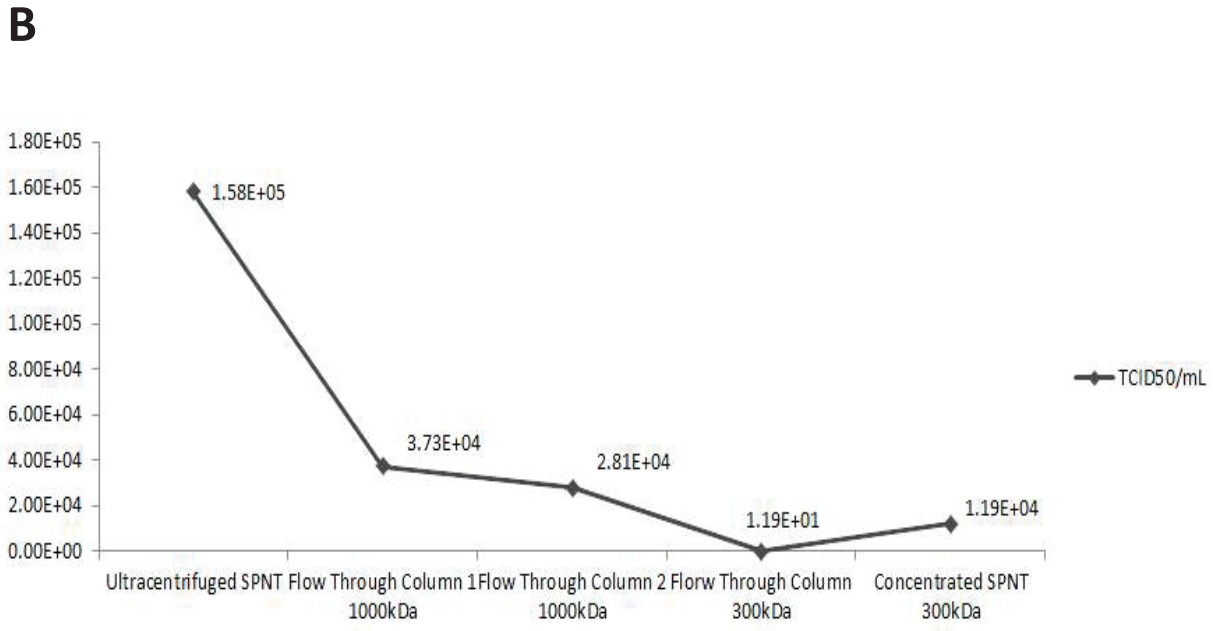

FIGURE 53. RVSV-GP ULTRAFILTRATION

rVSV-GP-HS infected cells supernatant was ultracentrifugerd for 2 hours, 28000 rpm (rotor SW32), on a 20% cushion sucrose. This ultracentrifuged supernatant (SPNT) was then loaded on an ultrafiltration column with a molecular weight cut off (MWCO) value of 10000 kDa and ultrafiltrated by centrifugation. The flow-through 1 was collected and passed on a second ultrafiltration column with a MWCO of 1000 kDa. Finally, the flow-through 2 was passed on a 300 kDa MCWO ultrafiltration column to concentrate the soluble viral glycoproteins (A). The ultracentrifuged supernatant, all flow-throughs and the concentrated supernatant were all titrated by TCID50 and the results are shown (B). The number above each point represents the infectious titration obtained.

Considering that it was not possible to entirely remove the virus using ultrafiltration columns we decided to perform nanofiltration using the Planova™ 35N virus removal filter that is made of cuprammonium-regenerated cellulose hollow fibres with pore size of 35 nm, that allows to retain any viruses with a size > 35 nm such as VSV (Fig. 54A).
In this respect, VeroE6 cells were infected with rVSV-GP-HS at a MOI of 0.01 and 48 hours post infection, the supernatant was collected and clarified by low speed centrifugation. Fifty mL of clarified supernatants were then passed onto the virus removal filter. Western-blotting analysis showed that before nanofiltration, two GP_2 bands are visible: The virion-bound GP_2 and the soluble truncated $GP_{2\Delta}$. Following nanofiltration, only the $GP_{2\Delta}$ band was detected indicating that a significant amount of rVSV-GP-HS viruses were removed to a point where that it cannot be detected anymore by western-blotting (Fig. 54B, left panel). However, signal quantification showed that at least half of the initial amounts of $GP_{2\Delta}$ were retained in the filter (Fig. 54B, right panel, and see $GP_{2\Delta}$ levels in grey, before and after nanofiltration). Virus removal was then confirmed by TCID50. In the initial product, the titre was of $2.87x10^7$ TCID50/mL whereas after nanofiltration the infectious titre was lower than our detection limit, which is of $1.25x10^0$ TCID50/mL, demonstrating a logarithmic reduction value of >7.33 (Fig. 54C). Similar results were obtained with cells infected with VSV Indiana (data not shown). Western-blotting quantification showed that after nanofilitration, the concentration of $GP_{2\Delta}$ was of 5µg/mL. Of interest, this showed that it was possible to obtain 5 times more $GP_{1,2\Delta}$ than what was obtained by Escudero-Pérez B *et al.* (2014), without the need to concentrate the cell culture media (Fig. 54D) [131].

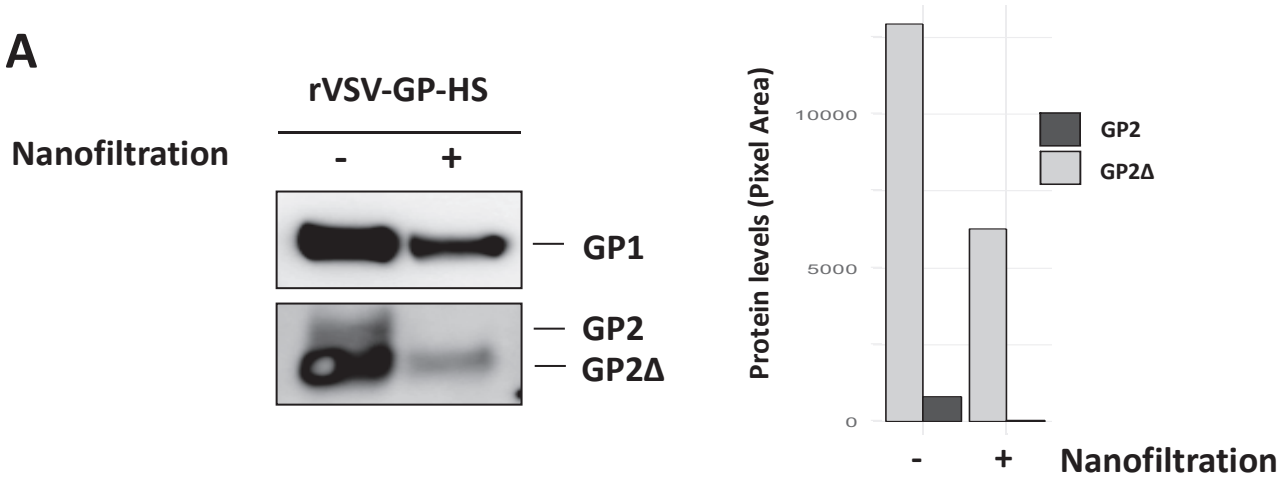
A
rVSV-GP-HS
Nanofiltration
-
+
GP1
GP2
GP2Δ
Protein levels (Pixel Area)
10000
5000
0
GP2
GP2Δ
-
+
Nanofiltration

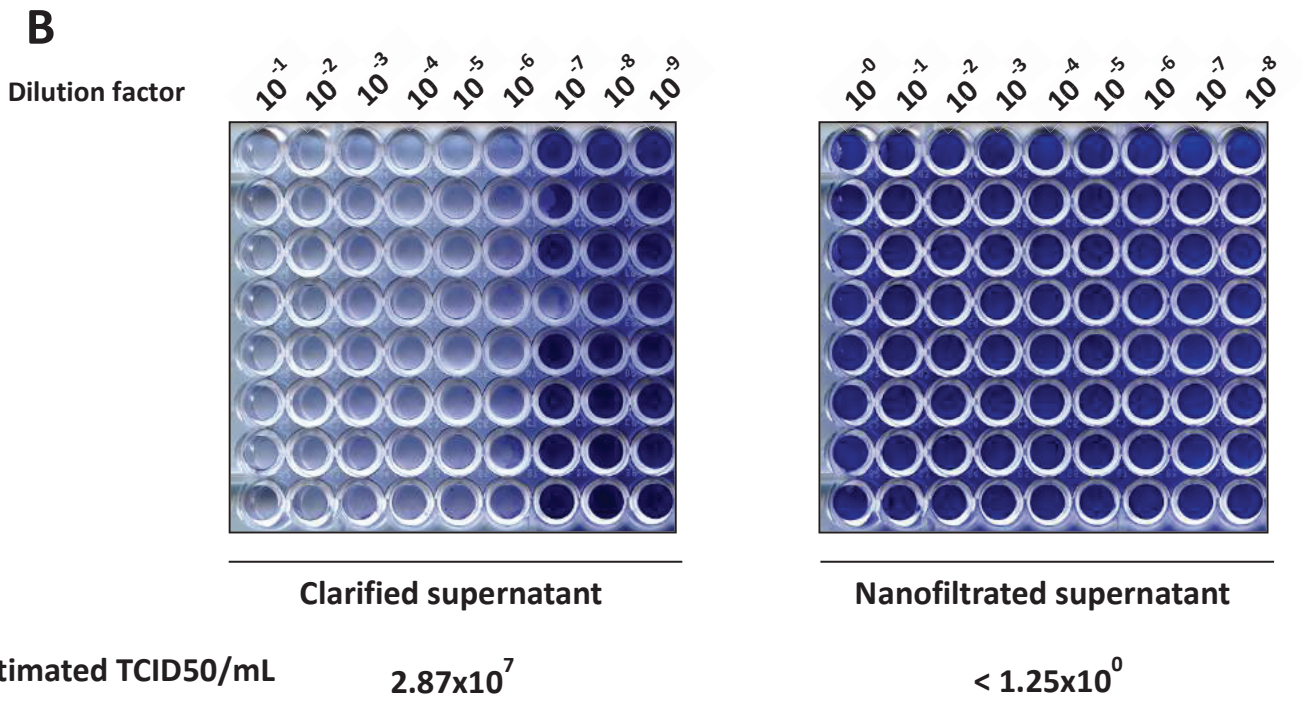
B
Dilution factor
10-1 10-2 10-3 10-4 10-5 10-6 10-7 10-8 10-9
10-0 10-1 10-2 10-3 10-4 10-5 10-6 10-7 10-8
Clarified supernatant
Nanofiltrated supernatant
Estimated TCID50/mL
2.87x10^7
< 1.25x10^0

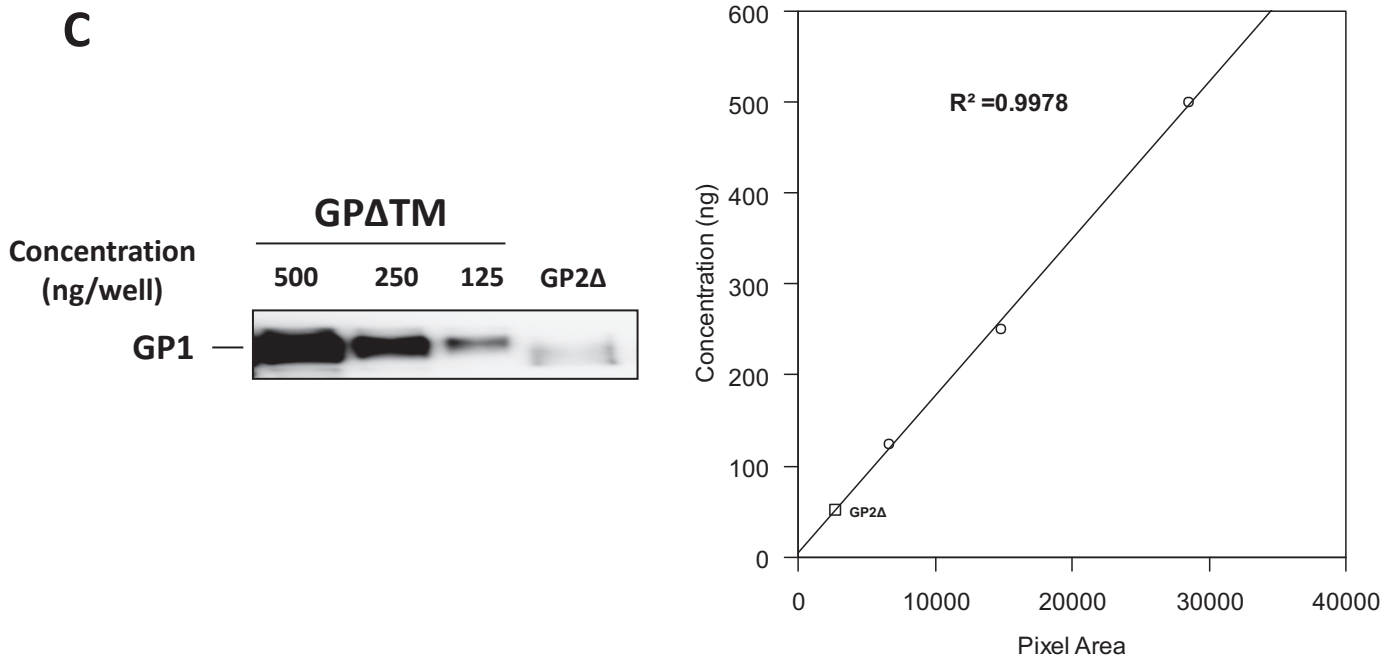
C
GPΔTM
Concentration (ng/well)
500
250
125
GP2Δ
GP1
R² =0.9978
Concentration (ng)
600
500
400
300
200
100
0
GP2Δ
0
10000
20000
30000
40000
Pixel Area

FIGURE 54. RVSV-GP NANOFILTRATION

rVSV-GP-HS supernatant was clarified by low-speed centrifugation and then nanofiltrated using a Planova™ 35N 0.001m2 filter (A). The presence of $GP_{1,2\Delta}$ was verified before and after nanofiltration by western-blotting using rabbit sera recognising GP_1 and GP_2 (B). Virus removal was confirmed by TCID50 (C) and the amount of $GP_{2\Delta}$ was quantified as before (D) [126]

Consequently, we were able to entirely remove the virus from of infectious supernatant through nanofiltration allowing to obtain a reliable and inexpensive source of $GP_{1,2\Delta}$ for further functional studies.

Platelets are megakaryocytes-derived cell fragments and the second most abundant cell population in the blood, with about $2x10^8$ platelets/mL of blood. They play a key role in maintaining haemostasis by rapidly detecting vessel integrity damages. In response, platelets bind to the damaged vessel wall and undergo a strong structural reorganisation that will lead to the recruitment of other platelets and immune cells, through the release of their intracellular stored granule contents in the bloodstream, and the initiation of the primary hemostasis to allow wound healing. In the last decades, it has been shown that in addition to control primary hemostasis, platelets were able to modulate the inflammatory response, either directly or by interacting with other components of the immune response pathways. Indeed, it was shown that platelets possess TLR, including TLR-4, as well as other receptors that are used as viral attachment factors, such as DC-SIGN or CLEC-2 [359–363]. Additionally, both HIV and DENV were shown to be able to be internalised inside of activated platelets [364,365]. Upon activation, platelets will typically form aggregates with other platelets to create a platelet plug but can also interact with resting or activated monocytes, and modulate their activity. Indeed, activated monocytes, by upregulating TF, are able to bind platelets that will decrypt TF present on the monocyte plasma membranes to render it active [366].
Thrombocytopenia is a hallmark of EBOV infection in human and NHP which is observed at the early stages of the infection and that is accompanied by the release of platelet-derived mediators such as sCD40L indicating that during the course of the disease, platelets are activated [74,182,216,220]. However, so far, it is not known whether this platelet activation is due to a direct interaction between the virus and its different glycoproteins with platelets or if this is the result of the dysregulated inflammatory response. Interestingly, a thrombocytopenia has been observed in patients vaccinated with the rVSV-GP-based vaccine and as such, we decided to use the virus to try to investigate the role of the viral glycoprotein in the activation of platelets during EBOV infections.

Platelets are very easily activated by different stimulants, including storage temperature and time, but also by the presence of different cell media culture components such as phenol red. Therefore, it was first necessary to identify which cell culture media would be best for the study of platelet activation. In this respect, platelet-rich plasma (PRP) was prepared by low speed centrifugation from blood tubes obtained from healthy donors. PRP are commonly used to study the induction of platelet as it 99.9% free of red and white blood cells and that it has all plasma factors that can support platelet activation [367]. PRP were then diluted with different cell culture media containing either phenol red and or/FBS and incubated for 30 minutes at 37°C (Fig. 55A). The thrombin-receptor activating peptide (TRAP) was used as a positive control and for negative control, platelets were left unstimulated. PRP activation was then monitored by flow cytometry by gating platelets using the platelet-specific marker CD41a and by following the upregulation of the gold standard marker of activation, CD62P (P-Selectin) (Fig. 55B). CD41a and CD62P limit of positivity was set up using appropriate isotype controls. As expected, following TRAP stimulation, 80% of the platelets were CD62P+, while less than 5% of the unstimulated platelets were CD41a+/CD62P+. When stimulated with the different cell media, platelets were maintained in a resting state with all media tested, until a certain dilution. Indeed, after diluting platelets more than 5 times (1:5 ratio compared to 1:1 ratio), at the exception of the Hank's Balanced Salt Solution (HBSS) buffer and the Phosphate buffer solution (PBS), all media (with or without phenol red and/or FBS) induced platelet activation and aggregation (noted by a + in the figure).

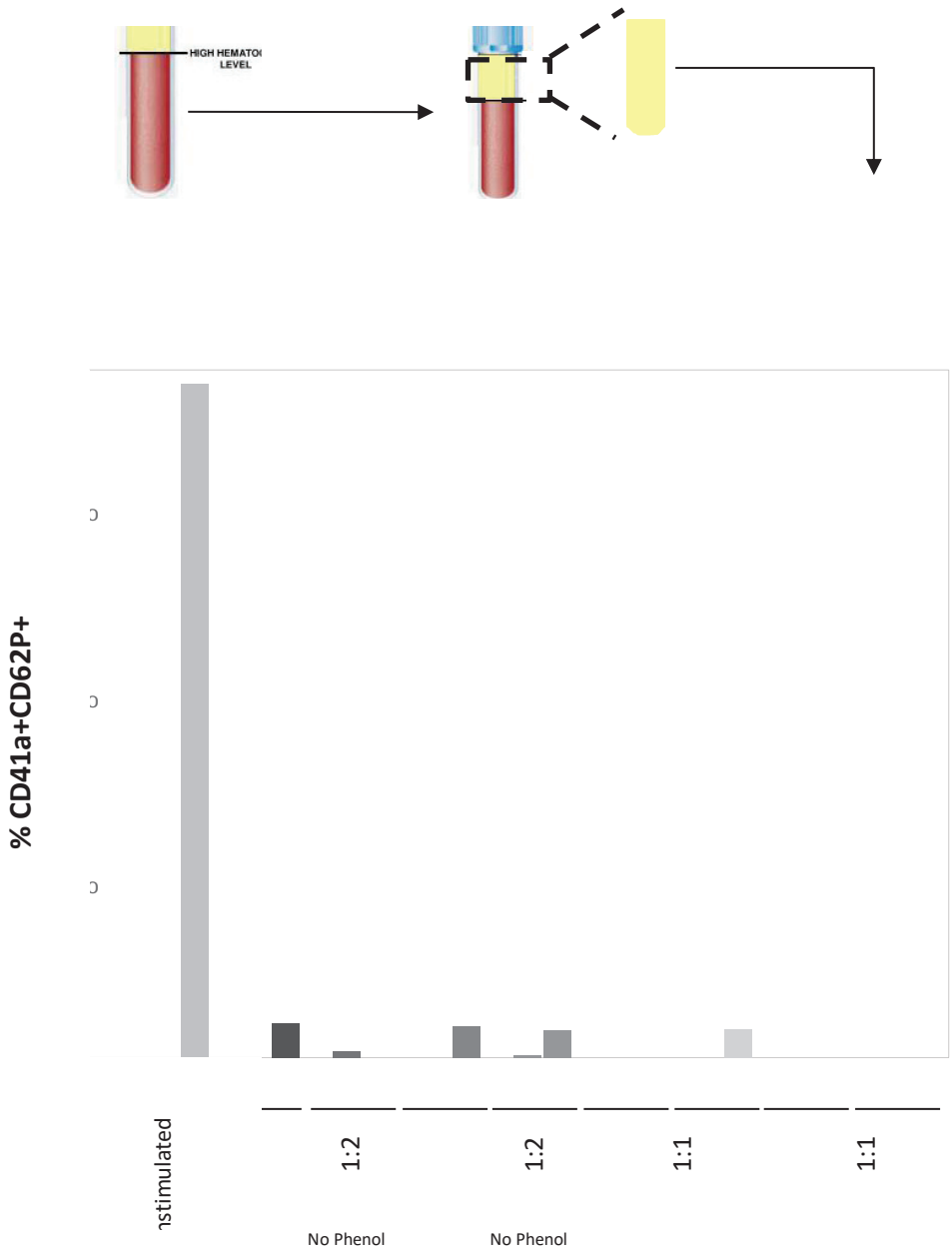

Schematical representation of the protocol used to obtain PRP from healthy blood donors (A). PRP activation by cellular media containing or no phenol red or FBS were evaluated by flow cytometry by measuring the upregulation of $CD62P^+$ of $CD41a^+$ positive cells. FBS: Fetal bovine serum

In parallel to PRP stimulation, it is common to study the role of plasma proteins in controlling platelet activation. In this respect, it is possible to wash plasma away from platelets to obtain so called 'washed platelets' through different centrifugation steps (Fig. 56A). For each step that leads to the obtention of washed platelets, their activation was monitored as before (Fig. 56B). Unsurprisingly and as also noticed by others, all washing steps lead to platelet activation, with about 35% of the total platelets which were activated at the end of the washing process (Fig. 56B, 'PRP' condition compare to 'Washed PLT' condition).

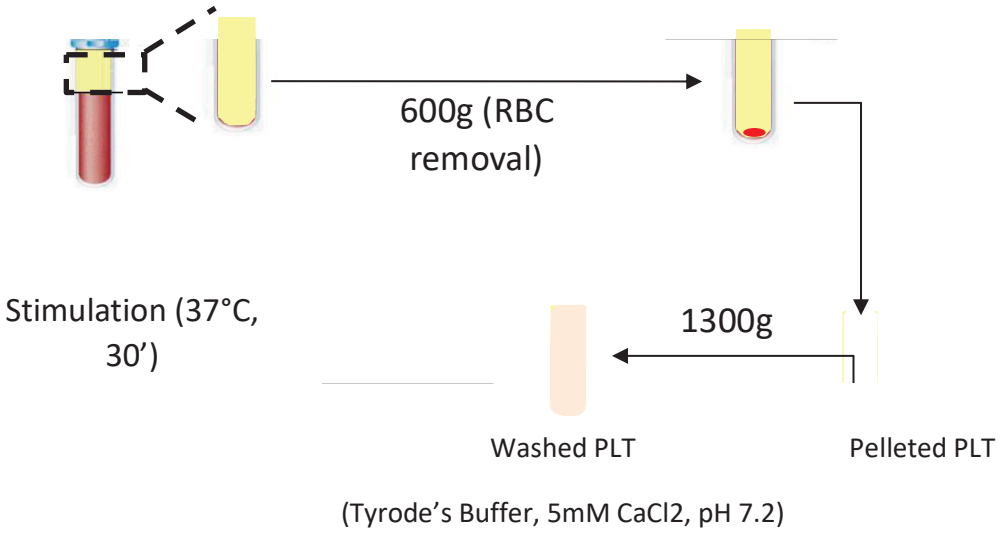

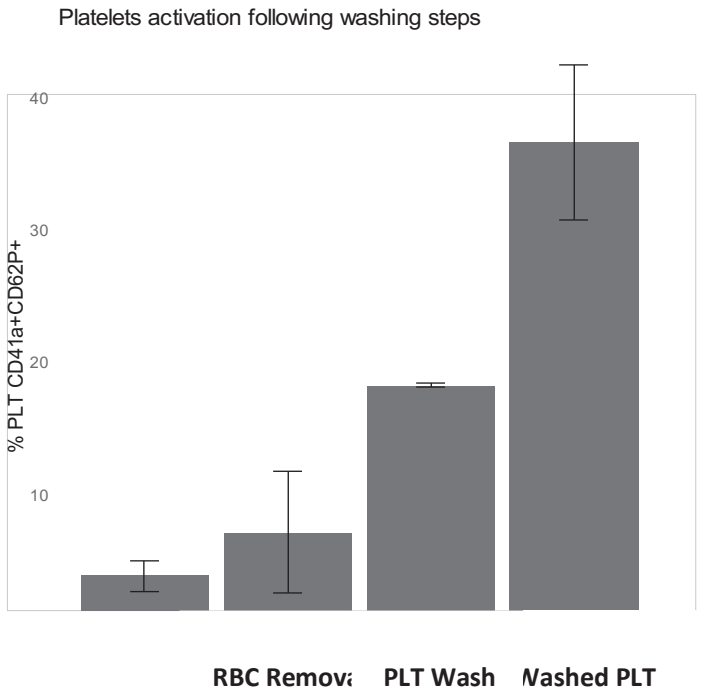

FIGURE 56. ANALYSIS OF WASHED PLATELETS ACTIVATION

Protocol for washing platelets from plasma (A). Following obtention of the Platelet-Rrich Plasma (PRP), red blood cells (RBC) were pelleted by centrifugation. The platelets in the PRP were then pelleted and washed twice. For each steps leading that lead to the obtention of the washed platelets, CD62P upregulation was analysed by flow cytometry.

Considering the high concentration of platelets in PRP compared to what is present in whole blood ($2.6x10^6$/µL $3.x10^5$/µL platelets, respectively) and the results obtained previously, that suggest that PRP can be diluted only until a certain point (Fig. 53), concentrated VSV and rVSV-GP stocks were produced to ensure to be able to observe an effect following stimulation. VeroE6 cells were either infected with VSV (strain Indiana) or rVSV-GP viruses and the supernatants were collected when cytopathic effects were evident. Viruses were then pelleted by ultracentrifugation and concentrated in PBS and both viruses were titrated and different virus dilutions were loaded and analysed by western-blotting using anti-VSV M monoclonal antibody to quantify the amount of total viral particles. As observed in Fig. 56, comparable levels of M protein were obtained between the undiluted VSV virus and the rVSV-GP viruses that was diluted 5 times (Fig. 56, 'Dilution factor 1', row VSV compared to 'Dilution factor 0.2', row rVSV-GP). A similar result was observed with the infectious titers, with VSV that titrated at $1x10^9$ TCID50/mL against $8x10^9$ TCID50/mL for rVSV-GP, confirming that it exists a difference of about 5 to 8 times between the stocks of rVSV-GP and VSV viruses.

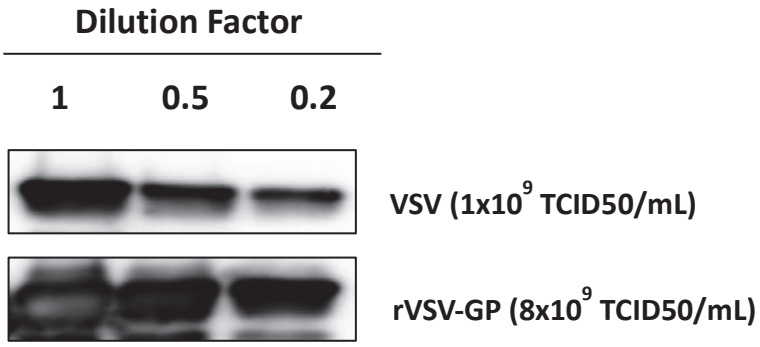

FIGURE 57. VIRUS PRODUCTION FOR PLATELET STIMULATION

Supernatants from VeroE6 cells infected with rVSV-GP or VSV were collected and clarified from dead cells and debris by low speed centrifugation. The viruses were then pelleted as before and resuspended and concentrated in PBS 1X, with No CA^{2+} and no Mg^{2+}. Samples were analysed by western-blotting and the amount of VSV protein M were detected. The titers of the undiluted viruses are indicated.

After PRP and washed platelets obtention, platelets were either left unstimulated or challenged with TRAP or different amount of viruses for 30 minutes, at 37°C. Platelet activation was measured similarly to before and the cytometry results obtained for one donor are shown Fig. 58A. Expectedly, CD62P+ levels were around 2 to 3% when PRP were stimulated with PBS whereas following TRAP treatment, a marked increase in P-selectin expression was observed (Fig. 57A, 'PRP' conditions 'PBS and 'TRAP', CD62P+: 9.54% and 57.9% respectively). On the opposite, PRP stimulated with either VSV or rVSV-GP showed no difference compared to the unstimulated control (Fig. 58A, 'PRP', 'VSV' and 'rVSV-GP', compared to 'PBS'). After plasma removal ('Washed PLT') and as observed before, a significant increase in CD62P levels was observed, which lead to a reduced capacity of TRAP to activate washed platelets (Fig. 58A, 'Washed PLT', see 'PBS' and 'TRAP' conditions, as well as Fig. 56B, for washed platelet activation). Surprisingly, similarly to platelets stimulated with VSV, washed platelets challenged with rVSV-GP showed no upregulation of CD62P levels. However, they displayed a strong downregulation of the CD41a maker (Fig. 58A, 'Washed PLT', 'rVSV-GP'. Of note, this CD41a- population showed similar CD62P levels than the CD41a+ population. Similar results were obtained for different donors (Fig. 58B).

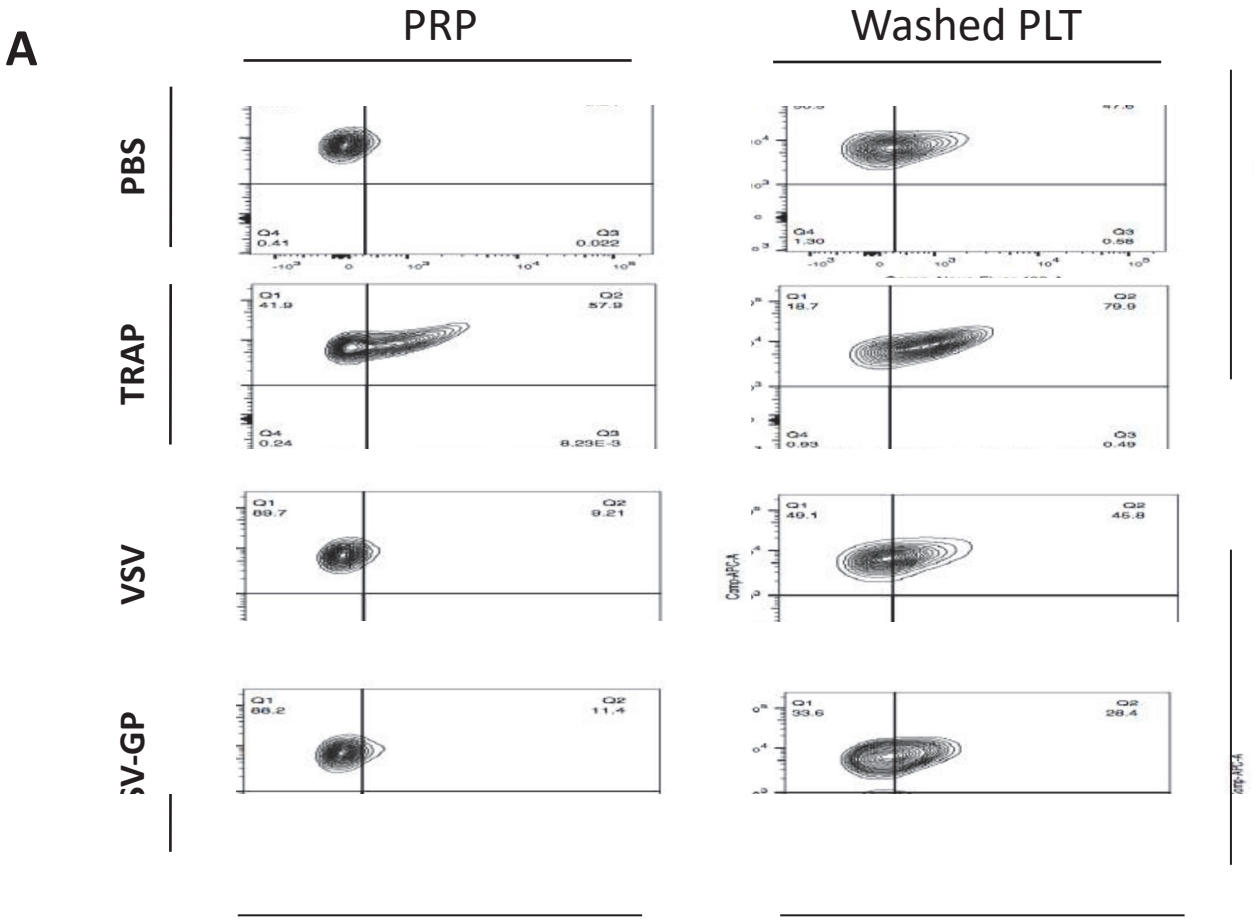

B

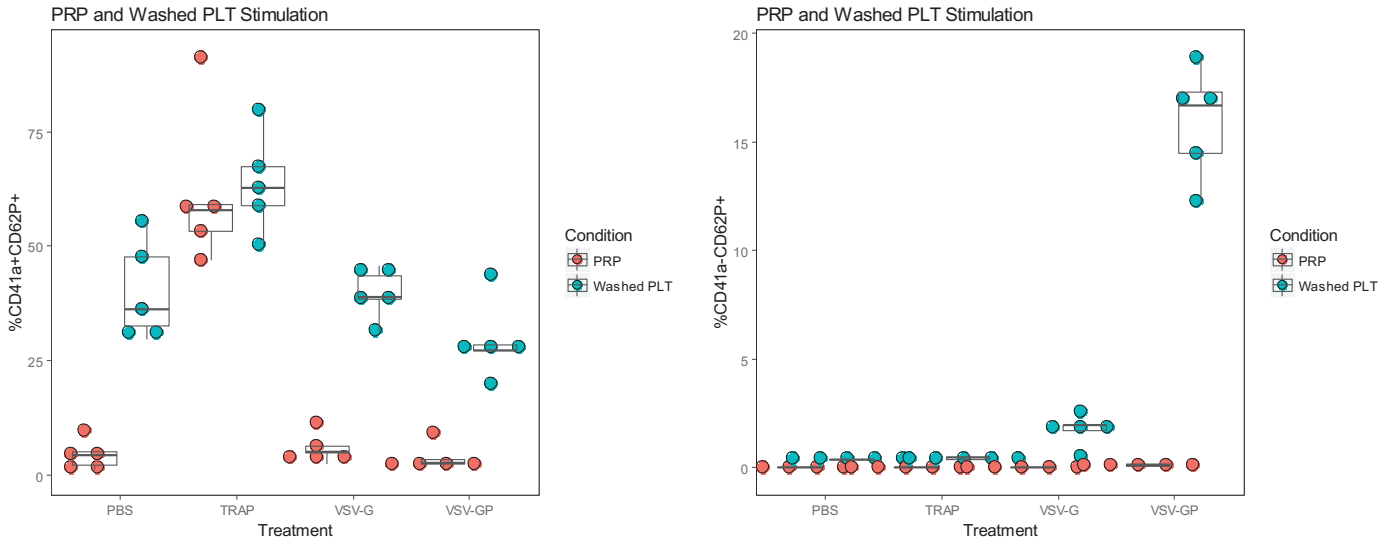

FIGURE 58. PRP AND WASHED PLATELETS STIMULATION WITH rVSV-GP AND VSV

PRP and washed platelets were obtained as described previously and were stimulated for 30 minutes at 37°C, with equal amounts of rVSV-GP and VSV, or were treated with PBS or TRAP as controls. Samples were then fixed and analysed by flow cytometry using the CD41a and CD62P markers. Isotype controls were used to set up the limit of positivity of the different markers and a representative flow cytometry results is presented in (A). In (B) are plotted the results for 5 independent donors. Left panel is showing the % of CED41a+CD62P+ and the right panel the % of CD41a-CD62P+ events.

To understand if this effect was specific to rVSV-GP or if it was due to a larger amount of rVSV-GP viral particles, washed platelets were prepared and either stimulated with a fixed amount of rVSV-GP or with an increasing amount of VSV Indiana and analysed as before (Fig. 58). In the analysis, the CD42b marker was also included to see if the observed CD41a downregulation was specific or if other membrane proteins were downregulated upon rVSV-GP stimulation. As it was observed before, platelets showed an important activation following washing and while they could still respond to TRAP, this effect was limited (Fig. 59, left panel, 'PBS' and 'TRAP'). Following rVSV-GP stimulation, the apparition of this CD41a population was observed again (Fig. 59, left panel, 'rVSV-GP'). Of interest, washed platelets that were incubated with increasing amount of VSV responded similarly to rVSV-GP stimulation (Fig. 59, left panel, 'VSV'; 'VSV 5X' and 'VSV 10X'). Indeed, when platelets were stimulated with the same amount of viral particles than rVSV-GP, the same amount of CD41a- platelets were detected (Fig. 59, left panel 'VSV 5X', compared to 'rVSV-GP). In addition, by stimulating the platelets with twice the amount of rVSV-GP particles (Fig. 59, left panel 'VSV 10X'), it was possible to increase the proportion of this CD41a- population from 13% to 18%. Furthermore, analysis using the CD42b marker, showed that this platelet population is also CD42b-, suggesting that another surface glycoprotein could be downregulated.

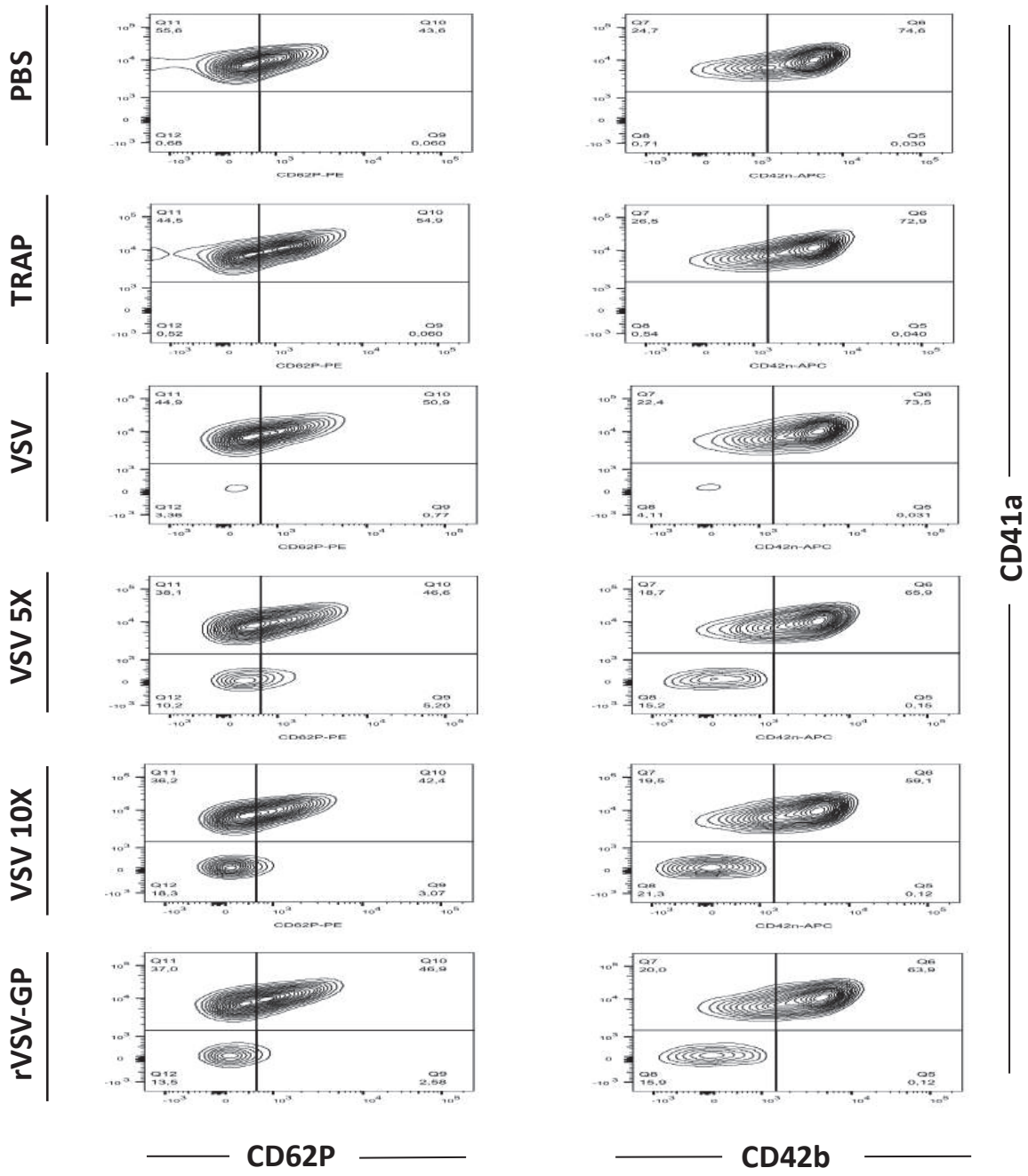

FIGURE 59. PLATELET ACTIVATION FOLLOWING STIMULATION WITH DIFFERENT AMOUNT OF VSV

Washed platelets were obtained and stimulated with different amounts of VSV (5 times: 5X, 10 times: 10X, in comparison to rVSV-GP amount). VSV-stimulated platelet activation was then investigated and compared to rVSV-GP stimulation using CD41a, CD42b and CD62P staining. Similar results were obtained for three independent donors.

While our results show that the observed CD41a and CD42b downregulation is not $GP_{1,2}$-dependant but appears to be a general response to the viral stimulation, it is to our knowledge, the first time that such population was identified and further studies are required to understand its role in viral infection. However, it already appears that plasma proteins are able to control this population apparition.

BIBLIOGRAPHY

1. Ebola virus infectons. Br Med J 1977, 2:539–540.

2. Kuhn JH, Radoshitzky SR, Bavari S, Jahrling PB: The International Code of Virus Classification and Nomenclature (ICVCN): proposal to delete Rule 3.41. Arch Virol 2013, 158:297–299.

3. Negredo A, Palacios G, Vázquez-Morón S, González F, Dopazo H, Molero F, Juste J, Quetglas J, Savji N, de la Cruz Martínez M, et al.: Discovery of an ebolavirus-like filovirus in europe. PLoS Pathog 2011, 7:e1002304.

4. He B, Feng Y, Zhang H, Xu L, Yang W, Zhang Y, Li X, Tu C: Filovirus RNA in Fruit Bats, China. Emerg Infect Dis 2015, 21:1675–1677.

5. Yang X-L, Zhang Y-Z, Jiang R-D, Guo H, Zhang W, Li B, Wang N, Wang L, Waruhiu C, Zhou J-H, et al.: Genetically Diverse Filoviruses in Rousettus and Eonycteris spp. Bats, China, 2009 and 2015. Emerg Infect Dis 2017, 23:482–486.

6. Kemenesi G, Kurucz K, Dallos B, Zana B, Földes F, Boldogh S, Görföl T, Carroll MW, Jakab F: Re-emergence of Lloviu virus in Miniopterus schreibersii bats, Hungary, 2016. Emerg Microbes Infect 2018, 7:66.

7. Baize S, Pannetier D, Oestereich L, Rieger T, Koivogui L, Magassouba N 'faly, Soropogui B, Sow MS, Keïta S, De Clerck H, et al.: Emergence of Zaire Ebola virus disease in Guinea. N Engl J Med 2014, 371:1418–1425.

8. Plowright RK, Foley P, Field HE, Dobson AP, Foley JE, Eby P, Daszak P: Urban habituation, ecological connectivity and epidemic dampening: the emergence of Hendra virus from flying foxes (Pteropus spp.). Proc Biol Sci 2011, 278:3703–3712.

9. Lawrence P, Danet N, Reynard O, Volchkova V, Volchkov V: Human transmission of Ebola virus. Curr Opin Virol 2017, 22:51–58.

10. Lindahl JF, Grace D: The consequences of human actions on risks for infectious diseases: a review. Infect Ecol Epidemiol 2015, 5:30048.

11. Singh SK: Viral Infections and Global Change. John Wiley & Sons; 2013.

12. Judson S, Prescott J, Munster V: Understanding ebola virus transmission. Viruses 2015, 7:511–521.

13. Geisbert TW, Strong JE, Feldmann H: Considerations in the Use of Nonhuman Primate Models of Ebola Virus and Marburg Virus Infection. J Infect Dis 2015, 212 Suppl 2:S91–7.

14. Alfson KJ, Avena LE, Beadles MW, Staples H, Nunneley JW, Ticer A, Dick EJ Jr, Owston MA, Reed C, Patterson JL, et al.: Particle-to-PFU ratio of Ebola virus influences disease course and survival in cynomolgus macaques. J Virol 2015, 89:6773–6781.

15. Van Kerkhove MD, Bento AI, Mills HL, Ferguson NM, Donnelly CA: A review of epidemiological parameters from Ebola outbreaks to inform early public health decision-making. Sci Data 2015, 2:150019.

16. Caviness K, Kuhn JH, Palacios G: Ebola virus persistence as a new focus in clinical research. Curr Opin Virol 2017, 23:43–48.

17. Mate SE, Kugelman JR, Nyenswah TG, Ladner JT, Wiley MR, Cordier-Lassalle T, Christie A, Schroth GP, Gross SM, Davies-Wayne GJ, et al.: Molecular Evidence of Sexual Transmission of Ebola Virus. N Engl J Med 2015, 373:2448–2454.

18. Christie A, Davies-Wayne GJ, Cordier-Lassalle T, Cordier-Lasalle T, Blackley DJ, Laney AS, Williams DE, Shinde SA, Badio M, Lo T, et al.: Possible sexual transmission of Ebola virus - Liberia, 2015. MMWR Morb Mortal Wkly Rep 2015, 64:479–481.

19. Subissi L, Keita M, Mesfin S, Rezza G, Diallo B, Van Gucht S, Musa EO, Yoti Z, Keita S, Djingarey MH, et al.: Ebola Virus Transmission Caused by Persistently Infected Survivors of the 2014-2016 Outbreak in West Africa. J Infect Dis 2018, doi:10.1093/infdis/jiy280.

20. Fischer R, Judson S, Miazgowicz K, Bushmaker T, Prescott J, Munster VJ: Ebola Virus Stability on Surfaces and in Fluids in Simulated Outbreak Environments. Emerg Infect Dis 2015, 21:1243–1246.

21. Prescott J, Bushmaker T, Fischer R, Miazgowicz K, Judson S, Munster VJ: Postmortem stability of Ebola virus. Emerg Infect Dis 2015, 21:856–859.

22. HICPAC | CDC. 2018,

23. HICPAC | CDC. 2018,

24. Roels TH, Bloom AS, Buffington J, Muhungu GL, Mac Kenzie WR, Khan AS, Ndambi R, Noah DL, Rolka HR, Peters CJ, et al.: Ebola hemorrhagic fever, Kikwit, Democratic Republic of the Congo, 1995: risk factors for patients without a reported exposure. J Infect Dis 1999, 179 Suppl 1:S92–7.

25. Martines RB, Ng DL, Greer PW, Rollin PE, Zaki SR: Tissue and cellular tropism, pathology and pathogenesis of Ebola and Marburg viruses. J Pathol 2015, 235:153–174.

26. Bausch DG, Towner JS, Dowell SF, Kaducu F, Lukwiya M, Sanchez A, Nichol ST, Ksiazek TG, Rollin PE: Assessment of the Risk of Ebola Virus Transmission from Bodily Fluids and Fomites. J Infect Dis 2007, 196:S142–S147.

27. Mekibib B, Ariën KK: Aerosol Transmission of Filoviruses. Viruses 2016, 8.

28. Dowell SF, Mukunu R, Ksiazek TG, Khan AS, Rollin PE, Peters CJ: Transmission of Ebola hemorrhagic fever: a study of risk factors in family members, Kikwit, Democratic Republic of the Congo, 1995. Commission de Lutte contre les Epidémies à Kikwit. J Infect Dis 1999, 179 Suppl 1:S87–91.

29. Bower H, Johnson S, Bangura MS, Kamara AJ, Kamara O, Mansaray SH, Sesay D, Turay C, Checchi F, Glynn JR: Exposure-Specific and Age-Specific Attack Rates for Ebola Virus Disease in Ebola-Affected Households, Sierra Leone. Emerg Infect Dis 2016, 22:1403–1411.

30. Kondoh T, Letko M, Munster VJ, Manzoor R, Maruyama J, Furuyama W, Miyamoto H, Shigeno A, Fujikura D, Takadate Y, et al.: Single-Nucleotide Polymorphisms in Human NPC1 Influence Filovirus Entry Into Cells. J Infect Dis 2018, doi:10.1093/infdis/jiy248.

31. Carette JE, Raaben M, Wong AC, Herbert AS, Obernosterer G, Mulherkar N, Kuehne AI, Kranzusch PJ, Griffin AM, Ruthel G, et al.: Ebola virus entry requires the cholesterol transporter Niemann-Pick C1. Nature 2011, 477:340–343.

32. Rasmussen AL, Okumura A, Ferris MT, Green R, Feldmann F, Kelly SM, Scott DP, Safronetz D, Haddock E, LaCasse R, et al.: Host genetic diversity enables Ebola hemorrhagic fever pathogenesis and resistance. Science 2014, 346:987–991.

33. Identifying Reservoirs of Infection: A Conceptual and Practical Challenge. Emerg Infect Dis 2002, 8:1468–1473.

34. Amman BR, Swanepoel R, Nichol ST, Towner JS: Ecology of Filoviruses. Curr Top Microbiol Immunol 2017, 411:23–61.

35. Swanepoel R: Experimental Inoculation of Plants and Animals with Ebola Virus. Emerg Infect Dis 1996, 2:321–325.

36. Morvan J: Identification of Ebola virus sequences present as RNA or DNA in organs of terrestrial small mammals of the Central African Republic. Microbes Infect 1999, 1:1193–1201.

37. Luis AD, O'Shea TJ, Hayman DTS, Wood JLN, Cunningham AA, Gilbert AT, Mills JN, Webb CT: Network analysis of host-virus communities in bats and rodents reveals determinants of cross-species transmission. Ecol Lett 2015, 18:1153–1162.

38. Hassanin A, Nesi N, Marin J, Kadjo B, Pourrut X, Leroy É, Gembu G-C, Musaba Akawa P, Ngoagouni C, Nakouné E, et al.: Comparative phylogeography of African fruit bats (Chiroptera, Pteropodidae) provide new insights into the outbreak of Ebola virus disease in West Africa, 2014-2016. C R Biol 2016, 339:517–528.

39. Towner JS, Amman BR, Sealy TK, Carroll SAR, Comer JA, Kemp A, Swanepoel R, Paddock CD, Balinandi S, Khristova ML, et al.: Isolation of genetically diverse Marburg viruses from Egyptian fruit bats. PLoS Pathog 2009, 5:e1000536.

40. Marburg Outbreaks 2005-2014 | Marburg Hemorrhagic Fever (Marburg HF) | CDC. [date unknown],

41. Amman BR, Jones MEB, Sealy TK, Uebelhoer LS, Schuh AJ, Bird BH, Coleman-McCray JD, Martin BE, Nichol ST, Towner JS: Oral shedding of Marburg virus in experimentally infected Egyptian fruit bats (Rousettus aegyptiacus). J Wildl Dis 2015, 51:113–124.

42. Schuh AJ, Amman BR, Sealy TK, Spengler JR, Nichol ST, Towner JS: Egyptian rousette bats maintain long-term protective immunity against Marburg virus infection despite diminished antibody levels. Sci Rep 2017, 7:8763.

43. Schuh AJ, Amman BR, Jones MEB, Sealy TK, Uebelhoer LS, Spengler JR, Martin BE, Coleman-McCray JAD, Nichol ST, Towner JS: Modelling filovirus maintenance in nature by experimental transmission of Marburg virus between Egyptian rousette bats. Nat Commun 2017, 8:14446.

44. Jones MEB, Schuh AJ, Amman BR, Sealy TK, Zaki SR, Nichol ST, Towner JS: Experimental Inoculation of Egyptian Rousette Bats (Rousettus aegyptiacus) with Viruses of the Ebolavirus and Marburgvirus Genera. Viruses 2015, 7:3420–3442.

45. Leroy EM, Kumulungui B, Pourrut X, Rouquet P, Hassanin A, Yaba P, Délicat A, Paweska JT, Gonzalez J-P, Swanepoel R: Fruit bats as reservoirs of Ebola virus. Nature 2005, 438:575–576.

46. Ng M, Ndungo E, Kaczmarek ME, Herbert AS, Binger T, Kuehne AI, Jangra RK, Hawkins JA, Gifford RJ, Biswas R, et al.: Filovirus receptor NPC1 contributes to species-specific patterns of ebolavirus susceptibility in bats. Elife 2015, 4.

47. Rouquet P, Froment J-M, Bermejo M, Kilbourn A, Karesh W, Reed P, Kumulungui B, Yaba P, Délicat A, Rollin PE, et al.: Wild animal mortality monitoring and human Ebola outbreaks, Gabon and Republic of Congo, 2001-2003. Emerg Infect Dis 2005, 11:283–290.

48. Leendertz SAJ, Wich SA, Ancrenaz M, Bergl RA, Gonder MK, Humle T, Leendertz FH: Ebola in great apes - current knowledge, possibilities for vaccination, and implications for conservation and human health. Mamm Rev 2016, 47:98–111.

49. Bermejo M, Rodríguez-Teijeiro JD, Illera G, Barroso A, Vilà C, Walsh PD: Ebola outbreak killed 5000 gorillas. Science 2006, 314:1564.

50. Leroy EM: Multiple Ebola Virus Transmission Events and Rapid Decline of Central African Wildlife. Science 2004, 303:387–390.

51. Walsh PD, Breuer T, Sanz C, Morgan D, Doran-Sheehy D: Potential for Ebola transmission between gorilla and chimpanzee social groups. Am Nat 2007, 169:684–689.

52. Hayes CG, Burans JP, Ksiazek TG, Del Rosario RA, Miranda ME, Manaloto CR, Barrientos AB, Robles CG, Dayrit MM, Peters CJ: Outbreak of fatal illness among captive macaques in the Philippines caused by an Ebola-related filovirus. Am J Trop Med Hyg 1992, 46:664–671.

53. Barrette RW, Metwally SA, Rowland JM, Xu L, Zaki SR, Nichol ST, Rollin PE, Towner JS, Shieh W-J, Batten B, et al.: Discovery of swine as a host for the Reston ebolavirus. Science 2009, 325:204–206.

54. Jayme SI, Field HE, de Jong C, Olival KJ, Marsh G, Tagtag AM, Hughes T, Bucad AC, Barr J, Azul RR, et al.: Molecular evidence of Ebola Reston virus infection in Philippine bats. Virol J 2015, 12:107.

55. Booth TF, Rabb MJ, Beniac DR: How do filovirus filaments bend without breaking? Trends Microbiol 2013, 21:583–593.

56. Bharat TAM, Noda T, Riches JD, Kraehling V, Kolesnikova L, Becker S, Kawaoka Y, Briggs JAG: Structural dissection of Ebola virus and its assembly determinants using cryo-electron tomography. Proc Natl Acad Sci U S A 2012, 109:4275–4280.

57. Geisbert TW, Jahrling PB: Differentiation of filoviruses by electron microscopy. Virus Res 1995, 39:129–150.

58. Volchkov VE, Volchkova VA, Muhlberger E, Kolesnikova LV, Weik M, Dolnik O, Klenk HD: Recovery of infectious Ebola virus from complementary DNA: RNA editing of the GP gene and viral cytotoxicity. Science 2001, 291:1965–1969.

59. Volchkov VE, Volchkova VA, Chepurnov AA, Blinov VM, Dolnik O, Netesov SV, Feldmann H: Characterization of the L gene and 5' trailer region of Ebola virus. J Gen Virol 1999, 80 (Pt 2):355–362.

60. Sztuba-Solinska J, Diaz L, Kumar MR, Kolb G, Wiley MR, Jozwick L, Kuhn JH, Palacios G, Radoshitzky SR, J Le Grice SF, et al.: A small stem-loop structure of the Ebola virus trailer is essential for replication and interacts with heat-shock protein A8. Nucleic Acids Res 2016, 44:9831–9846.

61. Weik M, Enterlein S, Schlenz K, Mühlberger E: The Ebola virus genomic replication promoter is bipartite and follows the rule of six. J Virol 2005, 79:10660–10671.

62. Crary SM, Towner JS, Honig JE, Shoemaker TR, Nichol ST: Analysis of the role of predicted RNA secondary structures in Ebola virus replication. Virology 2003, 306:210–218.

63. Neumann G, Watanabe S, Kawaoka Y: Characterization of Ebolavirus regulatory genomic regions. Virus Res 2009, 144:1–7.

64. Mühlberger E: Filovirus replication and transcription. Future Virol 2007, 2:205–215.

65. Vidal S, Curran J, Kolakofsky D: A stuttering model for paramyxovirus P mRNA editing. EMBO J 1990, 9:2017–2022.

66. Brauburger K, Boehmann Y, Tsuda Y, Hoenen T, Olejnik J, Schümann M, Ebihara H, Mühlberger E: Analysis of the highly diverse gene borders in Ebola virus reveals a distinct mechanism of transcriptional regulation. J Virol 2014, 88:12558–12571.

67. Brauburger K, Boehmann Y, Krähling V, Mühlberger E: Transcriptional Regulation in Ebola Virus: Effects of Gene Border Structure and Regulatory Elements on Gene Expression and Polymerase Scanning Behavior. J Virol 2016, 90:1898–1909.

68. Banerjee AK, Barik S, De BP: Gene expression of nonsegmented negative strand RNA viruses. Pharmacol Ther 1991, 51:47–70.

69. Barr JN, Whelan SPJ, Wertz GW: Transcriptional control of the RNA-dependent RNA polymerase of vesicular stomatitis virus. Biochim Biophys Acta 2002, 1577:337–353.

70. Shabman RS, Jabado OJ, Mire CE, Stockwell TB, Edwards M, Mahajan M, Geisbert TW, Basler CF: Deep sequencing identifies noncanonical editing of Ebola and Marburg virus RNAs in infected cells. MBio 2014, 5:e02011.

71. Shabman RS, Hoenen T, Groseth A, Jabado O, Binning JM, Amarasinghe GK, Feldmann H, Basler CF: An upstream open reading frame modulates ebola virus polymerase translation and virus replication. PLoS Pathog 2013, 9:e1003147.

72. Sanchez A, Kiley MP, Holloway BP, Auperin DD: Sequence analysis of the Ebola virus genome: organization, genetic elements, and comparison with the genome of Marburg virus. Virus Res 1993, 29:215–240.

73. Pathogenesis of Viral Infections and Diseases. In Fenner's Veterinary Virology. . Elsevier; 2017:47–78.

74. Baskerville A, Bowen ET, Platt GS, McArdell LB, Simpson DI: The pathology of experimental Ebola virus infection in monkeys. J Pathol 1978, 125:131–138.

75. Hoenen T, Shabman RS, Groseth A, Herwig A, Weber M, Schudt G, Dolnik O, Basler CF, Becker S, Feldmann H: Inclusion bodies are a site of ebolavirus replication. J Virol 2012, 86:11779–11788.

76. Nanbo A, Watanabe S, Halfmann P, Kawaoka Y: The spatio-temporal distribution dynamics of Ebola virus proteins and RNA in infected cells. Sci Rep 2013, 3:1206.

77. Noda T, Ebihara H, Muramoto Y, Fujii K, Takada A, Sagara H, Kim JH, Kida H, Feldmann H, Kawaoka Y: Assembly and budding of Ebolavirus. PLoS Pathog 2006, 2:e99.

78. Beniac DR, Melito PL, Devarennes SL, Hiebert SL, Rabb MJ, Lamboo LL, Jones SM, Booth TF: The organisation of Ebola virus reveals a capacity for extensive, modular polyploidy. PLoS One 2012, 7:e29608.

79. Watanabe S, Noda T, Kawaoka Y: Functional Mapping of the Nucleoprotein of Ebola Virus. J Virol 2006, 80:3743–3751.

80. Huang Y, Xu L, Sun Y, Nabel GJ: The assembly of Ebola virus nucleocapsid requires virion-associated proteins 35 and 24 and posttranslational modification of nucleoprotein. Mol Cell 2002, 10:307–316.

81. Su Z, Wu C, Shi L, Luthra P, Pintilie GD, Johnson B, Porter JR, Ge P, Chen M, Liu G, et al.: Electron Cryo-microscopy Structure of Ebola Virus Nucleoprotein Reveals a Mechanism for Nucleocapsid-like Assembly. Cell 2018, 172:966–978.e12.

82. Wan W, Kolesnikova L, Clarke M, Koehler A, Noda T, Becker S, Briggs JAG: Structure and assembly of the Ebola virus nucleocapsid. Nature 2017, 551:394–397.

83. Leung DW, Borek D, Luthra P, Binning JM, Anantpadma M, Liu G, Harvey IB, Su Z, Endlich-Frazier A, Pan J, et al.: An Intrinsically Disordered Peptide from Ebola Virus VP35 Controls Viral RNA Synthesis by Modulating Nucleoprotein-RNA Interactions. Cell Rep 2015, 11:376–389.

84. Kirchdoerfer RN, Abelson DM, Li S, Wood MR, Saphire EO: Assembly of the Ebola Virus Nucleoprotein from a Chaperoned VP35 Complex. Cell Rep 2015, 12:140–149.

85. Wang BX, Fish EN: The yin and yang of viruses and interferons. Trends Immunol 2012, 33:190–197.

86. Kawai T, Akira S: Antiviral signaling through pattern recognition receptors. J Biochem 2007, 141:137–145.

87. Bray M, Mahanty S: Ebola hemorrhagic fever and septic shock. J Infect Dis 2003, 188:1613–1617.

88. Baize S, Leroy EM, Georges AJ, -C. Georges-Courbot M, Capron M, Bedjabaga I, Lansoud-Soukate J, Mavoungou E: Inflammatory responses in Ebola virus-infected patients. Clinical & Experimental Immunology 2002, 128:163–168.

89. Bosio CM, Javad Aman M, Grogan C, Hogan R, Ruthel G, Negley D, Mohamadzadeh M, Bavari S, Schmaljohn A: Ebola and Marburg Viruses Replicate in Monocyte-Derived Dendritic Cells without Inducing the Production of Cytokines and Full Maturation. J Infect Dis 2003, 188:1630–1638.

90. Leung DW, Prins KC, Basler CF, Amarasinghe GK: Ebolavirus VP35 is a multifunctional virulence factor. Virulence 2010, 1:526–531.

91. Mühlberger E, Weik M, Volchkov VE, Klenk HD, Becker S: Comparison of the transcription and replication strategies of marburg virus and Ebola virus by using artificial replication systems. J Virol 1999, 73:2333–2342.

92. Cárdenas WB, Loo Y-M, Gale M Jr, Hartman AL, Kimberlin CR, Martínez-Sobrido L, Saphire EO, Basler CF: Ebola virus VP35 protein binds double-stranded RNA and inhibits alpha/beta interferon production induced by RIG-I signaling. J Virol 2006, 80:5168–5178.

93. Spiropoulou CF, Ranjan P, Pearce MB, Sealy TK, Albariño CG, Gangappa S, Fujita T, Rollin PE, Nichol ST, Ksiazek TG, et al.: RIG-I activation inhibits ebolavirus replication. Virology 2009, 392:11–15.

94. Dilley KA, Voorhies AA, Luthra P, Puri V, Stockwell TB, Lorenzi H, Basler CF, Shabman RS: The Ebola virus VP35 protein binds viral immunostimulatory and host RNAs identified through deep sequencing. PLoS One 2017, 12:e0178717.

95. Hartman AL, Bird BH, Towner JS, -A. Antoniadou Z, Zaki SR, Nichol ST: Inhibition of IRF-3 Activation by VP35 Is Critical for the High Level of Virulence of Ebola Virus. J Virol 2008, 82:2699–2704.

96. Lubaki NM, Ilinykh P, Pietzsch C, Tigabu B, Freiberg AN, Koup RA, Bukreyev A: The lack of maturation of Ebola virus-infected dendritic cells results from the cooperative effect of at least two viral domains. J Virol 2013, 87:7471–7485.

97. Leung DW, Prins KC, Borek DM, Farahbakhsh M, Tufariello JM, Ramanan P, Nix JC, Helgeson LA, Otwinowski Z, Honzatko RB, et al.: Structural basis for dsRNA recognition and interferon antagonism by Ebola VP35. Nat Struct Mol Biol 2010, 17:165–172.

98. Prins KC, Binning JM, Shabman RS, Leung DW, Amarasinghe GK, Basler CF: Basic Residues within the Ebolavirus VP35 Protein Are Required for Its Viral Polymerase Cofactor Function. J Virol 2010, 84:10581–10591.

99. Madara JJ, Han Z, Ruthel G, Freedman BD, Harty RN: The multifunctional Ebola virus VP40 matrix protein is a promising therapeutic target. Future Virol 2015, 10:537–546.

100. Ruigrok RW, Schoehn G, Dessen A, Forest E, Volchkov V, Dolnik O, Klenk HD, Weissenhorn W: Structural characterization and membrane binding properties of the matrix protein VP40 of Ebola virus. J Mol Biol 2000, 300:103–112.

101. Stahelin RV: Membrane binding and bending in Ebola VP40 assembly and egress. Front Microbiol 2014, 5:300.

102. Scianimanico S: Membrane association induces a conformational change in the Ebola virus matrix protein. EMBO J 2000, 19:6732–6741.

103. Adu-Gyamfi E, Johnson KA, Fraser ME, Scott JL, Soni SP, Jones KR, Digman MA, Gratton E, Tessier CR, Stahelin RV: Host Cell Plasma Membrane Phosphatidylserine Regulates the Assembly and Budding of Ebola Virus. J Virol 2015, 89:9440–9453.

104. Adu-Gyamfi E, Digman MA, Gratton E, Stahelin RV: Investigation of Ebola VP40 assembly and oligomerization in live cells using number and brightness analysis. Biophys J 2012, 102:2517–2525.

105. Panchal RG, Ruthel G, Kenny TA, Kallstrom GH, Lane D, Badie SS, Li L, Bavari S, Aman MJ: In vivo oligomerization and raft localization of Ebola virus protein VP40 during vesicular budding. Proc Natl Acad Sci U S A 2003, 100:15936–15941.

106. Adu-Gyamfi E, Soni SP, Xue Y, Digman MA, Gratton E, Stahelin RV: The Ebola Virus Matrix Protein Penetrates into the Plasma Membrane. J Biol Chem 2013, 288:5779–5789.

107. Bornholdt ZA, Noda T, Abelson DM, Halfmann P, Wood MR, Kawaoka Y, Saphire EO: Structural rearrangement of ebola virus VP40 begets multiple functions in the virus life cycle. Cell 2013, 154:763–774.

108. Timmins J, Schoehn G, Ricard-Blum S, Scianimanico S, Vernet T, Ruigrok RWH, Weissenhorn W: Ebola virus matrix protein VP40 interaction with human cellular factors Tsg101 and Nedd4. J Mol Biol 2003, 326:493–502.

109. Han Z, Sagum CA, Bedford MT, Sidhu SS, Sudol M, Harty RN: ITCH E3 Ubiquitin Ligase Interacts with Ebola Virus VP40 To Regulate Budding. J Virol 2016, 90:9163–9171.

110. Licata JM, Simpson-Holley M, Wright NT, Han Z, Paragas J, Harty RN: Overlapping motifs (PTAP and PPEY) within the Ebola virus VP40 protein function independently as late budding domains: involvement of host proteins TSG101 and VPS-4. J Virol 2003, 77:1812–1819.

111. Yamayoshi S, Noda T, Ebihara H, Goto H, Morikawa Y, Lukashevich IS, Neumann G, Feldmann H, Kawaoka Y: Ebola virus matrix protein VP40 uses the COPII transport system for its intracellular transport. Cell Host Microbe 2008, 3:168–177.

112. Takamatsu Y, Kolesnikova L, Becker S: Ebola virus proteins NP, VP35, and VP24 are essential and sufficient to mediate nucleocapsid transport. Proc Natl Acad Sci U S A 2018, 115:1075–1080.

113. Gomis-Rüth FX, Dessen A, Timmins J, Bracher A, Kolesnikowa L, Becker S, Klenk HD, Weissenhorn W: The matrix protein VP40 from Ebola virus octamerizes into pore-like structures with specific RNA binding properties. Structure 2003, 11:423–433.

114. Hoenen T, Volchkov V, Kolesnikova L, Mittler E, Timmins J, Ottmann M, Reynard O, Becker S, Weissenhorn W: VP40 Octamers Are Essential for Ebola Virus Replication. J Virol 2005, 79:1898–1905.

115. Hoenen T, Biedenkopf N, Zielecki F, Jung S, Groseth A, Feldmann H, Becker S: Oligomerization of Ebola virus VP40 is essential for particle morphogenesis and regulation of viral transcription. J Virol 2010, 84:7053–7063.

116. Mehedi M, Falzarano D, Seebach J, Hu X, Carpenter MS, Schnittler H-J, Feldmann H: A new Ebola virus nonstructural glycoprotein expressed through RNA editing. J Virol 2011, 85:5406–5414.

117. Volchkov VE, Becker S, Volchkova VA, Ternovoj VA, Kotov AN, Netesov SV, Klenk HD: GP mRNA of Ebola virus is edited by the Ebola virus polymerase and by T7 and vaccinia virus polymerases. Virology 1995, 214:421–430.

118. Mehedi M, Hoenen T, Robertson S, Ricklefs S, Dolan MA, Taylor T, Falzarano D, Ebihara H, Porcella SF, Feldmann H: Ebola virus RNA editing depends on the primary editing site sequence and an upstream secondary structure. PLoS Pathog 2013, 9:e1003677.

119. Brauburger K, Deflubé LR, Mühlberger E: FILOVIRUS TRANSCRIPTION AND REPLICATION. In Biology and Pathogenesis of Rhabdo- and Filoviruses. . 2014:515–555.

120. Volchkov VE, Feldmann H, Volchkova VA, Klenk HD: Processing of the Ebola virus glycoprotein by the proprotein convertase furin. Proc Natl Acad Sci U S A 1998, 95:5762–5767.

121. Mohan GS, Li W, Ye L, Compans RW, Yang C: Antigenic subversion: a novel mechanism of host immune evasion by Ebola virus. PLoS Pathog 2012, 8:e1003065.

122. Bradley JH, Harrison A, Corey A, Gentry N, Gregg RK: Ebola virus secreted glycoprotein decreases the anti-viral immunity of macrophages in early inflammatory responses. Cell Immunol 2018, 324:24–32.

123. de La Vega M-A, Wong G, Kobinger GP, Qiu X: The multiple roles of sGP in Ebola pathogenesis. Viral Immunol 2015, 28:3–9.

124. Volchkov VE, Volchkova VA, Slenczka W, Klenk H-D, Feldmann H: Release of Viral Glycoproteins during Ebola Virus Infection. Virology 1998, 245:110–119.

125. Volchkova VA, Dolnik O, Martinez MJ, Reynard O, Volchkov VE: Genomic RNA editing and its impact on Ebola virus adaptation during serial passages in cell culture and infection of guinea pigs. J Infect Dis 2011, 204 Suppl 3:S941–6.

126. Volchkova VA, Dolnik O, Martinez MJ, Reynard O, Volchkov VE: RNA Editing of the GP Gene of Ebola Virus is an Important Pathogenicity Factor. J Infect Dis 2015, 212 Suppl 2:S226–33.

127. Gire SK, Goba A, Andersen KG, Sealfon RSG, Park DJ, Kanneh L, Jalloh S, Momoh M, Fullah M, Dudas G, et al.: Genomic surveillance elucidates Ebola virus origin and transmission during the 2014 outbreak. Science 2014, 345:1369–1372.

128. Volchkova VA, Klenk HD, Volchkov VE: Delta-peptide is the carboxy-terminal cleavage fragment of the nonstructural small glycoprotein sGP of Ebola virus. Virology 1999, 265:164–171.

129. Radoshitzky SR, Warfield KL, Chi X, Dong L, Kota K, Bradfute SB, Gearhart JD, Retterer C, Kranzusch PJ, Misasi JN, et al.: Ebolavirus delta-peptide immunoadhesins inhibit marburgvirus and ebolavirus cell entry. J Virol 2011, 85:8502–8513.

130. He J, Melnik LI, Komin A, Wiedman G, Fuselier T, Morris CF, Starr CG, Searson PC, Gallaher WR, Hristova K, et al.: Ebola Virus Delta Peptide is a Viroporin. J Virol 2017, doi:10.1128/JVI.00438-17.

131. Escudero-Pérez B, Volchkova VA, Dolnik O, Lawrence P, Volchkov VE: Shed GP of Ebola Virus Triggers Immune Activation and Increased Vascular Permeability. PLoS Pathog 2014, 10:e1004509.

132. Lee J, Nyenhuis DA, Nelson EA, Cafiso DS, White JM, Tamm LK: Structure of the Ebola virus envelope protein MPER/TM domain and its interaction with the fusion loop explains their fusion activity. 2017, doi:10.2210/pdb5t42/pdb.

133. Jeffers SA, Sanders DA, Sanchez A: Covalent Modifications of the Ebola Virus Glycoprotein. J Virol 2002, 76:12463–12472.

134. Yang ZY, Duckers HJ, Sullivan NJ, Sanchez A, Nabel EG, Nabel GJ: Identification of the Ebola virus glycoprotein as the main viral determinant of vascular cell cytotoxicity and injury. Nat Med 2000, 6:886–889.

135. Takada A, Watanabe S, Ito H, Okazaki K, Kida H, Kawaoka Y: Downregulation of beta1 integrins by Ebola virus glycoprotein: implication for virus entry. Virology 2000, 278:20–26.

136. Simmons G, Wool-Lewis RJ, Baribaud F, Netter RC, Bates P: Ebola virus glycoproteins induce global surface protein down-modulation and loss of cell adherence. J Virol 2002, 76:2518–2528.

137. Younan P, Iampietro M, Nishida A, Ramanathan P, Santos RI, Dutta M, Lubaki NM, Koup RA, Katze MG, Bukreyev A: Ebola Virus Binding to Tim-1 on T Lymphocytes Induces a Cytokine Storm. MBio 2017, 8.

138. Saphire EO: An update on the use of antibodies against the filoviruses. Immunotherapy 2013, 5:1221–1233.

139. Reynard O, Borowiak M, Volchkova VA, Delpeut S, Mateo M, Volchkov VE: Ebolavirus glycoprotein GP masks both its own epitopes and the presence of cellular surface proteins. J Virol 2009, 83:9596–9601.

140. Francica JR, Varela-Rohena A, Medvec A, Plesa G, Riley JL, Bates P: Steric shielding of surface epitopes and impaired immune recognition induced by the ebola virus glycoprotein. PLoS Pathog 2010, 6:e1001098.

141. Lennemann NJ, Rhein BA, Ndungo E, Chandran K, Qiu X, Maury W: Comprehensive functional analysis of N-linked glycans on Ebola virus GP1. MBio 2014, 5:e00862–13.

142. Favier A-L, Gout E, Reynard O, Ferraris O, Kleman J-P, Volchkov V, Peyrefitte C, Thielens NM: Enhancement of Ebola Virus Infection via Ficolin-1 Interaction with the Mucin Domain of GP Glycoprotein. J Virol 2016, 90:5256–5269.

143. Moller-Tank S, Maury W: Ebola Virus Entry: A Curious and Complex Series of Events. PLoS Pathog 2015, 11:e1004731.

144. Wang B, Wang Y, Frabutt DA, Zhang X, Yao X, Hu D, Zhang Z, Liu C, Zheng S, Xiang S-H, et al.: Mechanistic understanding of -glycosylation in Ebola virus glycoprotein maturation and function. J Biol Chem 2017, 292:5860–5870.

145. Nyakatura EK, Frei JC, Lai JR: Chemical and Structural Aspects of Ebola Virus Entry Inhibitors. ACS Infect Dis 2015, 1:42–52.

146. Saeed MF, Kolokoltsov AA, Albrecht T, Davey RA: Cellular Entry of Ebola Virus Involves Uptake by a Macropinocytosis-Like Mechanism and Subsequent Trafficking through Early and Late Endosomes. PLoS Pathog 2010, 6:e1001110.

147. Schornberg K, Matsuyama S, Kabsch K, Delos S, Bouton A, White J: Role of Endosomal Cathepsins in Entry Mediated by the Ebola Virus Glycoprotein. J Virol 2006, 80:4174–4178.

148. Chandran K, Sullivan NJ, Felbor U, Whelan SP, Cunningham JM: Endosomal proteolysis of the Ebola virus glycoprotein is necessary for infection. Science 2005, 308:1643–1645.

149. Wang H, Shi Y, Song J, Qi J, Lu G, Yan J, Gao GF: Ebola Viral Glycoprotein Bound to Its Endosomal Receptor Niemann-Pick C1. Cell 2016, 164:258–268.

150. Dolnik O, Volchkova V, Garten W, Carbonnelle C, Becker S, Kahnt J, Ströher U, Klenk H-D, Volchkov V: Ectodomain shedding of the glycoprotein GP of Ebola virus. EMBO J 2004, 23:2175–2184.

151. Gooz M: ADAM-17: the enzyme that does it all. Crit Rev Biochem Mol Biol 2010, 45:146–169.

152. Black RA, Rauch CT, Kozlosky CJ, Peschon JJ, Slack JL, Wolfson MF, Castner BJ, Stocking KL, Reddy P, Srinivasan S, et al.: A metalloproteinase disintegrin that releases tumour-necrosis factor-alpha from cells. Nature 1997, 385:729–733.

153. Miller MA, Sullivan RJ, Lauffenburger DA: Molecular Pathways: Receptor Ectodomain Shedding in Treatment, Resistance, and Monitoring of Cancer. Clin Cancer Res 2017, 23:623–629.

154. Chemaly M, McGilligan V, Gibson M, Clauss M, Watterson S, Alexander HD, Bjourson AJ, Peace A: Role of tumour necrosis factor alpha converting enzyme (TACE/ADAM17) and

associated proteins in coronary artery disease and cardiac events. Arch Cardiovasc Dis 2017, 110:700–711.

155. Tellier E, Canault M, Rebsomen L, Bonardo B, Juhan-Vague I, Nalbone G, Peiretti F: The shedding activity of ADAM17 is sequestered in lipid rafts. Exp Cell Res 2006, 312:3969–3980.

156. Sommer A, Kordowski F, Büch J, Maretzky T, Evers A, Andrä J, Düsterhöft S, Michalek M, Lorenzen I, Somasundaram P, et al.: Phosphatidylserine exposure is required for ADAM17 sheddase function. Nat Commun 2016, 7:11523.

157. Modrof J: Phosphorylation of VP30 Impairs Ebola Virus Transcription. J Biol Chem 2002, 277:33099–33104.

158. Biedenkopf N, Lier C, Becker S: Dynamic Phosphorylation of VP30 Is Essential for Ebola Virus Life Cycle. J Virol 2016, 90:4914–4925.

159. Lier C, Becker S, Biedenkopf N: Dynamic phosphorylation of Ebola virus VP30 in NP-induced inclusion bodies. Virology 2017, 512:39–47.

160. Biedenkopf N, Schlereth J, Grünweller A, Becker S, Hartmann RK: RNA Binding of Ebola Virus VP30 Is Essential for Activating Viral Transcription. J Virol 2016, 90:7481–7496.

161. Martinez MJ, Biedenkopf N, Volchkova V, Hartlieb B, Alazard-Dany N, Reynard O, Becker S, Volchkov V: Role of Ebola Virus VP30 in Transcription Reinitiation. J Virol 2008, 82:12569–12573.

162. Kirchdoerfer RN, Moyer CL, Abelson DM, Saphire EO: The Ebola Virus VP30-NP Interaction Is a Regulator of Viral RNA Synthesis. PLoS Pathog 2016, 12:e1005937.

163. Xu W, Luthra P, Wu C, Batra J, Leung DW, Basler CF, Amarasinghe GK: Ebola virus VP30 and nucleoprotein interactions modulate viral RNA synthesis. Nat Commun 2017, 8:15576.

164. Han Z, Boshra H, Sunyer JO, Zwiers SH, Paragas J, Harty RN: Biochemical and functional characterization of the Ebola virus VP24 protein: implications for a role in virus assembly and budding. J Virol 2003, 77:1793–1800.

165. Licata JM, Johnson RF, Han Z, Harty RN: Contribution of ebola virus glycoprotein, nucleoprotein, and VP24 to budding of VP40 virus-like particles. J Virol 2004, 78:7344–7351.

166. Mateo M, Carbonnelle C, Martinez MJ, Reynard O, Page A, Volchkova VA, Volchkov VE: Knockdown of Ebola virus VP24 impairs viral nucleocapsid assembly and prevents virus replication. J Infect Dis 2011, 204 Suppl 3:S892–6.

167. Noda T, Halfmann P, Sagara H, Kawaoka Y: Regions in Ebola virus VP24 that are important for nucleocapsid formation. J Infect Dis 2007, 196 Suppl 2:S247–50.

168. Banadyga L, Hoenen T, Ambroggio X, Dunham E, Groseth A, Ebihara H: Ebola virus VP24 interacts with NP to facilitate nucleocapsid assembly and genome packaging. Sci Rep 2017, 7:7698.

169. Mateo M, Reid SP, Leung LW, Basler CF, Volchkov VE: Ebolavirus VP24 Binding to Karyopherins Is Required for Inhibition of Interferon Signaling. J Virol 2009, 84:1169–1175.

170. Schwarz TM, Edwards MR, Diederichs A, Alinger JB, Leung DW, Amarasinghe GK, Basler CF: VP24-Karyopherin Alpha Binding Affinities Differ between Ebolavirus Species, Influencing Interferon Inhibition and VP24 Stability. J Virol 2017, 91.

171. Mateo M, Carbonnelle C, Reynard O, Kolesnikova L, Nemirov K, Page A, Volchkova VA, Volchkov VE: VP24 is a molecular determinant of Ebola virus virulence in guinea pigs. J Infect Dis 2011, 204 Suppl 3:S1011–20.

172. Trunschke M, Conrad D, Enterlein S, Olejnik J, Brauburger K, Mühlberger E: The L-VP35 and L-L interaction domains reside in the amino terminus of the Ebola virus L protein and are potential targets for antivirals. Virology 2013, 441:135–145.

173. Rimmelzwaan GF, Berkhoff EGM, Nieuwkoop NJ, Smith DJ, Fouchier RAM, Osterhaus ADME: Full restoration of viral fitness by multiple compensatory co-mutations in the nucleoprotein of influenza A virus cytotoxic T-lymphocyte escape mutants. J Gen Virol 2005, 86:1801–1805.

174. Deng L, Liu M, Hua S, Peng Y, Wu A, Xiao-Feng Qin F, Cheng G, Jiang T: Network of co-mutations in Ebola virus genome predicts the disease lethality. Cell Res 2015, 25:753–756.

175. Dietzel E, Schudt G, Krähling V, Matrosovich M, Becker S: Functional Characterization of Adaptive Mutations during the West African Ebola Virus Outbreak. J Virol 2017, 91.

176. Albariño CG, Wiggleton Guerrero L, Jenks HM, Chakrabarti AK, Ksiazek TG, Rollin PE, Nichol ST: Insights into Reston virus spillovers and adaption from virus whole genome sequences. PLoS One 2017, 12:e0178224.

177. Feldmann H, Geisbert TW: Ebola haemorrhagic fever. Lancet 2011, 377:849–862.

178. Bray M, Geisbert TW: Ebola virus: The role of macrophages and dendritic cells in the pathogenesis of Ebola hemorrhagic fever. Int J Biochem Cell Biol 2005, 37:1560–1566.

179. Baseler L, Chertow DS, Johnson KM, Feldmann H, Morens DM: The Pathogenesis of Ebola Virus Disease. Annu Rev Pathol 2017, 12:387–418.

180. Akerlund E, Prescott J, Tampellini L: Shedding of Ebola Virus in an Asymptomatic Pregnant Woman. N Engl J Med 2015, 372:2467–2469.

181. Chertow DS, Kleine C, Edwards JK, Scaini R, Giuliani R, Sprecher A: Ebola virus disease in West Africa--clinical manifestations and management. N Engl J Med 2014, 371:2054–2057.

182. Rollin PE, Bausch DG, Sanchez A: Blood chemistry measurements and D-Dimer levels associated with fatal and nonfatal outcomes in humans infected with Sudan Ebola virus. J Infect Dis 2007, 196 Suppl 2:S364–71.

183. Baize S, Leroy EM, Georges-Courbot MC, Capron M, Lansoud-Soukate J, Debré P, Fisher-Hoch SP, McCormick JB, Georges AJ: Defective humoral responses and extensive intravascular apoptosis are associated with fatal outcome in Ebola virus-infected patients. Nat Med 1999, 5:423–426.

184. Lanini S, Portella G, Vairo F, Kobinger GP, Pesenti A, Langer M, Kabia S, Brogiato G, Amone J, Castilletti C, et al.: Blood kinetics of Ebola virus in survivors and nonsurvivors. J Clin Invest 2015, 125:4692–4698.

185. de La Vega M-A, Caleo G, Audet J, Qiu X, Kozak RA, Brooks JI, Kern S, Wolz A, Sprecher A, Greig J, et al.: Ebola viral load at diagnosis associates with patient outcome and outbreak evolution. J Clin Invest 2015, 125:4421–4428.

186. Mattia JG, Vandy MJ, Chang JC, Platt DE, Dierberg K, Bausch DG, Brooks T, Conteh S, Crozier I, Fowler RA, et al.: Early clinical sequelae of Ebola virus disease in Sierra Leone: a cross-sectional study. Lancet Infect Dis 2016, 16:331–338.

187. Steptoe PJ, Scott JT, Harding SP, Beare NAV, Semple MG, Vandy MJ, Sahr F: Ocular Complications in Survivors of the Ebola Outbreak in Guinea. Am J Ophthalmol 2017, 181:180.

188. Karafillakis E, Jalloh MF, Nuriddin A, Larson HJ, Whitworth J, Lees S, Hageman KM, Sengeh P, Jalloh MB, Bunnell R, et al.: “Once there is life, there is hope” Ebola survivors’ experiences, behaviours and attitudes in Sierra Leone, 2015. BMJ Global Health 2016, 1:e000108.

189. Barton GM: A calculated response: control of inflammation by the innate immune system. J Clin Invest 2008, 118:413–420.

190. Okumura A, Pitha PM, Yoshimura A, Harty RN: Interaction between Ebola virus glycoprotein and host toll-like receptor 4 leads to induction of proinflammatory cytokines and SOCS1. J Virol 2010, 84:27–33.

191. Olejnik J, Forero A, Deflubé LR, Hume AJ, Manhart WA, Nishida A, Marzi A, Katze MG, Ebihara H, Rasmussen AL, et al.: Ebolaviruses Associated with Differential Pathogenicity Induce Distinct Host Responses in Human Macrophages. J Virol 2017, 91.

192. Wahl-Jensen V, Kurz SK, Hazelton PR, Schnittler H-J, Ströher U, Burton DR, Feldmann H: Role of Ebola virus secreted glycoproteins and virus-like particles in activation of human macrophages. J Virol 2005, 79:2413–2419.

193. McElroy AK, Shrivastava-Ranjan P, Harmon JR, Martines R, Silva-Flannery L, Flietstra TD, Kraft CS, Mehta AK, Marshall Lyon G, Varkey J, et al.: Activated macrophages as pathogenesis factors in Ebola virus disease in humans. The Journal of Immunology 2018, 200:126.12–126.12.

194. Ebihara H, Rockx B, Marzi A, Feldmann F, Haddock E, Brining D, LaCasse RA, Gardner D, Feldmann H: Host response dynamics following lethal infection of rhesus macaques with Zaire ebolavirus. J Infect Dis 2011, 204 Suppl 3:S991–9.

195. Bixler SL, Goff AJ: The Role of Cytokines and Chemokines in Filovirus Infection. Viruses 2015, 7:5489–5507.

196. Wauquier N, Becquart P, Padilla C, Baize S, Leroy EM: Human fatal zaire ebola virus infection is associated with an aberrant innate immunity and with massive lymphocyte apoptosis. PLoS Negl Trop Dis 2010, 4.

197. Ruibal P, Oestereich L, Lüdtke A, Becker-Ziaja B, Wozniak DM, Kerber R, Korva M, Cabeza-Cabrerizo M, Bore JA, Koundouno FR, et al.: Unique human immune signature of Ebola virus disease in Guinea. Nature 2016, 533:100–104.

198. Wong G, Kobinger GP, Qiu X: Characterization of host immune responses in Ebola virus infections. Expert Rev Clin Immunol 2014, 10:781–790.

199. Villinger F, Rollin PE, Brar SS, Chikkala NF, Winter J, Sundstrom JB, Zaki SR, Swanepoel R, Ansari AA, Peters CJ: Markedly elevated levels of interferon (IFN)-gamma, IFN-alpha, interleukin (IL)-2, IL-10, and tumor necrosis factor-alpha associated with fatal Ebola virus infection. J Infect Dis 1999, 179 Suppl 1:S188–91.

200. Hutchinson KL, Rollin PE: Cytokine and chemokine expression in humans infected with Sudan Ebola virus. J Infect Dis 2007, 196 Suppl 2:S357–63.

201. Martinez O, Johnson JC, Honko A, Yen B, Shabman RS, Hensley LE, Olinger GG, Basler CF: Ebola virus exploits a monocyte differentiation program to promote its entry. J Virol 2013, 87:3801–3814.

202. Cimini E, Viola D, Cabeza-Cabrerizo M, Romanelli A, Tumino N, Sacchi A, Bordoni V, Casetti R, Turchi F, Martini F, et al.: Different features of Vδ2 T and NK cells in fatal and non-fatal human Ebola infections. PLoS Negl Trop Dis 2017, 11:e0005645.

203. Geisbert TW, Hensley LE, Larsen T, Young HA, Reed DS, Geisbert JB, Scott DP, Kagan E, Jahrling PB, Davis KJ: Pathogenesis of Ebola hemorrhagic fever in cynomolgus macaques: evidence that dendritic cells are early and sustained targets of infection. Am J Pathol 2003, 163:2347–2370.

204. Soghoian DZ, Streeck H: Cytolytic CD4 T cells in viral immunity. Expert Rev Vaccines 2010, 9:1453–1463.

205. Sant AJ, McMichael A: Revealing the role of CD4(+) T cells in viral immunity. J Exp Med 2012, 209:1391–1395.

206. Marzi A, Engelmann F, Feldmann F, Haberthur K, Shupert WL, Brining D, Scott DP, Geisbert TW, Kawaoka Y, Katze MG, et al.: Antibodies are necessary for rVSV/ZEBOV-GP-mediated protection against lethal Ebola virus challenge in nonhuman primates. Proc Natl Acad Sci U S A 2013, 110:1893–1898.

207. Nu Zhang MJB: CD8+ T Cells: Foot Soldiers of the Immune System. Immunity 2011, 35:161.

208. Iampietro M, Younan P, Nishida A, Dutta M, Lubaki NM, Santos RI, Koup RA, Katze MG, Bukreyev A: Ebola virus glycoprotein directly triggers T lymphocyte death despite of the lack of infection. PLoS Pathog 2017, 13:e1006397.

209. Gupta M, Spiropoulou C, Rollin PE: Ebola virus infection of human PBMCs causes massive death of macrophages, CD4 and CD8 T cell sub-populations in vitro. Virology 2007, 364:45–54.

210. Sobarzo A, Ochayon DE, Lutwama JJ, Balinandi S, Guttman O, Marks RS, Kuehne AI, Dye JM, Yavelsky V, Lewis EC, et al.: Persistent immune responses after Ebola virus infection. N Engl J Med 2013, 369:492–493.

211. Agrati C, Castilletti C, Casetti R, Sacchi A, Falasca L, Turchi F, Tumino N, Bordoni V, Cimini E, Viola D, et al.: Longitudinal characterization of dysfunctional T cell-activation during human acute Ebola infection. Cell Death Dis 2016, 7:e2164–e2164.

212. Sakabe S, Sullivan BM, Hartnett JN, Robles-Sikisaka R, Gangavarapu K, Cubitt B, Ware BC, Kotliar D, Branco LM, Goba A, et al.: Analysis of CD8 T cell response during the 2013-2016 Ebola epidemic in West Africa. Proc Natl Acad Sci U S A 2018, 115:E7578–E7586.

213. Ksiazek TG, Rollin PE, Williams AJ, Bressler DS, Martin ML, Swanepoel R, Burt FJ, Leman PA, Khan AS, Rowe AK, et al.: Clinical Virology of Ebola Hemorrhagic Fever (EHF): Virus, Virus Antigen, and IgG and IgM Antibody Findings among EHF Patients in Kikwit, Democratic Republic of the Congo, 1995. J Infect Dis 1999, 179:S177–S187.

214. McElroy AK, Akondy RS, Davis CW, Ellebedy AH, Mehta AK, Kraft CS, Lyon GM, Ribner BS, Varkey J, Sidney J, et al.: Human Ebola virus infection results in substantial immune activation. Proc Natl Acad Sci U S A 2015, 112:4719–4724.

215. Wong G, Richardson JS, Pillet S, Patel A, Qiu X, Alimonti J, Hogan J, Zhang Y, Takada A, Feldmann H, et al.: Immune parameters correlate with protection against ebola virus infection in rodents and nonhuman primates. Sci Transl Med 2012, 4:158ra146.

216. McElroy AK, Erickson BR, Flietstra TD, Rollin PE, Nichol ST, Towner JS, Spiropoulou CF: Ebola hemorrhagic Fever: novel biomarker correlates of clinical outcome. J Infect Dis 2014, 210:558–566.

217. Levi M, van der Poll T, Büller HR: Bidirectional relation between inflammation and coagulation. Circulation 2004, 109:2698–2704.

218. Esmon CT: Interactions between the innate immune and blood coagulation systems. Trends Immunol 2004, 25:536–542.

219. Foley JH, Conway EM: Cross Talk Pathways Between Coagulation and Inflammation. Circ Res 2016, 118:1392–1408.

220. Geisbert TW, Young HA, Jahrling PB, Davis KJ, Kagan E, Hensley LE: Mechanisms underlying coagulation abnormalities in ebola hemorrhagic fever: overexpression of tissue factor in primate monocytes/macrophages is a key event. J Infect Dis 2003, 188:1618–1629.

221. Marzi A, Chadinah S, Haddock E, Feldmann F, Arndt N, Martellaro C, Scott DP, Hanley PW, Nyenswah TG, Sow S, et al.: Recently Identified Mutations in the Ebola Virus-Makona Genome Do Not Alter Pathogenicity in Animal Models. Cell Rep 2018, 23:1806–1816.

222. Chu AJ: Tissue Factor, Blood Coagulation, and Beyond: An Overview. Int J Inflam 2011, 2011:1–30.

223. Geisbert TW, Hensley LE, Jahrling PB, Larsen T, Geisbert JB, Paragas J, Young HA, Fredeking TM, Rote WE, Vlasuk GP: Treatment of Ebola virus infection with a recombinant inhibitor of factor VIIa/tissue factor: a study in rhesus monkeys. Lancet 2003, 362:1953–1958.

224. Wu Y: Contact pathway of coagulation and inflammation. Thromb J 2015, 13.

225. Nanbo A, Maruyama J, Imai M, Ujie M, Fujioka Y, Nishide S, Takada A, Ohba Y, Kawaoka Y: Ebola virus requires a host scramblase for externalization of phosphatidylserine on the surface of viral particles. PLoS Pathog 2018, 14:e1006848.

226. Cross RW, Fenton KA, Geisbert JB, Ebihara H, Mire CE, Geisbert TW: Comparison of the Pathogenesis of the Angola and Ravn Strains of Marburg Virus in the Outbred Guinea Pig Model. J Infect Dis 2015, 212 Suppl 2:S258–70.

227. Fujita T: Evolution of the lectin-complement pathway and its role in innate immunity. Nat Rev Immunol 2002, 2:346–353.

228. Degn SE, Jensenius JC, Bjerre M: The lectin pathway and its implications in coagulation, infections and auto-immunity. Curr Opin Organ Transplant 2011, 16:21–27.

229. Jenny L, Dobó J, Gál P, Schroeder V: MASP-1 of the complement system promotes clotting via prothrombin activation. Mol Immunol 2015, 65:398–405.

230. Takahashi K, Chang W-C, Takahashi M, Pavlov V, Ishida Y, La Bonte L, Shi L, Fujita T, Stahl GL, Van Cott EM: Mannose-binding lectin and its associated proteases (MASPs) mediate coagulation and its deficiency is a risk factor in developing complications from infection, including disseminated intravascular coagulation. Immunobiology 2011, 216:96–102.

231. Hess K, Ajjan R, Phoenix F, Dobó J, Gál P, Schroeder V: Effects of MASP-1 of the complement system on activation of coagulation factors and plasma clot formation. PLoS One 2012, 7:e35690.

232. Kozarcanin H, Lood C, Munthe-Fog L, Sandholm K, Hamad OA, Bengtsson AA, Skjoedt M-O, Huber-Lang M, Garred P, Ekdahl KN, et al.: The lectin complement pathway serine proteases (MASPs) represent a possible crossroad between the coagulation and complement systems in thromboinflammation. J Thromb Haemost 2016, 14:531–545.

233. Ji X, Olinger GG, Aris S, Chen Y, Gewurz H, Spear GT: Mannose-binding lectin binds to Ebola and Marburg envelope glycoproteins, resulting in blocking of virus interaction with DC-SIGN and complement-mediated virus neutralization. J Gen Virol 2005, 86:2535–2542.

234. Michelow IC, Lear C, Scully C, Prugar LI, Longley CB, Yantosca LM, Ji X, Karpel M, Brudner M, Takahashi K, et al.: High-dose mannose-binding lectin therapy for Ebola virus infection. J Infect Dis 2011, 203:175–179.

235. Takada A, Feldmann H, Ksiazek TG, Kawaoka Y: Antibody-dependent enhancement of Ebola virus infection. J Virol 2003, 77:7539–7544.

236. Kuzmina NA, Younan P, Gilchuk P, Santos RI, Flyak AI, Ilinykh PA, Huang K, Lubaki NM, Ramanathan P, Crowe JE Jr, et al.: Antibody-Dependent Enhancement of Ebola Virus Infection by Human Antibodies Isolated from Survivors. Cell Rep 2018, 24:1802–1815.e5.

237. Keshwara R, Johnson RF, Schnell MJ: Toward an Effective Ebola Virus Vaccine. Annu Rev Med 2017, 68:371–386.

238. Pavot V: Ebola virus vaccines: Where do we stand? Clin Immunol 2016, 173:44–49.

239. Lupton HW, Lambert RD, Bumgardner DL, Moe JB, Eddy GA: Inactivated vaccine for Ebola virus efficacious in guineapig model. Lancet 1980, 2:1294–1295.

240. Geisbert TW, Pushko P, Anderson K, Smith J, Davis KJ, Jahrling PB: Evaluation in nonhuman primates of vaccines against Ebola virus. Emerg Infect Dis 2002, 8:503–507.

241. Rao M, Matyas GR, Grieder F, Anderson K, Jahrling PB, Alving CR: Cytotoxic T lymphocytes to Ebola Zaire virus are induced in mice by immunization with liposomes containing lipid A. Vaccine 1999, 17:2991–2998.

242. Wu X-X, Yao H-P, Wu N-P, Gao H-N, Wu H-B, Jin C-Z, Lu X-Y, Xie T-S, Li L-J: Ebolavirus Vaccines: Progress in the Fight Against Ebola Virus Disease. Cell Physiol Biochem 2015, 37:1641–1658.

243. Kibuuka H, Berkowitz NM, Millard M, Enama ME, Tindikahwa A, Sekiziyivu AB, Costner P, Sitar S, Glover D, Hu Z, et al.: Safety and immunogenicity of Ebola virus and Marburg virus glycoprotein DNA vaccines assessed separately and concomitantly in healthy Ugandan adults: a phase 1b, randomised, double-blind, placebo-controlled clinical trial. Lancet 2015, 385:1545–1554.

244. Warfield KL, Aman MJ: Advances in virus-like particle vaccines for filoviruses. J Infect Dis 2011, 204 Suppl 3:S1053–9.

245. Warfield KL, Bosio CM, Welcher BC, Deal EM, Mohamadzadeh M, Schmaljohn A, Aman MJ, Bavari S: Ebola virus-like particles protect from lethal Ebola virus infection. Proc Natl Acad Sci U S A 2003, 100:15889–15894.

246. Domi A, Feldmann F, Basu R, McCurley N, Shifflett K, Emanuel J, Hellerstein MS, Guirakhoo F, Orlandi C, Flinko R, et al.: A Single Dose of Modified Vaccinia Ankara expressing Ebola Virus Like Particles Protects Nonhuman Primates from Lethal Ebola Virus Challenge. Sci Rep 2018, 8:864.

247. Pushko P, Bray M, Ludwig GV, Parker M, Schmaljohn A, Sanchez A, Jahrling PB, Smith JF: Recombinant RNA replicons derived from attenuated Venezuelan equine encephalitis virus protect guinea pigs and mice from Ebola hemorrhagic fever virus. Vaccine 2000, 19:142–153.

248. Reynard O, Mokhonov V, Mokhonova E, Leung J, Page A, Mateo M, Pyankova O, Georges-Courbot MC, Raoul H, Khromykh AA, et al.: Kunjin virus replicon-based vaccines expressing Ebola virus glycoprotein GP protect the guinea pig against lethal Ebola virus infection. J Infect Dis 2011, 204 Suppl 3:S1060–5.

249. Halfmann P, Ebihara H, Marzi A, Hatta Y, Watanabe S, Suresh M, Neumann G, Feldmann H, Kawaoka Y: Replication-deficient ebolavirus as a vaccine candidate. J Virol 2009, 83:3810–3815.

250. Marzi A, Halfmann P, Hill-Batorski L, Feldmann F, Shupert WL, Neumann G, Feldmann H, Kawaoka Y: Vaccines. An Ebola whole-virus vaccine is protective in nonhuman primates. Science 2015, 348:439–442.

251. Regules JA, Beigel JH, Paolino KM, Voell J, Castellano AR, Hu Z, Muñoz P, Moon JE, Ruck RC, Bennett JW, et al.: A Recombinant Vesicular Stomatitis Virus Ebola Vaccine. N Engl J Med 2017, 376:330–341.

252. Agnandji ST, Huttner A, Zinser ME, Njuguna P, Dahlke C, Fernandes JF, Yerly S, Dayer J-A, Kraehling V, Kasonta R, et al.: Phase 1 Trials of rVSV Ebola Vaccine in Africa and Europe. N Engl J Med 2016, 374:1647–1660.

253. Garbutt M, Liebscher R, Wahl-Jensen V, Jones S, Möller P, Wagner R, Volchkov V, Klenk H-D, Feldmann H, Ströher U: Properties of replication-competent vesicular stomatitis virus vectors expressing glycoproteins of filoviruses and arenaviruses. J Virol 2004, 78:5458–5465.

254. Sharma R: Ebola Vaccine: How Far are we? J Clin Diagn Res 2017, doi:10.7860/jcdr/2017/22184.9863.

255. Rojek A, Horby P, Dunning J: Insights from clinical research completed during the west Africa Ebola virus disease epidemic. Lancet Infect Dis 2017, 17:e280–e292.

256. Bukreyev AA, Dinapoli JM, Yang L, Murphy BR, Collins PL: Mucosal parainfluenza virus-vectored vaccine against Ebola virus replicates in the respiratory tract of vector-immune monkeys and is immunogenic. Virology 2010, 399:290–298.

257. Sullivan NJ, Geisbert TW, Geisbert JB, Shedlock DJ, Xu L, Lamoreaux L, Custers JHHV, Popernack PM, Yang Z-Y, Pau MG, et al.: Immune protection of nonhuman primates against Ebola virus with single low-dose adenovirus vectors encoding modified GPs. PLoS Med 2006, 3:e177.

258. Geisbert TW, Bailey M, Hensley L, Asiedu C, Geisbert J, Stanley D, Honko A, Johnson J, Mulangu S, Pau MG, et al.: Recombinant adenovirus serotype 26 (Ad26) and Ad35 vaccine vectors bypass immunity to Ad5 and protect nonhuman primates against ebolavirus challenge. J Virol 2011, 85:4222–4233.

259. Wong G, Mendoza EJ, Plummer FA, Gao GF, Kobinger GP, Qiu X: From bench to almost bedside: the long road to a licensed Ebola virus vaccine. Expert Opin Biol Ther 2017, 18:159–173.

260. Ewer K, Rampling T, Venkatraman N, Bowyer G, Wright D, Lambe T, Imoukhuede EB, Payne R, Fehling SK, Strecker T, et al.: A Monovalent Chimpanzee Adenovirus Ebola Vaccine Boosted with MVA. N Engl J Med 2016, 374:1635–1646.

261. Lichty BD, Power AT, Stojdl DF, Bell JC: Vesicular stomatitis virus: re-inventing the bullet. Trends Mol Med 2004, 10:210–216.

262. Finkelshtein D, Werman A, Novick D, Barak S, Rubinstein M: LDL receptor and its family members serve as the cellular receptors for vesicular stomatitis virus. Proc Natl Acad Sci U S A 2013, 110:7306–7311.

263. Ge P, Tsao J, Schein S, Green TJ, Luo M, Zhou ZH: Cryo-EM model of the bullet-shaped vesicular stomatitis virus. Science 2010, 327:689–693.

264. Whelan SP, Ball LA, Barr JN, Wertz GT: Efficient recovery of infectious vesicular stomatitis virus entirely from cDNA clones. Proc Natl Acad Sci U S A 1995, 92:8388–8392.

265. Jones SM, Feldmann H, Ströher U, Geisbert JB, Fernando L, Grolla A, Klenk H-D, Sullivan NJ, Volchkov VE, Fritz EA, et al.: Live attenuated recombinant vaccine protects nonhuman primates against Ebola and Marburg viruses. Nat Med 2005, 11:786–790.

266. Geisbert TW, Daddario-Dicaprio KM, Lewis MG, Geisbert JB, Grolla A, Leung A, Paragas J, Matthias L, Smith MA, Jones SM, et al.: Vesicular stomatitis virus-based ebola vaccine is well-tolerated and protects immunocompromised nonhuman primates. PLoS Pathog 2008, 4:e1000225.

267. Marzi A, Ebihara H, Callison J, Groseth A, Williams KJ, Geisbert TW, Feldmann H: Vesicular Stomatitis Virus–Based Ebola Vaccines With Improved Cross-Protective Efficacy. J Infect Dis 2011, 204:S1066–S1074.

268. GHO | By category | Prevalence of HIV among adults aged 15 to 49 - Estimates by country. [date unknown],

269. Feldmann H, Jones SM, Daddario-DiCaprio KM, Geisbert JB, Ströher U, Grolla A, Bray M, Fritz EA, Fernando L, Feldmann F, et al.: Effective post-exposure treatment of Ebola infection. PLoS Pathog 2007, 3:e2.

270. Günther S, Feldmann H, Geisbert TW, Hensley LE, Rollin PE, Nichol ST, Ströher U, Artsob H, Peters CJ, Ksiazek TG, et al.: Management of accidental exposure to Ebola virus in the biosafety level 4 laboratory, Hamburg, Germany. J Infect Dis 2011, 204 Suppl 3:S785–90.

271. Marzi A, Hanley PW, Haddock E, Martellaro C, Kobinger G, Feldmann H: Efficacy of Vesicular Stomatitis Virus–Ebola Virus Postexposure Treatment in Rhesus Macaques Infected With Ebola Virus Makona. J Infect Dis 2016, 214:S360–S366.

272. Wong G, Audet J, Fernando L, Fausther-Bovendo H, Alimonti JB, Kobinger GP, Qiu X: Immunization with vesicular stomatitis virus vaccine expressing the Ebola glycoprotein provides sustained long-term protection in rodents. Vaccine 2014, 32:5722–5729.

273. Prescott J, DeBuysscher BL, Feldmann F, Gardner DJ, Haddock E, Martellaro C, Scott D, Feldmann H: Single-dose live-attenuated vesicular stomatitis virus-based vaccine protects African green monkeys from Nipah virus disease. Vaccine 2015, 33:2823–2829.

274. Rose NF, Roberts A, Buonocore L, Rose JK: Glycoprotein exchange vectors based on vesicular stomatitis virus allow effective boosting and generation of neutralizing antibodies to a primary isolate of human immunodeficiency virus type 1. J Virol 2000, 74:10903–10910.

275. Safronetz D, Mire C, Rosenke K, Feldmann F, Haddock E, Geisbert T, Feldmann H: A recombinant vesicular stomatitis virus-based Lassa fever vaccine protects guinea pigs and macaques against challenge with geographically and genetically distinct Lassa viruses. PLoS Negl Trop Dis 2015, 9:e0003736.

276. Tsuda Y, Safronetz D, Brown K, LaCasse R, Marzi A, Ebihara H, Feldmann H: Protective efficacy of a bivalent recombinant vesicular stomatitis virus vaccine in the Syrian hamster model of lethal Ebola virus infection. J Infect Dis 2011, 204 Suppl 3:S1090–7.

277. Marzi A, Feldmann F, Geisbert TW, Feldmann H, Safronetz D: Vesicular Stomatitis Virus–based Vaccines against Lassa and Ebola Viruses. Emerg Infect Dis 2015, 21.

278. Henao-Restrepo AM, Longini IM, Egger M, Dean NE, John Edmunds W, Camacho A, Carroll MW, Doumbia M, Draguez B, Duraffour S, et al.: Efficacy and effectiveness of an rVSV-vectored vaccine expressing Ebola surface glycoprotein: interim results from the Guinea ring vaccination cluster-randomised trial. Lancet 2015, 386:857–866.

279. Suder E, Furuyama W, Feldmann H, Marzi A, de Wit E: The vesicular stomatitis virus-based Ebola virus vaccine: From concept to clinical trials. Hum Vaccin Immunother 2018, 14:2107–2113.

280. Dowling W, Thompson E, Badger C, Mellquist JL, Garrison AR, Smith JM, Paragas J, Hogan RJ, Schmaljohn C: Influences of glycosylation on antigenicity, immunogenicity, and protective efficacy of ebola virus GP DNA vaccines. J Virol 2007, 81:1821–1837.

281. Francica JR, Matukonis MK, Bates P: Requirements for cell rounding and surface protein down-regulation by Ebola virus glycoprotein. Virology 2009, 383:237–247.

282. Lennemann NJ, Walkner M, Berkebile AR, Patel N, Maury W: The Role of Conserved N-Linked Glycans on Ebola Virus Glycoprotein 2. J Infect Dis 2015, 212 Suppl 2:S204–9.

283. Krause PR, Bryant PR, Clark T, Dempsey W, Henchal E, Michael NL, Regules JA, Gruber MF: Immunology of protection from Ebola virus infection. Sci Transl Med 2015, 7:286ps11.

284. Sullivan NJ, Hensley L, Asiedu C, Geisbert TW, Stanley D, Johnson J, Honko A, Olinger G, Bailey M, Geisbert JB, et al.: CD8+ cellular immunity mediates rAd5 vaccine protection against Ebola virus infection of nonhuman primates. Nat Med 2011, 17:1128–1131.

285. Dolnik O, Volchkova VA, Escudero-Perez B, Lawrence P, Klenk H-D, Volchkov VE: Shedding of Ebola Virus Surface Glycoprotein Is a Mechanism of Self-regulation of Cellular Cytotoxicity and Has a Direct Effect on Virus Infectivity. J Infect Dis 2015, 212 Suppl 2:S322–8.

286. Website. [date unknown],

287. Nakada-Tsukui K, Watanabe N, Kobayashi Y: Regulation of the processing and release of tumor necrosis factor α in a human macrophage cell line. J Leukoc Biol 1999, 66:968–973.

288. Cauwe B, Opdenakker G: Intracellular substrate cleavage: a novel dimension in the biochemistry, biology and pathology of matrix metalloproteinases. Crit Rev Biochem Mol Biol 2010, 45:351–423.

289. Schuck S, Honsho M, Ekroos K, Shevchenko A, Simons K: Resistance of cell membranes to different detergents. Proc Natl Acad Sci U S A 2003, 100:5795–5800.

290. Alazard-Dany N: Ebola virus glycoprotein GP is not cytotoxic when expressed constitutively at a moderate level. J Gen Virol 2006, 87:1247–1257.

291. Sullivan NJ, Peterson M, Yang Z-Y, Kong W-P, Duckers H, Nabel E, Nabel GJ: Ebola virus glycoprotein toxicity is mediated by a dynamin-dependent protein-trafficking pathway. J Virol 2005, 79:547–553.

292. Carrasco L, Otero MJ, Castrillo J: Modification of membrane permeability by animal viruses. Pharmacol Ther 1989, 40:171–212.

293. Browne EP, Taylor JA, Richard Bellamy A: Membrane-destabilizing activity of rotavirus NSP4 is mediated by a membrane-proximal amphipathic domain. J Gen Virol 2000, 81:1955–1959.

294. Cho MW, Teterina N, Egger D, Bienz K, Ehrenfeld E: Membrane rearrangement and vesicle induction by recombinant poliovirus 2C and 2BC in human cells. Virology 1994, 202:129–145.

295. Xu P, Derynck R: Direct activation of TACE-mediated ectodomain shedding by p38 MAP kinase regulates EGF receptor-dependent cell proliferation. Mol Cell 2010, 37:551–566.

296. Olival KJ, Hayman DTS: Filoviruses in bats: current knowledge and future directions. Viruses 2014, 6:1759–1788.

297. Han BA, Schmidt JP, Alexander LW, Bowden SE, Hayman DTS, Drake JM: Undiscovered Bat Hosts of Filoviruses. PLoS Negl Trop Dis 2016, 10:e0004815.

298. Goldstein T, Anthony SJ, Gbakima A, Bird BH, Bangura J, Tremeau-Bravard A, Belaganahalli MN, Wells HL, Dhanota JK, Liang E, et al.: The discovery of Bombali virus adds further support for bats as hosts of ebolaviruses. Nat Microbiol 2018, doi:10.1038/s41564-018-0227-2.

299. Hayman DTS, Emmerich P, Yu M, Wang L-F, Suu-Ire R, Fooks AR, Cunningham AA, Wood JLN: Long-term survival of an urban fruit bat seropositive for Ebola and Lagos bat viruses. PLoS One 2010, 5:e11978.

300. Hayman DTS, Yu M, Crameri G, Wang L-F, Suu-Ire R, Wood JLN, Cunningham AA: Ebola virus antibodies in fruit bats, Ghana, West Africa. Emerg Infect Dis 2012, 18:1207–1209.

301. Le Guenno B, Formenty P, Wyers M, Gounon P, Walker F, Boesch C: Isolation and partial characterisation of a new strain of Ebola virus. Lancet 1995, 345:1271–1274.

302. Peel AJ, McKinley TJ, Baker KS, Barr JA, Crameri G, Hayman DTS, Feng Y-R, Broder CC, Wang L-F, Cunningham AA, et al.: Use of cross-reactive serological assays for detecting novel pathogens in wildlife: Assessing an appropriate cutoff for henipavirus assays in African bats. J Virol Methods 2013, 193:295–303.

303. Hayman DTS, Suu-Ire R, Breed AC, McEachern JA, Wang L, Wood JLN, Cunningham AA: Evidence of henipavirus infection in West African fruit bats. PLoS One 2008, 3:e2739.

304. Hayman DTS, Wang L-F, Barr J, Baker KS, Suu-Ire R, Broder CC, Cunningham AA, Wood JLN: Antibodies to henipavirus or henipa-like viruses in domestic pigs in Ghana, West Africa. PLoS One 2011, 6:e25256.

305. Reynard O, Volchkov VE: Characterization of a Novel Neutralizing Monoclonal Antibody Against Ebola Virus GP. J Infect Dis 2015, 212 Suppl 2:S372–8.

306. Pan W, Song D, He W, Lu H, Lan Y, Tong J, Gao F, Zhao K: The matrix protein of vesicular stomatitis virus inhibits host-directed transcription of target genes via interaction with the TFIIH subunit p8. Vet Microbiol 2017, 208:82–88.

307. Waibler Z, Detje CN, Bell JC, Kalinke U: Matrix protein mediated shutdown of host cell metabolism limits vesicular stomatitis virus-induced interferon-alpha responses to plasmacytoid dendritic cells. Immunobiology 2007, 212:887–894.

308. Akpinar F, Timm A, Yin J: High-Throughput Single-Cell Kinetics of Virus Infections in the Presence of Defective Interfering Particles. J Virol 2016, 90:1599–1612.

309. Timm A, Yin J: Kinetics of virus production from single cells. Virology 2012, 424:11–17.

310. Hensel SC, Rawlings JB, Yin J: Stochastic kinetic modeling of vesicular stomatitis virus intracellular growth. Bull Math Biol 2009, 71:1671–1692.

311. Heldt FS, Frensing T, Reichl U: Modeling the intracellular dynamics of influenza virus replication to understand the control of viral RNA synthesis. J Virol 2012, 86:7806–7817.

312. Marozsan AJ, Fraundorf E, Abraha A, Baird H, Moore D, Troyer R, Nankja I, Arts EJ: Relationships between infectious titer, capsid protein levels, and reverse transcriptase activities of diverse human immunodeficiency virus type 1 isolates. J Virol 2004, 78:11130–11141.

313. Mohan GS, Ye L, Li W, Monteiro A, Lin X, Sapkota B, Pollack BP, Compans RW, Yang C: Less is more: Ebola virus surface glycoprotein expression levels regulate virus production and infectivity. J Virol 2015, 89:1205–1217.

314. Medaglini D, Siegrist C-A: Immunomonitoring of human responses to the rVSV-ZEBOV Ebola vaccine. Curr Opin Virol 2017, 23:88–94.

315. Kotwal GJ, Buller ML, Wunner WH, Pringle CR, Ghosh HP: Role of glycosylation in transport of vesicular stomatitis virus envelope glycoprotein. A new class of mutant defective in glycosylation and transport of G protein. J Biol Chem 1986, 261:8936–8943.

316. Neumann G, Feldmann H, Watanabe S, Lukashevich I, Kawaoka Y: Reverse genetics demonstrates that proteolytic processing of the Ebola virus glycoprotein is not essential for replication in cell culture. J Virol 2002, 76:406–410.

317. Teuchert M, Schäfer W, Berghöfer S, Hoflack B, Klenk H-D, Garten W: Sorting of Furin at the Trans-Golgi Network. J Biol Chem 1999, 274:8199–8207.

318. Bavari S, Bosio CM, Wiegand E, Ruthel G, Will AB, Geisbert TW, Hevey M, Schmaljohn C, Schmaljohn A, Aman MJ: Lipid raft microdomains: a gateway for compartmentalized trafficking of Ebola and Marburg viruses. J Exp Med 2002, 195:593–602.

319. Russ WP, Engelman DM: The GxxxG motif: a framework for transmembrane helix-helix association. J Mol Biol 2000, 296:911–919.

320. Hacke M, Björkholm P, Hellwig A, Himmels P, Ruiz de Almodóvar C, Brügger B, Wieland F, Ernst AM: Inhibition of Ebola virus glycoprotein-mediated cytotoxicity by targeting its transmembrane domain and cholesterol. Nat Commun 2015, 6:7688.

321. Lee JE, Fusco ML, Hessell AJ, Oswald WB, Burton DR, Saphire EO: Structure of the Ebola virus glycoprotein bound to an antibody from a human survivor. Nature 2008, 454:177–182.

322. Leung K, Kim J-O, Ganesh L, Kabat J, Schwartz O, Nabel GJ: HIV-1 Assembly: Viral Glycoproteins Segregate Quantally to Lipid Rafts that Associate Individually with HIV-1 Capsids and Virions. Cell Host Microbe 2008, 3:285–292.

323. Her L-S: Inhibition of Nucleocytoplasmic Transport by the Matrix Protein of Vesicular Stomatitis Virus. 2001.

324. Noser JA, Mael AA, Sakuma R, Ohmine S, Marcato P, Lee PW, Ikeda Y: The RAS/Raf1/MEK/ERK signaling pathway facilitates VSV-mediated oncolysis: implication for the defective interferon response in cancer cells. Mol Ther 2007, 15:1531–1536.

325. Luo H, Yanagawa B, Zhang J, Luo Z, Zhang M, Esfandiarei M, Carthy C, Wilson JE, Yang D, McManus BM: Coxsackievirus B3 replication is reduced by inhibition of the extracellular signal-regulated kinase (ERK) signaling pathway. J Virol 2002, 76:3365–3373.

326. Pleschka S, Wolff T, Ehrhardt C, Hobom G, Planz O, Rapp UR, Ludwig S: Influenza virus propagation is impaired by inhibition of the Raf/MEK/ERK signalling cascade. Nat Cell Biol 2001, 3:301–305.

327. Yang X, Gabuzda D: Regulation of human immunodeficiency virus type 1 infectivity by the ERK mitogen-activated protein kinase signaling pathway. J Virol 1999, 73:3460–3466.

328. Guibinga GH, Miyanohara A, Esko JD, Friedmann T: Cell surface heparan sulfate is a receptor for attachment of envelope protein-free retrovirus-like particles and VSV-G pseudotyped MLV-derived retrovirus vectors to target cells. Mol Ther 2002, 5:538–546.

329. Chen Y, Leask A, Abraham DJ, Pala D, Shiwen X, Khan K, Liu S, Carter DE, Wilcox-Adelman S, Goetinck P, et al.: Heparan sulfate-dependent ERK activation contributes to the overexpression of fibrotic proteins and enhanced contraction by scleroderma fibroblasts. Arthritis Rheum 2008, 58:577–585.

330. Dreyfuss JL, Regatieri CV, Jarrouge TR, Cavalheiro RP, Sampaio LO, Nader HB: Heparan sulfate proteoglycans: structure, protein interactions and cell signaling. An Acad Bras Cienc 2009, 81:409–429.

331. Marozin S, Altomonte J, Apfel S, Dinh PX, De Toni EN, Rizzani A, Nussler A, Kato N, Schmid RM, Pattnaik AK, et al.: Posttranslational Modification of Vesicular Stomatitis Virus Glycoprotein, but Not JNK Inhibition, Is the Antiviral Mechanism of SP600125. J Virol 2012, 86:4844–4855.

332. Renukaradhya GJ, Webb TJR, Khan MA, Lin YL, Du W, Gervay-Hague J, Brutkiewicz RR: Virus-induced inhibition of CD1d1-mediated antigen presentation: reciprocal regulation by p38 and ERK. J Immunol 2005, 175:4301–4308.

333. Johnson JC, Martinez O, Honko AN, Hensley LE, Olinger GG, Basler CF: Pyridinyl imidazole inhibitors of p38 MAP kinase impair viral entry and reduce cytokine induction by Zaire ebolavirus in human dendritic cells. Antiviral Res 2014, 107:102–109.

334. Martinez O, Valmas C, Basler CF: Ebola virus-like particle-induced activation of NF-κB and Erk signaling in human dendritic cells requires the glycoprotein mucin domain. Virology 2007, 364:342–354.

335. Matsuzawa A, Saegusa K, Noguchi T, Sadamitsu C, Nishitoh H, Nagai S, Koyasu S, Matsumoto K, Takeda K, Ichijo H: ROS-dependent activation of the TRAF6-ASK1-p38 pathway is selectively required for TLR4-mediated innate immunity. Nat Immunol 2005, 6:587–592.

336. Huang G, Shi LZ, Chi H: Regulation of JNK and p38 MAPK in the immune system: signal integration, propagation and termination. Cytokine 2009, 48:161–169.

337. Halfmann P, Neumann G, Kawaoka Y: The Ebolavirus VP24 protein blocks phosphorylation of p38 mitogen-activated protein kinase. J Infect Dis 2011, 204 Suppl 3:S953–6.

338. Younan P, Iampietro M, Santos RI, Ramanathan P, Popov VL, Bukreyev A: Disruption of Phosphatidylserine Synthesis or Trafficking Reduces Infectivity of Ebola Virus. J Infect Dis 2018, doi:10.1093/infdis/jiy489.

339. Younan P, Iampietro M, Santos RI, Ramanathan P, Popov VL, Bukreyev A: Role of Transmembrane Protein 16F in the Incorporation of Phosphatidylserine Into Budding Ebola Virus Virions. J Infect Dis 2018, doi:10.1093/infdis/jiy485.

340. Lorenzen I, Lokau J, Korpys Y, Oldefest M, Flynn CM, Künzel U, Garbers C, Freeman M, Grötzinger J, Düsterhöft S: Control of ADAM17 activity by regulation of its cellular localisation. Sci Rep 2016, 6:35067.

341. Chan Y-P, Yan L, Feng Y-R, Broder CC: Preparation of recombinant viral glycoproteins for novel and therapeutic antibody discovery. Methods Mol Biol 2009, 525:31–58, xiii.

342. Cha GW, Cho JE, Ju YR, Hong Y-J, Han MG, Lee W-J, Choi EY, Jeong YE: Comparison of four serological tests for detecting antibodies to Japanese encephalitis virus after vaccination in children. Osong Public Health Res Perspect 2014, 5:286–291.

343. De Ory F, Sánchez-Seco MP, Vázquez A, Montero MD, Sulleiro E, Martínez MJ, Matas L, Merino FJ, Working Group for the Study of Zika Virus Infections: Comparative Evaluation of Indirect Immunofluorescence and NS-1-Based ELISA to Determine Zika Virus-Specific IgM. Viruses 2018, 10.

344. Groen J, v. d. Groen G, Hoofd G, Osterhaus A: Comparison of immunofluorescence and enzyme-linked immunosorbent assays for the serology of Hantaan virus infections. J Virol Methods 1989, 23:195–203.

345. Nakayama E, Yokoyama A, Miyamoto H, Igarashi M, Kishida N, Matsuno K, Marzi A, Feldmann H, Ito K, Saijo M, et al.: Enzyme-linked immunosorbent assay for detection of filovirus species-specific antibodies. Clin Vaccine Immunol 2010, 17:1723–1728.

346. Ogawa H, Miyamoto H, Nakayama E, Yoshida R, Nakamura I, Sawa H, Ishii A, Thomas Y, Nakagawa E, Matsuno K, et al.: Seroepidemiological Prevalence of Multiple Species of Filoviruses in Fruit Bats (Eidolon helvum) Migrating in Africa. J Infect Dis 2015, 212 Suppl 2:S101–8.

347. Fischer K, Jabaty J, Suluku R, Strecker T, Groseth A, Fehling SK, Balkema-Buschmann A, Koroma B, Schmidt KM, Atherstone C, et al.: Serological Evidence for the Circulation of Ebolaviruses in Pigs From Sierra Leone. J Infect Dis 2018, 218:S305–S311.

348. Glynn JR, Bower H, Johnson S, Houlihan CF, Montesano C, Scott JT, Semple MG, Bangura MS, Kamara AJ, Kamara O, et al.: Asymptomatic infection and unrecognised Ebola virus disease in Ebola-affected households in Sierra Leone: a cross-sectional study using a new non-invasive assay for antibodies to Ebola virus. Lancet Infect Dis 2017, 17:645–653.

349. Leroy EM, Baize S, Volchkov VE, Fisher-Hoch SP, Georges-Courbot MC, Lansoud-Soukate J, Capron M, Debré P, McCormick JB, Georges AJ: Human asymptomatic Ebola infection and strong inflammatory response. Lancet 2000, 355:2210–2215.

350. O'Hearn AE, Voorhees MA, Fetterer DP, Wauquier N, Coomber MR, Bangura J, Fair JN, Gonzalez J-P, Schoepp RJ: Serosurveillance of viral pathogens circulating in West Africa. Virol J 2016, 13:163.

351. Bower H, Glynn JR: A systematic review and meta-analysis of seroprevalence surveys of ebolavirus infection. Sci Data 2017, 4:160133.

352. Mafopa NG, Russo G, Wadoum REG, Iwerima E, Batwala V, Giovanetti M, Minutolo A, Turay P, Turay TB, Kargbo B, et al.: Seroprevalence of Ebola virus infection in Bombali District, Sierra Leone. J Public Health Africa 2017, 8:732.

353. Amman BR, Carroll SA, Reed ZD, Sealy TK, Balinandi S, Swanepoel R, Kemp A, Erickson BR, Comer JA, Campbell S, et al.: Seasonal pulses of Marburg virus circulation in juvenile Rousettus aegyptiacus bats coincide with periods of increased risk of human infection. PLoS Pathog 2012, 8:e1002877.

354. Website. [date unknown],

355. Boilard E, Paré G, Rousseau M, Cloutier N, Dubuc I, Lévesque T, Borgeat P, Flamand L: Influenza virus H1N1 activates platelets through FcγRIIA signaling and thrombin generation. Blood 2014, 123:2854–2863.

356. Sanchez A, Ksiazek TG, Rollin PE, Miranda ME, Trappier SG, Khan AS, Peters CJ, Nichol ST: Detection and molecular characterization of Ebola viruses causing disease in human and nonhuman primates. J Infect Dis 1999, 179 Suppl 1:S164–9.

357. Thomas D, Newcomb WW, Brown JC, Wall JS, Hainfeld JF, Trus BL, Steven AC: Mass and molecular composition of vesicular stomatitis virus: a scanning transmission electron microscopy analysis. J Virol 1985, 54:598–607.

358. Vallance TM, Zeuner M-T, Williams HF, Widera D, Vaiyapuri S: Toll-Like Receptor 4 Signalling and Its Impact on Platelet Function, Thrombosis, and Haemostasis. Mediators Inflamm 2017, 2017:9605894.

359. Hamzeh-Cognasse H, Berthelot P, Tardy B, Pozzetto B, Bourlet T, Laradi S, Garraud O, Cognasse F: Platelet toll-like receptors are crucial sensors of infectious danger moieties. Platelets 2018, 29:533–540.

360. Cognasse F, Semple J, Garraud O: Platelets as Potential Immunomodulators: Is There a Role for Platelet Toll-Like Receptors? Curr Immunol Rev 2007, 3:109–115.

361. Cognasse F, Hamzeh H, Chavarin P, Acquart S, Genin C, Garraud O: Evidence of Toll-like receptor molecules on human platelets. Immunol Cell Biol 2005, 83:196–198.

362. Chaipan C, Soilleux EJ, Simpson P, Hofmann H, Gramberg T, Marzi A, Geier M, Stewart EA, Eisemann J, Steinkasserer A, et al.: DC-SIGN and CLEC-2 mediate human immunodeficiency virus type 1 capture by platelets. J Virol 2006, 80:8951–8960.

363. Youssefian T: Host defense role of platelets: engulfment of HIV and Staphylococcus aureus occurs in a specific subcellular compartment and is enhanced by platelet activation. Blood 2002, 99:4021–4029.

364. Zapata JC, Cox D, Salvato MS: The role of platelets in the pathogenesis of viral hemorrhagic fevers. PLoS Negl Trop Dis 2014, 8:e2858.

365. Osterud B: The role of platelets in decrypting monocyte tissue factor. Semin Hematol 2001, 38:2–5.

366. Chabert A, Damien P, Verhoeven PO, Grattard F, Berthelot P, Zeni F, Panicot-Dubois L, Robert S, Dignat-George F, Eyraud M-A, et al.: Acetylsalicylic acid differentially limits the activation and expression of cell death markers in human platelets exposed to Staphylococcus aureus strains. Sci Rep 2017, 7:5610.

367. Cook JD, Lee JE: The secret life of viral entry glycoproteins: moonlighting in immune evasion. *PLoS Pathog* 2013, 9:e1003258.

368. Beniac DR, Booth TF: Structure of the Ebola virus glycoprotein spike within the virion envelope at 11 Å resolution. *Sci Rep* 2017, 7:46374.

369. Daugherty MD, Malik HS: How a virus blocks a cellular emergency access lane to the nucleus, STAT! *Cell Host Microbe* 2014, 16:150–152.

Molecular characterisation of the recombinant *Vesicular Stomatitis Virus*-ZEBOV-GP virus, prototype vaccine against Ebola virus

Abstract

The filovirus Ebolavirus (EBOV) is the causative agent of severe viral haemorrhagic fevers in humans that can be lethal in 90% of cases. The current outbreak in the Democratic Republic of Congo and the extraordinary scale of the 2014-2016 outbreak in West Africa, that caused the death of more than 11 000 disease victims, lead the international public health agencies to test several therapeutic approaches to limit viral spreading and mortality. Amongst those, the recombinant replication-competent rVSV-ZEBOV virus, that expressed EBOV GP glycoprotein, appears to offer the best protection in animal models and outbreak settings. While its effectiveness and safety have been widely investigated before human trials and despite numerous studies that showed the importance the nature of the glycoproteins which are produced during the infection from the EBOV GP gene that has been inserted in VSV genome are unknown. In this respect, the molecular characterisation of the viral glycoproteins synthesised during rVSV-GP presented in this thesis, offer new insights with which to understand the success of the rVSV-GP vaccine but also the potential viral origins of the severe adverse side effects observed during vaccination and could help in developing a safer vaccine, which currently cannot be used in an immunocompromised population.

Keywords*: Ebolavirus, rVSV-ZEBOV, vaccine, glycosylations, R. aegyptiacus, Marburgvirus*

Tour Cervi, 21 Avenue Tony Garnier, 69365, Lyon CEDEX 07.